eman ta zabal zazu

Universidad del País Vasco
Euskal Herriko Unibertsitatea

DEPARTMENT OF PHARMACOLOGY / FARMAKOLOGIA SAILA
DEPARTAMENTO DE FARMACOLOGÍA

Human Postmitotic Neurons Derived from NTERA2/D1 Cells by Short Exposure to Cytosine-β-D-Arabinofuranoside: Characterization of Neurotransmitter Phenotypes and Role of Phospholipase C β1 in Differentiation

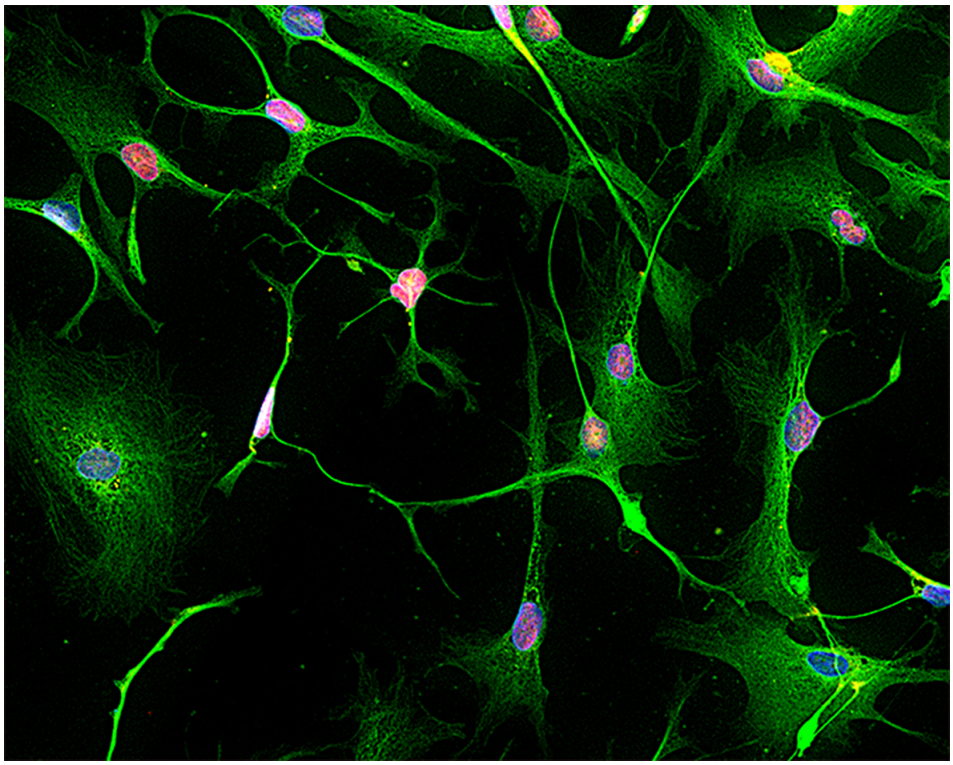

Imanol González-Burguera
Vitoria-Gasteiz, 2015

Cover illustration: Terminally differentiated NT2N neurons by treatment with AraC during 6 days. Cells were doubly immunolabeled for NeuN/Fox-3 (red) and β-III-tubulin (green), combined with Hoechst 33342 nuclear staining (blue).

Quisiera mostrar mi agradecimiento a todas aquellas personas que, de muy diversa forma, han posibilitado la realización satisfactoria de la presente tesis doctoral.

A los doctores Maider López de Jesús y Gontzal García del Caño, directores de mi tesis, no tengo palabras para agradecerles todo lo que me han enseñado a lo largo de estos años y darles las gracias por todo el apoyo y el tiempo que han dedicado a estar conmigo para que pudiese entender el por qué de todo. Gracias por vuestra paciencia, dedicación y comprensión, no he podido tener mejores directores que vosotros.

Al doctor Joan Sallés por haberme brindado la oportunidad de desarrollar este trabajo de investigación y a su vez por haberme dado la oportunidad de formarme mejor realizando una estancia en el extranjero. Gracias por haber confiado en este proyecto y en mí para desarrollarlo.

Al doctor Sergio Barrondo por estar siempre dispuesto a ayudarme en cualquier momento desde corregir la tesis, presentaciones etc. Siempre transmitiendo positividad en tus palabras, y como no, por hacer más ameno el trabajo en el laboratorio.

A mis compañeros de laboratorio, Mario, Xabi, Ana y Leyre por los buenos momentos vividos que han permitido al trabajo rutinario de laboratorio parecer mucho más ameno.

Mención especial al que fue técnico del departamento de Neurociencias Juan Pablo Villamor, siempre me preguntabas cuando iba a ser la defensa de mi tesis y ahora que tenemos una fecha, tú no estás. Desde donde estés solo te puedo decir que muchas gracias por todo y por todos los momentos vividos en el laboratorio.

Al grupo de la doctora Suzanne Scarlata, Bonnie, Sid, Shriya, Urszula, Jean, Giuseppe y Finly en Stony Brook (Nueva York), gracias por hacerme sentir como en casa.

Y por último pero no menos importante, a mi familia, a mi kuadrilla, patxanga y demás amigos por haberme animado en todo momento. Y por último a ti June, porque tú me has tenido que aguantar en mis días buenos y malos pensando que el día de la defensa nunca llegaría.

Financial support:

- Predoctoral Grant of the University of the Basque Country UPV/EHU 243/2011.
- Grants of the Basque Government: GIC/IT-330-10, GIC/IT-589/13, SAIOTEK (S-PE08UN29, S-PE11UN124, S-PE11UN125)
- Instituto de Salud Carlos III, Centro de Investigación Biomédica en Red de Salud Mental, CIBERSAM.
- Research and Training Unit of Neurochemistry, Neuropsychopharmacology and Psychiatry of the University of the Basque Country (UPV/EHU UFI11/35).

INDEX

Page

I. INTRODUCTION

1. PHOSPHOLIPASE Cβ1

1.1. Phosphatidylinositol-specific phospholipase C

Transduction of extracellular signals into intracellular responses mediated by G protein-coupled membrane receptors requires amplification systems, which are usually based on the ability of transmembrane receptors to regulate the activity of membrane-associated and/or cytosolic enzymes. Upon activation, these enzymes promote a rapid increase in the intracellular concentration of reaction products (known as second messengers), which transduce extracellular signals into intracellular signaling cascades, thus promoting specific physiological responses relevant for survival, proliferation, differentiation, and intercellular communication.

Among plasma membrane-associated enzymes, two major families emerge as the most important players in signal amplification: the so-called effector proteins adenylate cyclase and phosphatidylinositol-specific phospholipase C (also known as PtdIns-PLC or PI-PLC, but hereafter referred to as PLC). Because there is a wide variety of G protein-coupled receptors, each responding to specific agonists (such as hormones and neurotransmitters), different extracellular signals converge to affect the catalytic activity of these effector enzymes.

1.1.1. Catalytic activity of PLC isozymes

Phosphatidylinositol-specific phospholipase C is the target of several transducer mechanisms in response to a plethora of physiological stimuli, such as agonist (hormones, neurotransmitters, growth factors, chemokines…) activation of G-protein coupled receptors, or elevation of intracellular calcium levels. In this way, phosphoinositide hydrolysis in response to one or more extracellular signal type has been detected in all mammal tissues studied.

The major substrate of PLC phosphatidylinositol is the minor plasma membrane phosphoinositide inositol 4,5-bisphosphate (PtdIns 4,5-P_2. Hereinafter, we refer to this phosphoinositide as PIP_2; and positions of phosphate groups in the inositol ring will be mentioned only if necessary for disambiguation). By catalyzing the hydrolysis of the phosphodiester bond on the third position (sn-3) of the glycerol backbone, PLC generates the second messengers cyclic inositol 1,4,5-triphosphate (Ins 1,4,5-P_3 or IP_3) and diacylglycerol (DAG). Water-soluble IP_3 diffuses to the cytosol and bind its receptor on the ER, causing Ca^{2+} release from intracellular stores, whereas hydrophobic

DAG remains bound to inner layer of the plasma membrane, where it can activate different isoenzymes belonging to the family of protein kinase C (PKC) (Berridge, 1983; Nishizuka, 1984). The substrates used by the enzymatic activity of PLC are still under study and discussion. Clearly, the discussion is not sterile and should be maintained the importance of this question, given that the substrate used determines the percentage that IP_3 represents over other inositol phosphates (see Figure 1B), with only IP_3 having a well defined intracellular function. Considering the increasing number of functions assigned to PIP_2, the regulation of its plasma membrane concentration may have important functional consequences, as it will be described later. Focusing on the central nervous system, it can be concluded that the matter is not fully resolved. Specifically, the use of intact cells or membrane preparations, the presence or absence of detergents or divalent ions (like Ca^{2+} and Mg^{2+}), or the presence of exogenous or endogenous substrates appear to be determinant factors to direct the findings in either direction. Simultaneously, the first studies performed in platelets and proposing PIP_2 as the main substrate (Berridge, 1983; Downes and Wusterman, 1983), demonstrated that the partially purified PLC enzymatic activity was able to hydrolyze not only exogenous PIP_2, but also (PI) PtdIns and PtdIns 4-P (PIP), but not non-phosphorylated inositides. A few years later, it was described that stimulation of PLC enzymatic activity with the muscarinic acetylcholine receptor agonist carbachol, promoted hydrolysis of exogenous PI, PIP and PIP_2 in membrane preparations of rat cerebral cortex (Claro et al., 1989). All the three substrates required the Ca^{2+} ion, within the range of physiological concentrations, and the ionic detergent deoxycholate, although PI hydrolysis required slightly higher Ca^{2+} concentration than PIP and PIP_2 (Claro et al., 1989). The importance of deoxycholate *in vitro* has been linked to facilitation of PLC access to endogenous polyphosphates (Chung et al., 1985; Plantavid et al., 1986). However, PLCs appear to act primarily on PIP_2 in their native cellular environment, although few studies addressed this question rigorously (Fisher et al., 1990; Batty and Nahorski, 1992; for review, Balla T, 2013).

Finally, the work of several independent laboratories has consistently demonstrated that the phosphoinositide cycle (biosynthetic and hydrolytic machinery) is present in the cell nucleus, and may be important for various nuclear events such as mRNA export, DNA repair, and gene transcription (Irvine, 2003). The presence of phosphoinositide metabolism in the nuclear envelope was first reported by Smith and Wells (1983) using nuclear preparations from rat liver. Later, Cocco et al. (1987) demonstrated for the first

time that envelope-depleted nuclei were able to synthesize PIP and PIP_2 *in vitro*, showing that phosphoinositide cycle also occurred at internal nuclear domains (see also, Payrastre et al., 1992; Garcia-Bustos et al., 1994). At present, it is widely accepted the existence of phosphoinositide signaling within the nucleus, where the major PLC substrate PIP_2 and its products IP_3 and DAG are involved in a variety of nuclear events (mRNA export, DNA repair, gene transcription, splicing pre-mRNA transcripts…) and cellular responses, including differentiation, proliferation and neoplastic transformation (Neri et al., 1999; D'Santos et al., 2000; Irvine, 2003).

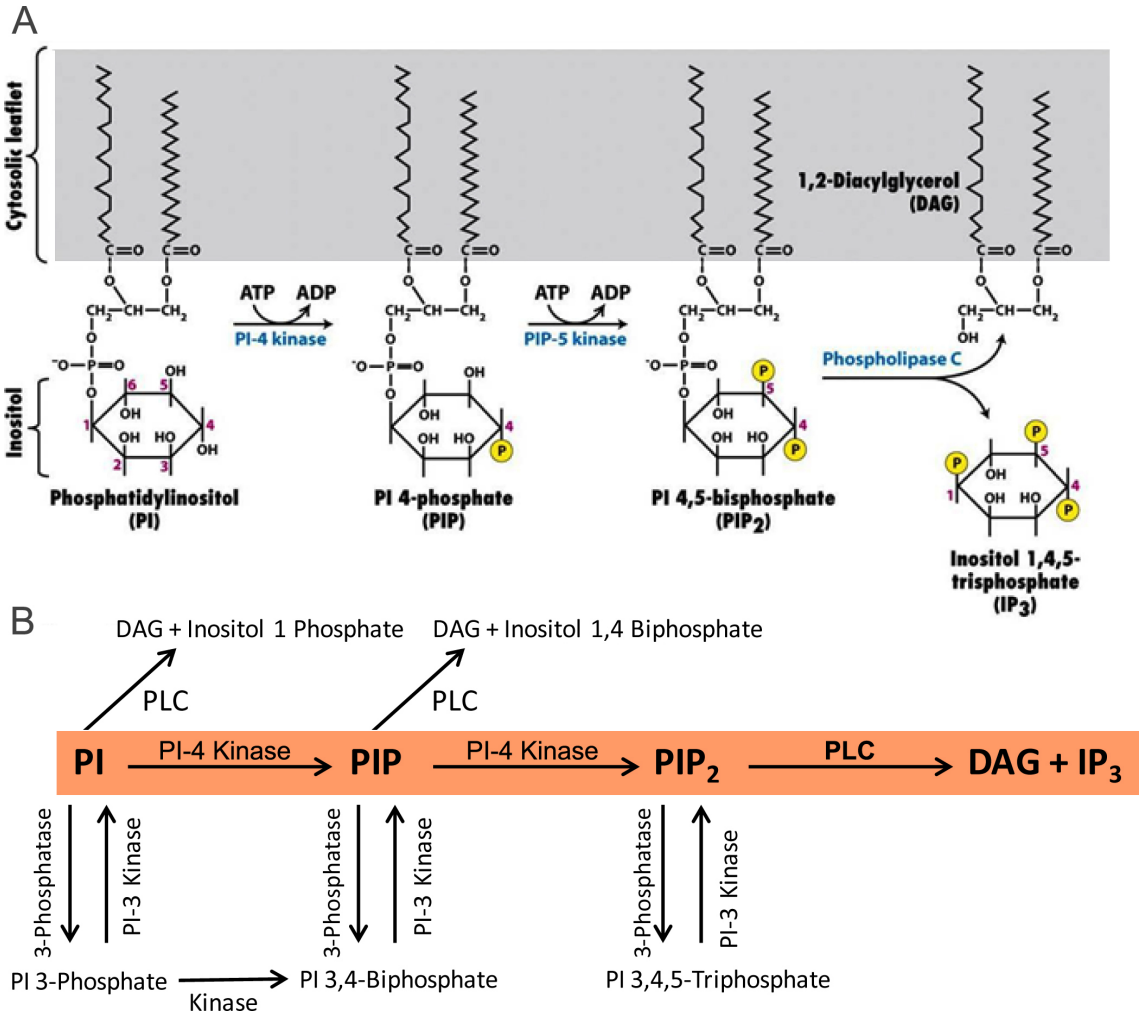

Figure 1. A. Schematic representation of phosphoinositide phosphorylation and PIP_2 hydrolysis to generate the second messengers DAG and IP_3. B. Possible metabolic routes of phosphoinositides involve 3-phosphatase, PI-3 kinase, PI-4 kinase and PLC enzymatic activity. Modified from Lodish et al. (2000).

1.1.2. Structural and functional domains of PLC isozymes

PLC activity comprises a large and diverse group of enzymes that differ in structure and cellular distribution. Until the XX century, there were identified 10 PLC isozymes in mammalians, which were classified into three different families; four PLCβ (1, 2, 3,

4), two PLCγ (1, 2) and three PLCδ (1, 3, 4), excluding from this later group an isozyme, originally called PLCα, that corresponds to a proteolytic fragment of PLCδ1 (Rhee et al., 1989; Bae and Rhee, 1997). Later three new PLC families were discovered: PLCη, PLCζ and PLCε (Lopez et al., 2001; Song et al., 2001; Kelley et al., 2001; for review Suh et al., 2008 and Balla, 2013), making up a total of 13 isolated PLC isoforms in mammals, excluding splicing variants (Fig. 2). The PLC isozyme families differ in size, although the amino acid sequences are relatively conserved among the different families. The catalytic domains, termed X-Y, share at more than 60% sequence homology among the isoforms of the same PLC family (Rhee et al., 1989; Rhee and Bae, 1997). The linker amino acid sequence between the X and Y regions of the catalytic domain varies considerably when the different families are compared. For example, it is composed of 40, 110 and 190 aminoacids in PLCβ, PLCδ and PLCε isoforms, respectively, whereas the X-Y linker of PLCγ contains 400 residues and includes two Src homology domain 2 (SH2) and one Src homology domain 3 (SH3). SH2 domains bind phosphotyrosine containing peptide sequences, whereas SH3 binds proline-rich sequences. In general, these SH domains are involved in the negative regulation of the PLCγ kinase activity, since they confer a conformation to the protein that somehow prevents the access of the substrate to the catalytic domains of the enzyme, and only upon phophsorilation a suitable conformation for catalytic activity is adopted (Carpenter and Ji, 1999). In its turn, SH3 domain confers mitogenic properties to PLCγ by allowing it to interact with several Ras/p21 protein activators.

The catalytic activity of all PLC isozymes strictly depends on the presence of Ca^{2+} ions, with PLCδ being the more sensitive to this ion. Different structural and mutational studies with the PLCδ have managed to identify those residues of the catalytic domains that contribute to the recognition of the substrate, Ca^{2+} ion binding, and catalytic activity. In this way, it has been determined that Lys-438, Ser-522 and Arg-549 are critical for the preferential hydrolysis of polyphosphoinositides against monophosphoinositides, while the substitution of the Lys-440 affects selectively the hydrolysis of PIP_2, indicating that Lys-438, Ser-522 and Arg-549 would be involved in the interaction with the 4-phosphate group, whereas Lys-440 would be related to the interaction of 5-phosphate groups. It should be noted that these residues are conserved in both PLCβ and γ isozymes (Ellis et al., 1998). Finally, recent structural studies of PLCβ2 isozyme have led to the characterization of a sequence (residues 516-535),

located between the X and Y catalytic domains, which exert an inhibitory function on the catalytic activity of the enzyme. This sequence is preserved in PLCβ1 and PLCβ3, and will confer an autoinhibitory function to these isoforms (Hicks et al., 2008).

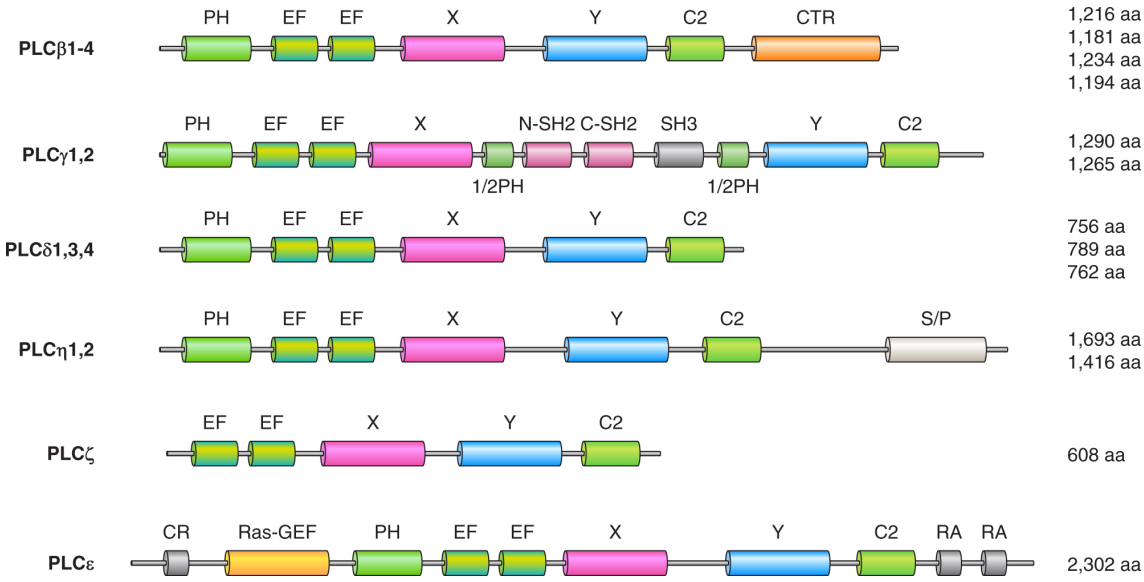

Figure 2. Organization of the structural and functional domains of the different PLC isozime families. All share in common X-Y catalytic, PH, EF-hand and C2 domains. Comments of other family-specific domains are incorporated in the introduction text. Taken from Balla, 2013.

Similarly to many different proteins involved in intracellular signaling mechanisms, the PLCβ, PLCγ and PLCδ isozymes share in common a pleckstrin homology (PH) domain, consisting of 100 residues within the amino-terminal region, critical for binding of some PLC isozymes to polyphosphoinositides and IP3 (Rameh et al., 1999; Harlan et al., 1994). PLCγ isozyme contains a second split PH domain flanking the SH2-SH2-SH3 tandem repeat. This additional PH domain has no affinity for phospholipids and has been implicated to interact directly with the TRPC3 calcium channel, suggesting a role in direct coupling between PLCγ and agonist-induced calcium entry (Wen et al., 2006). The well-characterized PH domain of PLCδ1 binds stereospecifically and with high affinity to the head group PIP_2, IP_3, and has become a valuable tool for studying cellular PIP_2 functions. The amino acid sequences of the PLCδ1 PH domain responsible for the interaction with PIP_2 have been elucidated, showing that they are necessary for plasma membrane targeting of and catalytic activity of PLCδ1. Thus, PIP_2 binding facilitates plasma membrane anchoring required for catalysis of phosphoinositides, whereas IP_3 production leads to sequestration and translocation of PLCδ1 to the cytoplasm. In this way, changes in PIP_2 and IP_3 levels due to activation of other PLC

isozymes could modulate the catalytic activity of PLCδ1 (Essen et al., 1996; Ferguson et al., 1995). The dissimilarity in the amino acid sequences of the PH domain among PLC isozymes accounts for differences in phoshpoinositide binding affinity and for the diverse mode of membrane interaction. For example, various studies reported that the PH domain of PLCγ has a high affinity for PtdIns 3,4,5-P_3 but not for PIP_2, suggesting a role for PtdIns 3,4,5-P_3 polyphosphoinositide in activation of PLCγ by its translocation to the plasma membrane (Razzini et al., 2000). On the other hand, the plasma membrane anchoring of PLCβs is not altered by PIP_2 levels, suggesting that the PH domain is not directly involved in targeting of PLCβs isozymes to the plasma membrane (Wang et al., 1999). By contrast, the PH domain of PLCβ1 shows affinity for PtdIns 3-P, suggesting that this phophoinositide would play an important role in the recruitment and activation of PLCβ isozymes in systems activated by PtdIns 3-kinases (Razzini et al., 2000) (Fig. 1). In addition, the PH domain of PLCβs seems to contain a binding sequence for βγ subunits of G proteins. Therefore, we could conclude that the PH domain facilitates plasma membrane anchoring of the different PLC isozymes but with different modes of interactions with phoshpoinositides and even βγ subunits of G heterotrimeric proteins in the case of PLCβ isozymes.

The analysis of the three-dimensional structure of PLCδ1 revealed the presence of two additional domains: the EF-hand located between the PH and the X catalytic domains, and the C2 domain, which is usually represented as an extension of the Y catalytic domain. As shown in figure 2, both the EF-hand and the C2 domain are present in all PLC isozymes (Essen et al., 1996; Lopez et al., 2001; Suh et al., 2008; Balla et al., 2013). The EF-hand domain consists of a duplication of two EF-hand units, each composed of two alpha helices linked by a short loop region of about 12 amino acids. The EF-hand domain of PLCδ1 is able to bind Ca^{2+}, as it has been observed in calcium binding proteins (Maki et al., 2002), and this binding appears to be required for the correct interaction between the PH domain and PIP_2 (Yamamoto et al., 1999; Rhee, 2001). However, the role of the EF-hand domain in other PLC families is unclear. As described below, a loop between the third and fourth EF-hands of PLCβs interacts with GTP-activated Gαq and is involved in regulating GTPase activating protein (GAP) activity of PLCβ (Waldo et al., 2010). The C2 domain of PLCs is composed of approximately 120 residues and is also present in many membrane-associated proteins.

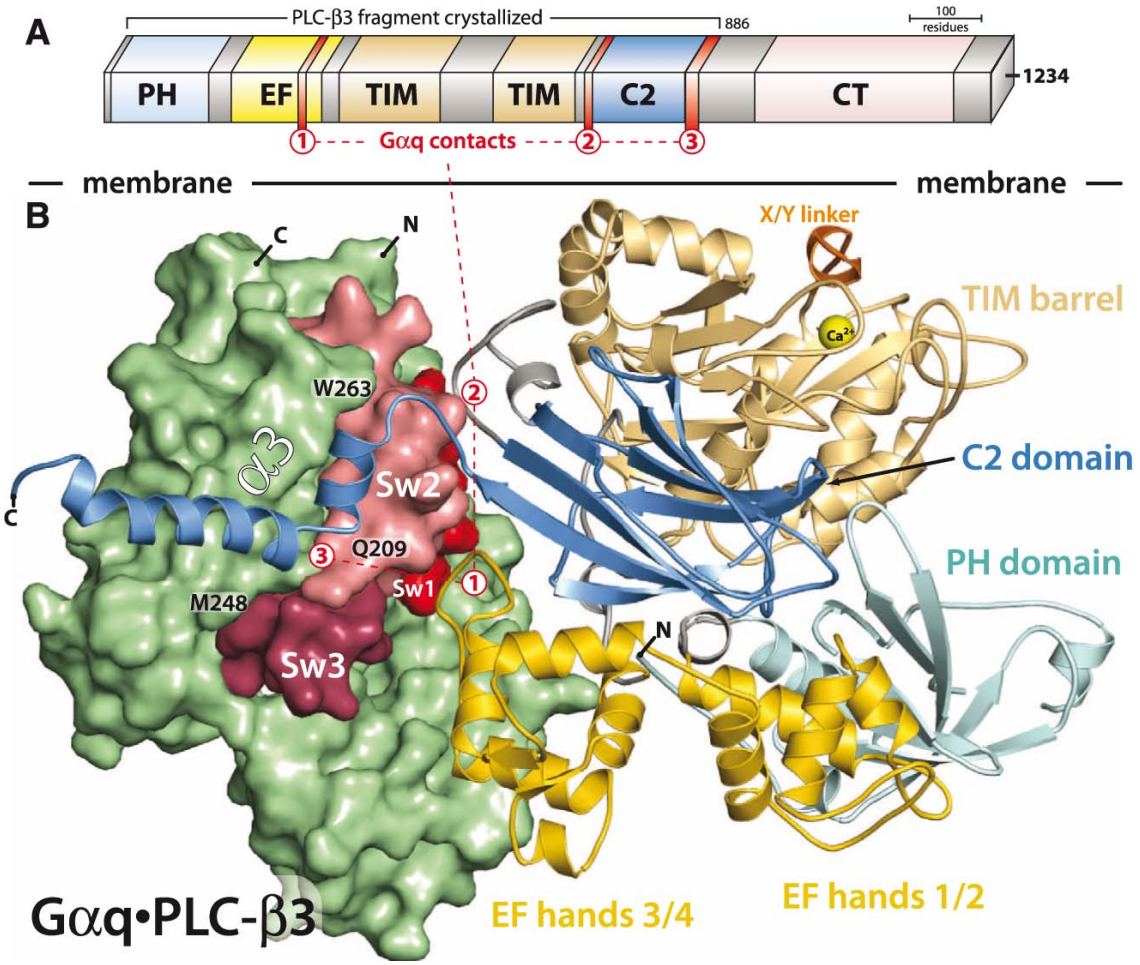

Figure 3. Structure of $G_{\alpha q}$•PLCβ3. A. Domain architecture of PLCβ3 drawn to scale and consisting of a N-terminal PH domain, a series of four EF hands, a catalytic TIM barrel, a C2 domain, and a carboxy-terminal (CT) domain. The CT domain is not necessary for $G_{\alpha q}$ binding, and, therefore, PLCβ3 truncated at residue 886 was used to facilitate crystallization. Three distinct regions of PLCβ3 that interact with $G_{\alpha q}$ are indicated by red numerals. **B.** Overall structure of the AlF_4^--dependent complex of $G_{\alpha q}$•PLCβ3 as viewed from the plane of the membrane. PLCβ3 is depicted as a ribbon cartoon with domains coloured as in (A). Activated $G_{\alpha q}$ is depicted as a green surface with nucleotide-dependent switches (Sw1 to Sw3) in shades of red. Hα1/Hα2 (red 3) at the end of the C2 domain of PLC-b3 lies within the canonical effector-binding region of $G_{\alpha q}$ formed by α3 starting at M248, the subsequent loop containing W263, and switch 2 containing Q209. The X/Y linker (orange) connects the two halves of the catalytic TIM barrel, and an ordered portion of the linker occludes the active site of the lipase highlighted by the Ca^{2+} (yellow ball) cofactor. Adapted from Waldo et al. (2010).

The C2 domain of PLCδ1 contains up to four Ca^{2+}-binding sites that modulate the Ca^{2+}-dependent membrane anchoring, thus facilitating the interaction of the enzyme with the phosphoinositides (Essen et al., 1996; Grobler and Hurley, 1998). In contrast, the C2 domain of PLCβ1 and PLCβ2 does not participate in Ca^{2+}-dependent interaction with the plasma membrane, but it associates with high affinity and specificity to activated Gαq (Gαq-GTP) subunits (Wang et al., 1999). Recently, the crystal structure of the activated Gαq-GTP/PLCβ interface has been resolved (Waldo et al., 2010),

showing the presence of two Gαq-GTP-interaction sites C2 domain flanking amino acid sequences highly conserved among the four PLCβ isoforms.

All the PLCβ isoforms, except one of the PLCβ4 splice variants, contain a long carboxy-terminal sequence downstream the Y domain of approximately 450 residues, whereas this region is very short or almost absent in PLCγ or PLCδ isozymes. This region has been shown to contain many of the determinants for interaction with Gαq as well as for other functions such as membrane binding and nuclear localization (Rebecchi and Pentyala, 2000; Rhee, 2001; Drin and Scarlata, 2007; Faenza et al., 2008; for review, Suh et al., 2008). Thus, C-terminal truncation of PLCβ2 generated enzymes that were activated by Gβγ but not by Gαq (Lee et al., 1993). Similarly, Wu et al. (1993) demonstrated that truncation of the long carboxy-terminal coil of PLCβ1 impaired Gαq. However, a recent high-resolution structural study of the interaction between the active-state Gαq and PLCβ3 revealed that the absence of the long C-terminal extension of PLCβ3 did not affect high affinity binding of PLCβ3 to Gαq (Waldo et al., 2010). In contrast, this study demonstrates that three distinct regions of PLCβ3, highly conserved among PLCβ isozymes, are involved in active-state Gαq-PLCβ interaction: [i] a loop between the third and fourth EF hands, [ii] a region of that connects the catalytic Y and the C2 domais, and [iii] a segment composed of a helix-turn-helix at the C terminus of the C2 domain. Of these three regions, the former and the later also contain critical residues for GAP activity (Fig. 3, 5). Of note, none of the three sites are located within the regions previously thought to be essential for interaction for Gαq. As discussed by these authors the C-terminal domain is important for membrane association, but whether it has additional function(s) in the signaling complex remains unclear. The model proposed by Waldo et al. (2010) considers that the carboxy-terminal domain of PLCβs basally associates with membranes, whereas the X/Y linker blocks the lipase active site. Upon activation of heterotrimeric Gq, Gαq-PLCβ complex formation anchors and orients the lipase active site at membranes, leading to repulsion of the X/Y linker and freeing the active site for PIP_2 hydrolysis (Reviewed from Waldo et al., 2010; Fig. 4). Indeed, in a recent report, the same group has demonstrated that neither Gαq nor $G\beta_1\gamma_2$ are able, by themselves, to activate PLCβ3-mediated hydrolysis of a PIP_2 analog in the absence of membranes or detergents, despite both Gαq and $G\beta_1\gamma_2$ robustly activated PIP_2 hydrolysis at membranes (Charpentier et al., 2014). Moreover, deletion of the autoinhibitory X-Y linker (Figs. 4, 5) drastically sped up PLCβ3 activation kinetics of PIP_2 in membranes, but not of the soluble analog in membrane free

preparations. Additionally, a short helix-turn-helix region downstream the C2 domain (Lyon et al., 2011; Charpentier et al., 2014; Figs. 3, 5) cooperates with the X-Y linker to prevent the productive association of PLCβ isozymes with membranes. In this way, membranes would act as a channel between Gαq and Gβγ on the one side and these autoinhibitory elements on the other side.

Apart from the different identified structural and functional domains described for the different PLC isoforms, it has been determined for PLCε the existence of an amino-terminal domain similar to the GEF protein, a nucleotide exchange factor of guanine specific for Ras, and at least one carboxy-terminal domain for Ras binding (Fig. 2), which probably would replace the function of the PH domain in the other PLC families (Kelley et al., 2001; López et al., 2001; Song et al., 2001).

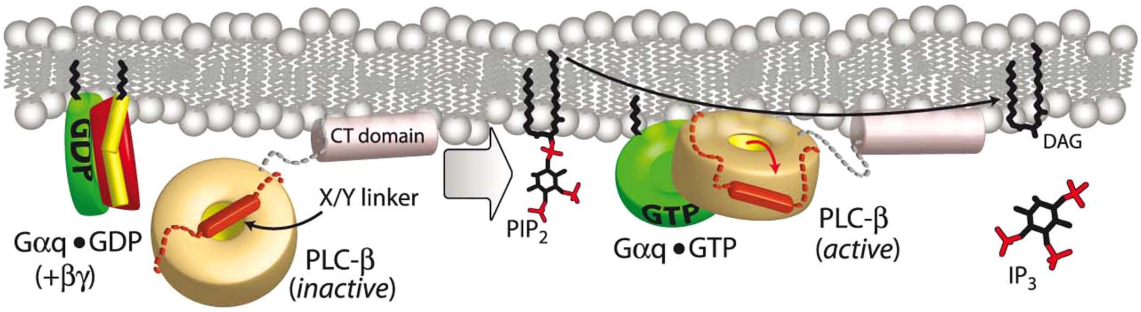

Figure 4. Model for activation of PLCβ3 by GTP-activated Gαq. Gαq (green) bound to GDP is sequestered by Gβγ (red and yellow) and does not interact with PLCβ, depicted as a gold toroid except for its CT domain (light pink) and X/Y linker (orange cylinder and dotted lines). The CT domain basally associates with membranes, whereas the X/Y linker blocks the lipase active site. Upon activation of heterotrimeric Gq, Gαq-GTP dissociates from Gβγ and interacts with the main portion of PLCβ. Complex formation anchors and orients the lipase active site at membranes, leading to repulsion of the X/Y linker and freeing the active site for hydrolysis of PIP_2 into IP_3 and DAG. Adapted from Waldo et al. (2010).

Of particular interest, PLC isozymes are subjected to alternative splicing, resulting in different expression variants. For example, this phenomenon affects the carboxy-terminal region of PLCβ1 and PLCβ4 transcripts, leading to the expression of different splice variants (Bahk et al., 1994; Kim et al., 1998). To date, three PLCδ4 splice variants have been described (ALTI, II, and III), of which ALTI and II contain additional amino acids between the X and Y domains, while ALTIII variant undergoes a change in the X domain becoming catalytically inactive. Curiously, the PH domain of this variant displays high affinity for PIP_2 and it has been proposed to negatively regulate the activity of other PLCs by competing with their PH domains for PIP_2 binding (Lee and Rhee, 1996). Indeed, overexpression of the PH domain of PLCδ4-

ALTIII was sufficient to decrease basal resting levels of IP_3, and suppress its elevation despite treatment with agonists known to stimulate IP_3 production (Nagano et al., 1999). Another PLC-related catalytically inactive protein known as p130, originally identified as an IP_3-binding protein similar to PLCδ, lacks a number of amino acids in the X catalytic domain. This catalytically inactive PLCδ-like protein inhibits Ca^{2+} mobilization from intracellular stores by sequestering IP_3. In this way, p130 counteracts PLC-IP_3 signalling (Takeuchi, 2000).

1.2. The PLCβ1 isoform

The detailed analysis of the human gene PLCβ1 gene hosted on chromosome 20 by fluorescence *in situ* hybridization (FISH) and PCR screening enabled to determine the entire structure of exons and introns (Caricasole et al., 2000; Peruzzi et al., 2000, 2002). Moreover, in rodent and human tissues (Bahk et al., 1994; Caricasole et al., 2000; Peruzzi et al., 2002), PLCβ1 exists as two alternatively splice variants, the 138 kDa PLCβ1a (1216 aa) and the 134 kDa PLCβ1b (1141 aa), derived from alternative splicing at the 3' end of the gene (Caricasole et al., 2000; Peruzzi et al., 2002). The PLCβ1b variant replaces the 75 C-terminal residue of PLCβ1a with 32 residues unique to PLCβ1b (Fig. 5). The importance of the PLCβ1 C-terminal domain may rely in two aspects. First of all, C-terminal region contains determinants for Gαq and phosphatidic acid stimulation (but not Gαq interaction, see above), electrostatic dependent association with membrane lipids, nuclear localization, and phosphorylation/regulation by protein kinase Cα and MA Pkinase (Bahk et al., 1994; Litosch, 2000; Martelli et al., 2000; Xu et al., 2001a,b; Fig. 5).

The classical role of PLCβ1 in phosphoinositide metabolism at the plasma membrane and cytoplasm in response to many extracellular stimuli is well established and, since more than two decades, it is known that this signal transduction mechanism also exists in the nucleus. In various cell types, PLCβ1 seems to be the predominant isoform in the nucleus, and its activation is independent of the plasma membrane PLCβ1. Even though PLCβ1 expression increases during cell growth and differentiation in various cell types, the activation mechanism of this isozyme has not been fully elucidated. Before a detailed description of the available experimental evidences, it must be noted that a systematic analysis of signal transduction mechanisms, enzymatic activity and protein expression in the nucleus of neural cells has not been addressed for the different PLC families and isoforms.

Martelli et al. (1992) demonstrated for the first time the presence of PLCβ1 in the nucleus of quiescent Swiss 3T3 fibroblasts, whereas PLCγ1 was exclusively cytoplasmic. In addition, this group demonstrated that PLCβ1 activity was increased by 2-3 fold in the nucleus, in response to mitogenic stimulation by insulin-like growth factor-1 (IGF-1) (Martelli et al., 1992). Thereafter, the presence of PLCβ1 in the nuclear matrix has been confirmed by various research groups in different cell lines and tissues (Divecha et al., 1993; Marmiroli et al., 1994; Fee et al., 1994; Liu et al. 1996). Of note, it has been shown that PLCβ1 is the most abundant PLC isozyme in the nucleus of several cell types (Martelli et al., 1992; Divecha et al, 1995) and, moreover, the amount of hydrolyzed PIP_2 correlates well with PLCβ1 abundance (Divecha and Irvine, 1995). Currently, a consensus exists that PLC-β1 is the major PLC isozyme in the nucleus of various cells, even though also PLCβ2, PLCβ3 and PLCβ4 have been shown to be in this organelle (Bertagnolo et al., 1997; Cocco et al., 1999)

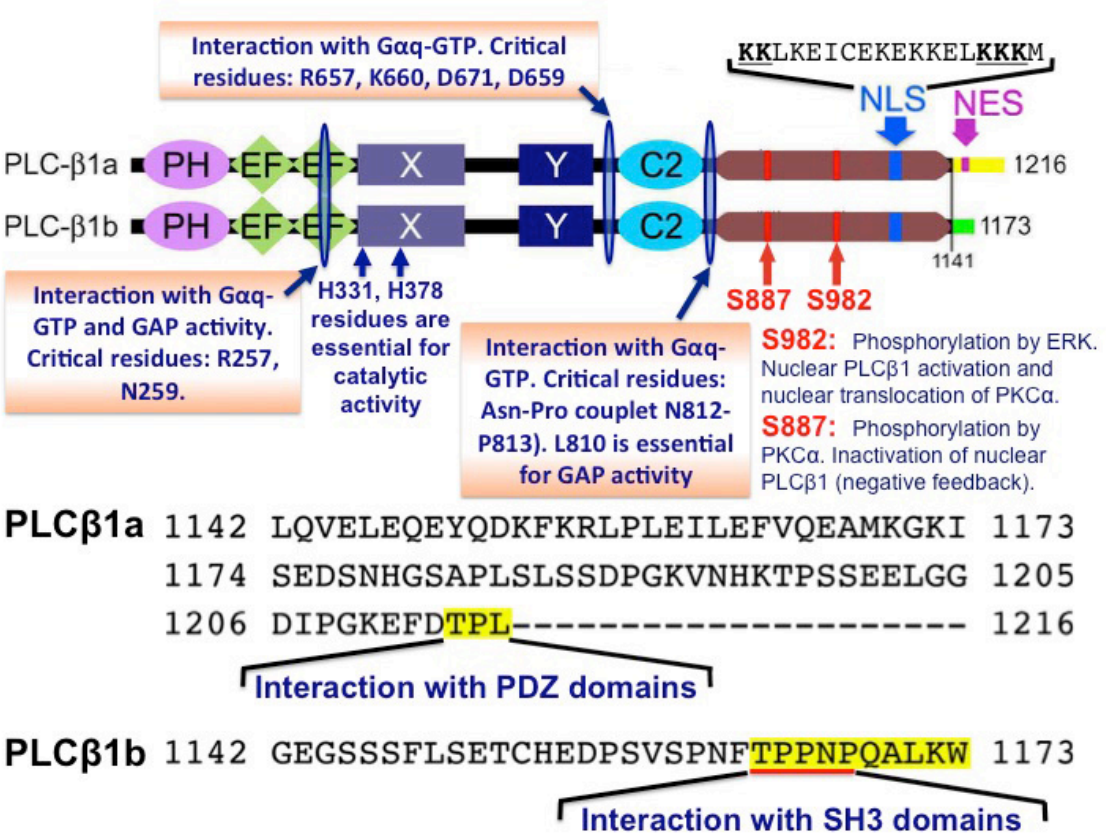

Figure 5. Schematic representation of the domains of the different domains and residues critical of PLCβ1a and PLCβ1b splice variants critical for catalytic activity, Gαq interaction, GAP activity and subcellular localization.

The molecular determinant for nuclear localization of PLCβ1 was identified as a consensus domain known as bipartite nuclear localization signal (NLS) (Kim et al., 1996). The bipartite NLS is defined as (K/R)(K/R)X10–12$(K/R)_{3/5}$, where $(K/R)_{3/5}$

represents at least three of either lysine or arginine of five consecutive amino acids, in which the linker region has been found to be tolerant to amino acid conversion (Robbins et al., 1991). Notably, substitution of the cluster of basic lysine residues 1056, 1063, and 1070 (called a mutant cDNA M2b) with isoleucine, prevents nuclear localization of PLCβ1. Nevertheless, the relative distribution of this isoenzyme between the nuclear fraction and other cellular compartments is highly variable depending on the cell type analyzed, suggesting the presence of other molecular determinants for subcellular localization of PLCβ1. For example, Martelli et al. (1992) and Marmiroli et al. (1994) found PLCβ1 to be exclusively expressed in the nucleus of osteosarcoma SaOS-2 cells and Swiss 3T3 cells, respectively, whereas Divecha et al. (1993) observed that only about 2% of the total PLCβ1 was localized in nuclei of rat liver cells. This apparent inconsistency may be due to differences between nuclear isolation methods and/or cell types. Also to the existence of PLCβ1a and PLCβ1b splice variants, which could be expressed at different relative levels in different cell types could account for the discrepancy. Indeed, although a bipartite NLS has been mapped to a cluster of basic residues common to both variants (Kim et al., 1996), PLCβ1a has in its unique carboxy-terminal tail a typical nuclear export signal (Fig. 5), which may result in this variant being less concentrated in the nucleus (Bahk et al., 1994). This could explain, at least in part, why PLCβ1a is usually equally distributed in the plasma membrane, cytoplasm and nucleus, whereas PLCβ1b is almost completely nuclear in several cell lines (C6Bu-1 glioma and Friend murine erythroleukaemia cells -MEL- cells). In this regard, at difference with the absence of nuclear PLCβ1 protein in rat liver tissue reported by Divecha et al. (1993), later studies demonstrated that PLCβ1b variant is almost exclusively nuclear in rat liver tissue (Bahk et al., 1998; Faenza et al., 2000; Crljen et al., 2004; Fiume et al., 2005), suggesting that the antibody used in the study by Divecha et al. (1993) only recognized the PLCβ1a isoform.

In the last years, a critical role for the PLCβ1b-specific C-terminal tail in targeting this variant to the sarcolemma of cardiomyocytes has been demonstrated (Grubb et al., 2008, 2011). Thus, PLCβ1b contains a proline-rich domain near the extreme carboxyl-terminus that interacts with the SH3 motifs of the scaffold protein Shank3 in cardiomyocytes, whereas the three carboxy-terminal amino acids of PLCβ1a constitute a PDZ-interacting domain. As shown by Grubb et al. (2008), the proline-rich domain of PLCβ1b is responsible for the selective targeting of this splice variant to the sarcolemma via interaction with Shank3 (Grubb et al., 2011), whereas PLCβ1a remains

cytosolic. Moreover, the integrity of a PLCβ1b-Shank3-Homer 1c protein complex is required for Gq-mediated signaling at the sarcolemma (Grubb et al., 2011, 2012). Interestingly, Shank3 belongs to a family of scaffold proteins of the postsynaptic density, where it provides multiple connections between glutamate receptor complexes and cytoskeleton (Böckers et al., 2001), such as coupling of mGluR5-Homer with PSD-95 (Tu et al., 1999). This makes plausible that the splice variant-specific carboxy-terminal tail is a key determinant of PLCβ1a and PLCβ1b subcellular localization in neurons.

In summary, although the two splice variants of PLCβ1 have identical Gαq-interacting domains and are comparably stimulated by Gαq, a myriad of evidence supports that the variant-specific extremes carboxy-termini of PLCβ1a and PLCβ1b contain molecular determinants for subcellular distribution. However, a deep analysis of the expression of PLCβ1a and PLCβ1b splice variants in nervous tissue or mammalian cell lines is still to be made.

1.3. Nuclear phosphoinositides and PLCβ1 activity

There is now abundant and solid evidence that phosphoinositides constitute a true component of the nuclear envelope and matrix. Smith and Wells (1983) carried out the first study reporting that phosphoinositide metabolism is also present in the nuclear membrane. Later, Cocco et al. (1987) demonstrated for the first time that envelope-depleted nuclei from MEL cells were able to synthesize PIP and PIP_2 *in vitro*, showing that the phosphoinositide metabolism also exists within internal nuclear domains (see also, Payrastre et al., 1992; Garcia-Bustos et al., 1994). Moreover, about 50% of nuclear PIP_2 remains in envelope-depleted nuclei, along with more than 80% of the enzymes involved in phosphoinositide metabolism, such as DAG kinase and PtdIns(4)P-5-kinase and PtdIns(5)P-4-kinase activities. During the last two decades, much experimental data about the involvement of phosphoinositide cycle in a variety of cellular responses, such as, differentiation, proliferation, neoplasic transformation and DNA repair have been accumulated (Neri et al., 1999; D'Santos et al., 2000). Kuriki et al. (1992), using a rat model of hepatocyte regeneration, detected increased levels of PLC activity and inositol phosphate accumulation in isolated nuclei 20-22 h after partial hepatectomy. The identification of sequences which are essential for nuclear localization and the possibility to express mutated recombinant proteins that have lost their capacity to localize in the nucleus have unequivocally demonstrated intranuclear localization of

phosphoinositide metabolism-related enzymes, such as type II PtdIns(5)P-4-kinase PIPKIIβ, diacylglycerol kinase-zeta (DGKζ), and PLCβ1 (Topham et al., 1998; Ciruela et al., 2000; Faenza et al., 2003).

1.3.1. Nuclear speckles as nuclear subdomains for phosphoinositide signaling

The experimental data showing that both polyphosphoinositides and their metabolizing enzymes are localized within internal nuclear domains arose the question of which would be their precise distribution. Data accumulated in recent years, identify "nuclear speckles" (Fig. 6) as major candidates (For review, Cocco et al., 2006; Schramp et al., 2012). Several approaches, combining subcellular fractionation techniques, western blot analysis and colocalization with pre-mRNA probes (Osborne et al., 2001) concluded that these domains organize in "clusters" formed by chromatin granules, which would be wrapped by newly transcribed mRNA. It is thought that these regions are nuclear storage sites of transcription factors, small nuclear ribonucleoproteins (snRNPs) and hyperphosphorylated forms of RNA polymerase II (Mortillaro et al., 1996; Spector et al., 1991, 1993; Lamond and Spector, 2003). The presence of many enzymes involved in the phosphoinositide cycle such as kinases necessary for the synthesis of PIP_2, various PLC isoforms, and DGKs has been demonstrated in these domains. Therefore, "nuclear speckles" emerge as important subnuclear domains for the phosphoinositide signaling, strengthening the idea of the role of nuclear phosphoinositides in mRNA processing.

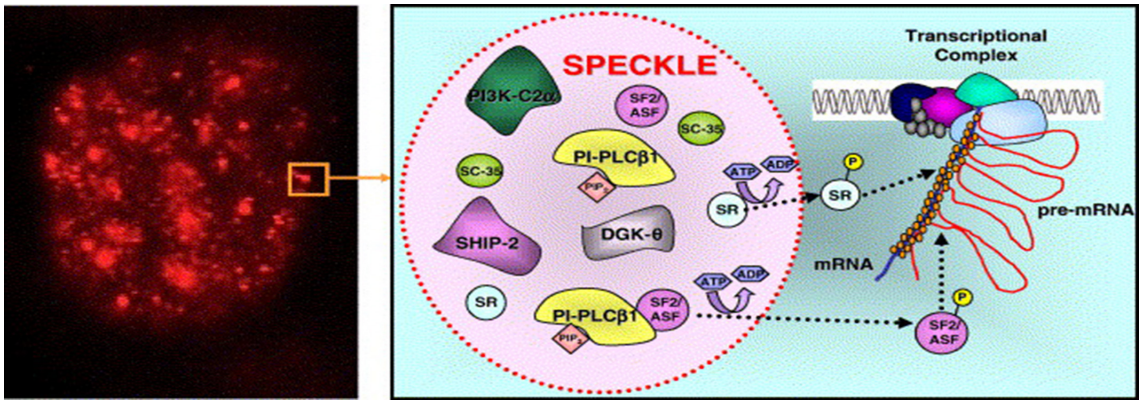

Figure 6. Schematic diagram illustrating the nuclear localization of the most representative elements of the PtdIns nuclear cycle. The picture on the left shows the "nuclear speckles" within the core using a specific marker. On the right, the elements forming the "speckles" and known relationships with transcription factors are observed. Modified from L. Cocco et al. (2006).

1.3.2. Role and synthesis of PIP_2 in nuclear speckles

The nuclear phosphoinositide cycle can be distinguished from that present at the plasma membrane at different levels. For instance, several agonists exclusively stimulate the membrane or nuclear cycles, whereas others stimulate both but with different kinetics (Martelli et al., 1999; Cocco et al., 2001; Irvine, 2003; Cocco et al., 2009), and the regulation mechanisms of nuclear phosphoinositide metabolism differs from that operating at the plasma membrane. Nuclear phospholipid signaling requires an array of coordinated of lipid kinases, phosphatases, and effectors. Of these elements, phosphatidylinositol phosphate kinases (PIPKs) tightly regulate the spatial and temporal generation of PIP_2. Using laser scanning confocal microscopy and immunofluorescence staining, intranuclear phosphoinositides (PIP, PIP_2, and PtdIns 3,4-P_2), and type I (also known as PIPKI or PIP5K) and type II PIP (known as PIPKII PIP4K) kinases have been identified (Boronenkov et al., 1998). Specifically type I kinases PIPKIα and PIPKIβ and type II, PIPKIIα and PIPKIIβ were identified at nuclear speckles (Boronenkov et al., 1998). Although the amount of PtdIns 4-P (the substrate of type I PIP kinases) is about 20-fold higher than that of PtdIns 5-P (the substrate of type II PIP kinases) in the nucleus, the relative generation of PtdIns 4,5-P_2 at the 5 *vs*. 4 OH position has been shown to be only ~1.8, suggesting that both substrates and enzyme types are relevant for PIP_2 synthesis (Vann et al., 1997; Keune et al., 2011). However, using an elegant biochemical approach to discard that radiolabeling of the 4-position is due to new synthesis of PtdIns 4-P by PI phosphorylation rather than to the synthesis of PtdIns 4,5-P_2 (PIP_2) from PtdIns 5-P_2 by type I PIP kinases, Vann et al. (1997) showed that at least 90% of nuclear PIP2 is derived from type I PIP kinases, suggesting a role for type II PIP kinases in regulating PtdIns 5-P levels rather than in generating PIP_2. Coming back to type I PIP kinases, it has been demonstrated that the carboxy-terminus of PIPKIα interacts with Star-PAP (nuclear speckle targeted PIPKIα regulated-poly(A) polymerase), a novel nuclear poly(A) polymerase that couples with the transcriptional machinery. In response to oxidative stress, PIPKIα-generated PIP_2 specifically modulates Star-PAP at the 3'-end of pre-mRNAs to control the expression of select group of genes, including the ones involved in stress responses (For review, Li et al., 2013). However, the upstream regulators of nuclear speckle-associated PIPKIα has not yet been identified. One proposed major candidate is the tumor suppressor retinoblastoma protein RB (pRB), which interacts with and stimulates PIPKIα in the

nucleus but not the plasma membrane (Divecha et al., 2002), indicating a role for pRB in regulating the levels of nuclear PIP_2. It has been suggested that transcriptional regulators and/or chromatin remodelling complexes may interact with and recruit type I PIP kinases to control local synthesis of PIP_2 (Jones and Divecha, 2004).

Although nuclear phosphoinositides are known to change in response to external stimuli, how these changes are transduced is poorly understood. Early studies using purified nuclei showed that exogenous phospholipids could affect transcription and replication of DNA *in vitro* (Capitani et al., 1986), with negatively charged lipids leading to chromatin decondensation, whereas positively charged ones have the opposite effect (Kuvichkin, 2002). Interestingly, binding of PIP_2 to the carboxy-terminal tail of histones H1 and H3 reverses histone H1-mediated inhibition of basal RNA transcription (Yu et al., 1998). Additionally, PIP_2 has been shown to regulate the chromatin structure of T cells by interaction with the chromatin-remodelling complex BAF (Zhao et al., 1998). Thus, exogenously added PIP_2 leads to translocation of BAF complex from a nuclear soluble fraction to an insoluble fraction, mimicking the effects of T-cell stimulation with anti-T-cell receptor/CD3 complex antibodies or with phorbol 12-myristate 13-acetate (PMA)/ionomycin. Although there is no experimental evidence showing that nuclear PIP_2 levels are increased upon T-cell activation, the data are consistent with a role for PIP_2 in regulating BAF complex localization. One central component of the BAF chromatin-remodeling complex is BRG-1, an ATPase subunit homologous to the yeast SWI/SNF2 protein, a member of the DEAD/H superfamily of DNA and RNA helicases (Eisen et al., 1995) that are critical for remodeling activities such as nucleosomal assembly, sliding and positioning. Among components of mammalian chromatin-remodeling complexes there are actin or actin-related proteins, which modulate remodeling activity both *in vitro* and *in vivo* (Shen et al., 2003). BRG-1 has two domains that can interact with actin, one of which contains a lysine-rich patch that can interact also with PIP_2. It has been suggested that PIP_2 disrupts actin-BRG-1 interaction, thus allowing binding of actin to nuclear matrix components (Rando et al., 2002), a phenomenon analogous to PIP_2-mediated uncapping of actin, which stimulates actin polymerisation (Yin and Janmey, 2003). Additionally, upon transcriptional activation, BRG-1 is the first component of the BAF complex recruited to the active promoter (Memedula and Belmont, 2003). It has been proposed that locally synthesized or H1/H3-bound PIP_2 may allosterically stimulate BRG-1 to interact and recruit other

components of the BAF complex and/or increase its interaction with the nuclear matrix leading to its stabilization at the promoter (Jones and Divecha, 2004).

Apart from its specific roles, intranuclear PIP_2 is the source of downstream second messengers including PtdIns 3,4,5-P3 (PIP_3), which can be generated from PIP_2 by class I and class II PI3Ks. These enzymes have been found in nucleus, with class IA PI3Ks being the major responsible for synthesis of nuclear PIP_3 (D'Santos et al. 1998; Gonzales and Anderson, 2006). Additionally, the presence of nuclear PTEN and SHIP-2 phosphatases acting on PIP_3 has been reported. PTEN and SHIP-2 preferentially dephosphorylate the 3- and 4-positions of PIP_3, thus generating two different di-phoinositide species, PtdIns 4,5-P_2 and PtdIns 3,4-P_2 (Cocco et al., 2006). Therefore, PI3Ks and PTEN activities likely impact on PLC-hydrolysable PIP_2 levels, whereas PtdIns 3,4-P_2 generated by SHIP-1 might constitute an additional second messenger with proper functions, as it could be the case for PIP_3.

Despite the wealth of knowledge accumulated during the last years about nuclear PI3K activity, the important physiological roles assigned to it and the potential physiological relevance of the products of PI3K-mediated PIP_2 hydrolysis, of more importance to the present work are the role of nuclear PLCβ1 and its catalytic activity in nuclear signaling cascades.

1.3.3. Regulation of nuclear PLCβ1 enzyme activity

The above-mentioned experimental data reveal a key role of PIP_2 in regulating chromatin remodeling and transcription. Being the most abundant PLC isozyme in the nucleus (Martelli et al., 1992; Divecha et al., 1995), PLCβ1 emerges as a major player in regulating PIP_2 levels and, consequently, nuclear PIP_2-mediated signaling. Moreover, DAG and IP_3, generated by the hydrolysis of PIP_2 by PLCβ1, are known regulators of gene transcription, DNA synthesis, stress response, mitosis and cell cycle progression (D'Santos et al., 1998), as it will be described below.

One interesting question regarding activation of nuclear PLCβ1 isoform is whether the mechanisms described in the plasma membrane also take place in the nucleus. Activation of PLCβs by G-protein coupled receptors at the plasma membrane and the participation of α subunits (αq, α11, α14, and α16) belonging to the Gq family and βγ dimers belonging to other families of G proteins is well known (Rhee and Bae, 1997). By contrast, there are few studies reporting the existence of such signal transduction mechanism for nuclear PLCβs. Of the few ones dealing with this topic, two reports by

O'Malley and colleagues stand out. Thus, O'Malley et al. (2003) demonstrated that the metabotropic glutamate receptor mGluR5 is localized in nuclear membranes of mGlurR5-overexpressing HEK cells, and of midbrain and cortical neurons. Moreover, nuclei isolated from mGluR5-expressing HEK cells and brain neurons responded to the addition of glutamate, but not carbachol, with Ca^{2+} oscillatory responses that were blocked by the mGluR5-selective antagonist 2-methyl-6-(phenylethynyl)-pyridine (MPEP) or EGTA. Five years later, the same group (Kumar et al., 2008) demonstrated that these responses were dependent on PtdIns-PLC activity. Thus, nuclear Ca^{2+} oscillations elicited by mGluR activation were abrogated in nuclei pretreated with either the general PLC inhibitor U73122 or the PtdIns-PLC inhibitor 1-O-octadecyl-2-O-methyl-sn-glycero-3-phosphorylcholine (ET-18-OCH3). Of note, Ca^{2+} oscillations were also abrogated in nuclei isolated from cells transfected with small interfering RNA (siRNA) targeted to PLCβ1 mRNA. Because blockade of ryanodine and IP_3 receptors prevented Ca^{2+} oscillations, it was concluded that the second messenger IP_3 generated by hydrolysis of PIP_2 by PLCβ1 mediated this response. Indeed, Kumar et al. (2008) elegantly demonstrated that IP_3 is generated in the nucleus following activation of nuclear mGluR5 receptors. To this end, HEK cells were transfected with a PIP_2/IP_3 "biosensor", consisting of a construct containing the PH domain of PLCδ1 fused to enhanced green fluorescent protein (pEGFP-C1-PLCδ1-PH). Because the PH domain of PLCδ1 binds with 20-fold higher affinity to IP_3 than to PIP_2, it could be possible to demonstrate translocation IP_3 from the nuclear envelope to the nucleoplasm upon glutamate treatment. Collectively, these results showed that nuclear PLCβ1 can be activated in a similar way to membrane PLCβ1 but independently from signal transduction mechanisms linked to plasma membrane receptors.

However, within the nucleus, the above-mentioned metabotropic receptor-mediated signal transduction mechanisms is circumscribed to the nuclear envelope, whereas most studies have described the bulk of nuclear PLCβ1 protein to be localized in discrete foci within the nuclear matrix (Avazeri et al., 2000; Tabellini et al., 2003; Martelli et al., 2005; Bavelloni et al., 2006; Miyara et al., 2008; Fiume et al., 2009). Currently, a consensus exists that activation of intranuclear PLCβ1 is dependent on mitogen-activated protein kinases (MAPKs). Early studies demonstrated the existence of a polyphosphoinositide cycle under the control of IGF-1 in nuclei isolated from Swiss 3T3 cells (Divecha et al., 1991), and showed that IGF-1 stimulation promoted nuclear DAG synthesis and translocation of protein kinase C-α (PKCα) to the nucleus (Neri et

al., 1998). One year later, Martelli et al. (1999) reported that impairment of extracellular signal-regulated kinase (ERK) translocation to the nucleus by pretreatment of Swiss 3T3 cells with the microtubule-depolymerizing compound colchicine prevented activation of nuclear PLCβ1 by IGF-1. Thereafter, Xu et al. (2001a) demonstrated ERK-PLCβ1 interaction and mapped the ERK phosphorylation target on PLCβ1 at serine 982 (Fig. 7). This residue is located within a Pro-Ser-Ser-Pro motif, common to PLCβ1a and

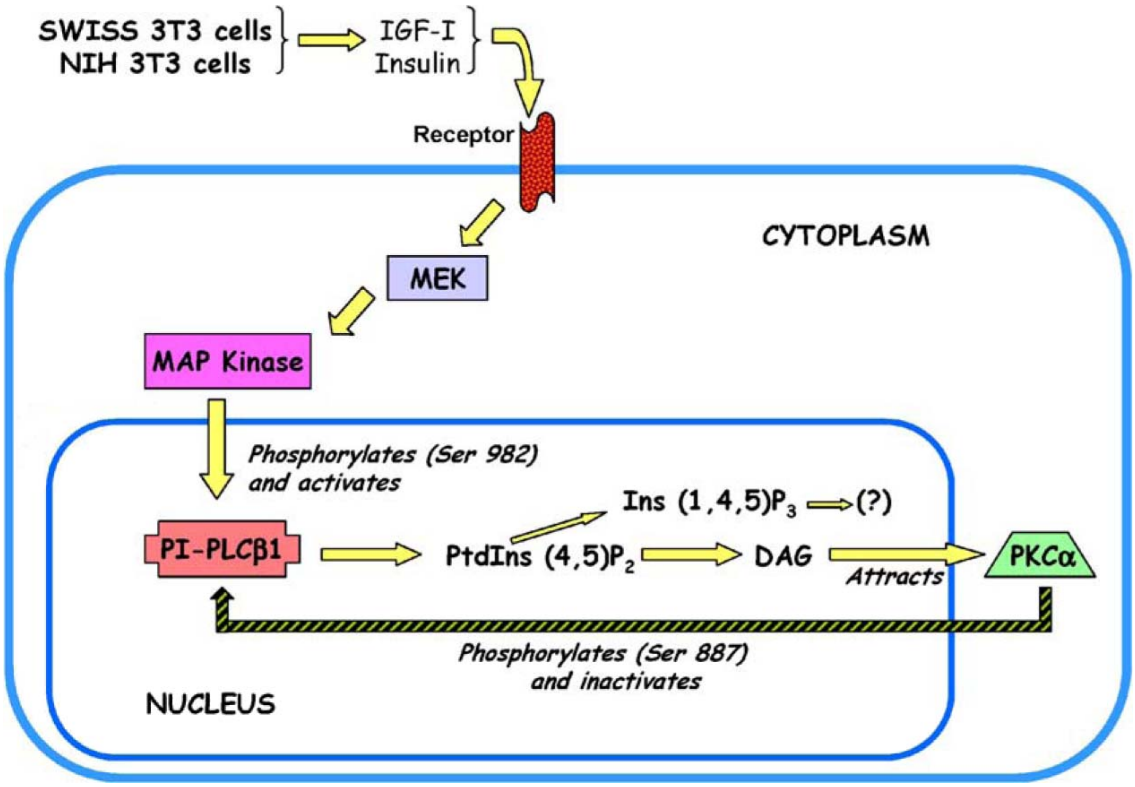

Figure 7. Schematic diagram depicts regulation mechanisms of PLCβ1 enzymatic activity in the nucleus of IGF-1-stimulated mouse fibroblasts. Activation and termination of PLCβ1 activation depends on phosphorylation at serine residues 982 and 887, respectively. Illustration from Cocco et al. (2006).

PLCβ1b splice variants (Fig. 5). Further evidence of the key role of serine 982 came from the analysis of the effect of glycine substitution of this residue (S982G). In fact, overexpression of the PLCβ1-S982G mutant prevented initiation of the phosphoinositide cycle and DAG production stimulated by IGF-1 (Xu et al., 2001a). The same group demonstrated that DAG production by transient activation of nuclear PLCβ1 results in nuclear translocation of PKCα, leading to phosphorylation of Serine 887 (Xu et al., 2001b; Figs. 5,7). Moreover, alanine substitution of this residue (S887A) and negative dominants of PKCα leads to a sustained activation of nuclear PLC activity following IGF-1 stimulation (Xu et al., 2001b). Their results, showing that DAG production drives nuclear translocation of PKCα for termination of the IGF-1-dependent

PLCβ1 activation, are the first evidence of a specific role for downstream PLCβ1 second messengers in the nucleus. These mutants have proved to be invaluable tools in the elucidation of the role of nuclear PLCβ1 in cell cycle control and differentiation (see next sections).

1.4. Role of PLCβ1 enzyme activity in cell physiology

Early studies aimed at determining the role of nuclear phosphoinositide metabolism in proliferative responses provided some insight into the importance that phosphoinositide hydrolysis might have in cell cycle control. York and Majerus (1994) monitored the levels of PI, PIP and PIP_2 during the cell cycle of HeLa cells after release from block at G1/S boundary by thymidine/aphidicolin. Nuclear levels of PI, PIP and PIP_2 decreased by about 50-70% during S phase, with plasmatic phosphoinositide levels remaining unchanged. Also, nuclear levels of phosphoinositides inversely correlated with nuclear PLC activity and DNA synthesis in response to growth factors and cell differentiation. Cocco et al. (1987), found very low levels of PIP_2 levels in envelope depleted nuclei isolated from growing MEL cells, whereas nuclei cells induced to differentiate with dimethyl sulphoxide (DMSO) displayed high levels in nuclear concentrations of phosphoinositides in parallel with the cessation of DNA synthesis. The fact that no differences were observed between growing and differentiating MEL in the amount of kinases responsible for PIP and PIP_2 synthesis suggested that phosphoinositide-hydrolizing activity accounted for cell cycle-dependent changes in phosphoinositide mass.

1.4.1. Role of PLCβ1 in the control of cell proliferation and cell differentiation

The first studies assigning a role to PLCβ1 in proliferation and differentiation were published in the mid 90s of last century. In cultured MEL cells, Divecha et al. (1995) showed that PLC activity, DAG production and PLCβ1 expression correlate directly positively with cell proliferation and negatively with cell differentiation. DMSO-induced differentiation of MEL cells is paralleled with a corresponding decrease in PLCβ1 expression, whereas transfection of cells with wild-type PLCβ1 attenuates DMSO-induced differentiation (Matteucci et al., 1998). In contrast, transfection with a construct encoding for PLCβ1 lacking the bipartite NLS had no effect, showing that nuclear but not cytoplasmic PLCβ1 is responsible for the maintenance of the undifferentiated state of MEL cells. Some observations suggest that PLCβ1 is also

involved in DNA replication during rat liver regeneration. After partial hepatectomy, nuclear PLC activity increases transiently in the S phase (Kuriki et al., 1992). A later study (Albi et al., 2003) demonstrated that increased activity of nuclear PLC in regenerating rat liver occurs before the peak of DNA replication and involves the enzyme activity associated to the chromatin but not to the nuclear membrane. Furthermore, Albi et al. (2003) reported that PLCβ1 co-localizes at DNA replication sites much more than PLCγ, which was also detected at the nuclear envelope. These authors suggested that increased activity of PLCβ1 could trigger DNA replication, PLCγ be involved in G2/M phase transition through lamin phosphorylation.

One piece of evidence that implicates PLCβ1 in the control of cell proliferation comes from two studies in two isolated Swiss 3T3 cell clones. Both clones express IGF-1 receptor that binds IGF-1 peptide but only one of them is mitogenically-responsive and shows a very high rate of DNA synthesis under IGF-1 stimulation. Indeed, nuclei isolated from responsive cells showed a marked decrease in PIP and PIP_2 levels upon IGF-1 stimulation, whereas irresponsive cells did not (Martelli et al., 1991). Additionally, PKC was seen to be activated only in responsive cells, suggesting a direct link between polyphosphoinositide metabolism, PKC activation and early events leading to cell division. The same authors pointed to PLCβ1 as the nuclear enzyme responsible for hydrolysis of phosphoinositides in response to IGF-1 (Martelli et al., 1992). A later report from the same group, using antisense RNA and overexpression based approaches, showed that PLCβ1 isoform is required in these cells for initiation of DNA synthesis in in response to IGF-1 (Manzoli et al., 1997). Using an inducible construct in which recombinant PLCβ1 transcription was under the control of the Lac repressor, Billi et al. (1997) were able to analyze the subcellular localization and partitioning of PLCβ1 after IGF-1 stimulation of 3T3 cells, showing that PLCβ1 levels increased in the nucleus in coincidence with DNA synthesis during the S phase of the cell cycle.

Several studies carried out by the group of Lefevre and colleagues have highlighted the importance of nuclear PLCβ1 activity in the control of mouse oocyte meiosis (Avazeri et al., 2000, 2003). In mammals, oogonia proliferate mitotically in ovaries during fetal life and then become primary oocytes that enter the meiotic cell cycle before they arrest at prophase I until puberty. At this time a few oocytes enter a growth phase (folliculogenesis), with the rest remaining quiescent. During folliculogenesis oocytes remain arrested in prophase I but enlarge about 100-fold and display a large

nucleus known as germinal vesicle (GV). Acquisition of meiotic competence by oocytes requires germinal vesicle breakdown (GVBD) before successful fertilization can take place. This process is preceded by Ca^{2+} oscillations in the region close to the nucleus. PLCβ1 is translocated to the GV within the hour preceding GVBD (Avazeri et al., 2000), this process is Ca^{2+} dependent as the Ca^{2+} chelator BAPTA prevents translocation (Avazeri et al., 2003). More recently, Igarashi et al. (2007) have shown that the amplitude of Ca^{2+} oscillations that follow PLCζ-dependent initial transient elevation of intracellular Ca^{2+} at early stages of mammalian egg fertilization (Saunders et al., 2002) is PLCβ1-dependent. Taken together these results show that PLCβ1 plays a key role in oocyte maturation in egg activation, in concert with sperm-derived PLCζ.

As described in the previous section, there is evidence that mitogens such as IGF-1 are able to activate PLCβ1 via MAPK/ERK pathway. Translocation of ERK to the nucleus phosphorylates PLCβ1 at serine 982 leading to increased catalytic activity and production of nuclear DAG, which in turn recruits PKCα to the nucleus for termination of mitogen-activation of PLCβ1 via phosphorylation at residue serine 887 (Xu et al., 2001a,b; Lukinovic-Skudar et al., 2005). Several lines of evidence have demonstrated that catalytic activity, phopsphorylation at serine 982 and nuclear localization of PLCβ1 are necessary for cell differentiation. However, the cellular responses demonstrated to be PLCβ1-dependent are distant from the initiation point of the signaling cascade, and intermediate molecular events are far from being totally understood. Among data linking PLCβ1 activity and cell cycle control, considerable experimental evidence has been accumulated on the involvement of PLCβ1 in the regulation of cyclins and cyclin-dependent kinases (cdks) and cell cycle progression. In this regard, Faenza et al. (2000) demonstrated that MEL cells transfected with either PLCβ1a or PLCβ1b splice variants overexpressed cyclin D3 and its kinase (cdk4) even though cells were serum-starved (which induces arrest in the G0/G1 phase). As a result of PLCβ1 overexpression, these authors observed that a significant increase of pRb phosphorylation on serines 795, 780, and 807/811 and activation of the E2F1 transcription factor. It is known that phosphorylation of pRb by cyclin/CDK complexes releases E2F1 to enable transcription of genes necessary for G1/S and cell cycle progression (Mittnacht, 1998) (Fig. 8). Of note, these effects were not observed when cells were transfected with the M2b mutant that prevents nuclear localization of PLCβ1 (PLCβ1M2b). In conclusion, nuclear PLCβ1-dependent signaling triggers cyclin D3/cdk4 activation and cell cycle progression.

In contrast with results reported in MEL cells, PLCβ1 expression increases during withdrawal of C2C12 myoblasts from the cell cycle, leading to differentiation into multinucleated myotubes (Faenza et al., 2003). By combining microarray mRNA, phenotypic analysis and siRNA, the same group demonstrated that overexpression of PLCβ1 but not PLCβ1M2b in MEL cells results in upregulation of the CD24 antigen, which is involved in differentiation and hematopoiesis (Fiume et al., 2005). Moreover, overexpression of the PLCβ1M2b mutant prevented formation of mature multinucleated myotube, strongly suggesting that PLCβ1 plays a key role in myoblast differentiation.

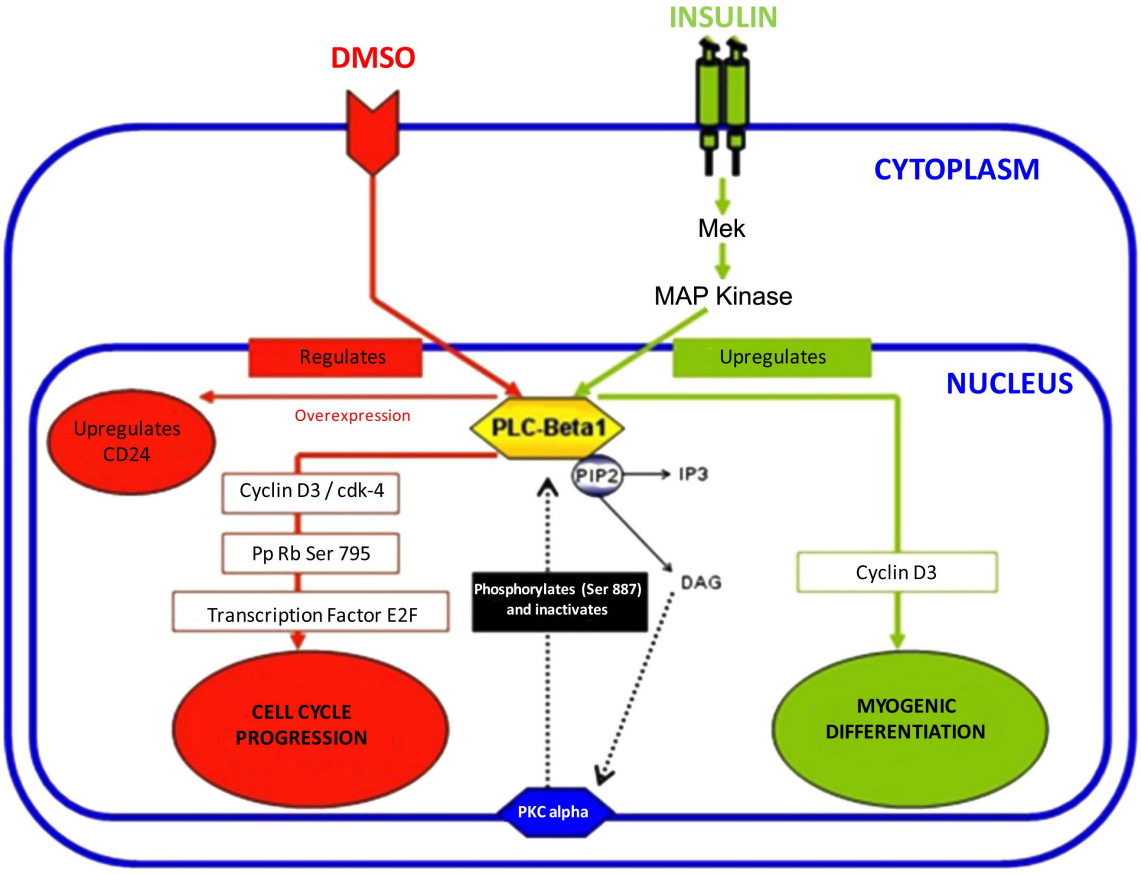

Figure 8. Schematic diagram showing the role PLCβ1 in cell cycle progression and differentiation.

More recently, a role for PLCβ1 in concert with PLCγ1 in the activation of the cyclin D3 promoter has been demonstrated during differentiation of C2C12 myoblasts (Faenza et al., 2007). The question of whether not only nuclear localization of PLCβ1 but also its catalytic activity is necessary for activation of the cyclin D3/cdk4 pathway and differentiation of C2C12 myoblasts was resolved by Ramazzotti et al. (2008) using a catalytically inactive PLCβ1 by mutation of histidines 331 and 378 located at the X domain (Fig. 5). Thus, overexpression of the catalytically inactive PLCβ1 results in lower levels of cyclin D3 mRNA after insulin treatment. Additionally, this study

provided interesting data, showing that PLCβ1 signaling activity results in upregulation of c-jun (a member of AP-1 transcription complex) and its binding to the cyclin D3 promoter during myoblast differentiation.

Studies in the adipocyte differentiation model of 3T3-L1 fibroblasts have provided further evidence of the role of nuclear PLCβ1 and its catalytic activity in cell differentiation (O'Carroll et al., 2009). Similar to that observed in C2C12 myoblasts, PLCβ1 activity is upregulated in two phases during differentiation. The first one takes place within 5 min after induction of differentiation, is regulated by pERK and PKCα, and is not dependent on nuclear translocation of PLCβ1. The second one begins after 48 h, is independent of pERK and PKCα, and requires both upregulation and nuclear translocation of PLCβ1 protein. Overexpression of PLCβ1M2b and PLCβ1-S982G, which impair nuclear translocation and phosphorylation by ERK, respectively (see section 1.2.3. and Fig. 5) revealed that both phases of PLCβ1 activity are required for 3T3-L1 fibroblasts to differentiate into adipocytes (O'Carroll et al., 2009).

Collectively, these data highlight the key role of nuclear PLCβ1 and its catalytic activity in cell cycle control and differentiation.

1.4.2. Role of PLCβ1 in neuronal differentiation

PLCβ1 is strongly regulated during development of human cortex, being almost absent in fetal cerebral cortex and highly expressed in adults, as demonstrated at both gene transcript and protein levels (Caricasole et al., 2000; Peruzzi et al., 2002; Ruiz de Azua et al., 2006; Montaña et al., 2012). Moreover, functional activity difference increases drastically postnatally as demonstrated by measurement of IP_3 production after stimulation of membranes with guanosine-5'-o-3 thiotriphosphate (GTPγS) or carbachol (in the presence of GTPγS). The involvement of PLCβ1, activated by the type I metabotropic receptor mGluR5, in cerebral cortex development has been analyzed in Plcb1- and mGluR5-knockout mice (Hannan et al., 2001; Böhm et al., 2002; Spires et al., 2005). The fact that both $Plcb1^{-/-}$ and $mGluR5^{-/-}$ mice exhibit alterations in the formation of the so-called "barrels" of the somatosensory cortex emphasizes the importance of this signal transduction for correct cortical development. It has been suggested that morphological reorganization of cortical neurons to form "barrels" depends on the transmitted signals during a critical period of postnatal development (Fox et al., 1996; O'Leary et al., 1994). Therefore, the primary somatosensory cortex of rodents provides an excellent model for the study of activity-dependent cortical

development. In this context, Spires et al. (2005) analyzed the neuronal ultrastructure, synapse formation and morphology of dendritic spines in "barrels" of Plcb1$^{-/-}$ mice. This study revealed a decrease in the proportion of symmetrical synapses in the postnatal day 5 and their disappearance on day 19, suggesting a transient imbalance in excitatory and inhibitory circuits (Spires et al., 2005). These observations indicate that PLCβ1 signaling pathway play a key role in the coordinated development of the cerebral cortex. In line with this idea, Plcb1-/- mice generated by Kim et al. (1997) died suddenly at early postnatal stages and death was preceded by status epilepticus or recurrent seizures characterized by tonic–clonic or tonic extension of the whole body. These seizures were similar to those induced by the GABAA-receptor antagonist pentamethylenetetrazole (metrazol), Also, Plcb1$^{-/-}$ mice have been shown to develop aberrant mossy fiber projections and hippocampal degeneration, which correlates with spontaneous seizures during early postnatal development (Böhm et al., 2002). Moreover, the murine model recapitulates the human phenotype described by Kurian et al. (2010), which described that an homozygous deletion, involving the promoter element and exons 1, 2 and 3 of human PLCB1 gene led to tonic seizures in early infancy, subsequently infantile spasms and death. Other Plcb1-/- mice display schizophrenia-related behaviors but a less severe phenotype with no spontaneous seizures (Koh et al., 2008; McOmish et al., 2008a,b; Koh, 2013). Interestingly, deficits of PLCβ1 expression in prefrontal cortex (Udawela et al., 2011) or deletion in the PLCB1 gene (LoVasco et al., 2012) have been observed in human schizophrenic patients. Also, missense mutations in the SH3 domain of the human SHANK3 gene (an interaction site for PLCβ1b, see section 1.1.4. and Fig. 5), lead to a schizoaffective phenotype and epileptic seizures (Gauthier et al., 2010).

The above described evidences in animal models and humans point to a role of PLCβ1 in postnatal development of cortical neurons. The fact that functional and morphological deficits appear during postnatal life and mutations of the scaffold protein of the postsynaptic density Shank3 mimic PLCβ1 deficits suggests that PLCβ1 signaling, rather than necessary for neuronal differentiation of cortical neurons, is required for synaptic activity-dependent neuronal maturation. This assumption would imply that membrane but not nuclear PLCβ1 is involved in maturation of cortical neurons. However, it must be noted that all isoforms of the PLCβ family are expressed in brain cortex (Ruiz de Azúa et al., 2006), contain a nuclear localization signal (Rebecchi and Pentylana, 2000) and are expressed in neuronal nuclei (García del Caño et al., 2015). Consequently, redundant PLCβs could compensate for the loss of PLCβ1

during early neuronal differentiation. Therefore, cell models are necessary to ascertain whether PLCβ1 is required for differentiation of neurons as it has been observed for several cell types. In this regard, the pluripotent NTERA2/D1 (NT2) cell line, which can be induced to differentiate *in vitro* into postmitotic NT2N neurons (Andrews, 1984), represents a valuable model to study molecular mechanisms underlying neuronal differentiation, including the role of PLCβ1 enzyme. Interestingly, it has been shown that differentiation of NT2 progenitors into NT2N mature neurons is associated with increased expression levels of the Gαq/11, PLCβ1 isoform and PLC activity (Novak et al., 2000). These data on the expression of elements leading to PLCβ1-induced signaling during NT2 cell differentiation are still very scarce, but provide an encouraging start point to address one the major issues in the present study.

1.5. Translin-Associated Factor X: a novel binding partner of PLCβ1 involved in RNA silencing

Recently, using the carboxy-terminal coil of PLCβ1 as bait in a yeast two-hybrid approach, Aisiku et al. (2010) have identified the protein translin-associated factor X (TRAX) a new binding partner of PLCβ1. TRAX is a 33 kDa protein that forms a DNA and RNA binding complex with translin (26 kDa), the only known binding partner of TRAX before the discovery of TRAX-PLCβ1 association (Jaendling and McFarlane, 2010). Translin is a single-stranded DNA and RNA-binding protein with proposed functions in chromosomal translocations in lymphoid cells and mRNA transport and storage in brain and testis (Wang et al., 2004), and both TRAX and translin have been found to be essential for normal cell proliferation (Hecht et al., 2004; Wang et al., 2004; Yang et al., 2004; Jaendling, 2010).

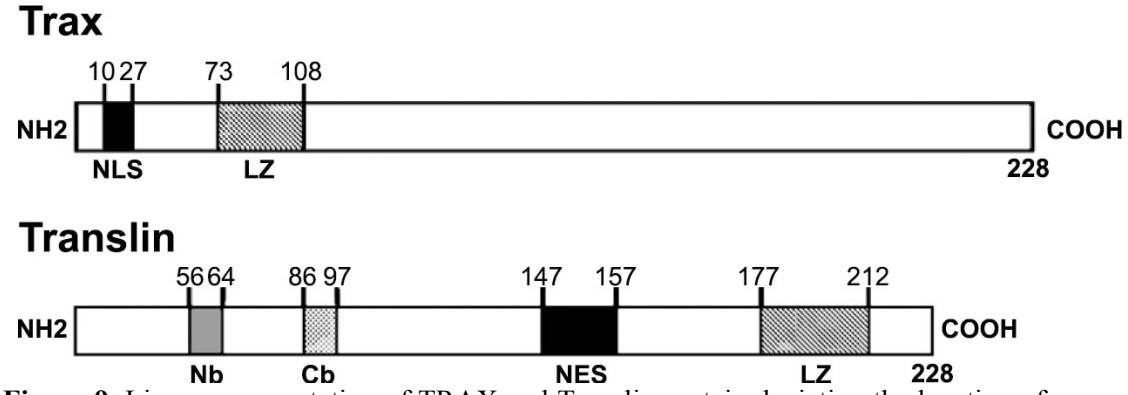

Figure 9. Linear representation of TRAX and Translin protein depicting the location of several domains. Nb and Cb, refer to basic domains located closer to the N-terminus and C-terminus, respectively, that mediate nucleic acid binding activity; NES, nuclear export signal, LZ, putative leucine zipper domain; NLS, nuclear localization signal. Modified from Li et al. (2008).

As seen in figure 9, TRAX contains a nuclear localization signal (NLS) and Translin is thought to possess a nuclear export signal (NES), and it has been suggested that TRAX-Translin complex mediates dynamic changes in the subcellular localization of the complex, allowing for shuttling between nuclear and cytoplasmic compartments. Under conditions where the level of TRAX is higher than translin, the NLS of TRAX would be exposed, leading to nuclear localization of the complex. In contrast, when translin is in excess the complex would move to the cytosol (Aoki et al., 1997; Cho et al., 2004).

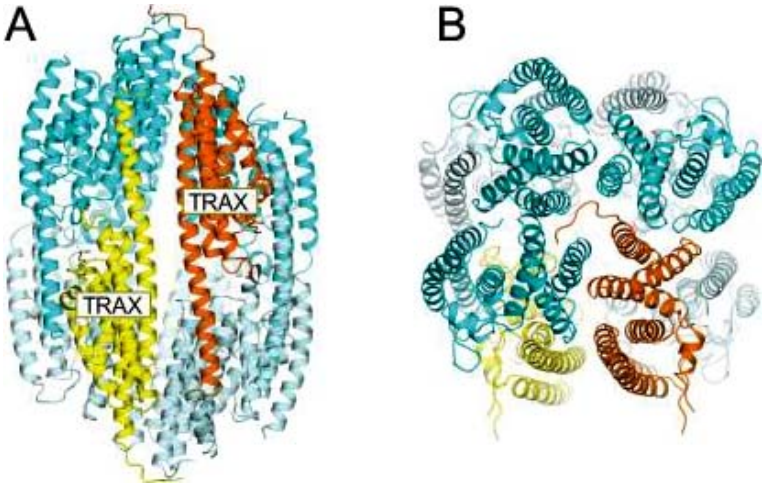

Figure 10. A. Ribbon representation of C3PO complex, in which the two TRAX subunits are colored in yellow and orange, and the six Translin subunits are colored in cyan or light cyan. **B.** Orthogonal view of A from the top of C3PO of the complex. Modified from Ye et al. (2011).

The conserved Translin-TRAX complex, also known as Component 3 Promoter of RISC (C3PO), is a complex formed by six Translin and two TRAX subunits that form an asymmetric octamer with the RNase catalytic residues located on the TRAX subunits (Fig. 10). C3PO helps guiding double stranded RNA into the silencing machinery as part of the RNA-induced complex (RISC) (Liu et al., 2009), whose other two major components are Argonaute-2 (Ago2) and Dicer-2 (Dcr-2). It has been demonstrated TRAX-Translin complex is necessary for efficient RNA interference (RNAi) mediated by small interfering RNAs (siRNAs) (Liu et al., 2009; Ye et al., 2011). RNA interference regulates gene expression by the slicer activity of Ago2, which degrades target mRNA with the aid of siRNA (Hammond et al., 2001). In this pathway, double strand RNA is transferred to the RLC (consisting of Dcr-2 and R2D2) and processed into 21-25 bp duplex RNA. The TRAX-Translin complex binds to the RLC and RISC (consisting of Ago2, Dcr-1, Tudor staphylococcal nuclease -TSN-, vasa intronic gene -VIG- and Drosophila FMR -dFMR-), thus forming the holo-RISC through an interaction between Drc-2 and Ago2. This allows the passenger strand to be endonucleolytically cleaved from the duplex RNA to form the single-stranded siRNA, this process being enhanced by C3PO (TRAX-Translin) activity. Then, the guide strand

targets the holo-RISC complex to the complementary mRNA for degradation (Fig. 11; Jaendling and McFarlane, 2011)

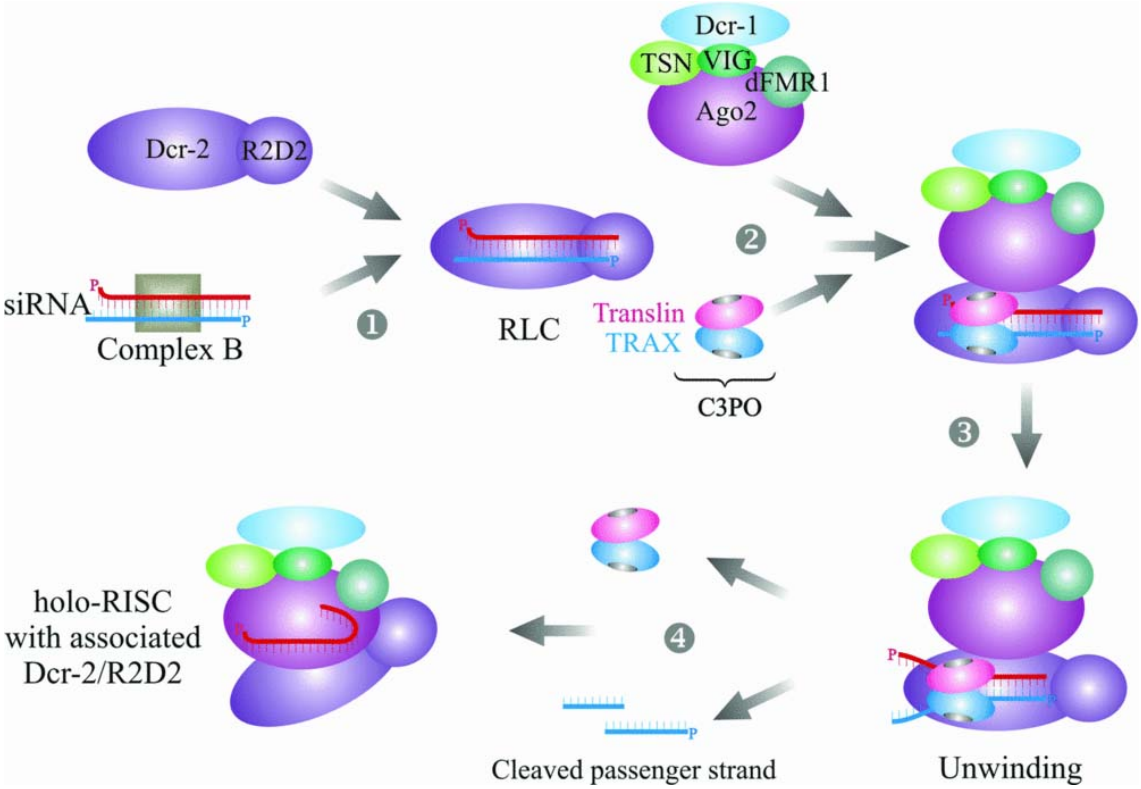

Figure 11. Schematic drawing showing the siRNA mediated RNA interference pathway and the proposed role of C3PO. Illustration taken from Jaendling and McFarlane (2011).

Noticeably, Aisiku et al. (2010) demonstrated that TRAX competes with activated Gαq (Gαq-GTPγS) but not unactivated Gαq (Gαq-GDP) for binding to PLCβ1 without affecting its affinity for membrane association. Because, the carboxy-terminal sequence used for yeast two-hybrid screening of PLCβ1-interacting partners encompassed the Gαq-interacting sequences flanking the C2 domain of PLCβ1 (Wang et al., 1999; Waldo et al., 2010; Lyon et al., 2011; Figs. 3, 5), it is very likely that TRAX interacts in at least one of these two regions, although the interaction sequence in PLCβ1 has not been mapped.

Recently, the same research group (Philip et al., 2012) has demonstrated a crosstalk between metabotropic receptor-mediated Gαq activation, subcellular localization of TRAX and the machinery involved in RNA interference. Thus, consistent with the ability of TRAX to disrupt the association between PLCβ1 and Gαq-GTPγS, Ca^{2+} signals observed after carbachol stimulation of PLCβ1- and Gαq-overexpressing HEK cells are abrogated upon co-transfection with TRAX. Conversely, carbachol stimulation of HEK cells overexpressing PLCβ1 (but having normal endogenous levels of Gαq and

TRAX) promotes translocation of a population of TRAX to the nucleus, indicating that TRAX localization is responsive to Gαq activation. But the most interesting finding by Philip et al. (2012) was that association between TRAX and PLCβ1 regulates the activity of the RISC complex affecting siRNA regulation of specific genes. They observed that overexpression of PLCβ1 reversed the activity of glyceraldehyde 3-phosphate dehydrogenase (GADPH) and lactate dehydrogenase (LDH) siRNAs, but did not affect siRNA silencing of other genes such as cyclophilin, Hsp90, translin. Moreover, overexpression of PLCβ1 rescued cells from cell death caused by transfection with GADPH and LDH siRNAs. This effect was independent of PLCβ1 catalytic activity and could be reversed by overexpression of a constitutively active form of Gαq, which very likely results from displacement of TRAX from its association with PLCβ1. In addition, they observed that GADPH siRNA, but not Hsp90 siRNA, increased co-localization of PLCβ1 with Ago2 and Dcr-2, indicating that only specific siRNA sequences trigger association of PLCβ1 to the RISC complex to reverse endonucleolytical cleavage of the duplex siRNAs, which impairs efficient degradation of specific target mRNAs (for review, Philip et al., 2013).

Interestingly, endogenously encoded, short (21–25 nt), single-stranded microRNAs (miRNAs) that posttranscriptionally regulate gene expression are temporally and spatially expressed during neuronal differentiation, acting as switches for neuronal stem cell differentiation (Shi et al., 2010; Coolen et al., 2012; Palm et al., 2013). This function requires incorporation of miRNAs to the RISC silencing machinery to target mRNAs for mRNA degradation and translational repression. In mammalian brain, many miRNAs are particularly enriched, where they participate in neuronal differentiation and even act locally controlling growth cone and synapse formation (Sun et al., 2013). Moreover, altered miRNA function or expression in neural stem cells has been shown to be associated with neurological disorders, such as Parkinson´s and Alzheimer's diseases (Palm et al., 2012; Maffioletti et al., 2014). Additionaly, TRAX- and translin-knockout mice display a wide spectrum of neurological deficits (Chennathukuzhi et al., 2003; Stein et al., 2006; Li et al., 2008). Therefore, it is conceivable that PLCβ1 could play a key role in neuronal differentiation by regulating endogenous miRNA activity thanks to its ability to associate to the RISC complex via TRAX. As a first step in testing this hypothesis, it is required an initial characterization of TRAX expression, subcellular localization and of PLCβ1-TRAX interaction during neuronal differentiation.

2. NT2-DERIVED POSTMITOTIC NEURONS: A MODEL OF TERMINALLY DIFFERENTIATED ADULT HUMAN NEURONS

Neuronal differentiation is a complex, developmentally regulated neurobiological phenomenon that involves proliferation arrest of neural progenitors and expression of neuron-specific genes, followed by neurite extension and morphological and functional polarization. In the vertebrate nervous system, the two broad types o neural progenitors (neural crest-derived cells and multipotent cells of the ventricular zone) have the ability to differentiate into neurons, astrocytes or oligodendrocytes. Neuronal differentiation appears to follow a common pattern in which proneural genes (members of the basic helix-loop-helix (bHLH) family of transcription factors) select progenitor cells previously specified to a neuronal fate. Subsequent phases involve the activity of proneural genes, which either alone or in coordination with other genes, activate Notch signaling, cell cycle withdrawal, and pan-neuronal and neuron phenotype-specific gene expression (for review, Jessell, 2000; Bertrand et al., 2002, Briscoe and Ericson, 2001). However, a still major challenge in developmental neurobiology is to elucidate the factors that govern the progression of the cascade of morphological and biochemical events that encompass the process of neuronal differentiation from neural progenitors. For these studies, human neuronal cells can be obtained from three different sources: embryonic stem cells (ESCs) derived from inner cell mass of the preimplanted human embryo, embryonic germ cells (EGCs) derived from primodal germ cells isolated from embryonic gonads and embryonic carcinoma cells (ECCs) derived from tumors in adult humans (Fig. 12).

Of these possibilities mentioned above, continuously dividing ECCs with neuronal characteristics has proven to be a very potent tool for biochemical and molecular biological studies. On one hand, biochemical studies usually require a large amount of homogenous cells. On the other hand, at difference with primary neurons, most cell lines are easy to transfect with non-viral vectors, which enables inexpensive, easy, safe and quick gen transfer to dissect molecular mechanisms underlying neuronal differentiation or to generate novel cell lines stably expressing the desired foreign gene product. In this regard, the pluripotent NTERA2/D1 (NT2) cell line, derived from human testicular embryonic carcinoma cells (Andrews, 1984), represents a committed neuronal precursor cell that can be induced to differentiate *in vitro* into postmitotic cells, known as NT2N (or hNT) neurons. Moreover, NT2N cells have the ability to

establish functional synapses and to develop neuronal electrophysiological properties, including generation of action potentials and the presence of spontaneous excitatory and inhibitory postsynaptic currents (Hartley et al., 1999a; Podrygajlo et al., 2010; Öz et al., 2013). Consequently, the NT2N cell type is now widely accepted as a suitable model for the study of neuronal networks, and differentiation and synaptogenesis processes.

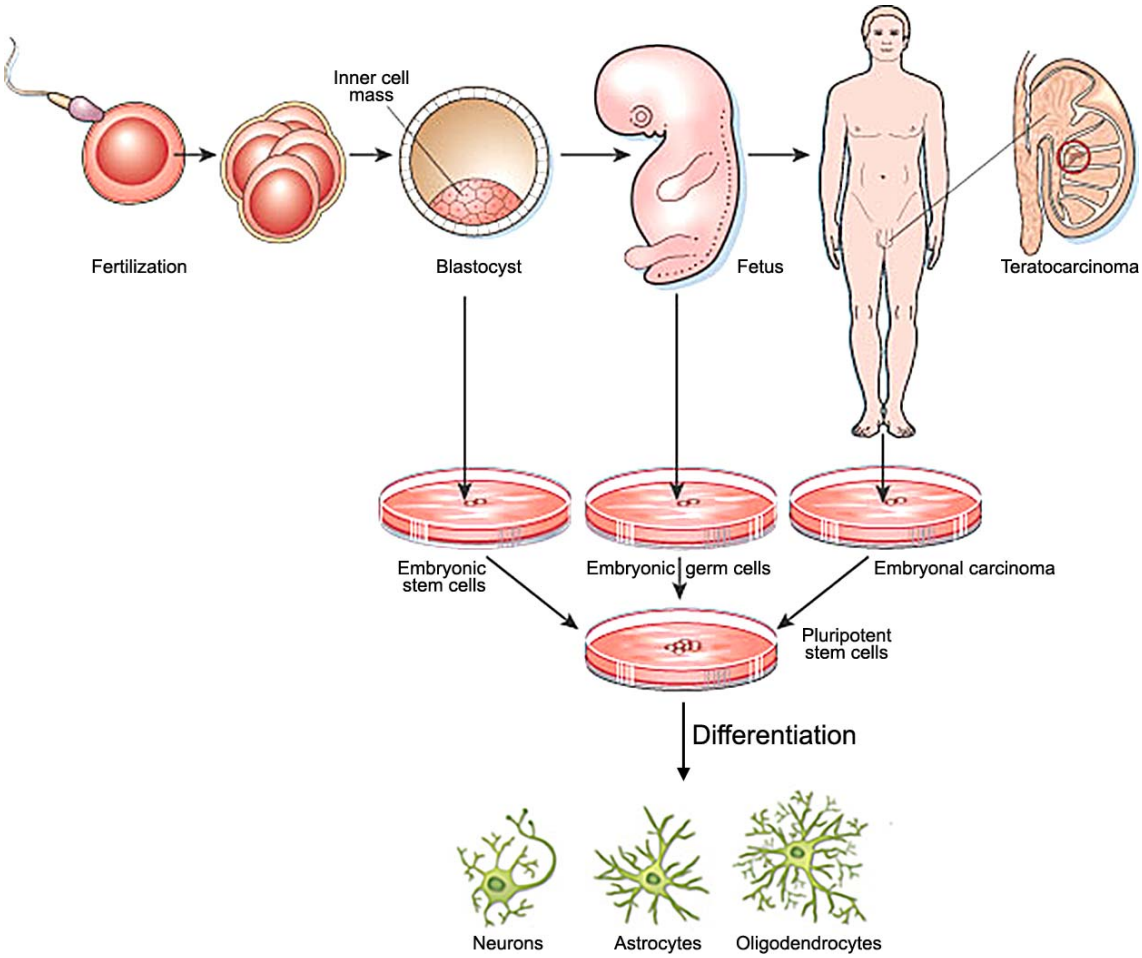

Figure 12. Sources of human neuronal cells. Modified from Donovan and Gearhart (2001).

In addition, the NT2 clonal line represents a promising cell source for neuronal replacement therapy applicable to the treatment of some neurological conditions, including neurodegenerative disorders such as Parkinson's, Huntington's and Alzheimer's diseases, and acute brain injury such as stroke and head trauma. To this end, grafts or cells in suspension from embryonic ventral mesencephalic tissue, adrenal medullary cells, other neuronal and non-neuronal cells, and even genetically modified cells have produced encouraging results, but none of them are fully satisfactory (Martínez-Morales et al., 2013). As a consequence, researchers have focused their efforts on either trying to increase the efficacy of existing tissue and cell candidates or searching for alternative sources of donor cells. In this sense, NT2N neurons maintain

their neuronal phenotype after transplantation into the rodent brain (Trojanowski et al., 1993; Kleppner et al., 1995; Baker and Mendez, 2005) and spinal cord (Hartley et al., 1999b; Lee et al., 2000). Furthermore, NT2N grafts have been shown to improve motor deficits in animal models of stroke (Borlongan et al., 1998a,b; Saporta et al., 1999) and Huntington's disease (Hurlbert et al., 1999), making NT2N neurons excellent candidates for cell replacement therapy in neurological disorders (Trojanowski et al., 1997; Lee et al., 2000; Nelson et al., 2002; Borlongan et al., 2006; Hara et al., 2008). Indeed, in a phase I clinical trial on 12 patients with basal ganglia stroke and stable motor deficits, NT2N cells were seen to integrate with the host brain tissue for long periods and with no detectable tumor formation (Kondziolka et al., 2000; Meltzer et al., 2001; Nelson et al., 2002), leading to a Phase II study in 18 patients with basal ganglia infarct (Kondziolka et al., 2005). Although statistical significance could not be reached due to the small population size analyzed, both studies showed an apparent trend towards functional improvement (Banerjee et al., 2010, for review).

Progress in the field of neuronal replacement using NT2 committed to differentiate with retinoic acid (RA) is limited by the long time frame necessary to generate postmitotic NT2N neurons and also by the low proportion of terminally differentiated neurons. Thus, neuronal differentiation of NT2 progenitors, first described by Andrews (1984) and later on improved by Pleasure et al. (1992), involves treatment of NT2 progenitors with RA during 4 weeks followed by mitotic inhibitors for 7-10 days, with only about 5% of the initial population of NT2 cells becoming differentiated. Recently, using nucleoside analogues, Musch et al. (2010) achieved successful differentiation of NT2 cells in less than one week, thus offering a rapid protocol to obtain postmitotic neurons, which could be potentially useful for neuronal replacement therapy. However, whereas NT2N neurons obtained by treatment with RA have been shown to express a variety of classical neurotransmitters, neurotransmitter-related enzymes and transporters, including γ-aminobutyric acid (GABA), tyrosine hydroxylase (TH), choline acetyltransferase (ChAT) and glutamate transporters (Podrygajlo et al., 2009; Coyle et al., 2011), there are no published data about neuronal phenotypes resulting from nucleoside-induced differentiation of NT2 cells. Therefore, one major objective of the present study will be to establish a quick and efficient method for neuronal differentiation of NT2 progenitors and to characterize the resulting neuronal phenotypes.

II. OBJECTIVES

As mentioned in the introduction, the involvement of PLCβ1 in cell differentiation has been extensively reported in a variety of cell lines (Cocco et al., 2009), and there is suggestive evidence that PLCβ1 plays a key role in neuronal differentiation. This later idea derives from observations that Plcb1$^{-/-}$ mice (Kim et al., 1997; McOmish et al., 2008a,b; Koh, 2013) and humans with deletions of the PLCB1 (Udawela et al., 2010; LoVasco et al., 2012) display functional and morphological deficits that become evident during postnatal life.

To address the issue of whether PLCβ1 plays an important role in neuronal differentiation, cell models suitable for gene and siRNA transfer to either force or knockdown the expression of the desired protein are necessary. In relation to the present project, these approaches will enable to ascertain whether PLCβ1 is necessary and/or sufficient for neuronal differentiation, and whether PLCβ1a and PLCβ1b splice variants play a specific role in this process. Among the cell lines available, the pluripotent NT2 embryonic carcinoma cells line is widely accepted as an excellent model for the study human neuronal differentiation. Currently, there is a wealth experimental evidence documenting that treatment with retinoic acid (RA) promotes differentiation of NT2 progenitors into postmitotic NT2N neurons (Andrews, 1984; Pleasure et al., 1992). Apart from being phenotypically characterized with regard to the expression of neurotransmitter-related enzymes and transporters, it has been shown that NT2N neurons are able to functionally integrate into the rodent and human brain and even to promote functional recovery in animal models of various neurological diseases (Banerjee et al., 2010).

However, the use of RA-differentiated NT2 progenitors is limited by the long time frame necessary to generate postmitotic NT2N cells and also by the low proportion of terminally differentiated neurons, making this procedure useless for transient transfection-based approaches. On the basis of a recent report showing that nucleoside analogues promote neuronal differentiation of NT2 cell in less than one week, the first objective of the present study will be to establish an alternative NT2 differentiation procedure that overcomes these drawbacks mentioned above.

The neurochemical characterization of a rapid and efficient method for neuronal differentiation of NT2 cells using nucleotide analogues will provide the basis for biochemical and molecular biological approaches aimed at determining the role of PLCβ1 in neuronal differentiation.

With these challenges in mind, the major objectives of this thesis are:

1. To establish and characterize an experimental model for human neuronal differentiation by short exposure of NT2 progenitors to nucleoside analogues.

2. To analyze the expression of PLCβ1a and PLCβ1b splice variants in subcellular fractions of the adult rat cerebral cortex and of NT2 cells.

3. To analyze the time-course expression of PLCβ1a and PLCβ1b variants during neuronal differentiation of NT2 cells.

4. To study the role of PLCβ1 in neuronal differentiation of PC12 and NT2 cells.

5. To analyze the expression and subcellular localization of TRAX during neuronal differentiation of NT2 cells.

6. To analyze the PLCβ1-TRAX interaction in differentiating NT2 cells and the effect of TRAX silencing on neuronal differentiation of PC12 and NT2 cells.

III. MATERIALS

1. GENERAL MATERIALS, CHEMICAL AND REAGENTS

- Acetone (Panreac, 211007).
- Chloral hydrate (Panreac, 141975).
- DL-Dithiothreitol (DTT) (Sigma-Aldrich, 43815).
- Ethylene glycol-bis(2-aminoethylether)-N,N,N′,N′-tetraacetic acid (EGTA, Sigma-Aldrich, E4378).
- Ethylenediaminetetraacetic acid (EDTA, Panreac, ED).
- Filter paper (Bio-Rad, 165-0962).
- Gelatin (Panreac, 142060).
- Glycerol (Sigma-Aldrich, G8773).
- Glycine (Bio-Rad, 161-0724).
- Hydrochloric acid 37% (Panreac, 141020).
- Magnessium Chloride Hexahydrate (Panreac, 131396).
- Methanol (Sigma-Aldrich, 32213).
- Mowiol (Calbiochem, 17951).
- P-phenylenediamine, 1,4-Benzenediamine hydrochloride (PPD, Sigma-Aldrich, P1519).
- Paraformaldehyde (PFA, Panreac, 141451).
- Potassium chloride (Sigma-Aldrich, P5405).
- Saponin (Sigma-Aldrich, 84510).
- Sodium azide (Panreac, 122712).
- Sodium chloride (Sigma-Aldrich, S7653).
- Sodium Hydroxide (Probus, 131687).
- Sodium phosphate dibasic (PO_4Na_2H, Sigma-Aldrich, S0876).
- Sodium phosphate monobasic (PO_4NaH_2, Sigma-Aldrich, S0751).
- Sucrose (Sigma-Aldrich, S0389).
- Tris(hydroxymethyl)aminomethane (Trizma® Base, Sigma-Aldrich, T1503).
- Tritón X-100 (Sigma-Aldrich, T8787).
- Tween-20 (Bio-Rad, 170-6531).
- Urea (Sigma-Aldrich, U5378).
- β-mercaptoethanol (Sigma-Aldrich, M7522).

2. SPECIFIC MATERIALS, CHEMICALS AND REAGENTS

2.1. Cell culture and transfection

2.1.1. Disposables

- 0.22-μm-pore-size syringe filters (Millipore, SLGP05010).
- 15 and 50 mL centrifuge tubes (Corning, 430791 and 430291).
- 25, 75 and 150 cm^2 cell culture flasks (Corning, 3055, 430725 and 430824).
- 5, 10 and 25 mL pipettes (Corning, 4487, 4487 and 4489).
- 6-, 12- and 24-well culture dishes (Corning, 3516, 3513 and 3526).
- 96-well EIA/RIA plates (Corning, 3590).
- Cell scrapers (Corning, 3011).
- Gene Pulser/MicroPulser Electroporation Cuvettes (Biorad, 165-2088).

2.1.2. Transfection media

- DharmaFECT 1 Transfection Reagent (Dharmacon, T-2001-02).
- Lipofectamine® 2000 (Invitrogen, 11668027).

2.1.3. Culture media, supplements, inductors and substrates

- BD Matrigel™ Basement Membrane Matrix (GIBCO, 354234).
- Dulbecco's Modified Eagle's Medium (DMEM, ATCC, 30-2002™).
- Dulbecco's Phosphate Buffered Saline (DPBS) (1X) (GIBCO, 14190-094).
- Fetal bovine serum (FBS, Sigma-Aldrich, F6178).
- Fetal horse serum (FHS, Sigma-Aldrich, H1270).
- Lithium chloride (Panreac, 141392).
- Nerve Growth Factor (NGF, Sigma-Aldrich, N0513).
- OptiMEM™ (Life Technologies, 51985-034).
- Poly-D-lysine hydrobromide (Sigma-Aldrich, P6407).
- Penicillin 10.000 U/mL, Streptomycin 10.000 μg/mL (Lonza, 17-602E).
- Trans retinoic acid (Sigma-Aldrich, R2625).

2.1.4. Antimitotics

- 2'-deoxy-5-azacytidine (DAC, Sigma-Aldrich, A1287).
- 5-Fluoro-2'-deoxiuridine (FUdR, Sigma-Aldrich, F8791).
- Citosine β-D-arabinofuranoside (AraC, Sigma-Aldrich, C1768).
- Uridine (Sigma-Aldrich, U3750).

2.1.5. Other products

- Cell culture grade dimethylsulfoxide (DMSO, ATCC, 4-X).
- Cell culture grade water (Sigma-Aldrich, W3500).
- Trypsin-EDTA (0,05%), phenol red (GIBCO, 25300-054).

2.2. Western blot

- Acrylamide/Bis-acrylamide, 40% solution (Bio-Rad, 161-0148).
- Ammonium persulfate (Bio-Rad, 161-0700).
- BCA Protein Quantification Kit (Abcam, ab102536).
- Blotting Grade Blocker Non-Fat Dry Milk (Bio-Rad, 170-6404).
- Bovine Serum Albumine (Sigma-Aldrich, A3608).
- Bio-Rad DC Protein Assay Kit I (Bio-Rad, 500-0111).
- Bromophenol blue (Sigma-Aldrich, 11439).
- CL-XPosure film (Thermo Scientific, 34089).
- Clarity Western ECL substrate (Bio-Rad, 170-5060).
- Coomassie brilliant blue dye (Bio-Rad, 161-0400).
- Developer (Sigma-Aldrich, 7042) and fixative (Sigma-Aldrich, P7167) for CL-XPosure films.
- IGEPAL (Sigma-Aldrich, 18896).
- Immun-Blot® PVDF Membrane (Bio-Rad, 162-0177).
- Iodoacetamide (Sigma-Aldrich, I1149).
- Laemmli Buffer (Bio-Rad, 161-0737).
- Phenylmethanesulfonyl fluoride (PMSF, Sigma-Aldrich, P7626).
- Precision Plus Protein™ Dual Color Standards (Bio-Rad, 161-0374).
- RNase-free recombinant DNase I (TaKaRa, TB 2270A).
- Sodium dodecyl sulfate (SDS, Amersham, L3771).
- TEMED (Bio-Rad, 161-0800).
- γ-Globulin (Bio-Rad, 500-0208).

2.3. Antibodies and sera for immunofluorescence and Western blot

2.3.1. Primary antibodies

Table 1. Primary antibodies used

Antibody	Dilution IF	Dilution WB	Species & clonality	Isotype	Immunizing antigen	Source, Cat. No.
BiP	-	1:500	Rabbit polyclonal	IgG	Synthetic peptide corresponding to amino acids within the last 660 residues of the C terminus of mouse GRP78/BiP.	Abcam, ab21685
ChAT	1:100	1:1000	Goat polyclonal	Serum	Human placental enzyme.	Millipore, AB144P
CyPA	-	1:500	Mouse monoclonal	IgG_{2a}	Recombinant CyPA protein of human origin.	Sta Cruz Biotech. Inc., sc-134310 clone 6-YD13
DCX	1:200	1:500	Goat polyclonal	IgG	Synthetic peptide mapping at the C-terminus of human doublecortin.	Sta Cruz Biotech. Inc., sc-8066
GAD67	1:100	1:1000	Mouse monoclonal	IgG_{2a}	Recombinant GAD67 protein.	Millipore, MAB5406, clone 1G10.2
GFP	-	1:2500	Rabbit polyclonal	IgG	GFP isolated from *Aequorea victoria.*	Invitrogen, A11122
Golgi	-	1:2000	Rabbit polyclonal	Serum	Synthetic peptide encompassing residues 200-300 of human 58K Golgi protein.	Abcam, ab5820
Gαq/11	1:200	1:1000	Rabbit polyclonal	IgG	Peptide mapping within a domain common to Gα 11 of mouse origin.	Sta Cruz Biotech. Inc., sc-392
HA	1:500	1:1000	Mouse monoclonal	IgG_1	Synthetic peptide corresponding to the hemagglutinin sequence CYPYDVPDYASL.	Covance, MMS-101P, clone 16B12
Histone H1	-	1:200	Mouse monoclonal	IgG_{2a}	Biopsy cells from human leukaemia.	Sta Cruz Biotech. Inc., sc-8030
Lamin B1	1:100	-	Mouse monoclonal	IgG_1	Purified cell nuclei from human epithelioid carcinoma.	Sta Cruz Biotech. Inc., sc-56144
MAP2	1:200	-	Mouse monoclonal	IgG_1	Bovine MAP2.	Sigma-Aldrich, M2320
Na^+/K^+ ATPase	-	1:450	Mouse monoclonal	IgG_1	α1 subunit of Na+/K+ ATPase purified from lamb kidney. The epitope maps at residues 496-506.	Sigma-Aldrich, A277, clone M8-P1-A3
Nav1.6 Na^+ channel	1:200	-	Mouse monoclonal	IgG_1	Synthetic peptide corresponding to amino acids 459-476 within the cytoplasmic loop I-II of rat Nav1.6.	NeuroMab, 75-026
NeuN	1:200	1:1000	Mouse monoclonal	IgG_1	Purified cell nuclei from mouse brain.	Millipore, MAB377 clone A60
NF200	1:400	1:10000	Rabbit polyclonal	IgG	NF200 protein purified from bovine spinal cord.	Sigma-Aldrich, N4142
NR1	-	1:1500	Rabbit polyclonal	Serum	Synthetic non-phosphopeptide around the phosphorylation site of human NMDAR1 at serine 897 (RSSKD).	Abcam, ab52177
Nuclear Pore Complex	-	1:1000	Mouse monoclonal	IgG_1	Nuclear pore complex mixture	Abcam, ab24609
PIP_2	1:100	-	Mouse monoclonal	IgM	Liposomes containing synthetic di-palmitoyl PtdIns (4,5)P_2.	Tocris, 2368, clone 2C11
PLCβ1 (D-8)	1:125	-	Mouse monoclonal	IgG_{2b}	Synthetic peptide mapping within amino acids 831-1063 of rat PLCβ1.	Sta Cruz Biotech. Inc., sc-5291
PLCβ1 (N-ter)	-	1:750	Mouse monoclonal	IgG_1	Synthetic peptide corresponding to amino acids 4–159 of the rat PLCβ1.	BD Transduction Laboratories, 610924
PLCβ1 (R-233)	1:500	-	Rabbit polyclonal	IgG	Synthetic peptide mapping within amino acids 831-1063 of rat PLCβ1.	Sta Cruz Biotech. Inc., sc-9050
PLCβ1a (G-12)	1:250	1:500	Rabbit polyclonal	IgG	Synthetic peptide corresponding to a unique C-terminal region of PLCβ1a splice variant.	Sta Cruz Biotech. Inc., sc-205
PLCβ4	-	1:500	Rabbit polyclonal	IgG	Synthetic peptide mapping at the C-terminus of rat PLCβ4.	Sta Cruz Biotech. Inc., sc-404

Antibody	Dilution		Species & clonality	Isotype	Immunizing antigen	Source, Cat. No.
SC-35	1:500	-	Mouse monoclonal	IgG	Synthetic peptide sequence corresponding to SC-35 splicing factor.	Abcam, ab11826
SNAP-25		1:4000	Mouse monoclonal	IgG1	Tissue cell preparation: this antibody was raised against a crude synaptic preparation from the post mortem human brain.	Abcam, ab24732
TH	1:100	1:1000	Rabbit polyclonal	Rabbit	SDS-denatured tyrosine hydroxylase from rat pheochromocytoma.	Millipore, AB152
TRAX (56)	-	1:2000	Mouse monoclonal	IgG1	Amino acids 1-207 of TRAX of human origin.	Sta Cruz Biotech. Inc., sc-136108
TRAX (FL-290)	1:125	-	Rabbit polyclonal	IgG	Full length TRAX of human origin.	Sta Cruz Biotech. Inc., sc-98554
VGluT1	1:200	1:1500	Rabbit polyclonal	IgG	Synthetic peptide from a cytoplasmic loop of rat (C-terminal) VGluT1.	Abcam, ab72311
β-Actin	-	1:40000	Mouse monoclonal	IgG1	An epitope mapping at the N-terminal end of β-actin.	Sigma-Aldrich, A5441
β-Tubulin	-	1:500	Mouse monoclonal	IgG1	An epitope in the carboxy-terminal part of all five isoforms of β-tubulin (between amino acids 281-446).	Sigma-Aldrich, T-4026
β-Tubulin-III	1:1000	1:1000	Chicken polyclonal	Chicken serum	Synthetic peptides corresponding to different regions shared by human and rat β-tubulin III.	Abcam, ab41489

2.3.2. Secondary antibodies for Immunofluorescence and fluorescent dyes

- Alexa Fluor 568 Goat anti-Rabbit (Invitrogen, A11036).
- Alexa Fluor 568 Goat anti-Mouse (Invitrogen, A11031).
- Alexa Fluor 488 Goat anti-Rabbit (Invitrogen, A11034).
- Alexa Fluor 488 Goat anti-Mouse (Invitrogen, A11029).
- Alexa Fluor 488 Donkey anti-Goat (Invitrogen, A11055).
- DyLight 549 Donkey anti-Rabbit (Jackson Immuno Research, 711-506-152).
- DyLight 549 Donkey anti-Mouse (Jackson Immuno Research, 715-506-151).
- DyLight 649 Donkey anti-Mouse (Jackson Immuno Research, 715-496-151).
- DyLight 649 Goat anti-Chicken (Jackson Immuno Research, 103-495-155).
- Cy 5 Donkey anti-Rabbit (Jackson Immuno Research, 711-176-152).
- DyLight 488 Donkey anti-Chicken (Jackson Immuno Research, 703-486-155).
- Hoescht 33342 (Sigma-Aldrich).

2.3.3. Secondary antibodies for Western blot

- Anti-rabbit IgG HRP conjugate (Amersham, NA934).
- Anti-mouse IgG HRP conjugate (Amersham, NXA931).
- Anti-Goat IgG HRP conjugate (Sigma-Aldrich, A5420).
- Rabbit anti-Chicken IgY HRP conjugate (Sigma-Aldrich, A9046).

2.3.4. Normal sera

- Normal goat serum (NGS, Vector Laboratories, U0328).

- Normal rabbit serum (NRS, Vector Laboratories, T1127).
- Normal donkey serum (NDS, Vector Laboratories, U0111).

2.4. Molecular biology

2.4.1. Agarose gel electrophoreis

- Agarose D1 Low EEO (Conda, 8016).
- 100 bp DNA ladder (Nippon Genetics, MWD100).
- 1kb DNA ladder (Nippon Genetics MWD1).
- 1kb DNA ladder (Thermo Scientific, SM1163).
- Low range DNA ladder (Thermo Scientific, SM1203).
- 50X TAE (Tris/AceticAcid/EDTA) buffer (Biorad, 161-0743).
- GelRed Nucleic Acid Stain 10000X (Biotium, 41003).

2.4.2. Bacterial culture

- Ampicillin Sodium Salt (Sigma-Aldrich, A9518).
- Kanamycin Sulphate Supplement (OXOID, SR0092).
- Medium for bacterial culture on agar, LB Agar (Lennox) (Conda, 1083).
- Medium for bacterial culture in suspension, LB Broth (Lennox) (Conda, 1231).
- Sterile Petri dishes (Kord, 905).

2.4.3. DNA purification

- NucleoBond® Xtra Midi Plus (Machery Nagel, 740412.50).
- Nucleospin® Gel and PCR Clean-Up (Machery Nagel, 740609.250).
- NucleoSpin® Plasmid (Machery Nagel, 740588.250).

2.4.4. PCR and cloning

- KAPA HiFi PCR Kit, including high-fidelity Taq polymerase, buffers and dNTPs (KAPA Biosystems, KK2101).
- PCR Tube Strips (Biorad, TCS0803).
- ONE Shot TOP 10 Chemically Competent *E. Coli* (Invitrogen, C4040).
- T4 DNA Ligase (Takara, 2011A).
- 10X T4 DNA Ligase Buffer (Takara, 2011A).
- Zero Blunt TOPO PCR Cloning Vector (Invitrogen, P/N 46-0757).
- Restriction Enzymes

Table 2. Restriction enzymes used. All from New England Biolabs.

Enzyme	Cleavage site	Ref.
AgeI	A^CCGGT	R0552S
BamHI	G^GATCC	R0136S
BglII	A^GATCT	R0144S
BsrGI	T^GTACA	R0575S
EcoRI	G^AATTC	R0101S
EcoRV	GAT^ATC	R0195S
HindIII	A^AGCTT	R0104S
KpnI	GGTAC^C	R0142S
MluI	A^CGCGT	R0198S
NheI-HF	G^CTAGC	R3131L
NotI	GC^GGCCGC	R0189L
PmlI	CAC^GTG	R0532S
XbaI	T^CTAGA	R0145S
XhoI	C^TCGAG	R0146S
XmaI	C^CCGGG	R0180L

- Buffers for restriction enzymes:

  - NE Buffer 1 (New England Biolabs, B7001S).
  - NE Buffer 2 (New England Biolabs, B7002S).
  - NE Buffer 3 (New England Biolabs, B7003S).
  - NE Buffer 4 (New England Biolabs, B7004S).
  - EcoRI Buffer (New England Biolabs, B0101S).
  - BSA 100X (New England Biolabs, B9001S).

2.4.5. Plasmid constructions

Table 3. Constructions used.

Name	Coding product	Use	Source	Cloning vector
PLCβ1a	Human PLCβ1a	Overexpression of the transgen in eukaryotic cells	1	pcDNA 3.0
PLCβ1b	Human PLCβ1b			
HA-PLCβ1a	N-terminal HA-tagged PLCβ1a			
HA-PLCβ1b	HA-tagged PLCβ1b			
PLC-β1a-eYFP	PLCβ1a-eYFP fusion protein	Overexpression of the transgen in eukaryotic cells for analysis of PLCβ1a-TRAX interaction by FRET	2	
TRAX-eCFP	TRAX-eCFP fusion protein			
eYFP	eYFP	Negative control for FRET		
eCFP	eCFP			
eCFP-eYFP	eYFP-eCFP fusion protein	Positive control for FRET		
shRNA-01	Scramble shRNA	Overxpression of non-target shRNA	1	pSuperior.gfp/neo (Origene) Contains an EGFP reporter gene to monitor transfection rate
shRNA-87	PLCβ1-shRNA	Overxpression of shRNA expression for PLCβ1 siRNA silencing		
shRNA-89				
shRNA-97				
shRNA-99				

[1]Own production by PCR and subcloning.
[2]Laboratory of Dr. Suzanne Scarlatta; Dept. of Physiology & Biophysics, Stony Brook University.

2.4.6. Small interfering RNAs

Table 4. ON-TARGET plus SMART pools from Dharmacon.

Name	Code	Protein encoded by the mRNA target
PLCB1 siRNA	L-010280-00-0020	Human PLCβ1
Plcb1 siRNA	L-092936-02-0020	Rat PLCβ1
Tsnax siRNA	L-097955-02-0020	Rat TRAX
Tsn siRNA	L-099674-02-0020	Rat Translin
Gna11 siRNA	L-092615-02-0020	Rat Gαq/11
Non-targeting Pool	D-001810-10-20	Negative control

IV. METHODS

1. CELL CULTURE AND TRANSFECTION

1.1. Culture of NT2 and PC12 cells

Human teratocarcinoma NTERA2-D1 (hereafter referred to as NT2) cells from the American Type Culture Collection (ATCC®, CRL-1973™) were maintained in complete medium (DMEM®, supplemented with 10% FBS and antibiotics -100 U/mL penicillin and 100 µg/mL streptomycin) at 37ºC under a humidified atmosphere containing 5% CO_2. PC12 cells were cultured in similar conditions except that DMEM was supplemented with 10% FHS and 5% FBS.

1.2. Transfection

1.2.1. Transfection of plasmidic DNA

Cells were allowed to grow to ~70-80% confluence and then transfected. NT2 cells were transfected with Lipofectamine® 2000 in antibiotic and serum-free medium according to the manufacturer's instructions, using a ratio of 2 µL of Lipofectamine for 1 µg DNA. The amount of DNA used was 0.5, 1 and 2.5 µg for 24-, 12- and 6-well plates, respectively.

PC12 cells were grown in 25 cm^2 culture flasks to ~70-80% confluence, washed with sterile PBS, trypsinized, centrifuged for 5 min at 1500 x g and resuspended in 10 mL of antibiotic and serum-free medium. 800 µL of the cell suspension were pipeted into a 4 mm BioRad cuvette and placed in an electroporator (BioRad Gene Pulser Xcell). Conditions for transfection were 10 µg DNA, 250 V, 500 µF, ∞ Ω. After a 10 ms pulse, cells were allowed to rest for 1-2 min, and 1 mL of DMEM was added to each cuvette. Then, cells were plated onto LabTek chambers coated with Poly-D-Lysine (Sigma-Aldrich). Three to four hours post-transfection, the wells were washed with 1 mL of PBS, and 1.5 mL of DMEM containing 100 ng/mL NGF. After 3 days, transfected cells were induced to differentiate (see below) and used for imaging.

1.2.2. Transfection of siRNAs

For small interfering (siRNA)-mediated gen knockdown in NT2 and PC12 cells, we used species-specific ON-TARGET plus SMART pool siRNAs (see Materials), which consist of four siRNAs to the same target gene mixed together. For control experiments, ON-TARGET plus Non-targeting Control siRNA Pool was used, which consists of four small RNAs designed for minimal targeting of human, mouse or rat genes and modified

to reduce potential off-targets. NT2 cells grown to ~70-80% in 12-well plates were transfected with 5 nmol siRNA, using DharmaFECT 1 Transfection Reagent in antibiotic and serum-free medium. The transfection mix was prepared according to the manufacturer's protocol, using a ratio using a ratio of 2.5 µL of DharmaFECT 1 Reagent for 5 nmol siRNA.

PC12 cells were transfected by electroporation as described above with 40 nmol siRNA (section 1.2.1.).

2. NEURONAL DIFFERENTIATION OF NT2 AND PC12 CELLS

2.1. Retinoic acid-induced differentiation of NT2 cells

For differentiation of NT2 progenitors with all-trans retinoic acid (RA, Sigma-Aldrich), cells were treated as previously described by Pleasure et al. (1992). NT2 cells at 80% confluence were treated during 4 weeks with 10 µM RA containing complete medium, which was replaced every 3 days. Cells were then treated briefly with 0.05% trypsin-EDTA (Sigma-Aldrich) and mechanically dislodged, that is, culture flasks were struck on each side 10 times. Floating cells were counted using the trypan-blue exclusion assay and replated at a density of 2.1×10^5 cells/cm^2, in either 75 cm^2 culture flasks or poly-D-lysine treated 12 mm glass coverslips, both pre-coated with 1:25 diluted *Matrigel*™ (BD Biosciences, Madrid, Spain), and maintained in complete medium. Twenty-four hours later, the culture medium was replaced with fresh medium containing mitotic inhibitors (10 µM uridine -Sigma-Aldrich, 10 µM 5-Fluoro-2'-deoxyuridine -Sigma-Aldrich, and 1 µM cytosine β-D-arabinofuranoside -AraC -Sigma-Aldrich) and maintained under these conditions for 2 weeks, thus obtaining RA-differentiated NT2N cells (hereafter referred to as RA/NT2N cells). Medium containing mitotic inhibitors was replaced every 3 days (Fig. 13, left panel).

2.2. Nucleoside analogue induced differentiation of NT2 cells

Induction of neuronal differentiation using 2'-deoxy-5-azacytidine (DAC) or Cytosine β-D-arabinofuranoside (AraC) was performed based on a previous report showing that exposure of NT2 cells for only 6 days leads to neuronal differentiation (Musch et al., 2010). For preliminary assays progenitor NT2 cells were exposed to equitoxic concentrations of DAC or AraC (Tan et al., 2007; Musch et al., 2010). Briefly, NT2 cells at 80-90% confluence were treated with 1 µM DAC or 20 µM AraC-

containing medium for 24 h, 48 h, 72 h or 6 days. Medium from cultures treated for more than 48 h, was replaced with fresh complete medium supplemented with the corresponding nucleoside analogue every two days. Results of preliminary experiments led us to choose AraC to induce neuronal differentiation (see Results) and, therefore, this compound was used for subsequent experiments (Fig. 13, right panel).

2.3. Modified AraC differentiation protocol

Because low cell density can compromise neuronal survival and differentiation, we tested whether increased confluence improves the yield of terminally AraC-differentiated neurons (hereafter referred to as AraC/NT2N cells). For this purpose, cells were trypsinized after 72 h of treatment (a time point at which most cell have acquired a neuron-like morphology, see results), counted and replated in complete medium on a 3-fold smaller growth surface area. Thus, cells from a 75 cm^2 culture flask were passed to either a 25 cm^2 flask (for Western blot analysis) or to 13 wells of a 24-well plate (for immunofluorescence analysis). These conditions corresponded to a density of 1,75 to 2 x 10^5 viable cells/cm^2. Next morning, culture medium was replaced with 20 µM AraC-containing complete medium (AraC-differentiation medium), and cells were maintained in this medium until day 6, starting from the initial culture of NT2 progenitors. Cells grown on 25 cm^2 flasks were dissociated with trypsin and the amount of viable cells was calculated using the trypan-blue dye-exclusion method. The amount of cells in the initial cultures was calculated by counting viable NT2 cells recovered from untreated cultures at a time point corresponding initiation of treatment in cultures exposed to 20 µM AraC (Fig. 13, right panel).

2.4. Differentiation of PC12 cells

The PC12 cell line from the American Type Culture Collection (ATCC® CRL1721™), derive from a pheochromocytoma of the rat adrenal medulla composed of a mixture of neural crest-derived neuroblastic and eosinophilic cells. This cell line has been widely used as a model of sympathetic neuron differentiation. When exposed to NGF, PC12 cells undergo cell cycle arrest and acquire neuronal polarity with abundant branching varicose processes similar to those observed in primary cultures of sympathetic neurons. Neurochemically, differentiated PC12 cells synthesize and store the catecholamines dopamine and norepinephrine (Greene and Tischler, 1976)

To induce differentiation, PC12 cells at ~50% density were treated with NFG at a final concentration of 100 ng/mL and the differentiation medium was renewed every two days. Cells were defined as differentiated when displayed neurites at least two cell body diameters (~30 μm) long, with a well (Ignatius et al., 1985).

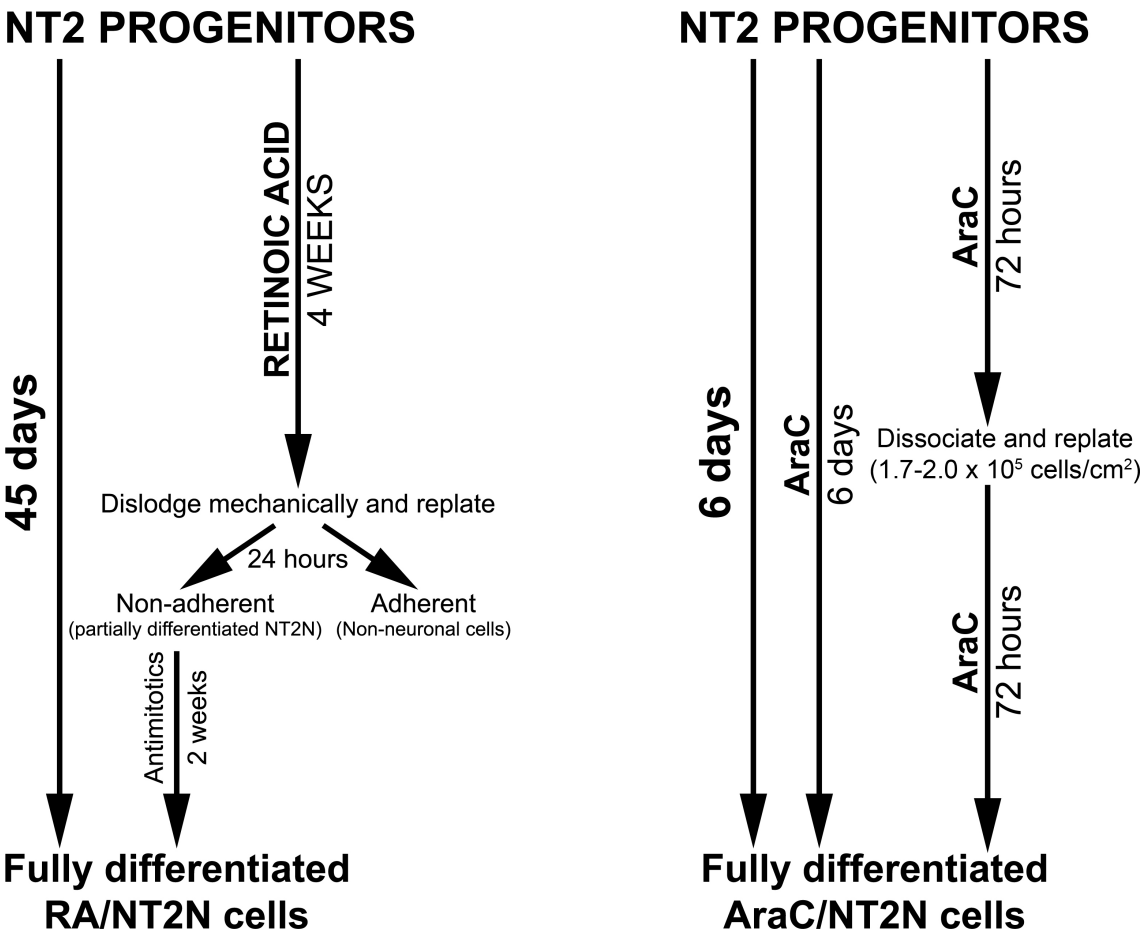

Figure 13. Schematic diagrams of the protocols used to induce differentiation of NT2 progenitors into postmitotic NT2N neurons. Left, RA-induced differentiation schedule. Right, AraC-induced differentiation following either a 6-day uninterrupted AraC treatment or a two-step schedule that involves dissociation of cells at mid at mid-treatment to increase cell density.

3. IMMUNOFLUORESCENCE

3.1. Fixation

For fixation, cells were washed twice with phosphate buffered saline 0.1 M, pH 7.4 (PBS) at room temperature and incubated with paraformaldehyde 4% in phosphate buffer 0.1 M, pH 7.4 (PB) for 10 min at room temperature. Thereafter, cells were washed three times with PBS and stored at 4ºC for no more than 4 days before immunofluorescence. Because RA- and AraC-differentiation protocols could not be

carried out in parallel, for assays involving comparison between these two conditions PBS was replaced with a a cryoprotectant solution (consisting of glycerol 50% in PB) and cells were stored at -20ºC for periods no longer than two months before immunostaining. For all antigens analyzed, preliminary assays showed no changes in immunoreactivity or immunostaining profile in cells treated under these conditions.

Isolated nuclei seeded on gelatin-coated slides were immersed in buffered 4% paraformaldehyde for 5 min at room temperature.

3.2. Immunofluorescence

NT2 cells were washed with 0.1 M PBS, pH 7.4 and fixed in buffered 4% paraformaldehyde for 4 min, both at 20°–25°C. Thereafter, cells were blocked for 1 h with gelatin-histology buffer (0.1 M PBS, pH 7.4, containing 0.22% gelatin, 0.05% saponin, 1% BSA, and 1% normal serum from the specie in which the secondary antibody was raised). Antibody dilutions and subsequent washes were also performed in this gelatin-histology buffer. Subsequently, cells were incubated overnight at 4ºC with the primary antibody at the appropriate dilution (see Table 1 in Materials for details), washed three times and incubated for 1 h at 20-25ºC in an adequate 1:400 diluted fluorescent dye-conjugated secondary antibody. All secondary antibodies were adsorbed against several species to prevent undesired cross-reactions (see Materials for details). Double-immunostaining was performed in the same way except that mixtures of primary antibodies from two different host species and species-specific secondary antibodies conjugated to different fluorophores were used. Nuclei were counterstained with Hoechst 33342 diluted to 0.1 μg/mL in gelatin histology buffer. Finally, cells were mounted onto glass slides using homemade Mowiol mounting medium containing anti-fade reagent PPD.

Immunofluorescence experiments in isolated nuclei from adult rat cortex were carried out identically, except that saponin was omitted in the first step.

3.3. Microscope studies and imaging

All microscope images were acquired with an epifluorescence microscope Carl Zeiss Axio Observer.Z1, equipped with a HXP120C metal halide lamp illumination source and a high-resolution monochromatic camera (AxioCam MRm, 1388 x 1040 pixels), all from Carl Zeiss MicroImaging, Inc (Gottigen, Germany). Conventional

epifluorescence images were acquired using a 20 x Plan-Apochromat objective (NA 0.8). Higher resolution images were acquired using a structured illumination module (ApoTome) and a XYZ motorized stage (Carl Zeiss MicroImaging, Inc), using a 63 x Plan-Apochromat objective (NA 1.4), and optical sections (0.24 μm intervals in the z-axis) were obtained with the Zeiss ApoTome device, with camera settings adjusted to obtain images with a pixel size of 0.01 μm^2. Bandpass filters used were 49 DAPI (Ex G 365/Em 445/50) for Hoecsht's staining, 38 HE eGFP (Ex 470/40, Em 525/50) for Alexa Fluor 488, and 43 HE Cy3 shift free (Ex 550/ 25, Em 605/70) for Alexa Fluor 568 and DyLight 549. Images were digitized using Zeiss Axio Vision 4.8 software (Carl Zeiss MicroImaging, Inc). A pseudocolor was assigned to each channel and minor despeckling was performed on ImageJ (NIH, Bethesda, MD, USA) software. For illustration, images were exported to TIFF format, and compiled and labeled using Adobe Photoshop CS3 (San Jose, CA, USA).

4. MORPHOMETRIC ANALYSES

4.1. AraC-induced differentiation: neuronal *vs*. non-neuronal phenotypes

Available markers for morphometric analyses, microtubule-associated protein 2 (MAP2), Tau, neurofilaments and β-III-tubulin differ somewhat to the degree that they are expressed in the cell body as opposed to neurites. Because β-III-tubulin was expressed in cell bodies and throughout all neurites of differentiated cells, delivering at the same time high contrast, we chose antibodies against β-III-tubulin as the primary marker for measurements of neurite length, area and arborization. In addition, cells classified as non-neuronal, on the basis of their low or no NeuN/Fox-3 expression and their polygonal morphology, were also immunopositive for β-III-tubulin (see Results). Thus, morphometric analysis of terminally differentiated AraC/NT2N neurons and non-neuronal cells remaining after the 6-day period of treatment with AraC was performed on fluorescence microscope images of cells doubly stained for β-III-tubulin and NeuN/Fox-3, and counterstained with Hoechst 33342. For this purpose, conventional epifluorescence images were acquired using a 20 x Plan-Apochromat objective (NA 0.8). Multiple images from cultures were taken using the Carl Zeiss Mosaic module with focus adjustment. Subsequent stitching and aligning individual images with an overlap of 10% resulted in 2.0 x 1.5 mm mosaic images. Measurements were performed on three mosaic images obtained from three independent experiments. A total of 33

neuronal and 33 non-neuronal cells per mosaic were analysed, starting from the centre of the image. Figures 35A-F correspond to a portion of a mosaic image used for morphometric analysis and depict the different steps of image processing to obtain values of the analysed parameters.

To identify neuronal and non-neuronal cells, absence of or very weak immunolabelling for the neuronal marker NeuN/Fox-3 was used as the first cut-off criterion to classify cells as non-neuronal. Additionally, cells showing weak to moderate immunoreactivity for NeuN/Fox-3 but displaying flat polygonal morphologies and no neurites were also classified as non-neuronal (Figs. 35A-C, arrows). To measure the area of nuclei, binary images were obtained by thresholding the Hoechst channel to include only nuclei using ImageJ software (NIH, Bethesda, MD, USA). Grayscale-converted images from the β-III-tubulin channel allowed for an easy visualization of the whole cell area, including lamellar extensions (Fig. 35D). The NeuN/Fox-3 channel, binary images corresponding to Hoechst staining and inverted grayscale images corresponding to the β-III-tubulin channel were loaded as separate image stacks in ImageJ software. Area of nucleus and total cell area were determined for each cell. In addition, area of cell body and length of neurites was determined for each AraC/NT2N neuron. The area of nuclei was selected on the corresponding stack with the wand (tracing) tool of ImageJ and then measured. Unhealthy or fragmented nuclei and false-positive particles were excluded from the analysis. The total area of cells, including nuclei, was measured after manually tracing cell boundaries, using the polygon selection tool, on the grayscale-converted images corresponding to the β-III-tubulin channel (schematically illustrated in fig. 35E). Cell somata were manually outlined and their area measured. When the boundaries were not clearly defined due to the presence of flat lamellar extensions, β-III-tubulin staining accumulation was used to define the limits of neuronal bodies (Fig. 35F). Neurites were traced using the segmented line tool and their length measured (Fig. 35F).

4.2. RA *vs.* AraC differentiated NT2N neurons

Cell bodies of RA/NT2N neurons were organized into aggregates, making it impossible to discern cell boundaries using conventional fluorescence microscopy. On the other hand, neuronal nuclei of RA/NT2N neurons were considerably smaller than those of AraC/NT2N neurons and could not be accurately analysed under the 20 x

objective. For these reasons, measurements of the area of somata and nuclei of RA/NT2N cells were performed on high-resolution images of virtual sections acquired under the 63 x Plan-Apochromat objective. Z-stacks were then loaded into NIH ImageJ and carefully examined to ensure that measurements were performed at the widest part of each cell soma and nucleus analysed. Measurements were performed using NIH ImageJ software, basically as described above. In our culture conditions, neurites of RA/NT2N cells were organized in bundles, which did not allow the assignment of neurites to individual neuronal bodies and prevented reliable length measurement their length. Hence, in the context of the present study, which focuses on the phenotypic characterization of neurons derived from NT2 progenitors upon AraC treatment, this was not assessed in our study (see also Discussion below).

All data (sections 4.1. and 4.2) represent average values obtained from 99 cells in three independent experiments (33 cells/experiment).

5. TISSUE SAMPLING AND PREPARATION OF SUBCELLULAR FRACTIONS

5.1. Preparation of subcellular fractions from the adult rat cerebral cortex

5.1.1. Animals

Male albine Sprague-Dawley rats, weighing 200–250 g at the time of arrival were obtained from Harlan Iberica (Barcelona, Spain). Upon arrival, animals were randomized and housed three per cage and kept in a controlled environment (12 h light-dark cycle, lights on at 08:00 h A.M., and 22 ± 2°C room temperature) with food and water provided *ad libitum*. The animals, received at 7-8 weeks of age (data provided by the manufacturer), were allowed to acclimate for 1 week prior to any experimentation. On the day of experiments, rats had a weight of at least 250 g. All experimental procedures were carried out during the morning (between 10:00 and 12:00 A.M.). Rats were carefully handled in accordance with the guidelines of the European Communities Council Directive of November 24, 1986 (86/609/EEC).

5.1.2. Tissue preparation

Rats were anesthetized with an overdose of choral hydrate (1 g/kg, i.p.) and then sacrificed by decapitation. For brain extraction, the skin that covers the skull is removed and the skull was opened by two posteroanterior cuts following the outer edge of the

temporal bones with the help of scissors that were introduced in the core hole. After separating these bones with the help of a gouge, the dura was cut and the piece was inverted and for sectioning of cranial nerves arising from the brainstem, optic tracts and olfactory bulbs, allowing the brain to be detached by gravity onto saline. Subsequently, it was placed on a metal plate located on a container with crushed ice to keep the tissue under refrigeration. Then, with the aid of scissors, forceps and filter paper, blood clots and the meninges were removed from the sample and the piece was dissected carefully to obtain different brain regions. Initially, a sagittal incision was made in the central part of the brain to allow the separation of the cerebral hemispheres. Once those are completely separated, the hippocampus was dissected and the cortex separated from diencephalon and basal ganglia. After removing white matter from the cortical sample as much as possible, tissue was stored at -80°C until use.

5.1.3. Tissue fractionation

Preparation of subcellular fractions from rat cerebral cortex, enriched in cytosolic (Cyt) and plasma membrane (P2) proteins, was performed essentially as previously described for rat and human brain tissues (Garro et al., 2001; Sallés et al., 2001). Cortical tissue, stored at -80°C, was cold thawed and transferred to a vessel containing homogenization buffer (20 mM Tris-HCl, 1 mM EGTA, 0.32 M sucrose and 0.01% v/v protease inhibitor cocktail for inhibition of aspartic, cysteine, serine and aminopeptidase peptidases, pH 7,4) in a 1:4 w/v proportion. The brain tissue was homogenized with a Potter-Elvejem glass with Teflon plunger (Braun biotech International), where the distance between the piston and the tubewall is from 0.15 to 0.20 mm. The homogenization process consisted of apply the Teflon plunger to homogenize the sample for a few seconds (7-10 times) at maximum speed (1500 rpm) by an electric motor. During the homogenization process, the mixture was kept refrigerated at 4°C with a ice jacket around the Potter-Elvejem glass to maintain the cold chain and prevent the degradation of the sample. Once that a homogeneous suspension was obtained, more homogenization buffer was added to obtain a 1:10 w/v proportion, again it was mixed gently and the whole solution was divided into centrifuge tubes. These tubes were subjected to a centrifugation at 1100 x g for 10 min at 4°C in a high speed refrigerated centrifuge (centrikon T-42K, KONTRON). The pellet (P1, containing unbroken cells, debris and nuclei) was discarded and the supernatant was centrifuged again at 4000 x g for 10 min, making a total of three cycles of resuspension-centrifugation with the

homogenization buffer keeping the proportion of 1:10 w/v with respect to the original tissue sample. The first of these supernatants constituted the cytosolic fraction (Cyt), which was divided in 1 mL aliquots and stored at -80°C until use. After the third centrifugation, the obtained pellet (P2) is enriched in plasmatic membrane (Fig. 14).

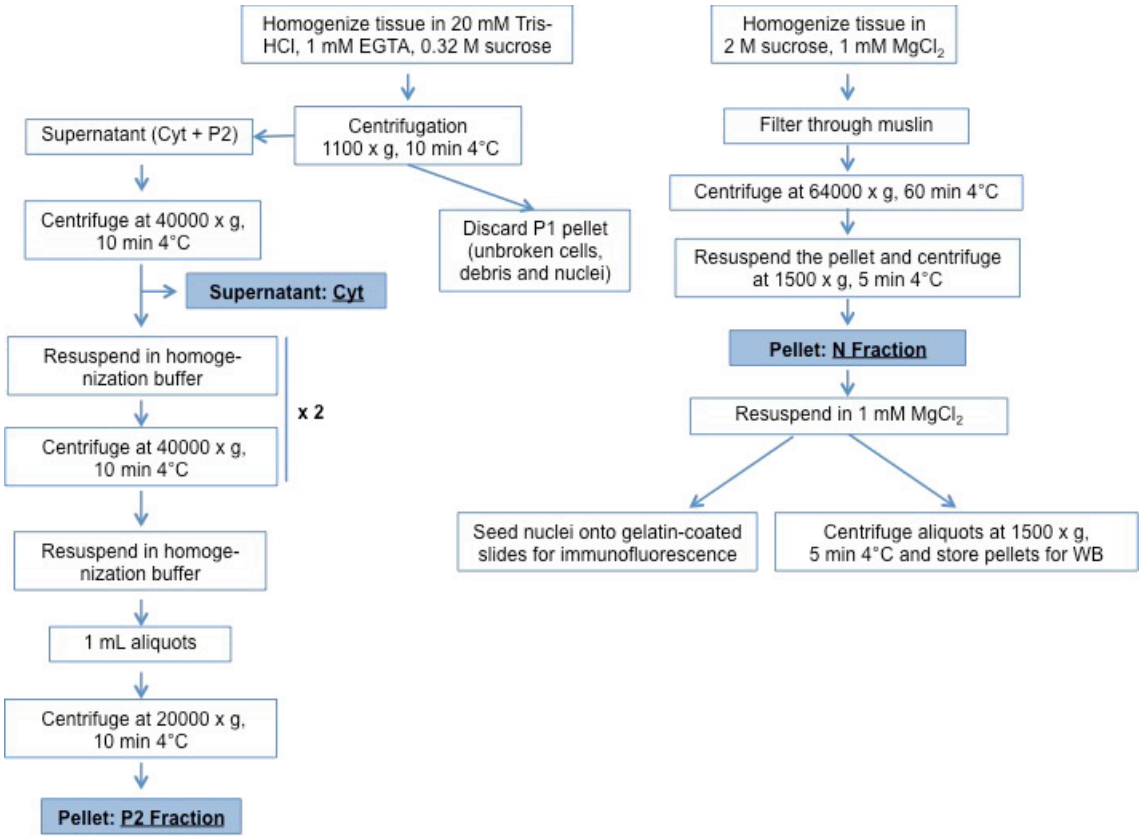

Figure 14. Schematic diagram showing the procedure to obtain subcellular fractions enriched in cytosol (Cyt), crude membranes (P2) and "isolated nuclei" (N).

To obtain highly purified intact nuclei, useful for both immunofluorescence and Western blot analyses, we used the procedure previously reported by Thompson (1973) and Dent et al. (2010) with slight modifications. Cerebral cortices dissected from four adult rats were placed in ice-cold 0.32 M sucrose containing 1 mM $MgCl_2$ and protease inhibitors. The cortices were then chopped finely and homogenized to give a 20% (w/v) homogenate in 2 M sucrose containing 1 mM $MgCl_2$ and protease inhibitors. The homogenate was then diluted with and equal volume of homogenizing medium, filtered through muslin and centrifuged at 4ºC for 60 min at 64000 x g in a SW40Ti rotor (Beckman, 331302) at 4ºC. The resulting pellet was washed with 0.32 M sucrose containing 1 mM $MgCl_2$ and protease inhibitors, and centrifuged for 5 min at 1500 x g to obtain a final pellet of highly purified intact nuclei (N fraction). Finally, nuclei were resuspended in a volume of 10 mL of 1 mM $MgCl_2$ (containing protease inhibitors) and

counted under a light-phase microscope. Nuclei set aside for Western blot analysis were divided into aliquots of 4 x 10^6 nuclei, pelleted by centrifugation at 1500 x g for 5 min, and stored at -80ºC until use. Nuclei used for immunofluorescence analysis were resuspended in TM2 buffer (10 mM Tris-HCl, pH 7.4, 2 mM $MgCl_2$, 0.5 mM PMSF, 50 μM iodoacetamide) at a dilution of 2 x 10^6 nuclei/mL. Finally, 25 μL drops were laid on gelatin-coated slides, allowed to dry at room temperature, and stored at -80ºC until use (Fig. 14).

The total protein content determination of each subcellular fraction was performed by the Bradford method (Bradford, 1976) using bovine γ-globulin as protein standard. All samples were resuspended in homogenization buffer and brought to an estimated concentration of ~1.0-2.0 μg/μL on the basis of our previous experience. Thereafter, the the γ-globulin stock (2.0 μg/μL) and the samples (~1.0-2.0 μg/μL) were diluted 80-fold with distilled H_2O, thus obtaining a 25 μg/μL γ-globulin solution (A solution) and a 80-fold diluted experimental sample (B solution). Before measurement, four serial dilutions of standard A solution and from each sample were prepared in duplicate as follows:

A solution: γ-globulin standard (25 μg/μL)			B solution: experimental sample	
[γ-globulin] = μg/mL	Volume A solution (μL)	H_20 (μL)	Volume B solution (μL)	H_20 (μL)
0	0	1000		
2.5	100	900	100	900
5.0	200	800	200	800
7.5	300	700	300	700
10.0	400	600	400	600

Table 5. Serial dilutions of γ-globulin standards and experimental samples for estimation of total protein concentration using the Bradford method.

Thereafter, a volume of 200 μL of Bradford dye reagent was added to each tube of the serial dilutions of γ-globulin standard and experimental samples. Tubes were then mixed by vigorous shaking or vortex for ~5 sec, and Bradford dye was allowed to react for 10 min. Thereafter, the absorbance was measured at 595 nm using a spectrophotometer. Blank was subtracted from the absorbance values, and data of absorbance *vs*. concentration (γ-globulin or experimental samples) were fitted by linear regression analysis. Protein concentration present in the original experimental samples (before the 80-fold dilution) of Cyt, P2, and N samples was calculated as follows:

$$[\text{Protein}]_{\text{sample}} = m'/m \text{ x } 80 \text{ x } 25 \text{ μg/mL}$$

Where m' and m are the slopes corresponding to the linear fits of the γ-globulin and the experimental sample, respectively, 80 is the fold dilution of the 2 μg/μL γ-globulin

stock and of the original samples and 25 µg/mL is the concentration γ-globulin in A solution (achieved by 80-fold dilution of the γ-globulin stock at 2 µg/µL).

5.2. Preparation of subcellular fractions from NT2 cultures

Isolation of cell nuclei from cells in culture usually involves a first solubilization step using non-ionic detergents, resulting in cells being fractionated in two fractions. One of them consisting of a mixture of plasma membrane, cytosol and intracellular organelles, and another one consisting of highly purified nuclei (Fiume et al., 2010). Here we carried out a modification of this procedure to enable obtaining a fraction of highly purified nuclei (N), on the one hand, and separating the plasma membrane (P2) and the intracellular heavy membranes (S2) from the cytosol (Cyt), on the other hand.

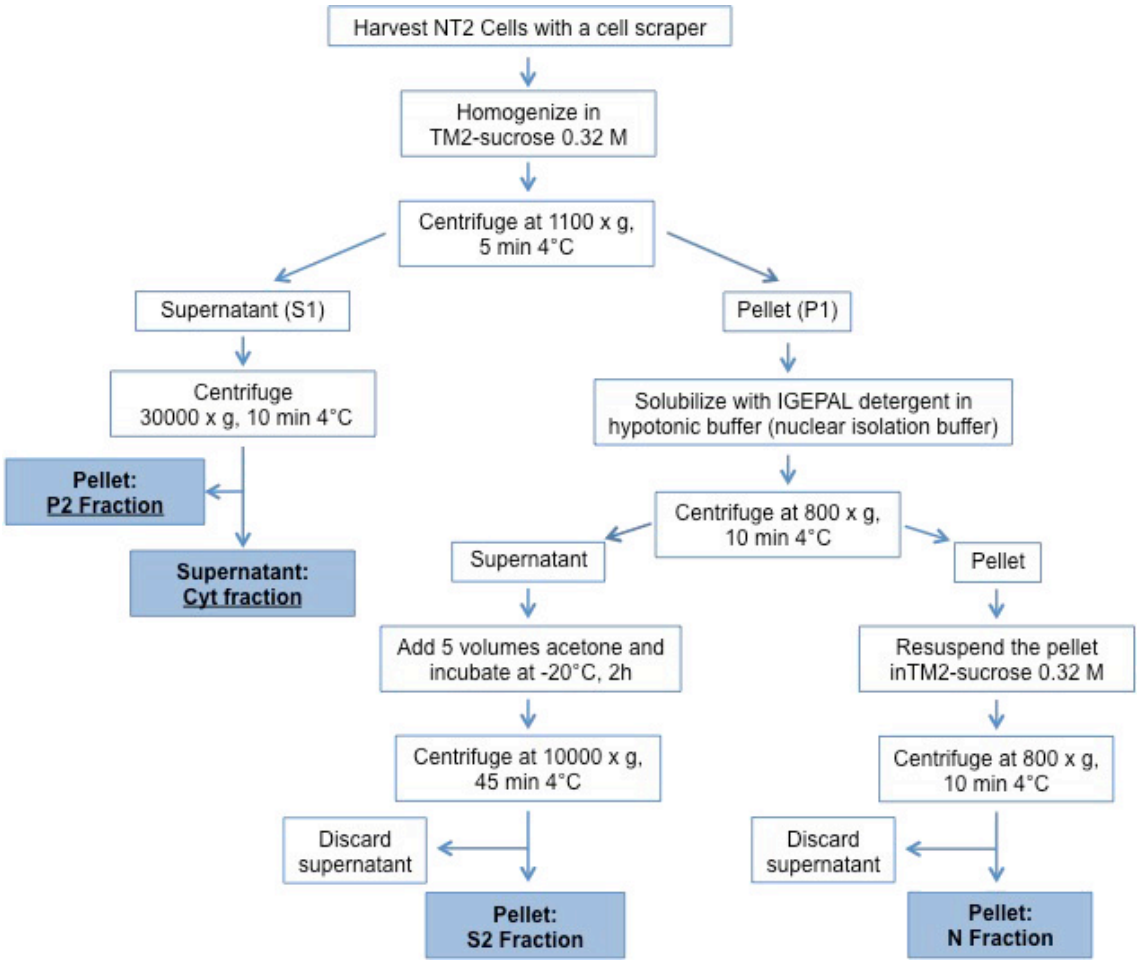

Figure 15. Schematic diagram showing processing of NT2 cells to obtain fractions enriched in cytosol (Cyt), plasma membrane (P2), heavy membranes (S2) and "isolated nuclei" (N) fractions.

NT2 progenitors, either untreated or treated with AraC during 72 h or 6 days, were harvested from 150 cm^2 flasks. Cells were released from the surface of the culture flasks

using a cell scraper, collected in cold PBS and spun down at 500 x g for 5 min at 4ºC. Cells harvested from each 150 cm^2 culture flask were resuspended in 500 µL of 0.32 M TM2 buffer (10 mM Tris-HCl, pH 7.4, 2 mM $MgCl_2$, 0.5 mM PMSF, 50 µM iodoacetamide) and homogenized by 20 strokes through a syringe with a 20-gauge needle. The homogenate was then subjected to a centrifugation at 1100 x g for 5 minutes at 4°C in a high speed refrigerated centrifuge (centrikon T-42K, KONTRON). The resulting supernatant (S1) and pellet (P1) were further processed to obtain plasma membrane (P2), cytosolic (Cyt), heavy membranes (S2) and highly purified nuclei (N).

Centrifugation of the first supernatant (S1) at 30000 x g for 10 min at 4°C allowed to obtain a plasma membrane pellet (P2) and cytosolic (Cyt supernatant) (Fig. 15). To separate nuclei (N) from heavy membranes (S2), the P1 pellet, resulting from the first low-speed centrifugation step, was resuspended in 500 µL of cold nuclear isolation buffer (TM2, 1% Igepal and 10 mM β-Mercaptoethanol) and then incubated for 8 min on ice. The presence of the non-ionic detergent Igepal in this solution leads to solubilization of membranes, thus allowing separation of nuclei from attached membranes. To remove the external nuclear membrane, 500 µL of pre-chilled distilled water was added to the 500 mL suspension. This suspension was then subjected to 20 passages through a syringe with a 21-gauge needle and checked on a phase contrast microscope to make sure that nuclei had lost their outer envelope. Passages through the needle were repeated as many times as needed, until nuclei completely stripped of the envelope, but still intact. The nuclear fraction was recovered in a translucent, glassy, and semitransparent pellet by centrifuging the suspension 800 x g for 10 min at 4°C. The supernatant was kept for acetone precipitation of proteins, whereas the nuclear pellet was resuspended in TM2 buffer containing 0.32 M sucrose and centrifuged at 800 x g to obtain a final white pellet of highly purified nuclei (N). The supernatant containing heavy membranes was mixed with 5 volumes of cold acetone (-20ºC) and incubated for 2 h at -20ºC. The protein precipitate (S2) was collected by centrifugation at 10000 x g for 45 min at 4°C. The supernatant was discarded and the pellet resuspended in distilled water. The suspensions were split into four aliquots at the final centrifugation steps. Aliquots of the N fraction were treated with 1 µL (10 IU) RNase-free recombinant DNase I (Takara Bio Inc.) in nuclear isolation buffer for 20 min at 37ºC to favor access of bicinchoninic acid (BCA) reagent, (used to determine protein concentration) to nuclear proteins. One of the DNAse I-treated aliquots was set aside for BCA assay and the rest were treated with 0.25 M $(NH_4)_2SO_4$ to release chromatin-

bound proteins. For this purpose, a volume of 2 M $(NH_4)_2SO_4$ was added dropwise to the DNase I-treated nuclear suspension to achieve a final concentration of 0.25 M, followed by 15 min incubation on ice. In our hands, optimal migration of nuclear proteins was only achieved by sequential treatment with DNase I and high-salt (0.25 M $(NH_4)_2SO_4$).

For BCA assays, all samples were brought to an estimated concentration of ~0.25-0.5 μg/μL, on the basis of our previous experience and three two-fold serial dilutions of each sample were made. 50 mL of each sample were loaded in duplicate to 96-well EIA/RIA plates and mixed with BCA copper reagent (100 μL/well). Reference BSA standards were loaded in parallel at increasing protein concentration (0, 0.02, 0.04, 0.08, 0.16, 0.32, 0.64 μg/μL). After a 1 h incubation at 37ºC, absorbance was measured at 562 nm using a Sunrise (Tecan) plate reader. Blank was subtracted from the absorbance values, and data of absorbance *vs*. BSA concentration were fitted by linear regression analysis, allowing determination of the actual protein concentration in Cyt, P2, S2 and N samples.

6. WESTERN BLOT ANALYSIS

6.1. Western blot

Western blot was performed as previously reported (Garro et al., 2001; López de Jesús et al., 2006; Ruiz de Azúa et al., 2006; Montaña et al., 2012) with minor modifications. Briefly, three volumes of sample were mixed with one volume of 4X urea denaturation buffer (300 mg urea, 50 mg SDS, 120 mg DTT, 500 μL 100 mM Tris-HCl, pH 8.0, 6 μL bromophenol blue 1% -w/v-) and boiled for 5 min. Denatured proteins were resolved by electrophoresis on sodium dodecyl sulfate-polyacrylamide (SDS–PAGE) gradient gels (5 to 10%, depending on the molecular mass of proteins to be resolved) using the Mini Protean II gel apparatus (Bio-Rad, Hercules, CA, USA) for about 2 h at 100 V. Proteins were transferred to 100% methanol-activated polyvinylidene fluoride (PVDF) membranes using the Mini TransBlot transfer unit (Bio-Rad, Hercules, CA, USA) at 90 V constant voltage for 1 h at 4ºC. Thereafter, PVDF membranes were then briefly washed with distilled H_2O and allowed to dry and re-activated in 100% methanol. After a washing step of 10 min in washing buffer (phosphate buffer 0.2 M, pH 7.5, Tween-20 0.1 %) at room temperature, membranes were incubated in blocking buffer (PB 0.2 M, pH 7.5, Tween-20 0.2 %, non-fat dry milk

5%, BSA 0.5%) for 1 h at room temperature, followed by overnight incubation at 4 ºC with the corresponding primary antibodies diluted in blocking buffer at the adequate concentrations (see Materials, Table 1). Blots were washed and incubated with specific HRP-conjugated secondary antibodies diluted to 1:10000 in blocking buffer for 2 h at room temperature. Immunoreactive bands were revealed with the Clarity Western ECL system from BioRad, according to the manufacturer instructions, and either developed on x-ray films or acquired using an ImageQuant 350 digital image system (GE Healthcare).

6.2. Immunodetection and measurements

Immunoreactive bands developed on X-ray films were digitized using a transmittance scanner. Digital images of immunoreactive bands, either digitized from X-ray films using a transmittance scanner or acquired using the ImageQuant 350 imager device, were quantified by densitometry using ImageJ image analysis software (ImageJ, NIH, Bethesda, MD, USA). For comparison of protein expression between samples, two types of semiquantitative analysis were performed depending on the amount of sample available. The most accurate determinations involved SDS-PAGE analysis of increasing concentrations of total protein from all samples to be compared, which were run in parallel. Integrated optical density (OD) values from bands were used for linear regression analysis, which enabled to obtain a linear regression equation for each sample. The fold-change was then obtained by calculating the ratio between the slope of the curve in a given experimental sample and the slope of the curve in the reference sample (control condition). When the amount of protein was limiting, the fold-change was determined by directly calculating the ratio between OD obtained from immunoreactive bands after resolving equal amounts of protein from all samples. When it was possible, data were normalized to β-Actin or CyPA. When these controls were useless because their expression was different among samples to be compared, Coomassie Brilliant Blue gel staining was used to check for equal protein loading.

7. FÖRSTER/FLUORESCENCE RESONANCE ENERGY TRANSFER MICROSCOPY (FRET)

Differentiating NT2 and PC12 living cells co-expressing TRAX-eCFP and PLCβ1-eYFP were viewed under an Olympus Fluoview FV1000 laser confocal microscope.

Only cells with similar expression of both eCFP and eYPF, such that both channels could be set at the same voltage and gain for a specific series of studies, were analyzed. Using Olympus software, FRET efficiency in TRAX-eCFP and PLCβ1-eYFP expressing cells was determined by sensitized emission after correction for spectral bleed through by analyzing images of control cells expressing donor proteins alone or acceptor proteins alone with the same intensity distributions as the sample, as previously described (Guo et al., 2010). The FRET efficiency (E) is calculated as shown in Equation 1,

$$E = 1 - \epsilon/(\epsilon + \mathrm{nFRET} \cdot r\Psi \cdot rQ) \qquad \text{(Eq. 1)}$$

where ϵ is the fluorescence in the CFP channel, $r\Psi$ is the ratio of the detector response of the CFP and YFP channels, and rQ is the ratio of the quantum yields of the CFP and YFP. nFRET is equal to the image obtained in the FRET channel minus bleed through in CFP (a) and YFP (b) channels as shown in Equation 2,

$$\mathrm{nFRET} = \mathrm{FRET} - a\mathrm{CFP} - b\mathrm{YFP} \qquad \text{(Eq. 2)}$$

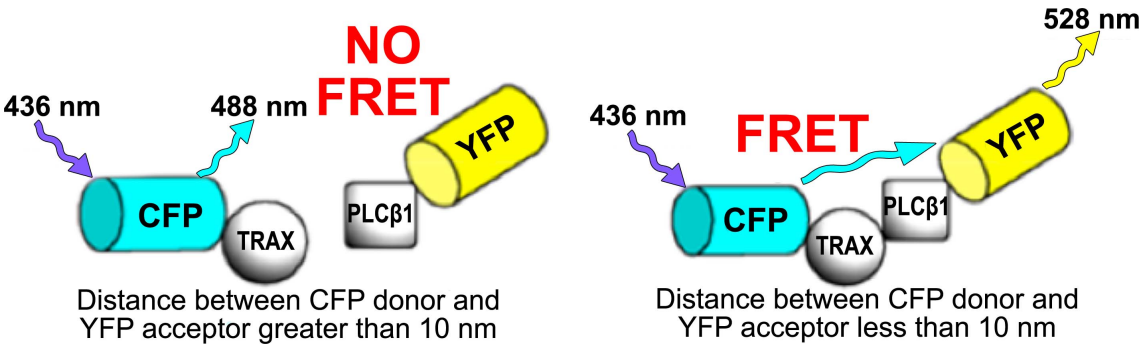

Figure 16. Schematic illustration of FRET experiments design. Constructions used consisted of TRAX-eCFP and PLCβ1-eYFP fusion proteins. Förster resonance energy transfer (FRET) consists of energy transfer between two light-sensitive fluorescent dyes (fluorophores). Fluorophores are chosen so that the emission spectrum of one of them (donor) overlaps significantly with the excitation spectrum of the other one (acceptor). During FRET, the CFP donor excited by a light source, transfers its energy to the YFP acceptor only if it they are in close proximity. This causes the YFP to emit light at a longer wavelength than the light emitted by CFP. The efficiency of this energy transfer is inversely proportional to the sixth power of the distance between donor and acceptor, making FRET extremely sensitive to small changes in distance and one of the best tools for the analysis of protein-protein interaction.

Using controls with the same intensity distributions as the samples, we found that FRET efficiency values did not change significantly over a 10-fold range of acceptor:donor intensity ratios. Background FRET values were obtained by imaging cells co-expressing eCFP and eYFP, resulting in an nFRET = 0.014 ± 0.001 for all negative controls, including free eCFP and free eYFP and free eCFP and eYFP-PLCβ1.

Positive control values were obtained using a dodecapeptide labeled with eCFP and eYFP on both ends (*i.e.* eCFP-X_{12}-eYFP), resulting in an FRET = 0.26 ± 0.006.

8. CLONING

8.1. General procedures

8.1.1. Agarose gel electrophoresis

To prepare 0.8 or 1% agarose gels used here, 50X TAE buffer was diluted to 1X using double distilled H_2O (final composition, 40 mM Tris-acetate, 1 mM EDTA). Thereafter, 1.2 g or 1.5 g of agarose were boiled in 150 mL TAE 1X under continuous stirring by a magnetic stirrer until the solution appeared homogeneous. Evaporated distilled H_2O was replenished when necessary to maintain the initial volume. The agarose solution was allowed to coil to approximately 60ºC before preparing the gel. Five volumes of DNA were mixed with one volume of 5X loading dye before gel loading. 100 bp and/or 1 kb DNA ladders were prepared and run in parallel with the DNA samples. For preparative gel electrophoresis, DNA samples were run at 90 V for about 2 h in cold 1X TAE buffer using a horizontal gel electrophoresis device (BioRad, BioRad, Wide Mini-Sub Cell GT System). For screening by restriction mapping, electrophoresis was performed using a electrophoresis device specially designed for minigel electrophoresis (Mupid® One Electrophoresis System, Eurogentec) at 135 V for 30 min. 100 bp and/or 1 kb DNA ladders were prepared and run in parallel to the samples. After electrophoresis, gels were stained with GelRed nucleic acid stain following the manufacturer's instructions. Visualization of DNA band and image acquisition was performed by UV light transillumination using an ImageQuant 350 digital image system (GE Healthcare) (see Materials section for details on reagents).

8.1.2. Extraction of DNA after preparative agarose gel electrophoresis

The DNA fragments were directly visualized on the UV light transilluminator and the DNA fragments were excised from the agarose gel with a clean scalpel. Extraction of the DNA fragments from the gel slice was performed using Nucleospin Gel and PCR Clean-Up following the manufacturer's instructions. DNA fragments were eluted in 30-50 µL ultrapure culture grade H_2O. DNA concentrations were estimated using NanoDrop ND-1000 Spectrophotometer by measuring absorbance at 260 nm. Protein contamination was assessed by the ratio of 260/280 nm absorbance readings. Ratios in

the range of 1.7-1.9 were considered acceptable. Other contaminants were assessed by the ratio of 260/230 nm absorbance reading. Values in the range of 2.0-2.2 were considered acceptable.

8.1.3. Transformation of chemically competent cells

10 µL of One Shot® TOP10 chemically competent *E. coli* cells were thawed on ice and 1 µl plasmid (diluted to 0.1 µg/µL) was added to the cells and mixed by gently stirring the pipette tip in a 500 µL Eppendorf tube. After 30 min on ice, were given a heat shock at 42°C for 30 sec in a water bath, followed by incubation on ice for 2 min. Thereafter, cells were grown in 200 µL LB at 37°C for 1 h with agitation and under aerobic conditions. After the hour cells were grown on agar plates with appropriate antibiotics for selection. Plates were incubated upside-down at 37°C overnight. Transformation with ligation products was performed identically except that 50 µL of chemically competent *E. coli* cells and 5 µL of ligation product were used for transformation.

8.1.4. Bacterial growth for amplification of plasmids

One individual colony from those grown in agar plate was inoculated in either 6 mL (for miniprep purification) or 45 mL (form midiprep purification) of LB containing the appropriate antibiotic for selection and grown overnight at 37°C with agitation and under aerobic conditions. Thereafter, bacteria were spun down by centrifugation at 5000 x g for 15 min, and plasmid was purified using NucleoSpin® Plasmid or NucleoBond® Xtra Midi Plus kits following the manufacturer's instructions (see Materials for further details).

8.2. shRNA constructions

8.2.1. Design

Small hairpin (or short hairpin) RNAs (shRNAs) consists of an artificial tight hairpin turn used to silence target genes via the endogenous RNA interference machinery (see Introduction, Fig. 11). Expression of shRNA in eukaryotic cells is typically accomplished by delivery of complementary DNA (cDNA) encoding for shRNA through either viral or plasmidic vectors. shRNA is an advantageous mediator of RNAi in that it has a relatively low rate of degradation and turnover. The use of

shRNA technology instead of duplex short RNAs encoding for siRNAs has two major advantages. First, vectors can be designed such that an inducible promoter controls the shRNA expression. Second, degraded siRNA is continuously replaced by newly synthesized shRNA. These features, overcome two major limitations of duplex siRNAs, i.e., the lack spatial and temporal control.

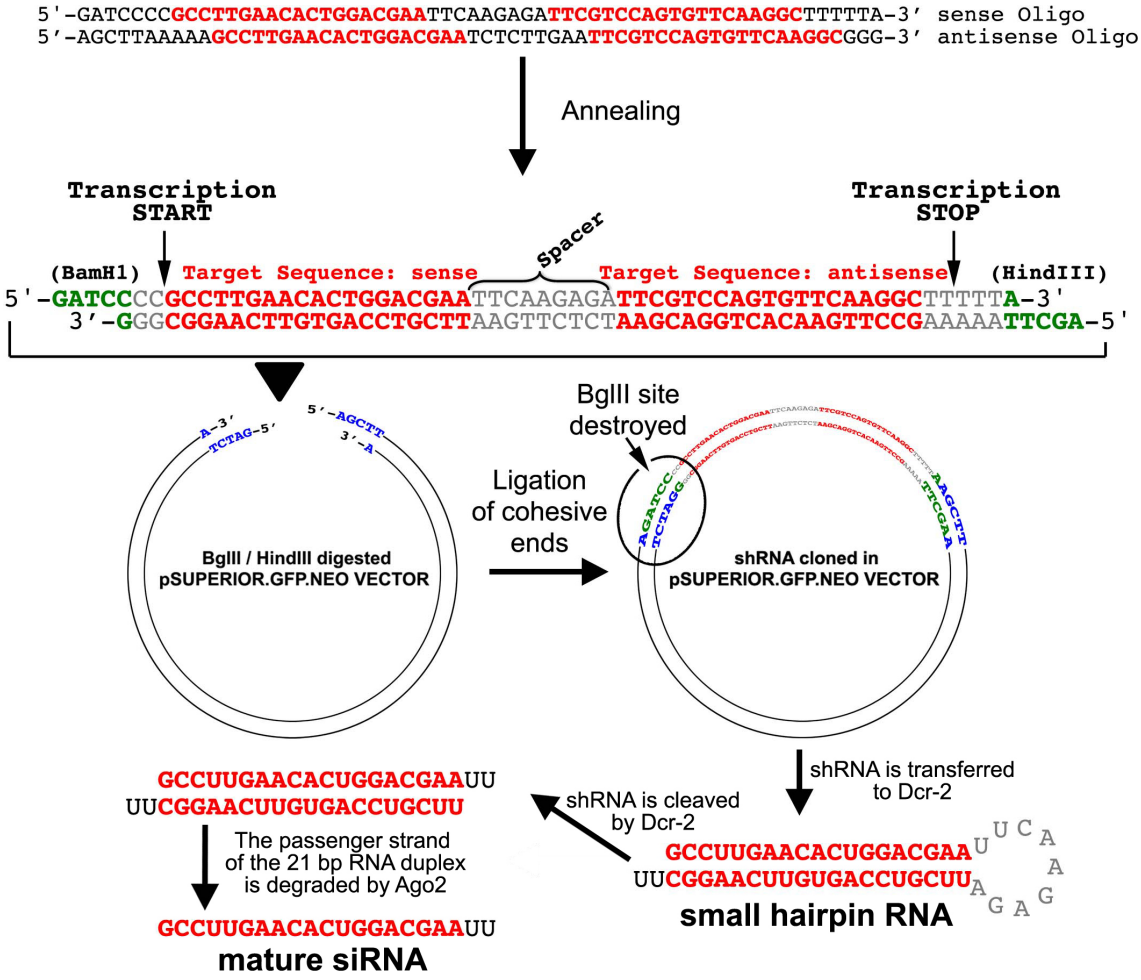

Figure 17. Schematic drawing summarizing the major steps for cloning of shRNAs into the eukaryotic expression vector pSuperior.gfp/neo and processing of shRNA to generate mature siRNA.

Here we used the pSuperior.gfp/neo plasmid (see Materials, Table 3), in which a DNA duplex encoding for the desired shRNA sequence can be easily inserted downstream the polymerase-III H1-RNA gene promoter. In the pSuperior.gfp/neo the H1 promoter is modified in a sequence between the TATA box and the RNA hairpin transcription start site to contain the tetracycline operator 2 (TetO2) site that serves as the binding site for two molecules of the Tet repressor. Although we did not use this feature in the present study, in the absence of tetracycline, transcription of shRNA is repressed in cell lines stably expressing the Tet repressor (TetR), and shRNA expression

can be induced by tetracycline. Additionally, the plasmid contains an EGFP reporter gene under the control of the PKG promoter to monitor transfection rate, and a neomycin resistance gene under control of separate PGK promoter for antibiotic selection of stable shRNA transfectant.

DNA duplexes encoding for shRNAs are obtained by annealing of synthetic oligonucleotide pairs containing the target sequence (21 nucleotides (nt)) in both sense and antisense orientation, separated by a 9-nucleotide spacer. DNA oligonucleotides are designed such that: [i] form BamHI and HindIII sticky ends upon annealing for insertion into the BglII/HindIII-digested vector, [ii] when inserted, DNA duplexes have a well-defined start of transcription and a termination signal consisting of five thymidines (T) in a row (T5) [iii] the cleavage of the transcript at the termination site is after the second uridine (U), yielding a transcript resembling the ends of synthetic siRNAs, which also contain two 3' overhanging T or U (nt). Because the BamH1 and BglII overhangs are cohesive, the resulting double stranded sequence can be inserted in the BglII/HindIII-digested pSuperior.gfp/neo vector. This leads to destruction of the BglII site, which facilitates screening of positive clones by digestion with BglII combined with a second restriction enzyme followed by agarose gel electrophoresis (Fig. 17).

8.2.2. Oligonucleotides

Code	Sequences
shRNA-01	Ss: 5' GATCCCC**GCGCGCTTTGTAGGATTCG**TTCAAGAGA**CGAATCCTACAAAGCGCGC**TTTTTA 3' As: 5' AGCTTAAAAA**GCGCGCTTTGTAGGATTCG**TCTCTTGAA**CGAATCCTACAAAGCGCGC**GGG 3'
	5' GATCCCC**GCGCGCTTTGTAGGATTCG**TTCAAGAGA**CGAATCCTACAAAGCGCGC**TTTTTA 3' 3' GGG**CGCGCGAAACATCCTAAGC**AAGTTCTCT**GCTTAGGATGTTTCGCGCG**AAAAATTCGA 5'
shRNA 87	Ss: 5' GATCCCC**GGAAAGTGACGACGACGA**TTTCAAGAGA**ATCGTCGTCGTCACTTTCC**TTTTTA 3' As: 5' AGCTTAAAAA**GGAAAGTGACGACGACGAT**TCTCTTGAA**ATCGTCGTCGTCACTTTCC**GGG 3'
	5' GATCCCC**GGAAAGTGACGACGACGA**TTTCAAGAGA**ATCGTCGTCGTCACTTTCC**TTTTTA 3' 3' GGG**CCTTTCACTGCTGCTGCT**AAAGTTCTCT**TAGCAGCAGCAGTGAAAGG**AAAAATTCGA 5'
shRNA-89	Ss: 5' GATCCCC**CGCAAAGTAAACGGCAAGA**TTCAAGAGA**TCTTGCCGTTTACTTTGCG**TTTTTA 3' As: 5' AGCTTAAAAA**CGCAAAGTAAACGGCAAGA**TCTCTTGAA**TCTTGCCGTTTACTTTGCG**GGG 3'
	5' GATCCCC**CGCAAAGTAAACGGCAAGA**TTCAAGAGA**TCTTGCCGTTTACTTTGCG**TTTTTA 3' 3' GGG**GCGTTTCATTTGCCGTTCT**AAGTTCTCT**AGAACGGCAAATGAAACGC**AAAAATTCGA 5'
shRNA-97	Ss: 5' GATCCCC**GGACCCCAAATTACGTGAA**TTCAAGAGA**TTCACGTAATTTGGGGTCC**TTTTTA 3' As: 5' AGCTTAAAAA**GGACCCCAAATTACGTGAA**TCTCTTGAA**TTCACGTAATTTGGGGTCC**GGG 3'
	5' GATCCCC**GGACCCCAAATTACGTGAA**TTCAAGAGA**TTCACGTAATTTGGGGTCC**TTTTTA 3' 3' GGG**CCTGGGGTTTAATGCACTT**AAGTTCTCT**AAGTGCATTAAACCCCAGG**AAAAATTCGA 5'
shRNA-99	Ss: 5' GATCCCC**GATTTCACTCCAGAAGTGT**TTCAAGAGA**ACACTTCTGGAGTGAAATC**TTTTTA 3' As: 5' AGCTTAAAAA**GATTTCACTCCAGAAGTGT**TCTCTTGAA**ACACTTCTGGAGTGAAATC**GGG 3'
	5' GATCCCC**GATTTCACTCCAGAAGTGT**TTCAAGAGA**ACACTTCTGGAGTGAAATC**TTTTTA 3' 3' GGG**CTAAAGTGAGGTCTTCACA**AAGTTCTCT**TGTGAAGACCTCACTTTAG**AAAAATTCGA 5'

Table 6. Sequences of sense (Ss) and antisense (As) oligonucleotide pairs used to generate duplex DNA with BamHI and HindIII sticky ends (blue dashed cells).

Oligonucleotides for cloning of shRNAs targeting human PLCB1 mRNA (NCBI accession, NM_015192) into the pSuperior.gfp/neo were purchased from OligoEngine

(Seattle, WA, USA). Two of the four shRNAs (shRNA-97 and shRNA-99) were designed by Dr. Marion Benoist (Mediterranean Institute of Neurobiology -INMED-, Luminy, Marseille) and the other two (shRNA-97 and shRNA-99) were designed using Oligoengine software (www. oligoengine.com). The oligonucleotides to generate the negative control or scramble shRNA (Table 6, shRNA-01) were purchased from OligoEngine.

8.2.3. BglII/HindIII digestion of pSuperior.gfp/neo plasmid

Digestion of pSuperior.gfp/neo vector was performed sequentially. HindIII digestion was performed for 1 h at 37 ºC in the following reaction mixture:

- 67 µL ultrapure culture grade H_2O (to achieve a final volume of 100 µL).
- 10 µL of plasmid (1 µg/µL).
- 10 µL NEB Buffer 2 10X.
- 3 µL HindIII enzyme.

The digestion product was purified by Nucleospin Gel and PCR Clean-Up DNA purification kit using the manufacturer's instructions, eluted in 50 µL and digested with BglII enzyme for 1 h at 37ºC in the following reaction mixture:

- 19 µL ultrapure culture grade H_2O (to achieve a final volume of 80 µL).
- 50 µL of Hind III-digested plasmid.
- 8 µL NEB Buffer 3 10X.
- 3 µL BglII enzyme.

After digestion, purification of the linearized plasmid was performed by extraction from a preparative 1% agarose gel after being resolved by electrophoresis (see sections 8.1.1. and 8.1.2.).

8.2.4. Oligonucleotide annealing

Stock oligonucleotides 100 µM were ditulted at a working concentration of 0.2 µM (1:500 dilution) in annealing buffer (100 mM NaCl, 50 mM HEPES, pH 7.4). For annealing of oligonucleotide pairs (Table 6) 1 µL of each of the complementary oligonucleotides (0.2 µM) were mixed with 48 µl of annealing buffer. Finally, annealing was performed in a thermocycler (BioRad, MyCycler™ Thermal Cycler System) using the following program: 94ºC for 4 min, 80ºC for 4 min, 75ºC for 4 min, 70ºC 4 min, 4ºC, with cooling rate of 2ºC/sec between annealing steps.

8.2.5. Ligation

For ligation of DNA 2 µl of each 10-fold diluted annealed oligonucleotides and 1 µl BglII/HindIII digested pSuperior.gfp/neo were added to 9.5 µL culture grade ultrapure H_2O. After adding 1.5 µl T4 DNA ligase buffer 10X and 1 µL T4 DNA ligase, the mixture was mixed by vigorous shaking or vortex for ~5 sec and incubated overnight at 16ºC. As a negative control ligation was performed in the absence of annealed oligonucleotides.

To minimize the appearance of false positives, 1 µL BglII was added to each tube containing the different ligation products before transforming chemically competent *E. coli* cells. Because the BglII site is destroyed upon ligation, only recircularized vectors with no insert are cleaved, thus preventing their replication. Transformation of bacteria with the different ligation products was performed as described above (see section 8.1.3.).

8.2.6. Screening of positive clones

For screening, three independent positive clones from each ligation were grown for miniprep plasmid purification as described above (see section 8.1.4.) and eluted in 50 µL ultrapure culture grade H_2O. Thereafter, purified plasmids were digested by HindIII and EcoRI restriction enzymes for 1 h at 37ºC in the following reaction mixture:

- 33 µL ultrapure culture grade H_2O.
- 10 µL of the plasmid eluate.
- 5 µL NEB Buffer 2 10X.
- 1 µL HindIII enzyme.

The digested DNA was resolved by agarose gel electrophoresis in a minigel system and DNA bands were visualized as described above (see section 8.1.1.).

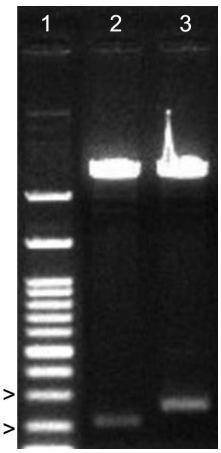

Figure 18. Example of a negative (lane 2) and a positive clone (lane 3) digested with EcoRI and HindIII restriction enzymes. The expected size of restriction fragments for the recircularized vector were 5020 and 228 bp, whereas those expected for shRNA insert-containing plasmid were 5202 and 282 bp. As it can be observed, the lower band in lanes 2 and 3 are consistent with restriction maps expected for a recircularized and a shRNA insert-containing vector, respectively.

Finally, sequencing of positive shRNA clones was performed by STAB-Vida (Lisbon, Portugal) with M13-RV primer. Once the clones were checked for the correct sequence, DNA from one clone corresponding to each shRNA was amplified for midiprep purification as described in 8.1.4. These plasmids were ready for cell transfection.

8.3. Generation of pCDNA3-N-PLCβ1a- and pCDNA3-N-PLCβ1b-cloning vectors

8.3.1. Design

We designed a cloning strategy to generate pCDNA3-N-PLCβ1a- and pCDNA3-N-PLCβ1b N-terminal cloning vectors for easy insertion of short DNA duplexes at the beginning of the human PLCB1a and PLCB1b coding sequences. By this way N-terminal cloning vectors can be easily engineered to encode native or N-terminal tagged human PLCβ1a and PLCβ1b proteins. At the same time, the cloning strategy served to remove large 5'- and 3' untranslated regions (UTRs) from the original plasmids pCMV6-XL6-PLCB1a and pCMV6-XL6-PLCB1b (OriGene Technologies, Burlington, Ontario, Canada), that could contain elements for endogenous regulation of translation (Chatterjee and Pal, 2009).

8.3.2. Generation of pCDNA3-N-PLCβ1a N-terminal cloning vector

To generate pCDNA3-N-PLCβ1a N-terminal cloning vector, AgeI and NotI restriction sites were introduced at the beginning and end of the human PLCB1a and PLCB1b coding sequences by polymerase chain reaction (PCR), using pCMV6-XL6-PLCB1a as matrix. AgeI restriction site was introduced downstream the ATG start codon of PLCB1a coding sequence and NotI restriction site was introduced a few bases downstream the TGA stop codon of PLCB1a. To this end, the following primer pairs were used:

PLCb1_AgeI_Fw 5' aCCGGtGTGCACGCCTTGCAAC 3'
PLCb1a_NotI_Rv 5' GcgGccGCCATGCAATTTCTG 3'

The sequences in yellow correspond to AgeI and NotI restriction sites. Lowercase letters correspond to nucleotides non complementary to the DNA sequence to be amplified by PCR.

8.3.2.1. Polymerase chain reaction (PCR)

The following master mixture was prepared by adding each component in the indicated order:

	Volume	**Final concentration**
H_2O	130 µl	
5 X PCR buffer	40 µl	1 x (contains 2 mM Mg^{++})
dNTPs mix 10 mM	6 µl	0.3 mM each
Primer Fw 10 µM	6 µl	0.3 µM
Primer Rv 10 µM	6 µl	0.3 µM
HiFi Taq Polymerase	6 µl	1.5 units / 50 µl
Total volume	**194 µl**	

Prepare four PCR tubes were prepared as follows:

Tube number	**Master mixture**	**Matrix (pCMV6-XL6-PLCb1a vector 1µg/µL)**
1	48.5 µL	1.5 µL H_2O
2	48.5 µL	1.5 µL matrix 1/10
3	48.5 µL	1.5 µL matrix 1/100
4	48.5 µL	1.5 µL matrix 1/1000

Place tubes in the thermocycler and run the following PCR program:

94°C 5 min
94°C 1 min
60°C 30 sec } 27 times
68°C 2 min
72°C 5 min
4°C Hold

5 µL of each of the PCR products were analyzed by agarose gel electrophoresis in a minigel system and DNA bands were visualized as described above (see section 8.1.1.). As it can be observed in figure 19, the three dilutions of the matrix yielded a net band of the expected size (3669 bp). Of the three reaction products we chose the one obtained with the lowest amount of matrix for preparative agarose gel electrophoresis and purification of the A3669 bp AgeI_PLCb1a_NotI amplicon as described in sections 8.1.1. and 8.1.2.

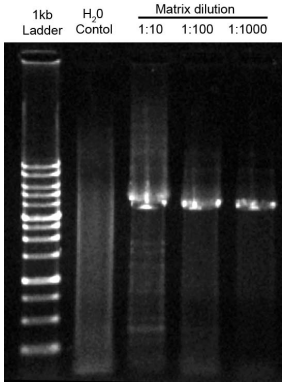

Figure 19. Analysis of PCR products. No product was observed in the lane corresponding to the H_2O negative control, whereas a net band of the expected size for the AgeI_PLCb1a_NotI amplicon was observed at the three dilutions of matrix.

8.3.2.2. Insertion of the amplicon in the pCR®-Blunt II-TOPO cloning vector

The purified 3669 bp AgeI_PLCb1a_NotI amplicon was inserted in the pCR®-Blunt II-TOPO cloning vector (hereinafter TOPO; Fig. 21) using two different amounts of insert.

	Conditons	
PCR product	1 µL	4 µL
H_2O	3 µL	-
Salt	1 µL	1 µL
pCR-Blunt-TOPO vector	1 µL	1 µL

After incubation of the mixtures during 30 min at room temperature, One Shot Top10 competent cells were transformed (see section 8.1.3.) and cultured on LB agar plates containing 50 µg/mL kanamycin. Although TOPO vector allows direct selection of recombinants via disruption of the lethal *E. coli* gene upon insertion of the PCR product (cells that contain non-recombinant vector are killed upon plating), we have observed the presence of surviving clones with no insert. Therefore, we took advantage of the possibility for blue/white selection coated the agar plates with 50 µL X-gal solution. Because amplicon insertion disrupts the LacZ gene present in TOPO, only white colonies are expected to have insert (Fig. 21).

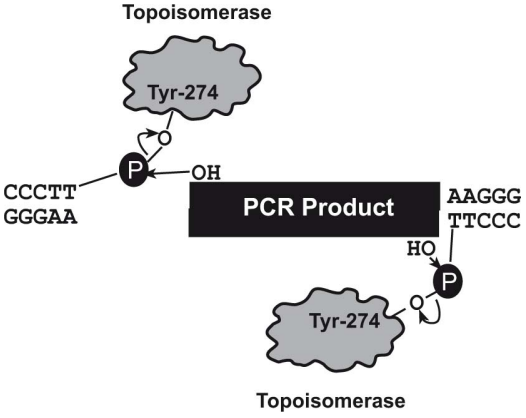

Figure 20. pCR®-Blunt II-TOPO is supplied linearized with *Vaccinia* virus DNA topoisomerase I covalently bound to the 3′ end of each DNA strand. Topoisomerase I binds to duplex DNA at specific sites and cleaves the phosphodiester backbone after 5′-CCCTT in one strand (Shuman, 1991). The energy from the broken phosphodiester backbone is conserved by formation of a covalent bond between the 3′ phosphate of the cleaved strand and a tyrosyl residue (Tyr-274) of topoisomerase I.
The phospho-tyrosyl bond between the DNA and enzyme can subsequently be attacked by the 5′ hydroxyl of the original cleaved strand, reversing the reaction and releasing topoisomerase (Shuman, 1994), which is very useful to efficiently clone PCR products.

Both conditions used for insertion of the AgeI_PLCb1a_NotI in TOPO yielded abundant colonies (Fig. 21).

Five white colonies were grown for miniprep plasmid purification as described above (see section 8.1.4.) and screening was performed with EcoRV and BglII restriction enzymes and NEB buffer 3, basically as described in section 8.2.6. Because the amplicon can be inserted into the plasmid in either direction, there are two possible restriction maps for positive clones:

	SENSE INSERTION	ANTISENSE INSERTION
Size of fragments	4503	6172
	2691	1022

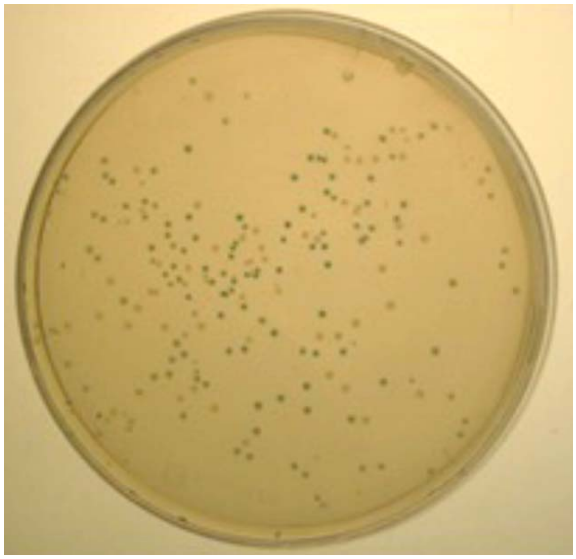

Figure 21. Degradation of the lactose analogue X-gal produces a blue precipitate. Because successful insertion of the amplicon disrupts the LacZ gene encoding for β-galactosidase, only white colonies are expected to be positive.

The restriction map of nearly all of the clones analyzed was consistent with the insertion of the AgeI_PLCb1a_NotI amplicon. Of them, one of them with the PCR product inserted in reverse was completely sequenced by STAB-Vida (Lisbon, Portugal) with the following primers:

M13_Fw	5' TGTAAAACGACGGCCAGT 3'
PLCb1_Int_5_Fw_1	5' AGCGAGATCCTCGGCTTAATG 3'
PLCb1_Int_5_Fw_2	5' ACTGCTGGAAGTGAGGCTATG 3'
PLCb1_Int_5_Fw_3	5' AGTGAAAGACTATGTGCCAGAC 3'
M13_Rv	5' CAGGAAACAGCTATGACC 3'

8.3.2.3. Construction of the pCDNA3-N-PLCβ1a N-terminal cloning vector

Once checked for the correct sequence, the TOPO clone containing the AgeI_PLCb1a_NotI amplicon was used to generate the pCDNA3-N-PLCβ1a N-terminal cloning vector by a digestion of the sequenced TOPO clone and pCDNA3.0 plasmid in EcoRV and NotI sites followed by ligation of the AgeI_PLCb1a_NotI insert into the linearized pCDNA3.0 plasmid.

EcoRV/NotI digestion of the TOPO clone and pCDNA3.0 plasmid was performed by incubation at 37ºC for 2 h in the in the following reaction mixture:

	pCR-TOPO clone	pCDNA3.0
H_20	75 µL	71 µL
Buffer 3 (10 X)	10 µL	10 µL
BSA (100 X)	1 µL	1 µL
Amount of vector	10 µg	10 µg
NotI	2 µL	4 µL
EcoRV	2 µL	4 µL

The digested DNA was resolved by preparative 0.8% agarose gel electrophoresis as described above (see section 8.1.1.). Then, two fragments of 3692 bp and 5430 bp, corresponding to the insert and the linearized pCDNA3.0 plasmid, purified by extraction from gel as described in section 8.1.2.

pCDNA3-N-PLCβ1a N-terminal cloning vector was generated by ligation of the above mentioned fragments. For this purpose, the following mixtures were prepared on ice:

	Ligation	**Control**
Ultrapure H_2O	8 µL	11 µL
Insert	3 µL	-
Linearized pCDNA vector	1.5 µL	1.5 µL
T4 DNA ligase buffer 10X	1.5 µL	1.5 µL
T4 DNA ligase	1 µL	1 µL

The mixture was mixed by vigorous shaking or vortex for ~5 sec and incubated overnight at 16ºC. The resulting ligation products were used to transform chemically competent *E. coli* cells. Bacteria were then cultured on LB agar plates containing 100 µg/ml ampicillin (section 8.1.3).

Five individual clones were chosen, inoculated in 6 mL of ampicillin-containing LB, grown in suspension and purified using NucleoSpin® Plasmid kit (see section 8.1.4.) and eluted in 30 µL ultrapure H_2O. For screening by restriction mapping BglII and AgeI enzymes were used. Double digestion was performed sequentially using NEB buffers 3 and 1 for BglII and AgeI, respectively. Digestion was performed as described in section 8.2.3., except that 5 µL of plasmid and only 1 µL of each enzyme was used in a final volume of 10 µL. The digested DNA was resolved by agarose gel electrophoresis in a minigel system and DNA bands were visualized as described above (see section 8.1.1.).

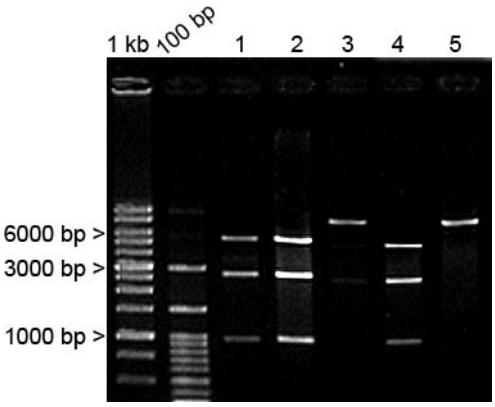

Figure 22. Screening of clones after ligation. The expected size of restriction fragments for the pCDNA3-N-PLCβ1a N-terminal cloning vector were 5492, 2669 and 958 bp. As it can be observed, restriction maps of clones 1, 2 and 5 were consistent with the theoretical one.

As seen in figure 22, three of the five clones had restriction maps coherent with the expected one. Therefore, one of them was chosen for sequencing (STAB-Vida) with the following primers:

Forward primers:

T7	5' AATACGACTCACTATAGGG 3'
PLCb1_Int_5_Fw_1	5' AGCGAGATCCTCGGCTTAATG 3'
PLCb1_Int_5_Fw_2	5' ACTGCTGGAAGTGAGGCTATG 3'
PLCb1_Int_5_Fw_3	5' AGTGAAAGACTATGTGCCAGAC 3'

Reverse primers:

PLCb1_Int_5_Rv_4	5' CCTGGATATATGACCGGATC 3'
SP6	5' ATTTAGGTGACACTATAG 3'

Once the clone was checked for the correct sequence, the pCDNA3-N-PLCβ1a N-terminal cloning vector was amplified for midiprep purification as described in 8.1.4., and used for cloning of PLCβ1a and HA-PLCβ1a in pCDNA3.0 plasmid.

8.4. Cloning of non-tagged and HA-tagged PLCβ1a in pCDNA3.0

8.4.1. Design

Using the pCDNA3-N-PLCβ1a N-terminal cloning vector DNA duplexes can be easily inserted at the 5' end of the sequence encoding for the human PLCB1a mRNA in the pCDNA3-N-PLCβ1a vector. These inserts are designed such that all contain a same Kozak consensus sequence GCCACCATGG (the underlined triplet is the ATG start codon), which plays a major role in the initiation of translation (De Angioletti et al., 2004). The rationale of engineering all constructs with an identical Kozak sequence (and also removing 5'- and 3'-UTRs, see section 8.3.1.) was to obtain constructs exhibiting similar translation efficiencies. The DNA duplexes can be designed to contain the initial codons corresponding to the native PLCB1a sequence, but also to contain a coding sequence for a given protein tag. Obviously, the design of DNA duplexes must consider the reading frame is maintained after being inserted.

8.4.2. DNA duplexes

DNA duplexes containing the initial triplets coding for the human PLCB1a mRNA, preceded or not by a sequence coding for the human *influenza hemagglutinin* (HA) tag were obtained by annealing of synthetic oligonucleotide pairs, thus obtained two DNA duplexes sequences with 5' KpnI- and 3' AgeI-cohesive overhangs. Duplexes were

designed to contain one AgeI site immediately upstream of the Kozak sequence and one EcoRV site a few nucleotides before. Therefore, the 3' AgeI-cohesive overhang was designed such that is destroyed upon ligation with the KpnI/AgeI-digested pCDNA3-N-PLCβ1a N-terminal cloning vector (Fig. 23).

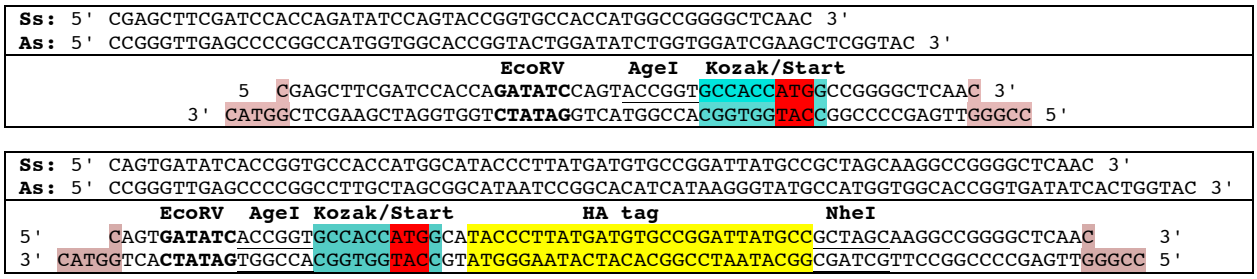

Figure 23. Sequences of sense (Ss) and antisense (As) oligonucleotide pairs used to generate DNA duplexes for insertion in KpnI/AgeI-digested pCDNA3-N-PLCβ1a N-terminal cloning vector, thus generating PLCβ1a and HA- PLCβ1a constructs cloned in pCDNA3.0 vector. The pink colored 5' and 3' sticky ends of the duplexes are KpnI- and AgeI-cohesive, respectively. The AgeI-cohesive 3' overhang destroys the AgeI site upon ligation with the KpnI/AgeI-digested pCDNA3-N-PLCβ1a cloning vector.

8.4.3. KpnI/AgeI digestion of pCDNA3-N-PLCβ1a cloning vector, ligation and screening

Digestion was performed sequentially. KpnI digestion was performed for 2 h at 37ºC in the following reaction mixture:

- 67 µL ultrapure culture grade H_2O (to achieve a final volume of 100 µL).
- 10 µL of plasmid (1 µg/µL).
- 10 µL NEB Buffer 1 10X.
- 1 µL BSA (100 X).
- 2 µL KpnI enzyme.

The digestion product was purified by Nucleospin Gel and PCR Clean-Up DNA purification kit using the manufacturer's instructions, eluted in 50 µL and digested with AgeI enzyme for 2 h at 37ºC in the following reaction mixture:

- 38 µL ultrapure culture grade H_2O (to achieve a final volume of 100 µL).
- 50 µL of KpnI-digested plasmid.
- 10 µL NEB Buffer 3 10X.
- 2 µL AgeI enzyme.

After digestion, purification of the linearized plasmid was performed by extraction from a preparative 1% agarose gel after being resolved by electrophoresis (see sections 8.1.1. and 8.1.2.).

8.4.4. Generation of PLCβ1a and HA-PLCβ1a constructs

Oligonucleotides shown in figure 13 were purchased from Integrated DNA Technologies (IDT Inc., Coralville, Iowa, USA) an annealed as described in section 8.2.4. Ligation of oligonucleotides was performed as described in section 8.4.4.

Screening was performed as described before (section 8.2.6.) using either EcoRI/MluI or NheI/PmlI enzyme combinations for pCDNA3-PLCβ1a and pCDNA3-HA-PLCβ1a constructs, respectively (Fig. 24).

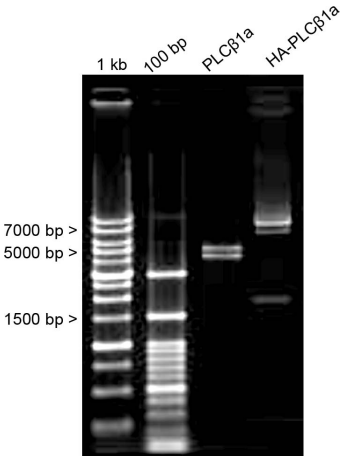

Figure 24. Screening of clones after ligation. The expected sizes of restriction fragments were 4906 and 4197 for the pCDNA3-PLCβ1a construct, and 7315 and 1810 for the pCDNA3-HA-PLCβ1a construct. As it can be observed, restriction maps of the PLCβ1a and HA-PLCβ1a clones were consistent with the theoretical ones. The appearance of a doublet band seen in the lane corresponding to HA-PLCβ1a is due to incomplete digestion of the plasmid.

One positive clone of each construct was chosen for full sequencing (STAB-Vida) with the following primers:

Forward primers:

T7	5' AATACGACTCACTATAGGG 3'
PLCb1_Int_5_Fw_1	5' AGCGAGATCCTCGGCTTAATG 3'
PLCb1_Int_5_Fw_2	5' ACTGCTGGAAGTGAGGCTATG 3'
PLCb1_Int_5_Fw_3	5' AGTGAAAGACTATGTGCCAGAC 3'

Reverse primers:

PLCb1_Int_5_Rv_4	5' CCTGGATATATGACCGGATC 3'
SP6	5' ATTTAGGTGACACTATAG 3'

Once they were checked for the correct sequence, the PLCβ1a and HA-PLCβ1a constructs were amplified for midiprep purification as described in 8.1.4.

8.4.5. Generation of PLCβ1b and HA-PLCβ1b constructs

The DNA sequences coding for both human PLCB1a and PLCB1b mRNAs encompass a unique PmlI unique site upstream of the splice variant-specific 3'-terminal sequence. On the other hand, the PLCB1b sequence in the pCMV6-XL6-PLCβ1b plasmid encompass a NotI site a few bases downstream the stop codon. Because, pCDNA3.0-PLCβ1a and pCDNA3.0-HA-PLCβ1a plasmids were cloned such that contain a unique NotI site a few bases downstream the stop codon (section 8.3.2.), it is

possible to generate pCDNA3.0-PLCβ1b and pCDNA3.0-HA-PLCβ1b constructs by PmlI/NotI digestion. Thus PmlI/NotI digestion of pCDNA3.0-PLCβ1a and pCDNA3.0-HA-PLCβ1a results in a linearized plasmid in which the PLCB1a specific splice-variant 3'-sequence is removed. The PLCB1b specific splice-variant 3'-sequence can be obtained by PmlI/NotI digestion of the pCMV6-XL6-PLCβ1b plasmid and inserted into the pCDNA3.0-PLCβ1a and pCDNA3.0-HA-PLCβ1a plasmids linearized by PmlI/NotI digestion, thus obtaining pCDNA3.0-PLCβ1b and pCDNA3.0-HA-PLCβ1b constructs.

8.4.5.1.PmlI/NotI digestion

Digestion was performed sequentially by incubation of pCDNA3-PLCβ1, pCDNA3-HA-PLCβ1a and pCMV6-XL6-PLCβ1b for 2 h at 37ºC in the following reaction mixture:

- 67 µL ultrapure culture grade H_2O (to achieve a final volume of 100 µL).
- 10 µL of plasmid (1 µg/µL).
- 10 µL NEB Buffer 1 10X.
- 1 µL BSA (100X).
- 2 µL PmlI enzyme.

The digestion product was purified by Nucleospin Gel and PCR Clean-Up DNA purification kit using the manufacturer's instructions, eluted in 50 µL and digested with BglII enzyme for 2 h at 37ºC in the following reaction mixture:

- 50 µL of PmlI-digested plasmid.
- 39 µL ultrapure culture grade H_2O (to achieve a final volume of 100 µL).
- 8 µL NEB Buffer 3 10X.
- 1 µL BSA (100X).
- 2 µL NotI enzyme.

8.4.5.2. Ligation

After being resolved by preparative agarose gel electrophoresis (see section 8.1.1.) the following fragments were purified (see section 8.1.2.) and eluted in 50 µL ultrapure H_2O:

Pml/NotI digestion of:	**Fragments of interest**
pCDNA3-PLCβ1a	7225 bp
pCDNA3-HA-PLCβ1a	7247 bp
pCMV6-XL6-PLCβ1b	1726 bp

The 1726 bp fragment was ligated with 7225 bp and 7247 bp fragments to obtain the pCDNA3-PLCβ1b and pCDNA3-HA-PLCβ1b plasmids coding for native human PLCβ1b and HA-tagged PLCβ1b.

For ligation the following conditions were used:

	Ligations	**Control**
Ultrapure H_2O	6,5 µL	10,5 µL
Insert	4 µL	-
Linearized Vector	2 µL	2 µL
T4 DNA ligase buffer 10X	1.5 µL	1.5 µL
T4 DNA ligase.	1 µL	1 µL

The mixture was mixed by vigorous shaking or vortex for ~5 sec and incubated overnight at 16ºC. The ligation products were used to transform chemically competent *E. coli* cells. Bacteria were then cultured on LB agar plates containing 100 µg/mL ampicillin (see section 8.1.3).

Five individual clones were chosen, inoculated in 6 mL of ampicillin-containing LB, grown in suspension and purified using NucleoSpin® Plasmid kit (see section 8.1.4.) and eluted in 30 µL ultrapure H_2O.

For screening by restriction mapping, EcoRV and BamHI enzymes were used. Plasmids were double digested by incubation at 37ºC for 1 h in the following solution reaction mixture:

Ultrapure H_20	1 µL.
Buffer 3 (10 X)	1 µL.
BSA (10 X)	1 µL.
Plasmid	5 µL.
BamHI	1 µL.
EcoRV	1 µL.

The digested DNA was resolved by agarose gel electrophoresis in a minigel system and DNA bands were visualized as described above (see section 8.1.1.).

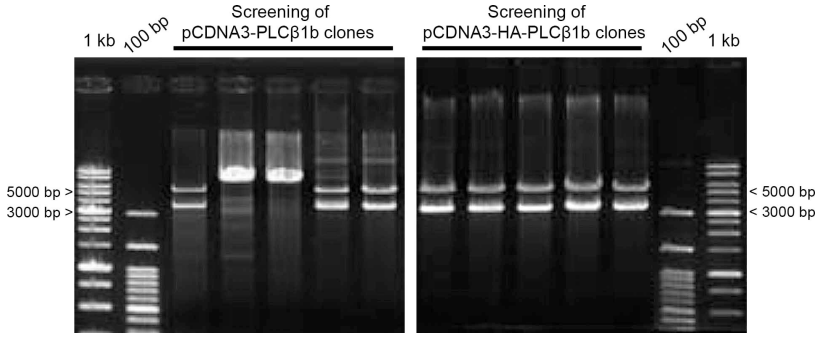

Figure 25. Screening of clones after ligation. The expected size of restriction fragments was 5465 and 3486 for the pCDNA3-PLCβ1b construct, and 5452 and 3521 for the pCDNA3-HA-PLCβ1b construct. Restriction maps 3 of the 5 PLCβ1a and of all HA-PLCβ1a clones analyzed clones were consistent with the theoretical ones.

As seen in figure 25, three of the five pCDNA3-PLCβ1b clones and all of the pCDNA3-HA-PLCβ1b clones had restriction maps coherent with the expected ones.

Therefore, one pCDNA3-PLCβ1b and one pCDNA3-HA-PLCβ1b was chosen for full sequencing (STAB-Vida) with the following primers:

Forward primers:

T7	5' AATACGACTCACTATAGGG 3'
PLCb1_Int_5_Fw_1	5' AGCGAGATCCTCGGCTTAATG 3'
PLCb1_Int_5_Fw_2	5' ACTGCTGGAAGTGAGGCTATG 3'
PLCb1_Int_5_Fw_3	5' AGTGAAAGACTATGTGCCAGAC 3'

Reverse primers:

PLCb1_Int_5_Rv_4	5' CCTGGATATATGACCGGATC 3'
SP6	5' ATTTAGGTGACACTATAG 3'

Once they were checked for the correct sequence, the PLCβ1b and HA-PLCβ1b constructs were amplified for midiprep purification as described in 8.1.4.

9. Statistical analysis

Data were analyzed using Prism (GraphPad Software, La Jolla, CA). The number of samples or cells analyzed, as well as the statistical analysis performed is detailed in each figure legend. Results in graphs are expressed as mean ± standard error (SEM). Significance of differences in mean values was calculated using Student's t-test or one-way ANOVA followed by Tukey´s post-test. For significance symbols, one symbol means $p < 0.05$, two symbols mean $p < 0.01$, and three symbols mean $p < 0.001$.

V. RESULTS

1. ANALYSIS OF PHOSPHOLIPASE Cβ1 EXPRESSION IN CORTICAL NUCLEI OF THE ADULT RAT

As mentioned in the introduction, PLCβ1 is expressed in the nucleus of several non-neuronal cell lines, where it plays a pivotal role in regulation of cell proliferation and differentiation (Cocco et al., 2006, 2009). Therefore, before focusing on the role of PLCβ1 in neuronal differentiation, the expression of PLCβ1 was analyzed in isolated intact nuclei by Western blot, double immunofluorescence staining and confocal laser scanning.

1.1. Expression of PLCβ1a and PLCβ1b in subcellular fractions of the rat cortex

In view of the essential roles attributed to PLCβ1 in several cell lines (for review, Cocco et al., 2006, 2009), and of the lack of data about the nuclear localization of this protein in neurons, PLCβ1-expression was analyzed in cytosol (Cyt fraction) and crude membranes (P2 fraction), and in highly purified nuclei (N fraction).

We first tested the purity of Cyt, P2 and N fractions. For that purpose, Western blot assays were carried out in every fraction of neocortical samples using antibodies raised against specific subcellular compartments. As shown in figure 26A, markers of the Cyt (β-tubulin), P2 (Na^+/K^+ ATPase, NR1 subunit of the NMDA receptor, SNAP-25 and 58K Golgi protein) and N (nuclear pore complex, NPCx) fractions were either preferentially (β -tubulin) or exclusively (the rest) expressed in the expected subcellular compartment. We then measured the expression levels of the splice variants PLCβ1a and PLCβ1b in N, P2 and Cyt fractions, using an antibody raised against a peptide mapping at the N-terminus of PLCβ1 (common to both PLCβ1a and PLCβ1b variants; Fig. 26A; Table 1). Immunoblot analysis revealed specific immunoreactivity for both PLCβ1a and PLCβ1b in every fraction (Fig. 26A-B). To fully investigate the subcellular distribution of PLCβ1a and PLCβ1b, we measured the immunoreactivity using increasing amounts of total protein in N, P2 and Cyt fractions (Fig. 26B).

Regression analysis of standard curves revealed a linear relationship between the amount of protein and the relative optical density of PLCβ1a- and PLCβ1b-immunoreactivity in the range of 2.5-15 µg in the Cyt and P2 fractions, and 10-25 µg in the N fraction. The correlation coefficients obtained using linear regression were between 0.89 and 0.99 (Cyt fraction PLCβ1a, r^2=0.98 and PLCβ1b, r^2=0.99; P2 PLCβ1a, r^2=0.99 and PLCβ1b, r^2=0.98; and N PLCβ1a, r^2=0.89 and PLCβ1b, r^2=0.92).

The analysis of the slopes revealed a higher immunoreactivity of PLCβ1a than of PLCb1b in all subcellular fractions, although the expression of PLCβ11a was significantly higher only in Cyt and P2 fractions (Fig. 26C). The comparative study between PLCβ1a/1b ratios revealed that it was significantly higher in Cyt than in N and P2 fractions (inset in Fig. 26C).

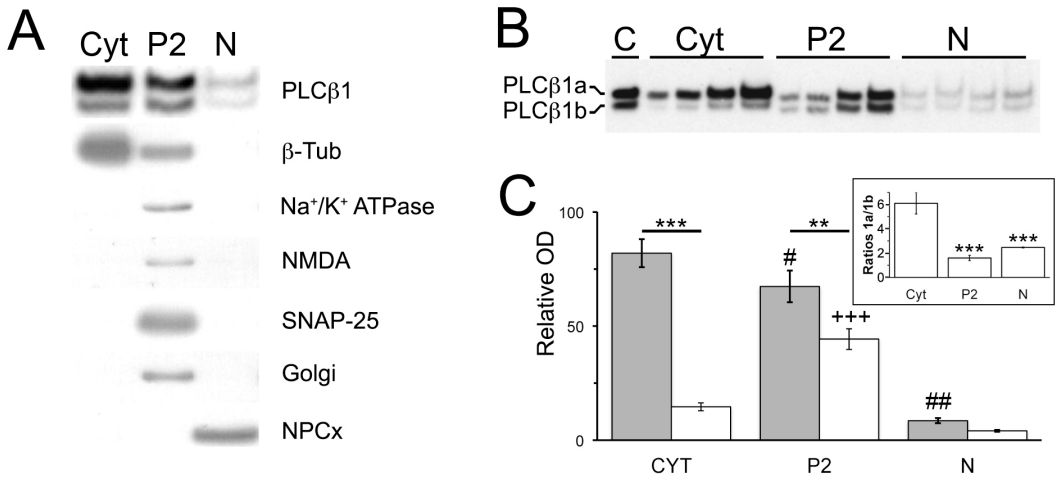

Figure 26. A. Western blot analysis of cytosolic (Cyt), crude membranes (P2) and "isolated nuclei" (N) fractions with antibodies against PLCβ1 and subcellular fraction-specific antigens. For each marker, equal amounts of total protein (10 μg) were loaded on the same gel. **B.** Western blot analysis of PLCβ1a and PLCβ1b in the reference control (C), and Cyt, P2 and N fractions. Increasing amounts of proteins were loaded (2.5, 5, 10 and 15 μg of from the Cyt and P2 fractions, and 10, 15, 20 and 25 μg from the N fraction) and run in parallel. **C.** Bar graph depicts the OD of PLCβ1a and PLCβ1b immunoreactivity for every fraction in lanes loaded with 15 μg protein, relative to the total optical density in the reference control ($n = 7$). Two-way ANOVA revealed significant differences between splice variants and subcellular fractions ($p < 0.0001$ both; $p < 0.005$ for splice variant-subcellular fraction interaction). Post hoc Bonferroni's test revealed a significantly higher expression of PLCβ1a than PLCβ1b in Cyt and P2 fractions ($^{***}p < 0.001$ and $^{**}p < 0.01$, respectively). PLCβ1a expression was significantly lower in P2 and N fractions than in Cyt ($^{\#}p < 0.05$ and $^{\#\#}p < 0.01$, respectively). PLCβ1b expression was significantly higher in P2 than in Cyt and N fractions ($^{+++}p < 0.001$). PLCβ1a/PLCβ1b ratios of immunoreactivity revealed significantly higher values in Cyt than in P2 and N fractions (inset; $^{**}p < 0.01$, $^{***}p < 0.001$) as shown by one-way ANOVA followed by post hoc Tukey's test. All values shown in the bars are the mean ± SEM of four independent experiments.

1.2. Subnuclear distribution of PLCβ1 in intact nuclei from adult rat cortex

In order to confirm and extend results obtained by Western blot analysis, we isolated intact nuclei from adult rat cortex to improve antibody penetration, and conducted different double labeling experiments. First, double-labeling assays using the polyclonal anti-PLCβ1 R-233 antibody and a monoclonal antibody to the postmitotic neuronal marker NeuN/Fox was combined with Hoechst staining, showing that nuclei

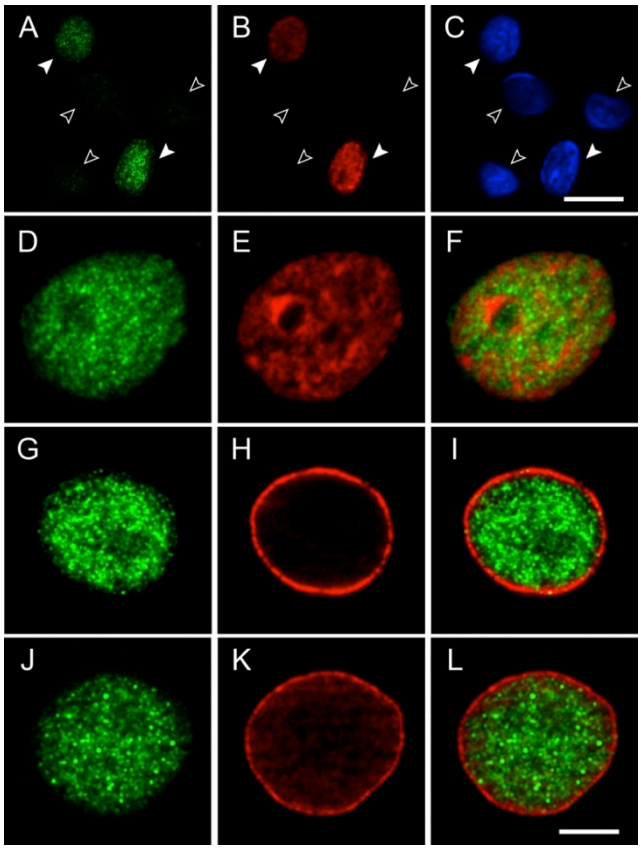

Figure 27. PLCβ1-immunofluorescence combined with NeuN (A-C), chromatin (D-F), nuclear pore complex (G-I) and lamin B1 (J-L) staining in intact nuclei isolated from the adult rat brain cortex. **A-C.** Double PLCβ1- (A) and NeuN-immunofluorescence (B) labeling combined with Hoechst (C). Every NeuN-immunopositive nucleus exhibited strong PLCβ1-immunoreactivity (filled arrowheads), whereas no PLCβ1-staining was observed in nuclei devoid of NeuN (empty arrow-heads). **D-F.** Higher magnification views of PLCβ1-immunollabeled nuclei (D) counterstained with Hoechst (E). No overlapping was observed between PLCβ1 spots and patches of intense Hoechst staining (F). **G-I.** Double PLCβ1- (G) and nuclear pore complex-immunofluorescence (H) showing that PLCβ1 localizes internal to the nuclear envelope (I). **J-L.** Double PLCβ1- (J) and lamin B1-immunofluorescence (K) showing that PLCβ1 localizes internal to the nuclear lamina (L). Scale bars = 20 μm in C (applies to A-C); 5 μm in L (applies to D-L).

of neuronal origin were PLCβ1-positive (Figs. 27A-C). At high resolution, PLCβ1-signal displayed a punctate pattern composed of bright foci distributed throughout the nucleoplasm in nuclear subdomains poor in Hoechst's chromatin staining (Figs. 27D-F), suggesting that PLCβ1 is a component of the nuclear matrix. The distribution of PLCβ1 within the nucleus was then analyzed in more detail by double immunofluorescence experiments with the R-233 antibody combined with markers of the nuclear envelope and lamina, and of different components of the nuclear speckles, where PLCβ1 has been detected in various cell types (Avazeri et al., 2000; Tabellini et al., 2003; Martelli et al., 2005; Bavelloni et al., 2006; Miyara et al., 2008; Fiume et al., 2009). In addition, we observed no overlap with antibodies to nuclear pore complex or to lamin B1 (Figs. 27G-L), indicating that PLCβ1 is internal to the nuclear envelope and lamina. Double immunofluorescence against PLCβ1 and the nuclear matrix component NeuN/Fox3, recently shown to be a marker of the nuclear speckles in neurons (Dent et al., 2010), revealed a similar distribution of both markers and a high overlap between PLCβ1- and NeuN/Fox-immunopositive puncta (Figs. 28A-C). Similar results were obtained when antibodies against PLCβ1 and SC-35 (a nuclear speckle marker) were combined (Figs. 28D-F). PLCβ1 was also highly expressed in PIP_2-rich regions of neuronal nuclei (Figs. 28G-I).

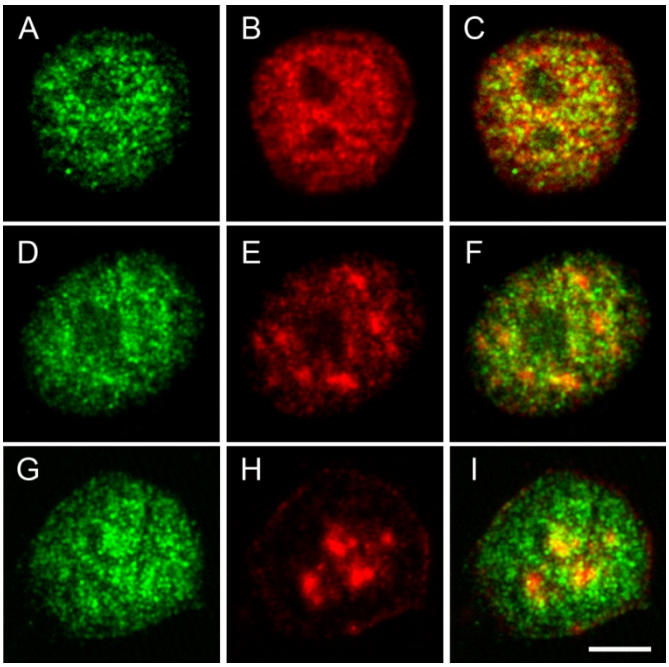

Figure 28. Combined immunofluorescence of PLCβ1 and nuclear matrix markers in neuronal nuclei isolated from the adult rat brain cortex. **A-C.** Double PLCβ1- (A) and NeuN-immunofluorescence (B). Both immunostainings exhibited similar distribution in the nucleo-plasm (C). Numerous PLCβ1-immunopositive puncta co-localized with or were in close apposition to NeuN-positive puncta. **D-F.** Double PLCβ1- (D) and SC-35-immunofluorescence (E). PLCβ1-immunlolabeling partially overlapped with SC-35-speckles (F). **G-I.** Double PLCβ1- (G) and PIP_2-immunofluorescence (H). The bulk of PIP_2-signal was confined to speckle-like structures. Domains exhibiting the most intense PLCβ1- and PIP_2-stainings overlapped or were closely apposed to each other (H). Scale bar = 5 μm.

Results described in this chapter form part of two peer-reviewed publications (Montaña et al., 2012; García del Caño et al., 2015) and one review article (García del Caño et al., 2014).

2. CHARACTERIZATION OF NT2-DERIVED POSTMITOTIC HUMAN NEURONS OBTAINED BY SHORT-TERM TREATMENT WITH THE NUCLEOSIDE ANALOGUE CYTOSINE B-D-ARABINOFURANOSIDE

As mentioned in the introduction, the use of RA/NT2N is limited by the long period needed for differentiation and by and the low differentiation rate. Moreover, these limitations make this procedure useless for transient transfection-based approaches. Thus, we tested the ability of the nucleoside analogues 2'-deoxy-5-azacytidine (DAC) and β-D-arabinofuranoside (AraC) to induce a rapid differentiation of NT2 cells and compared the results with those obtained by RA-treatment.

2.1. Short exposure of NT2 progenitors to AraC efficiently promotes acquisition of neuron-like morphology

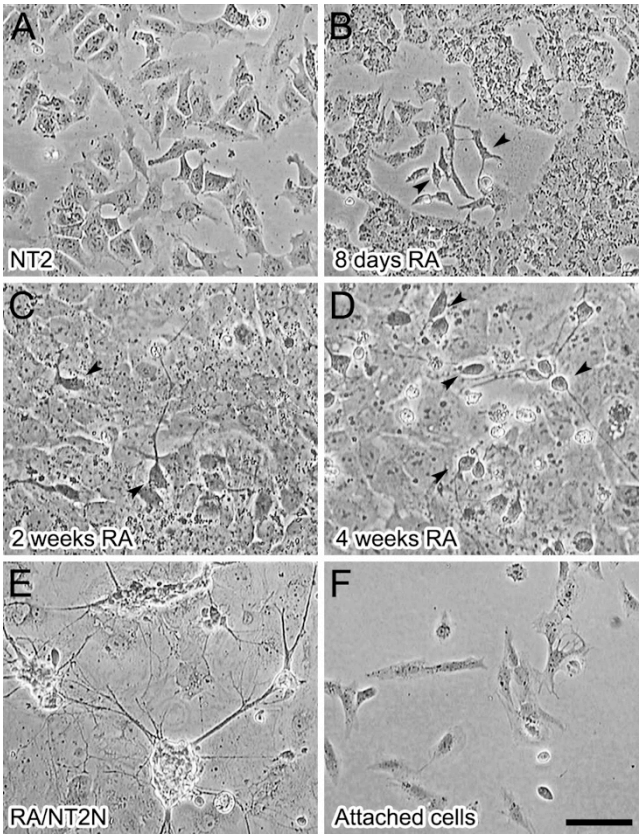

Figure 29. Phase-contrast micrographs showing cell morphology during the course of RA-induced differentiation. **A**. NT2 progenitors. **B-D**. NT2 cells following treatment with 10 μM RA during 8 days (B), 2 weeks (C) and 4 weeks (D). **E**. RA/NT2N cells isolated by mechanical dislodging at week 4 of the RA-treatment schedule and maintained with antimitotics for 2 additional weeks. **F**. Cells remaining attached to the flask after mechanical dislodging. Arrowheads indicate neuron-like cells at different time points during RA-induced differentiation. Scale bar = 50 μm.

First, we sought to reproduce the RA-induced differentiation protocol published by Pleasure et al. (1992). Eight days after initiation of treatment, a subpopulation of the flat and amorphous undifferentiated NT2 precursors (Fig. 29A) began to acquire a typical neuronal spindle shape and to develop short neurite extensions (Fig. 29B, arrowheads). Neuronal morphologies stood out more clearly after 2 and, even more, after 4 weeks (Figs. 29C-D, arrowheads), the time at which postmitotic neurons were mechanically isolated. As previously described, following replating of dislodged cells and treatment

with antimitotics for 2 weeks, cells organized into aggregates and displayed large processes that formed bridges linking clusters of perikarya (Fig. 29E). Our results, showing that only 4.4 ± 0.8% (SEM) of the initial population become terminally differentiated RA/NT2N cells, were also in line with the observations by Pleasure et al. (1992).

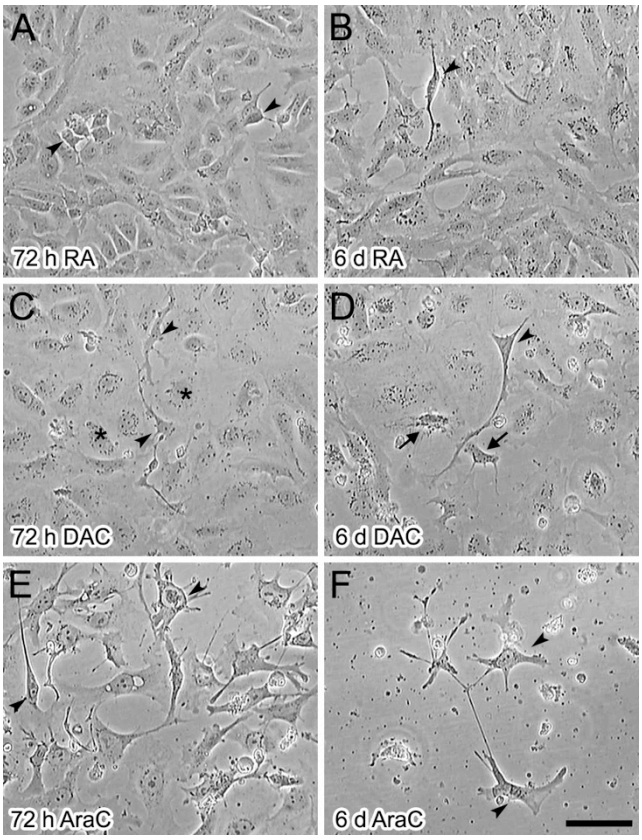

Figure 30. Phase-contrast micrographs comparing the effects of exposure of NT2 cells to equitoxic concentrations of RA (10 μM) (**A-B**), DAC (20 μM) (**C-D**) and cytosine β-D-arabino-furanoside (AraC, 20 μM) (**E-F**) during 72 h (A, C, E) and 6 days (B, D, F). Arrowheads indicate cells displaying neurite-like processes. Asterisks in C and arrows in D indicated different non-neuronal morphologies identified in cultures treated with DAC. Scale bar = 50 μm.

Subsequently, we tested the ability of DAC and AraC to promote short-term neuron-like differentiation and compared it to that of RA. After 3 days of treatment with RA, the vast majority of cells showed no morphological signs of differentiation, although a few cells displayed round phase-bright bodies and short processes (Fig. 30A, arrowheads). These cells developed longer neurite-like processes (Fig. 30B, arrowhead) 6 days post-treatment, but remained a very minor component of the total cell population. DAC treatment for 3 days resulted in a drastic decrease in cell number, although the culture remained confluent due to the large size of the majority of cells, which consisted of flat cells with a phase-translucent cytoplasm (Fig. 30C, asterisks). Intermingled with them, we could observe a small population of phase-darker cells bearing neurite-like processes (Fig. 30C, arrowhead). Six days after DAC treatment these later phenotype become more evident (Fig. 30D, arrowheads), but it constituted an even smaller minority of cell population. Among the rest of cells, large rounded

morphologies were still predominant, together with a less numerous population of smaller irregular-shaped cells bearing filopodia-like processes (Fig. 30D, arrows). In turn, treatment with AraC for only 3 days resulted in a culture consisting mostly of profusely branched large cells of variable morphology, highly suggestive of a neuronal phenotype (Fig. 30E, arrowheads). At this time point, the percentage of surviving cells relative to the initial NT2 population was 42.18 ± 2.78%. Many surviving cells showed a highly polarized morphology with long processes, indicative of their neuronal identity (Fig. 30F, arrowheads).

These cultures were extremely sparse and, indeed, only 10.5 ± 1.3% of the initial cell population survived AraC treatment. Therefore, we tested whether survival could be improved by increasing cell confluence. For this purpose, after 3 days of AraC treatment, cells were harvested, replated at higher density, and treated with AraC for 3 additional days. In fact, this procedure resulted in a 2-fold increase of surviving cells (20.2 ± 3.3% *vs*. 9.3 ± 1.1%). Figure 29 illustrates morphological changes occurring during the first 72 h of AraC-induced differentiation (Figs. 31A-D) and the features of the culture at the end of the standard (Fig. 31E) and modified schedules (Fig. 31F). As it can be observed, both procedures yielded a culture highly enriched in cells with neuronal morphology (AraC/NT2N cells).

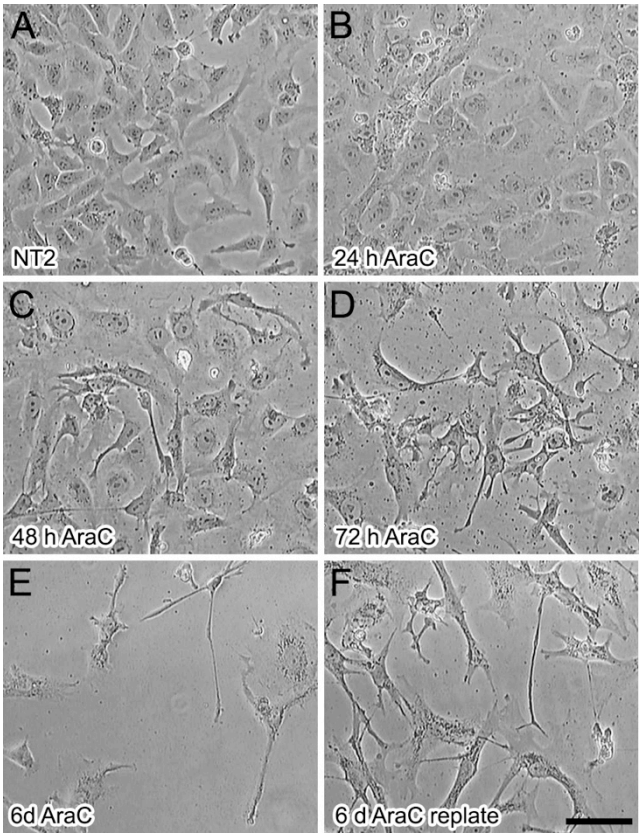

Figure 31. Phase-contrast micrographs illustrating the time-course of AraC-induced differentiation (**A-E**) and the effects of increasing cell confluence at 72 h of AraC treatment in the state of cultures after 6-day period of treatment (**F**). Asterisks indicate the presence of a population of flat cells with phase-translucent cytoplasm and non-neuronal morphology at the end of treatment. Scale bar = 50 µm.

2.2. Treatment of NT2 cells with AraC for 6 days induces terminal neuron differentiation with high efficiency

To ascertain whether AraC/NT2N cells expressed markers consistent with a neuronal phenotype, we analyzed the expression of the neuron-specific cytoskeletal proteins neurofilament 200 kDa (NF200), β-III tubulin and doublecortin (DCX) during the time-course of RA- and AraC-induced differentiation process. To this end, cell homogenates were subjected to SDS-PAGE, immunoblot and semiquantitative densitometric analysis (Fig. 32A). Both, RA and AraC led to an increase of NF200 expression, reaching a maximum at the end of the differentiation process, showing only subtle differences in the relative expression level during the time-course of treatments. In contrast, the temporal expression profile of β-III tubulin and DCX showed marked differences between the RA- and AraC-induction of differentiation. Thus, upon RA treatment of NT2 progenitors, the expression of β-III tubulin increased rapidly and then decreased, whereas it increased sharply at the end of the AraC treatment. DCX, in its turn, increased progressively in RA-treated cells, whereas it showed an up-down regulation pattern in AraC-treated cells (Fig. 32A). These distinct temporal expression patterns in the time-course RA- and AraC-induced differentiation are discussed (see Discussion chapter) in relation to the cell composition of cultures and immunocytochemical results.

Subsequently, we performed immunolabeling experiments for β-III tubulin, NF200 and DCX in NT2 progenitors, RA/NT2N and AraC/NT2N cells (Figs. 32B-J). No or barely detectable NF200-immunolabeling was observed in NT2 cells (Fig. 32B), whereas a bright signal could be observed in both RA/NT2N (Fig. 32E) and AraC/NT2N (Fig. 32H) cells. Also in good agreement with immunoblot results (Fig. 32A), β-III tubulin-immunolabeling was diffusely distributed in the cytoplasm of NT2 progenitors (Fig. 32C), whereas intense immunoreactivity was found in varicosities within the neurites of RA/NT2N cells (Fig. 32F) and throughout the cell body and neurites or AraC/NT2N cells (Fig. 32I). NT2 cells resulted diffusely stained by anti-DCX antibody, whereas it gave a strong fluorescent signal in neurites of RA/NT2N cells (Fig. 32G) and consistently delineated neurites of AraC/NT2N cells (Fig. 32J).

The neuronal identity of AraC/NT2N cells was further analyzed by immunofluorescence labeling for NeuN/Fox-3 (a marker of adult neurons), combined with staining β-III tubulin, in cell cultures treated with AraC for 6 days subjected or not to replating on day 3. This was useful to assess the impact these two culture schedules

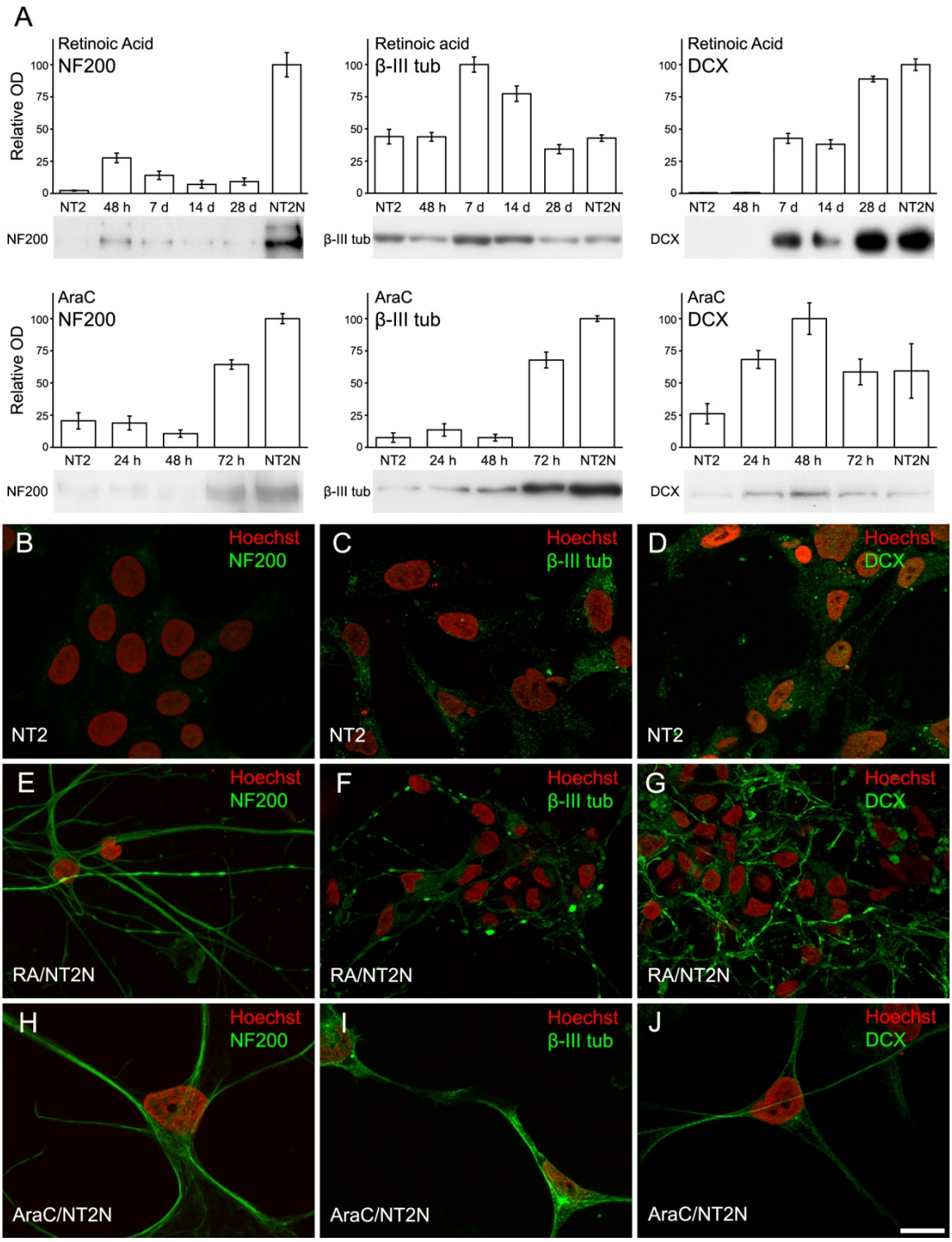

Figure 32. A. Results of immunoblots and semiquantitative densitometric analysis of immunoreactivity for neuronal markers NF200, β-III tubulin and DCX during RA- and AraC-induced differentiation. Immunoblots were performed in whole homogenates of cells harvested at different time points of differentiation using RA- (NT2 progenitors, 48 h, 7 days, 14 days, 28 days and terminally differentiated RA/NT2N neurons) and AraC (NT2 progenitors, 24 h, 48 h, 72 h and terminally differentiated AraC/NT2N neurons). The amount of protein loaded per lane was 5 µg for immunoblots against NF200 and β-III tubulin, and 20 µg for immunoblots against DCX. The y-axis of graphs shows percent optical density of each band normalized to the highest value found during the time-course of differentiation. Error bars indicate SEM (n=4).

(Continues in next page)

in neuronal enrichment and maturation. Nuclei of NT2 cells displayed a very weak NeuN/Fox-3 immunofluorescence signal (Figs. 33A-B), whereas dense immunoreactivity could be observed in nuclei of β-III tubulin-immunopositive AraC/NT2N neurons, irrespectively of the culture schedule used (Figs. 33C-F). Consistent with these results, NeuN/Fox-3 was almost undetectable by Western blot of NT2 cell homogenates. Immunoreactivity began to be clearly detectable after 48 h of AraC-treatment and reached a maximum at the end of the 6 days treatment period and no differences could between samples obtained from the two different treatment schedules (Fig. 33G).

Because cultures of NT2 cells treated for 6 days with AraC still contained a population of presumably non-neuronal cells, NeuN/Fox-3 staining, together with morphological features, was used to evaluate the efficiency of both schedules to induce neuronal differentiation. For this purpose we performed cell counts on cell cultures doubly immunolabeled for NeuN/Fox-3 and β-III tubulin, and cells negative for NeuN/Fox-3 and those displaying round shapes with no or short processes were considered to be non-neuronal. Using these criteria, we concluded that 55.4 ± 2.4% and 71.3 ± 3.9% of cells exposed to AraC for 6 days without replating and those subjected replating on day 3 fulfilled criteria to be considered as AraC/NT2N neurons, respectively. Using these values and the percentage of surviving cells following 6 days of treatment with AraC (see above) we could conclude that 5.14 ± 0.6% and 14.4 ± 2.3% of the initial population of NT2 progenitors became terminally differentiated AraC/NT2N neurons (Fig. 33H).

Finally, AraC/NT2N cells (Figs. 34B, D), but not NT2 progenitors (Figs. 34A, C), were strongly immunolabeled for MAP2 (Fig. 34B) and voltage-dependent sodium channel 1.6 (Nav 1.6) (Fig. 34D) proteins, further indicative of their adult phenotype and suggestive of their ability to generate action potentials, respectively.

Figure 32. B. Micrographs of NT2 cells (B-D) and terminally differentiated RA/NT2N (E-G) and AraC/NT2N (H-J) neurons immunolabeled (green) for NF200 (A, E, H), DCX (C, F, I) and β-III-tubulin (D, G, J) combined with chromatin staining using the Hoechst's dye (pseudocoloured red). Micrographs are maximum intensity projections of four consecutive optical sections separated by 0.24 μm, obtained using the structured illumination module (ApoTome) of a fluorescence microscope (Carl Zeiss Axio Observer) equipped with a XYZ motorized stage. Scale bar = 20 μm.

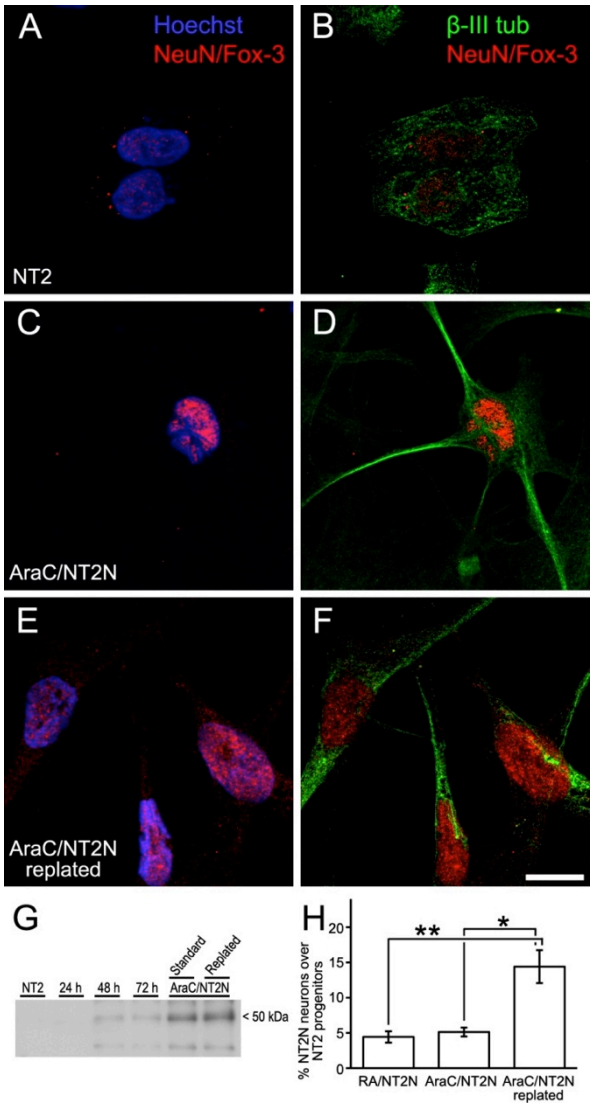

Figure 33. A-F. Fixed NT2 progenitors (A-B) and NT2 cells subjected to treatment with AraC under two different culture schedules (C-F), processed for double-immunofluores-cence against β-III-Tubulin (green) and NeuN/Fox-3 (red) combined with Hoechst's chromatin staining (blue). NT2 cells in C-D were treated uninterruptedly with AraC. Cells in E-F were treated for 3 days, replated at higher density on day 3, and then treated for 3 additional days. Micrographs are maximum intensity projections of four consecutive optical sections separated by 0.24 µm, obtained using the structured illumination module (ApoTome). Scale bar = 20 µm. **G.** Western blot analysis of NeuN/Fox-3 expression in total cell lysates (30 µg) at different time points of standard AraC-induced differentiation and under replating conditons. **H.** Bar graph shows the percentage yield of terminally differentiated NT2N neurons obtained by differentiation with RA and with AraC under the two culture schedules mentioned above. Data are mean ± SEM. One-way ANOVA followed by post hoc Bonferroni's test (n=3; **p*<0.05, ***p*<0.01).

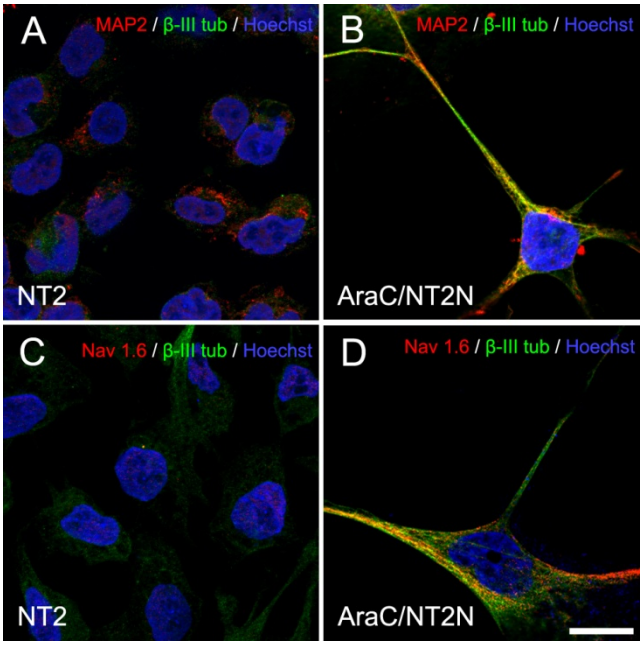

Figure 34. NT2 progenitors (A, C) and AraC/NT2N neurons (B, D) processed for double-immunofluorescence against MAP2 (red) and β-III-Tubulin (green) (A-B), or the voltage-dependent sodium channel Nav 1.6 (red) (C-D) and β-III-Tubulin (green), both combined with Hoechst's chromatin staining (blue). Micrographs are maximum intensity projections of four consecutive optical sections separated by 0.24 µm, obtained using the structured illumination module (ApoTome). Scale bar = 20 µm.

Collectively, these results demonstrate the effectiveness of AraC to promote neuronal differentiation of NT2 cells in a short time period and highlight the importance of optimizing culture conditions.

2.3. Cells identified as AraC/NT2N neurons are morphometrically distinguishable from non-neuronal cells

To assess whether phenotypes classified as neuronal and non-neuronal after AraC-induced differentiation were morphometrically distinguishable, we analyzed the average nuclear and whole cell area of both cell populations, classified on the basis of NeuN/Fox-3 expression and morphological features The methodology used for morphometric analysis is illustrated in figures 35A-F and described in detail in Methods.

The average nuclear area of cells classified as non-neuronal was considerably larger (851.53 ± 27.63 μm^2) than nuclear area of AraC/NT2N neurons (339.67 ± 11.91 μm^2), whereas no differences in total cell area were observed (3122.36 ± 95.06 and 3326.82 ± 177.68 μm^2, respectively). Consequently, the ratio of nuclear area to total cell body area was about 2-fold higher in non-neuronal cells (0.280 ± 0.007) than in AraC/NT2N cells (0.128 ± 0.008) (Fig. 35G). These results clearly reinforce the reliability of criteria used to classify cell phenotypes resulting from exposure of NT2 progenitors to AraC treatment.

Comparison of the nuclear area between neurons committed to differentiate with either RA or AraC showed that nuclei of AraC/NT2N neurons (339.78 ± 12.03 μm^2) were 4.7-fold larger than those of RA/NT2N neurons (72.37 ± 1.85 μm^2). Similarly, the average soma area of AraC/NT2N neurons (1103,15 ± 41.69 μm^2) was about 6.8-fold larger compared to that of RA/NT2N neurons (162.70 ± 4.46 μm^2). Consequently, the ratio of nuclear to body area tended to equalize in both phenotypes, although it was significantly lower in AraC/NT2N (0.344 ± 0.017) than in RA/NT2N (0.45 ± 0.008) neurons (Fig. 35H). The average value obtained here for area of nuclei of RA/NT2N neurons was more than double compared that obtained in a recent study (Haile et al., 2014). This difference is discussed (see Discussion chapter) in relation to the different culture conditions used. Finally, neurites of AraC/NT2N neurons were 105,33 ± 3,55 μm long in average, which represent less than half the value reported by Haile et al. (2014) in RA/NT2N neurons (Table 7). This, together with a lower number of neurites per cell (1.85 ± 0.10) found in AraC/NT2N neurons, makes total arborization 4.2-fold

longer in RA/NT2N neurons (Table 7).

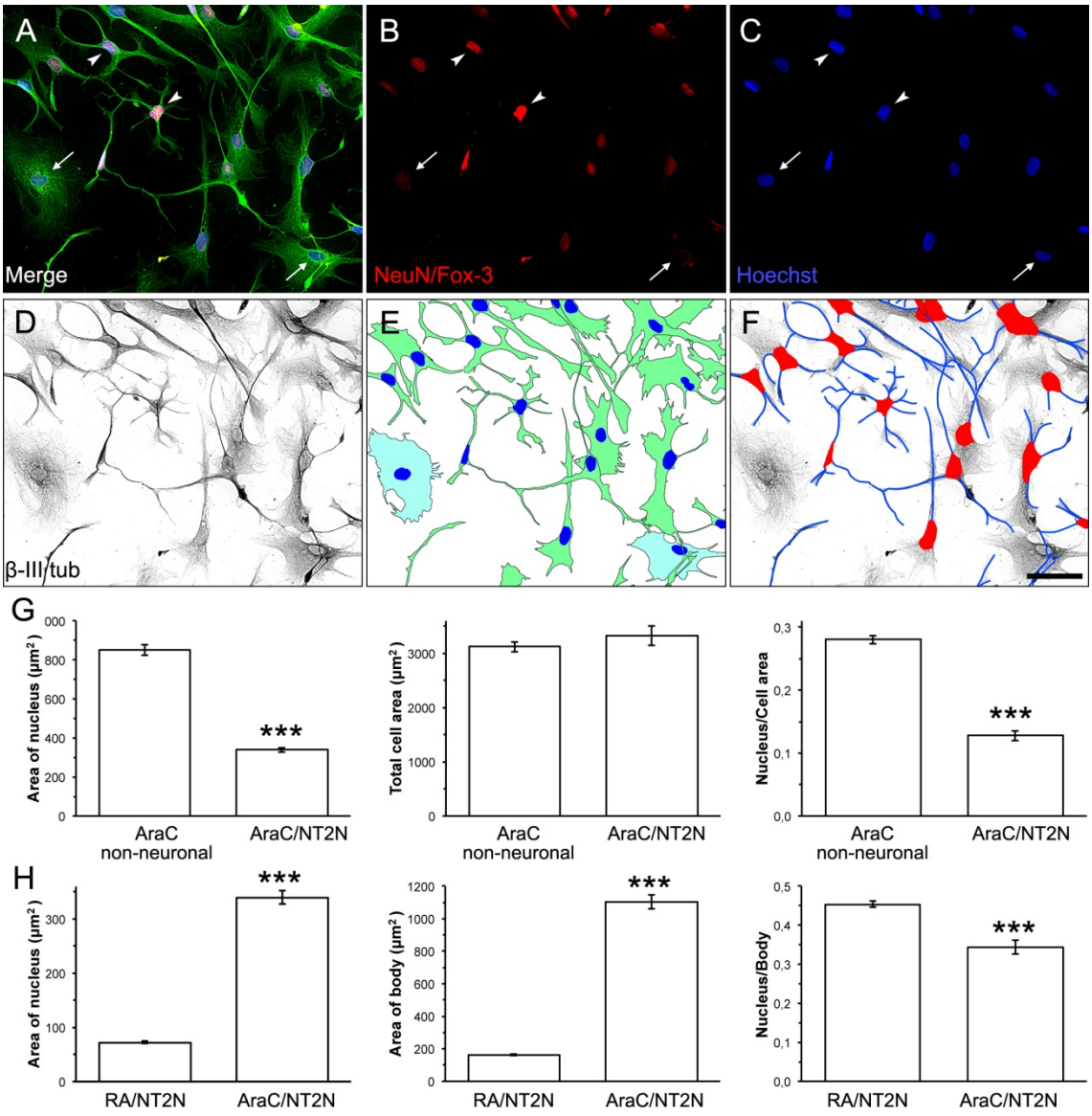

Figure 35. A-F. Illustration of image processing for morphometric analysis of non-neuronal and AraC/NT2N neuronal phenotypes. Mosaic images of cell cultures processed for double immunolabeling for NeuN/Fox-3 (red) and β-III-tubulin (green) combined with Hoechst' staining (blue) were captured under a 20 X objective (A). The β-III-tubulin and NeuN (B) channels were used to identify cells of non-neuronal (arrows) and neuronal (arrowheads) phenotypes. Binary images Hoechst-stained nuclei (C) and inverted grayscale images of β-III-tubulin immunostaining (D) were used to measure the nuclear and whole cell areas of non-neuronal (E, cyan-filled cells) and neuronal cells (E, green-filled cells). Neuronal somata and neurites were measured on grayscale images of β-III-tubulin immunostaining (F) (see Methods for further details). Scale bar = 100 µm. **G-H.** Bar graphs show results of morphometric analyses to compare non-neuronal and AraC/NT2N cells grown in identical conditions (G) and RA/NT2N and AraC/NT2N (H). All data represent average values obtained from 99 cells in three independent experiments. Two-tailed unpaired t-test (***$p < 0.001$).

Table 7. Neurite length of RA/NT2N and AraC/NT2N neurons.

	RA/NT2N[1]	**AraC/NT2N**
Average neurite length (μm^2)	239.56 ± 8.9	105.33 ± 3.55
Number of neurites/cell	3.17 ± 0.04	1.85 ± 0.10
Total neurite length/cell (μm^2)	759.40	179.96 ± 9.19

[1]Data of RA/NT2N cells are from Haile et al. (2014).

2.4. AraC/NT2N co-express glutamatergic and cholinergic phenotypic markers

To assess whether AraC/NT2N cells can be a source of specific neurotransmitter phenotypes, the expression of glutamatergic, cholinergic, GABAergic and dopaminergic specific-markers was analyzed by means of immunofluorescence microscopy and Western blot in cell homogenates. For this purpose, we used specific antibodies to vesicular glutamate transporter 1 (VGluT1), choline acetyl transferase (ChAT), glutamate decarboxylase 67 kDa (GAD67) and tyrosine hydroxylase (TH) enzymes. Rat brain homogenates and total cell lysates of the human U87 glioma cell line were used as positive and negative controls, respectively. In rat brain homogenates anti-VGluT1 antibody recognized several strong bands migrating below the 75 kDa marker, which were within the range of molecular sizes predicted for annotated splice variants of rat (61.6-64.3 kDa) origin. Additionally, a minor band slightly below the 50 kDa marker was observed, in agreement with the supplier's control (Fig. 36). VGluT1-immunoreactivity in undifferentiated samples from NT2 cells was slightly above the threshold level, whereas two clear bands were detected in NT2 cells treated with AraC for 72 h and in AraC/NT2N cells: an upper minor one located between the 75 and 50 kDa markers, probably corresponding to the human VGluT1 isoform 1 (61.6 kDa) and a lower major one slightly below the 50 kDa marker, close to the size predicted for the human VGluT1 isoform 2 (53.9 kDa). Indeed, this antibody recognizes both isoforms as described by supplier. VGluT1 signal was barely detectable in cell homogenates from NT2 cells treated with retinoic acid during 4 weeks and from RA/NT2N cells (Fig. 36). Remarkably, non-neuronal NT2A cells (those remaining attached to the flask after mechanical isolation of neuronal cells) displayed strong VGluT1-immunoreacivity. Only a weak signal at the level of the upper band seen in NT2A cells could be observed in U87 cells, along with two larger sized bands. A strong ChAT-immunoreactive band with an apparent molecular mass consistent with the predicted size for the ChAT

enzyme of rat origin (72,4 kDa) was detected in homogenates from adult brain (Fig. 36). A net immunoreactive band, migrating slightly below the one observed in rat brain homogenates, was clearly detectable in homogenates from NT2 progenitors, its apparent molecular mass being well consistent with the theoretical size of the human ChAT isoform R (70.4 kDa). ChAT-immunoreactivity increased markedly after 72 h of treatment with AraC and returned to levels observed in NT2 progenitors at day 6. ChAT protein could be detected in cell homogenates from cells treated during 4 weeks with RA, but not in RA/NT2N samples, and strong ChAT-immunoreactivity was found in homogenates from NT2A cells (Fig. 36). These data indicate that expression of ChAT in non-neuronal NT2A cells account for the immunoreactivity observed in samples from cultures at 4 weeks of RA treatment, which are composed of a mixture of neuronal and NT2A cells. A ChAT-positive band was also seen in immunoblots of U87 cell homogenates (Fig. 36). In rat brain samples, GAD67 antibody detected a strong band of a size consistent with the theoretical 66.6 kDa molecular mass of the rat protein. No detectable signal was observed in NT2 cell and AraC-treated samples. A positive band, consistent with the molecular mass of human GAD67 (66.9 kDA), appeared after 4 weeks of RA-treatment (Fig. 36). This signal increased markedly in RA/NT2N cells and was also detectable in NT2A but not U87 samples. An additional smaller-sized band was detected in samples of NT2, AraC-treated, RA/NT2N and NT2A cells, being particularly intense in the NT2A samples (Fig. 36). Because the antibody used does not cross-react with GAD65, this band is presumed to be either unspecific or a degradation product, although the possibility of posttranslational modification cannot be ruled out. Finally, in rat brain homogenates, TH antibody detected a strong specific band migrating above the 50 kDa marker, but we found no TH-immunoreactivity in any of the cell samples analyzed even after overexposure of Western blots (Fig. 36).

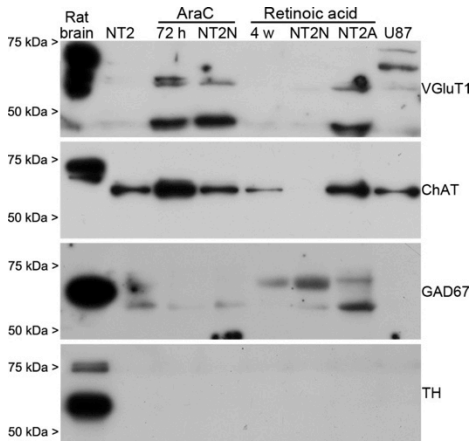

Figure 36. Western blot analysis of neurotransmitter phenotype markers in total cell lysates from NT2 cells (20 µg) during the RA- and AraC-induced differentiation. Rat brain homogenates (4 µg) and human U87 glioma cell line lysates (20 µg) were used as positive and negative controls, respectively. Specific antibodies to vesicular glutamate transporter 1 (VGluT1), choline acetyl transferase (ChAT), glutamate decarboxylase 67 kDa (GAD67) and tyrosine hydroxylase (TH) enzymes were used as glutamatergic, cholinergic, GABAergic and dopaminergic phenotype markers.

In agreement with the results of Western blot analysis, NT2 progenitors exhibited barely detectable VGlut1-immunofluorescence (Fig. 37A), whereas bright staining was detected throughout cells processes of cells differentiated into neurons by AraC treatment for 72 h and 6 days (Figs. 37B-C). In the same immunocytochemical staining conditions, VGluT1-signal was seen as bright foci restricted to varicosities on a small subset of neurites of RA/NT2N cells (Fig. 37D). ChAT-immunoreactivity was diffusely distributed throughout the cytoplasm of NT2 progenitors (Fig. 37E) and extended to neurites of AraC-differentiated cells (Figs. 37F-G), but no signal above the background level was detected in RA/NT2N neurons (Fig. 37H). NT2 progenitors and AraC-treated cells were nearly devoid of GAD67-immunofluorescence staining (Figs. 37I-K), whereas most neurites of RA/NT2N cell displayed bright staining (Fig. 37L).

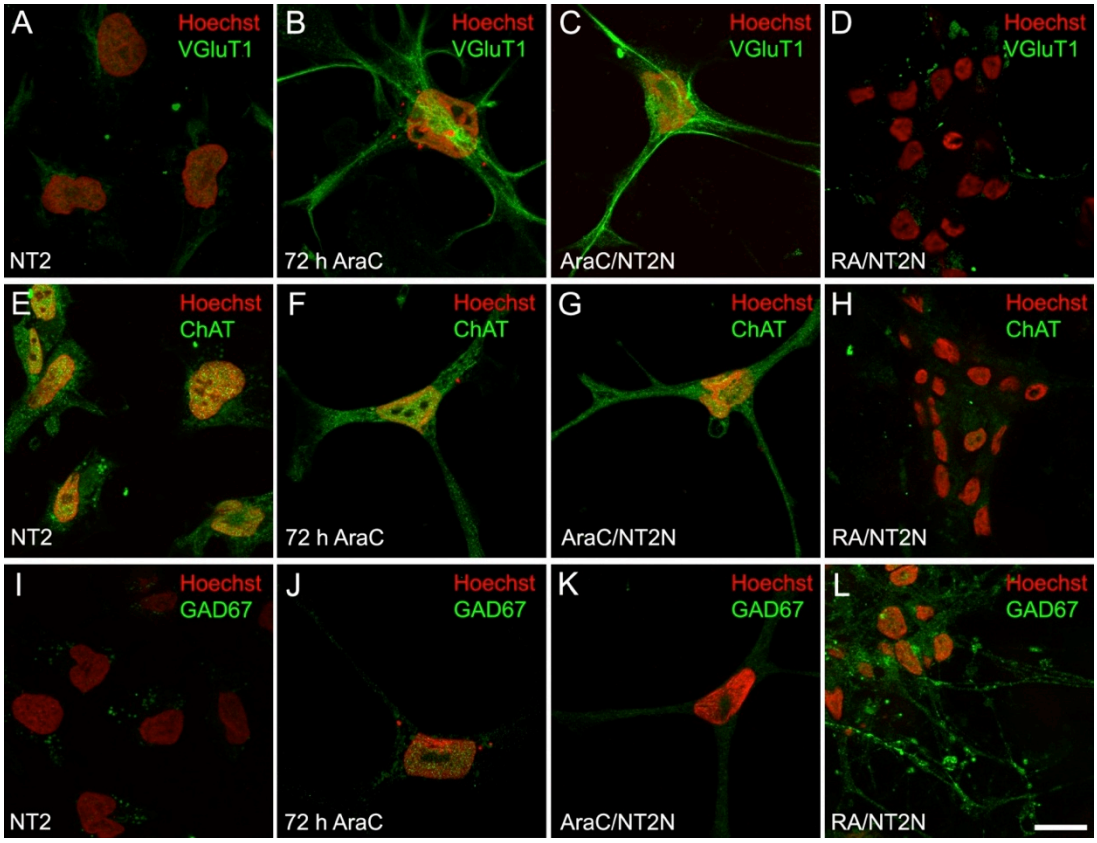

Figure 37. Immunolabeling (green) against VGlut1 (**A-D**), ChAT (**E-H**) and GAD67 (**I-L**) combined with Hoechst's chromatin staining (pseudocoloured in red) in fixed NT2 cells, cells treated for 72 h with AraC, and AraC/NT2N and RA/NT2N neurons. Micrographs are maximum intensity projections of three consecutive optical sections separated by 0.24 µm, obtained by structured illumination microscopy (ApoTome). Scale bar = 20 µm.

Immunofluorescence staining showed that virtually all AraC/NT2N neurons were both VGluT1- and ChAT-immunopositive, strongly indicating that these cells co-express glutamatergic and cholinergic markers. Thus, we carried out double VGluT1/ChAT-immunofluorescence staining, showing that every VGluT1-positive

neuron also expressed ChAT (Fig. 38A). Although both markers were distributed in neurites of AraC/NT2N cells, VGluT1-immunofluorescence was highly polarized to neurites, whereas anti-ChAT antibody also stained flat lamellipodia (Figs. 38B-D). Because cells committed to differentiate into neurons by AraC treatment cannot be physically separated from non-neuronal cells for Western blot analysis, immunofluorescence analysis allowed us to compare these two cell phenotypes with respect to the expression of VGluT1 and ChAT. VGlut1-immunoreactivity in flat polygonal non-neuronal cells (Figs. 36B-D, stars) was mostly restricted to perinuclear locations (Fig. 38B), whereas ChAT-staining extended further to the whole cytoplasm (Fig. 38C), even delineating the whole cellular perimeter.

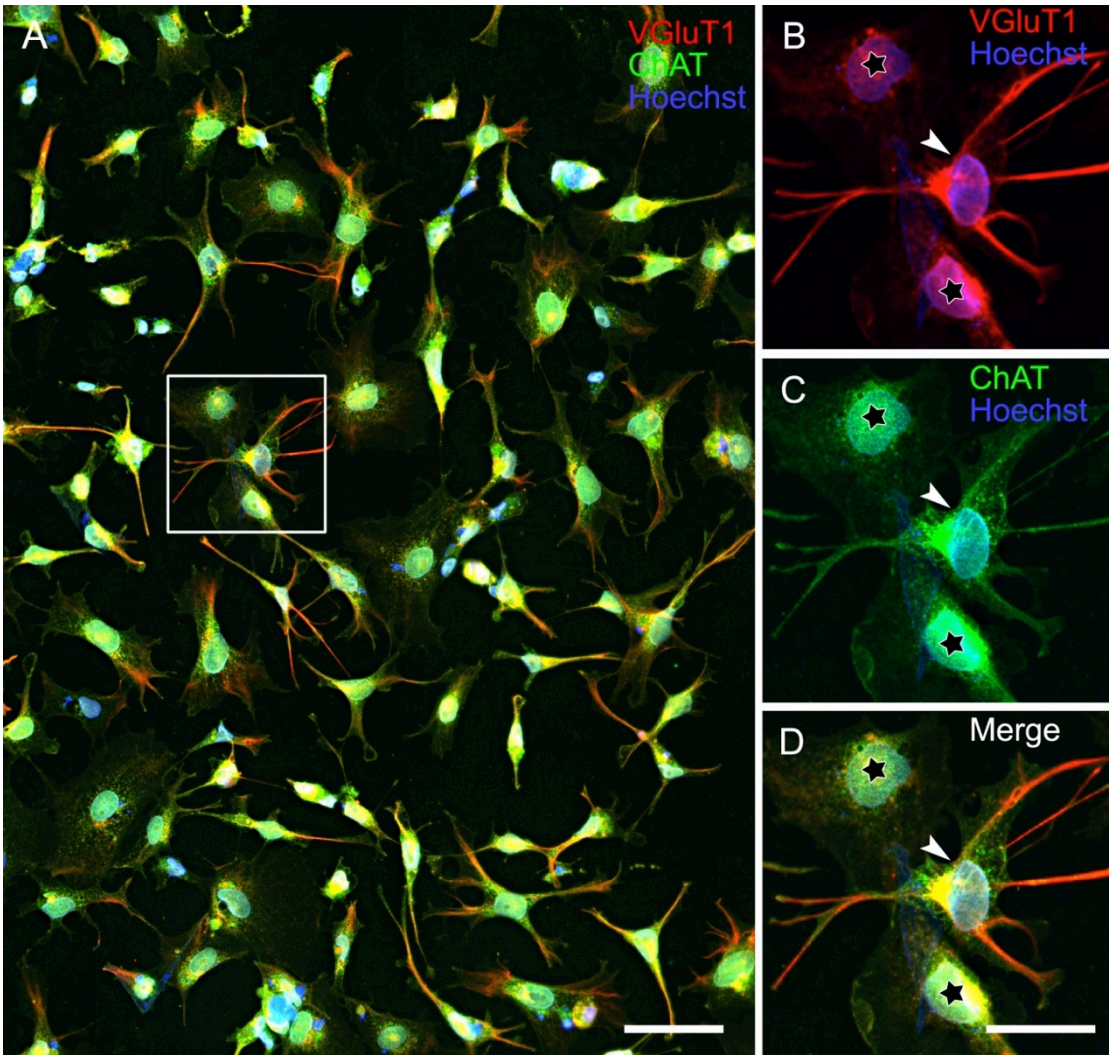

Figure 38. Epifluorescence microscopy images of AraC/NT2N cells processed for double immunofluorescence to VGlut1 (red) and ChAT (green) combined with Hoechst's staining (blue). **A.** Panoramic view corresponding to a mosaic from multiple images captured with a 20 X objective. **B-D.** Higher magnification of the area framed in A for a better view of VGlut1- (B) and ChAT-immunofluorescence (C) distribution in an AraC/NT2N neuron (arrowhead) and in non-neuronal cells (stars). Scale bars = 100 µm in A; 50 µm in D.

3. THE PC12 CELL LINE AS A MODEL OF NEURONAL DIFFERENTIATION

The PC12 cells line, derived from rat pheochromocytoma is a well-established model of sympathetic neuron differentiation. When exposed to NGF, PC12 cells undergo neuronal differentiation, acquire morphological and phenotypic features typical of sympathetic neurons, and synthesize and store the catecholamines dopamine and norepinephrine (Greene and Tischler, 1976).

3.1. Morphometric analysis

Proliferating PC12 cells, which are devoid of processes and display a rounded shape (Fig 39A), acquire a highly polarized morphology with long neurites and a triangular-shaped soma upon exposure to NGF (Fig. 39B). As described by Ignatius et al. (1985) cells are defined as differentiated when neurites are at least two cell body diameters long. Thus, we measured on phase-contrast images the diameter of cell bodies and neurite length (Figs. 39A-B) at 18, 24, 48, 72 and 96 h (100 cells per time point) after the beginning of NGF stimulation, and calculated the ratio between these two parameters. Then, we used this morphometric index to establish the time point at which differentiation is achieved after NGF treatment in our culture conditions. To this end mean values were fit by linear regression (Fig. 39C), and the resulting equation allowed us to calculate that 41 h after the beginning NGF treatment neurites reached a length of two body diameters (Fig. 39C, dashed line).

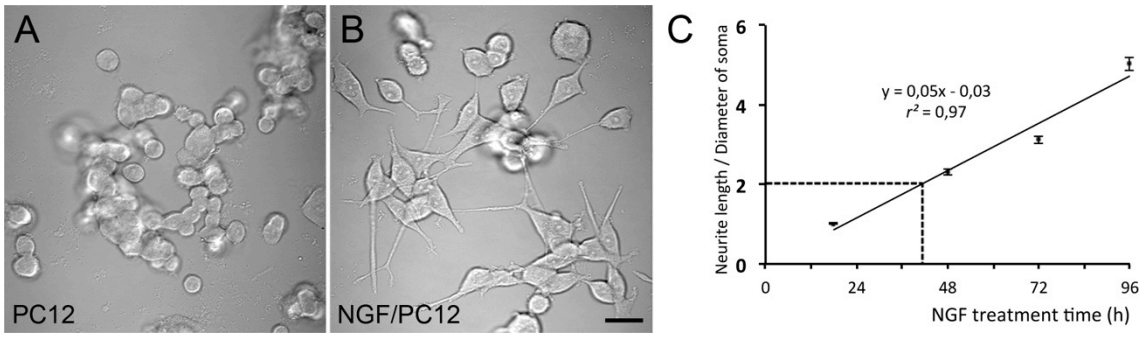

Figure 39. A-B. Phase-contrast micrographs of proliferating PC12 cells (A) and differentiated PC12 cells by treatment with NGF (50 ng/mL) during 96 h (B). **C.** Graph showing the ratio between neurite length and diameter of cell soma during time-course of NGF-induced differentiation. Values were fitted by linear regression analysis. Data are mean ± SEM (n=100). Scale bar = 25 μm.

3.2. Analysis of neurofilament 200 kDa expression

It has been described that NGF treatment leads to rapid upregulation of NF68 (68 kDa), NF160 (160 kDa), and NF200 (200 kDa) subunits in PC12 (Xu et al., 2012). Therefore, expression of these proteins can be used as an additional indicator of neuronal differentiation. Here we analyzed the expression of the neuronal marker NF200 in proliferating and differentiated PC12 cells. As shown in figures 40A-B, NF200-immunofluorescence increased in cells treated with NGF during 96 h. Consistently, NF200 was barely detectable in whole cell homogenates of untreated PC12 cells, whereas it was clearly detectable after 96 h of NGF treatment (Fig. 40C). Optical density analysis of immunoreactive bands showed that NF200-immunoreactivity increased significantly by about 3.5-fold in NGF treated PC12 cells with respect to proliferating cells (Fig. 40C).

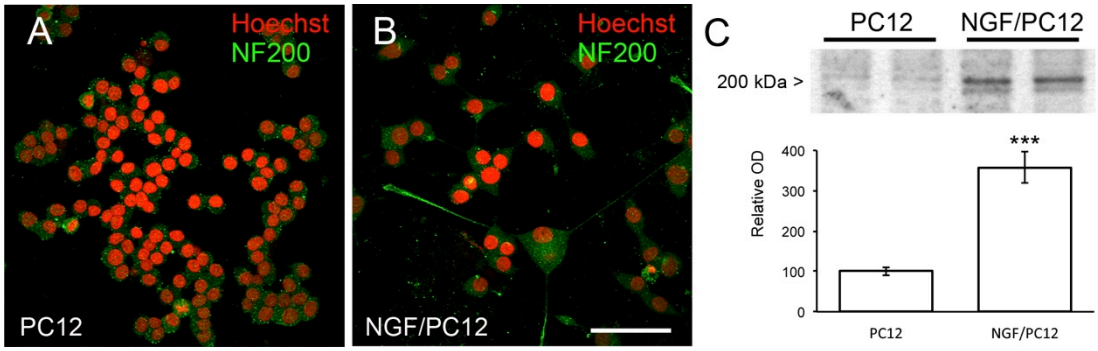

Figure 40. A-B. NF200-immunofluorescence (green) combined with Hoechst's chromatin staining (pseudocoloured in red) in fixed progenitor cells (A) and PC12 cells treated with NGF for 96 h (NGF/PC12 neurons). Scale bar = 50 µm. **C.** Results of immunoblots and semiquantitative densitometric analysis of immunoreactivity for the neuronal marker NF200. Immunoblots were performed in whole homogenates (5 µg of protein) of PC12 progenitors and NGF/PC12 neurons. The y-axis of the graph shows mean percent optical density normalized to the value in PC12 progenitor cells. Data are mean ± SEM (n=6). Two-tailed unpaired t-test (***$p < 0.001$).

4. PHOSPHOLIPASE Cβ1 DURING NEURONAL DIFFERENTIATION OF NT2 CELLS: EXPRESSION AND SUBCELLULAR LOCALIZATION

As a first descriptive approximation previous to the study of the role of PLCβ1 in neuronal differentiation of NT2 cells, using Western blot and high-resolution fluorescence microscopy, we performed an extensive analysis of the time-course of PLCβ1 expression during RA- and AraC-induced differentiation of NT2 cells.

4.1. PLCβ1a and PLCβ1b expression in subcellular fractions of NT2 cells

As described in the introduction, we carried out a modification of a well described subfractionation protocol (Fiume et al., 2010) that enables to obtain highly purified nuclei from cultured cells. By this modification it was possible to separate a fraction of highly purified nuclei (N) along with plasma membrane fraction (P2), a fraction enriched in intracellular membranes (S2) and a cytosolic fraction (Cyt).

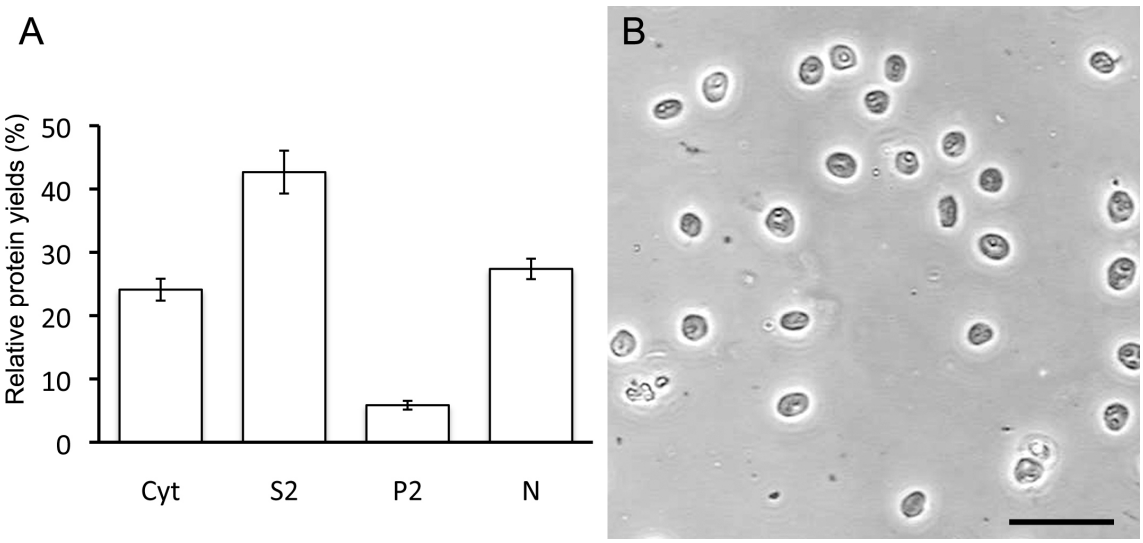

Figure 41. A. Percentage of protein recovered in each subcellular fraction of NT2 progenitors. Data are mean ± SEM (n=4). **B.** Phase-contrast micrograph of intact nuclei isolated from NT2 cells. Scale bar = 40 μm.

As depicted in the bar graph in figure 41A, the percentage of protein recovered in each fraction over the total was 24.1 ±1.7%, 42.7 ±0.7%, 5.9 ±0.7% and 27.4 ±1.6% in Cyt, S2, P2 and N fractions, respectively. This procedure preserved morphological features of isolated nuclei (Fig. 41B). Indeed, about 7 x 10^6 nuclei were isolated from each 150 cm^2 flask, which corresponds to an efficiency of more than 80% considering the amount of cells present in a 150 cm^2 flask at 70-80% confluence.

Subsequently, we analyzed by Western blot the enrichment of the Cyt, P2 and N fractions in specific markers of subcellular components. Specifically, antibodies against

to β-tubulin, α1 subunit of Na^+/K^+ ATPase and Histone H1 were used as specific markers of Cyt, P2 and N fractions. Additionally, antibodies against the endoplasmic reticulum (ER) chaperone binding immunoglobulin protein (BiP) and against the Golgi 58K protein were used to assess the possible cross-contamination of subcellular fractions.

As shown in figure 42, the cytoskeletal protein β-Tubulin was strongly detected in Cyt, whereas the α1 subunit of Na^+/K^+ ATPase and histone H1 were highly enriched in P2 and N fractions, respectively. None of the three markers was detected in 5 μg of whole cell homogenate. In contrast, strong immunoreactivity was observed for the Golgi marker Golgi 58K, indicating that Golgi membranes had been pelleted in the first centrifugation at low-speed and then completely solubilized and washed from intact nuclei by treatment with the non-ionic detergent Igepal. Indeed, no Golgi 58K-immunoreactivity was found in N fraction. BiP signal was similar in whole homogenate and P2 fraction, and weaker in Cyt fraction, suggesting some contamination of P2 and, to a lesser extent, of Cyt by ER components. In view that BiP is not enriched in P2 and that this fraction constitutes only 5.9 ±0.7% of the total protein (Fig. 41), it can be inferred that the bulk of ER is partitioned into the first pellet and then solubilized by treatment with Igepal.

Therefore, these results show that Cyt, P2 and N fractions are highly enriched in cytosolic, plasma membrane and nuclear proteins, respectively.

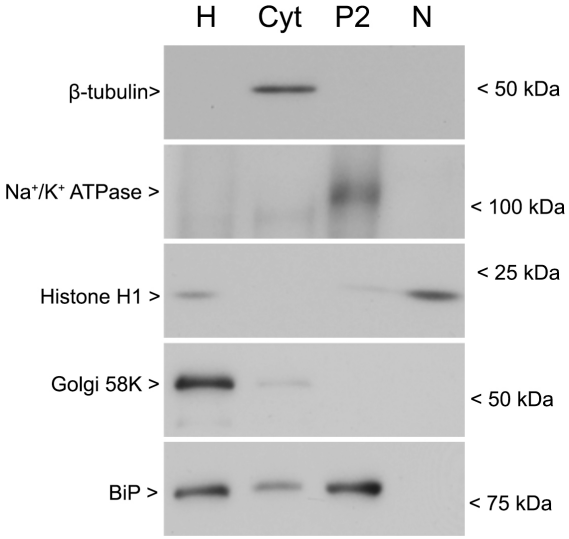

Figure 42. Western blot analysis of Cyt, P2 and N fractions obtained from NT2 progenitor cells with antibodies against subcellular fraction-specific antigens. For each marker, equal amounts of total protein (5 μg) were loaded on the same gel.

Once the different fractions had been tested for purity, we evaluated the partitioning of PLCβ1a and PLCβ1b isoforms into cytosolic, plasma membrane and nuclei. To this

end, equivalent volumes of Cyt, P2 and N were resolved in parallel by SDS-PAGE. Immunoblots were performed using a mouse monoclonal antibody raised against a peptide mapping at the N-terminus of PLCβ1 common to both PLCb1a and PLCb1b variants ($PLC\beta1_{N\text{-}ter}$ antibody, see Table 1 in Materials).

Western blot analysis showed that PLCβ1-immunoreactivity was highest in N, followed by P2 and Cyt fractions (Fig. 43), although no-significant differences were observed (Bar graph in Fig. 43).

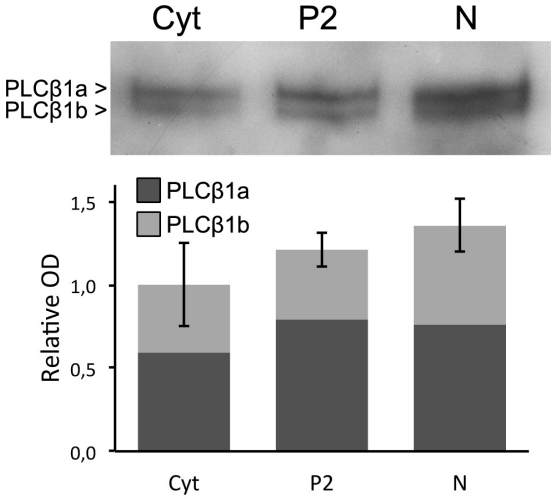

Figure 43. Western blot analysis of PLCβ1a and PLCβ1b expression in Cyt, P2 and N fractions obtained from NT2 progenitor cells. Equal volumes of each sample were loaded (40 μL) and run in parallel on the same gel. Bar graph depicts the OD of PLCβ1a and PLCβ1b immunoreactivity for each fraction, relative to total PLCβ1 (PLCβ1a and PLCβ1b) optical density in Cyt extract (normalized to 1). The different shading inside bars depicts the relative contribution of PLCβ1a and PLCβ1b to the total signal. Data are mean ± SEM (n=4).

Regarding the contribution of splice variants to the total signal, PLCβ1a was more abundant than PLCβ1b in all fractions analyzed. Thus, the PLCβ1a/PLCβ1b OD ratios were 1.41 ± 0.05%, 1.89 ± 0.13%, and 1.27 ± 0.07 in Cyt, P2 and N fractions, respectively. Statistically significant differences in PLCβ1a/b ratios were detected between Cyt and P2 and between P2 and N (both $p < 0.01$, one-way ANOVA followed by Tukey's test, n=4).

4.2. Time-course of expression of PLCβ1a and PLCβ1b variants during RA-induced differentiation of NT2 progenitors

4.2.1. Western blot analysis

Western blot analysis of whole homogenates from cells at different time points during RA-induced differentiation revealed a drastic increase of PLCβ1 immunoreactivity one week after initiation of RA treatment, which remained elevated until day 28. In contrast, PLCβ1-immunoreactivity in isolated RA/NT2N neurons was equivalent to that found in NT2 cells, whereas in non-neuronal NT2A cells (remaining attached to the flask after mechanical dislodging of neurons at day 28, see section 2 in Results) was as high as that in NT2 cells between days 7 and 28 (Fig. 44).

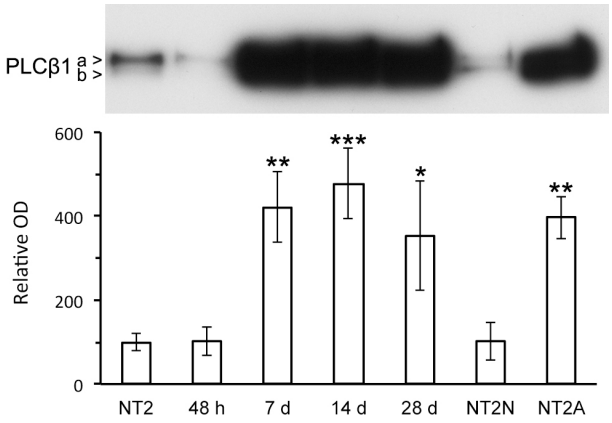

Figure 44. Results of Western blot and semiquantitative densitometric analysis of PLCβ1-immunoreactivity. Immunoblots were performed in whole homogenates of NT2 progenitors, RA-treated cells (48 h, 7 d, 14 d, 28 d), terminally differentiated RA/NT2N neurons and non-neuronal NT2A cells remaining attached to the flask after mechanical dislodging of neurons (see section 2 of Results). Equal amounts of total protein (12 µg) were loaded from each sample in the same gel (n=4). The y-axis of the graph shows relative optical density (OD) expressed as percent of that found in NT2 progenitor cells (normalized to 100%). Repeated measures one-way ANOVA followed by Tukey's post-hoc test. Significant differences between the different samples with respect to NT2 progenitors are shown (*$p < 0.05$; **$p < 0.01$; ***$p < 0.001$). Data are mean ± SEM (n=4).

The strong PLCβ1-immunoreactive signal made impossible to discern the splice-variant specific bands between days 7 and 28. To overcome this problem, the amount of total protein loaded was readjusted for each condition, such that non-saturating signals could be obtained at all time point (details in the legend of Fig. 45). This enabled to resolve quantifiable signals for PLCβ1a and PLCβ1b bands in all samples. The percent changes in expression were corrected for amount of protein loaded.

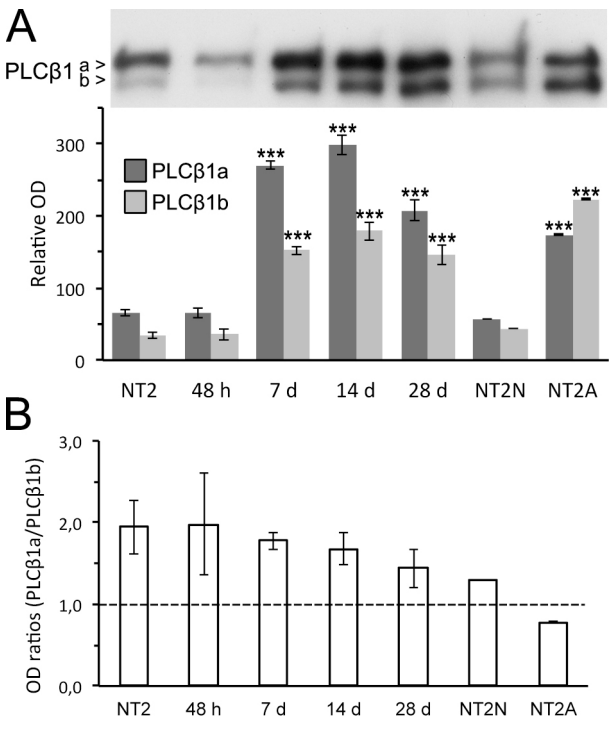

Figure 45. A. Western blot analysis of PLCβ1a and PLCβ1b expression during RA-induced differentiation. Immunoblots were performed in whole homogenates at the same time points shown in figure 44, but loading different amounts of total protein (from lane 1 to 7: 37.5, 37.5, 12.5, 12.5, 12.5, 37.5 and 12.5 µg). Relative optical density (OD) is expressed as percent of that found for total PLCβ1 (PLCβ1a + PLCβ1b) in NT2 progenitor cells (normalized to 100%). Two-way ANOVA with post-treatment time (NT2, 48 h, 7 d, 14 d, 28 d, NT2N and NT2A) and splice variant (PLCβ1a and PLCβ1b) as the main factors followed by Bonferroni's post-hoc test. Significant differences between ODs for each splice variant in different samples with respect to OD found for the corresponding splice variant in NT2 progenitors are shown (***$p < 0.001$). **B.** Time-course of ratios between PLCβ1a and PLCβ1b immunoreactivity during RA-induced neuronal differentiation of NT2 cells. All data are mean ± SEM (n=2).

As represented in figure 45, the expression of both splice variants increased significantly between days 7 and 28. However, the ratio between PLCβ1a and PLCβ1b

tended to equalize as differentiation progressed, and this ratio was inverted in non-neuronal NT2A cells (Fig. 45B), although no statistically significant changes were detected by one-way ANOVA analysis.

4.2.2. Fluoresecence microscopy analysis

Results obtained by Western blot analysis were extended by combined PLCβ1 and NF200 immunofluorescence and high-resolution fluorescence microscopy. For this study, the monoclonal PLCβ1 (D-8) antibody raised against a synthetic peptide corresponding to an epitope mapping within an internal region of PLCβ1 (amino acids 831-1063) common to PLCβ1a and PLCβ1b (see Table 1 in Materials).

As illustrated in figure 46, PLCβ1-signal was barely detectable in NT2 progenitors, which were NF200-negative (Figs. 46A-B). An increase in PLCβ1-immunoreactivity was observed 48 h after the onset of RA-treatment. At this time point, cells began to express NF200, which colocalized with PLCβ1 (Fig. 46C-D). PLCβ1-immunostaining consisted of a dense juxtanuclear ball form which fibrilar-like processes emanated. PLCβ1-immunolabeling displayed a similar distribution pattern after 7 days of RA treatment, although immunostaining intensity increased considerably. In contrast, NF200-immunoreactivity increased only in a small proportion of cells, whereas it was undetectable in the vast majority of them (Fig. 45F). This is consistent with Western blot results showing a rapid increase in NF200-immunoreactivity at 48 h followed by progressive decrease until day 28 (Fig. 32A). The most noticeable change at day 28 was that NF200-immunopositive cells showed considerable less PLCβ1-immunoreactivity than NF200-negative cells (Fig. 46H), suggesting that PLCβ1 is downregulated as cells acquire neuronal fate. In agreement with this, after removal of neuronal cells by mechanical dislodging, NF200-immunoreactivity virtually disappeared from cultures of remaining non-neuronal NT2A cells, which displayed bright PLCβ1-immunostaining (Figs. 46K-L). RA/NT2N neurons, treated with antimitotics for 2 weeks after mechanical dislodging, showed intense nuclear PLCβ1-immunoreactivity. PLCβ1-signal in the neuronal body and neurites was hardly visible when exposure settings were adjusted to avoid saturation of the nuclear signal (Figs. 46I-J). Notably RA/NT2N neurons displayed dense NF200 immunoreactivity (Fig. 46J), in agreement with Western blot analysis (Fig. 32A).

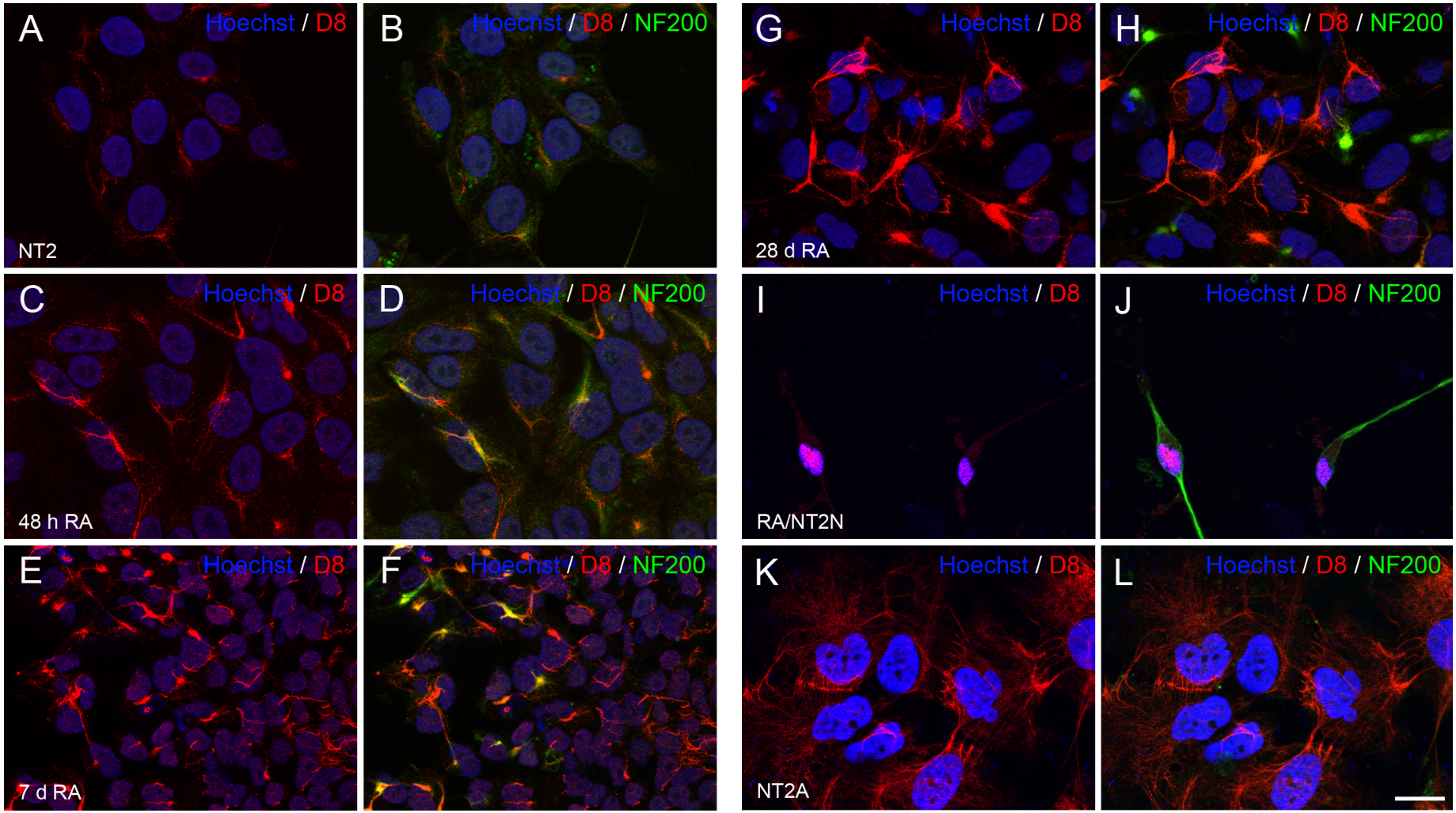

Figure 46. Double-immunofluorescence against PLCβ1 (D-8) (red) and NF200 (green) combined with Hoechst's chromatin staining (blue) in fixed NT2 progenitor cells (**A-B**), NT2 cells treated with RA 10 µM for 48 h (**C-D**), 8 days (**E-F**), 4 weeks (**G-H**), RA/NT2N neurons (**I-J**) and non-neuronal NT2A cells (**K-L**). Micrographs are maximum intensity projections of four consecutive optical sections separated by 0.24 µm, obtained using the structured illumination module (ApoTome). Scale bar = 20 µm.

4.3. Time-course of expression of PLCβ1a and PLCβ1b variants during AraC-induced differentiation of NT2 progenitors

4.3.1. Western blot analysis

Treatment of NT2 cells with AraC led to an progressive increase in PLCβ1-immunoreactivity over 72 h after the initiation of AraC treatment (Fig. 47). AraC appeared to have a more acute effect than RA (compare Figs. 44 and 47). Similarly to that observed during RA-induced differentiation, PLCβ1-immunoreactivity returned nearly to basal levels in terminally differentiated neurons.

Similarly to that observed during RA-induced differentiation, strong PLCβ1-immunoreactive signals at 48 and 72 h made impossible to discern the splice-variant specific bands. Therefore, the same strategy was used to overcome this inconvenience (see section 4.2.1.). Thus the amount of total protein loaded was readjusted for each condition, such that non-saturating signals could be obtained at all time point (details in the legend of Fig. 47) and the percent changes in expression were corrected for amount of protein loaded.

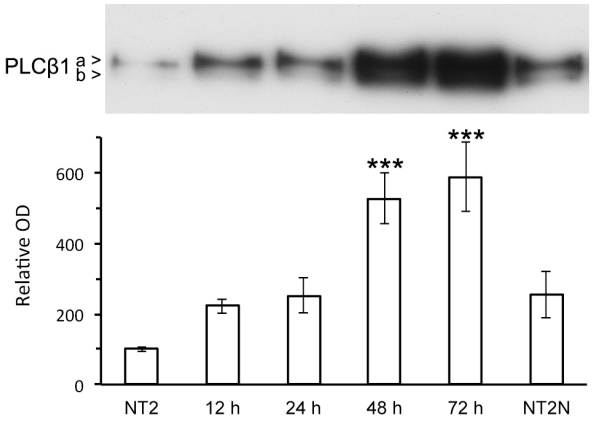

Figure 47. Results of immunoblots and semiquantitative densitometric analysis of PLCβ1-immunoreactivity. Immunoblots were performed in whole homogenates of NT2 progenitors, AraC-treated cells (12, 24, 48 and 72 h) and AraC/NT2N cells. Equal amounts of total protein (12 μg) were loaded from each sample in the same gel. The y-axis of the graph shows relative optical density (OD) expressed as percent of that found in NT2 progenitor cells (normalized to 100%). Repeated measures one-way ANOVA followed by Tukey's post-hoc test. Significant differences between the different samples with respect to NT2 progenitors are shown (***$p < 0.001$). Data are mean ± SEM (n=4).

As illustrated in figure 48A, two way-ANOVA and Tukey's post-hoc test showed that PLCβ1a- and PLCβ1b-expression remained significantly increased at all time points analyzed. The expression of both splice variants increased progressively, reaching a maximum between 48 and 72 h post-treatment and then decreasing at the end of differentiation. The ratio between PLCβ1a and PLCβ1b tended to equalize during the first 72 h of treatment, but returned to values found in NT2 progenitors at the end of

AraC treatment. In any case, no statistically significant changes were detected (Fig. 48B).

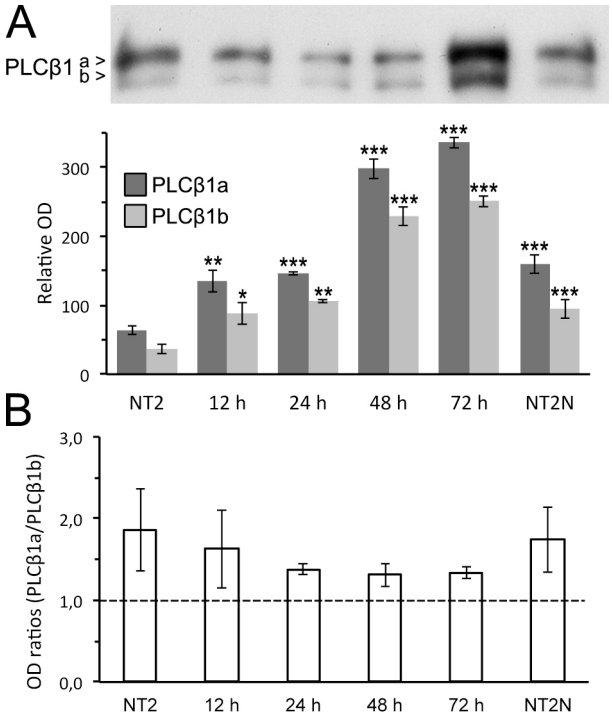

Figure 48. Western blot analysis of PLCβ1a and PLCβ1b expression during AraC-induced differentiation. Immunoblots were performed in whole homogenates at the same time points shown in figure 47, but loading different amounts of total protein (from lane 1 to 6: 37.5, 25, 12,5, 12,5, 25 and 37.5 μg). Relative optical density (OD) is expressed as percent of that found for total PLCβ1 (PLCβ1a + PLCβ1b) in NT2 progenitor cells (normalized to 100%). Two-way ANOVA with post-treatment time (NT2, 12 h, 24 h, 48 h, 72 h, AraC/NT2N) and splice variant (PLCβ1a and PLCβ1b) as the main factors followed by Bonferroni's post-hoc test. Significant differences between ODs for each splice variant in different samples with respect to OD found for the corresponding splice variant in NT2 progenitors are shown (***$p < 0.001$). **B.** Time-course of ratios between PLCβ1a and PLCβ1b immunoreactivity during RA-induced neuronal differeniation of NT2 cells. All data are mean ± SEM (n=2).

Comparison of the time-course of PLCβ1-, and neuronal markers-expression (NF200 and β-III-tubulin) during AraC-induced differentiation (Fig. 49), showed that PLCβ1-upregulation preceded the increment in expression levels observed for NF200 or β-III-tubulin, suggesting that PLCβ1 could be involved in modulation of neuron-specific gene expression.

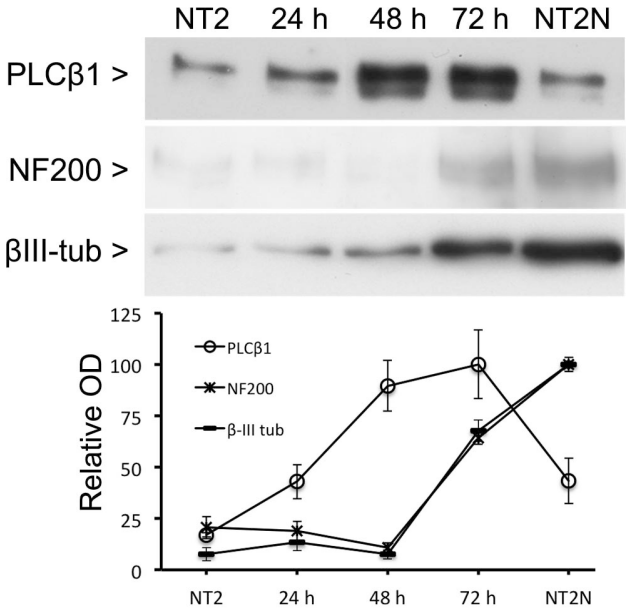

Figure 49. Comparison of the time-course of PLCβ1- and neuronal marker-expression (NF200 and β-III-tubulin) during AraC-induced differen-tiation. Optical density values were normalized to optical density at the time point showing the highest expression level for each protein. All data are mean ± SEM (PLCβ1, n=4; NF200 and β-III-tub, n=3).

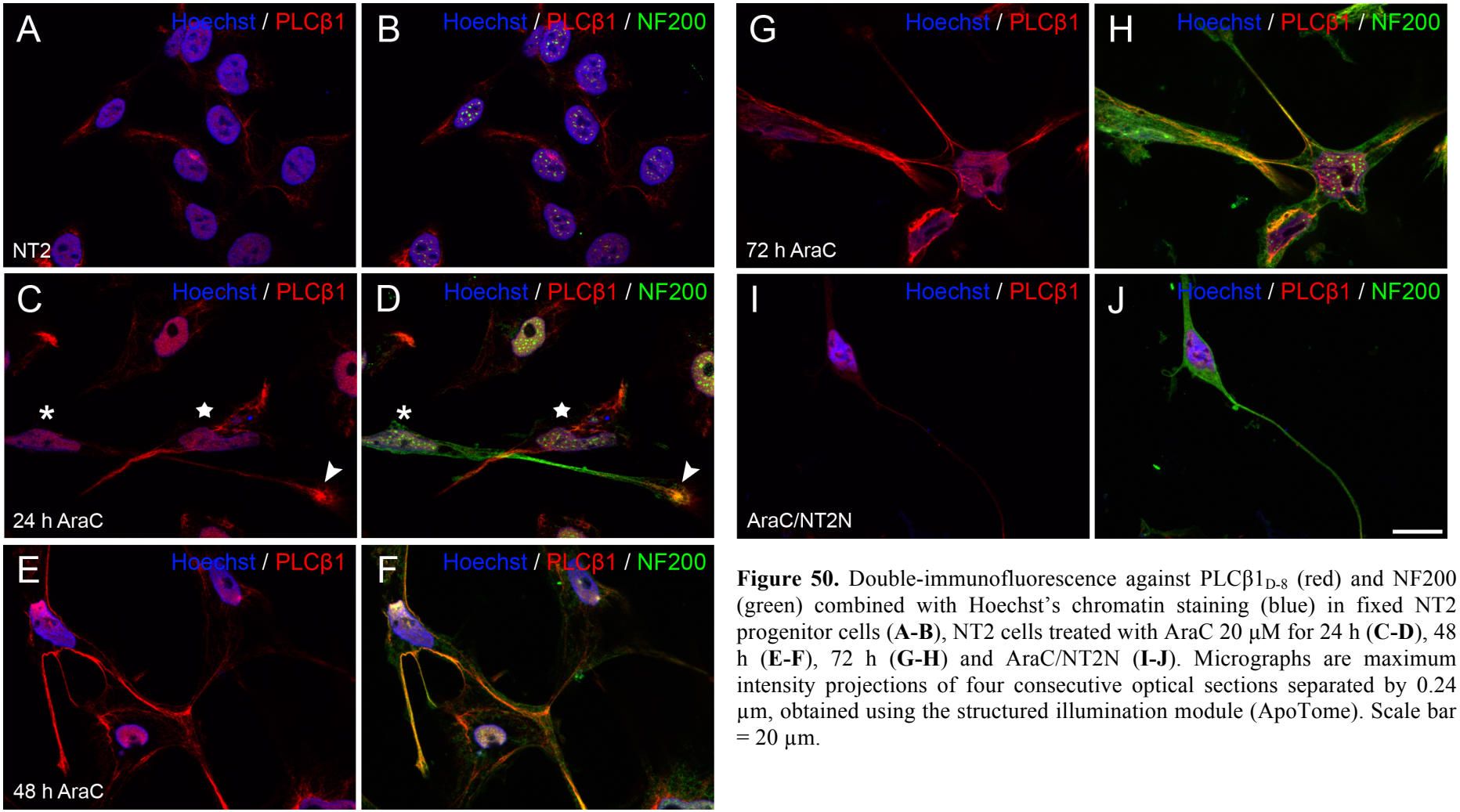

Figure 50. Double-immunofluorescence against PLCβ1$_{D\text{-}8}$ (red) and NF200 (green) combined with Hoechst's chromatin staining (blue) in fixed NT2 progenitor cells (**A-B**), NT2 cells treated with AraC 20 µM for 24 h (**C-D**), 48 h (**E-F**), 72 h (**G-H**) and AraC/NT2N (**I-J**). Micrographs are maximum intensity projections of four consecutive optical sections separated by 0.24 µm, obtained using the structured illumination module (ApoTome). Scale bar = 20 µm.

4.3.2. Fluorescence microscopy analysis

Results obtained by Western blot analysis were extended by combined PLCβ1 and NF200 immunofluorescence and high-resolution fluorescence microscopy using the monoclonal PLCβ1 ($PLC\beta1_{D-8}$) antibody (see Table 1 in Materials).

As illustrated in figure 50, PLCβ1-immunolabeling increased considerably in NT2 cells treated with AraC for 24 h when compared with NT2 progenitor cells (Figs. 50 A-D). PLCβ1-signal was intense in neurites and diffusely distributed in the cell nucleus. NF200 was highly upregulated in a subset of cells (Figs. 50C-D, asterisk), where it colocalized in growth-cone like structures (Figs. 50C-D, arrowhead). Noticeably, a subset of neurite-bearing cells with bright PLCβ1-immunostaining were NF200-negative (Figs. 50C-D, star), reinforcing the notion that upregulation of PLCβ1 precedes the appearance of neuron-specific markers as suggested above. After 48 h and 72 h post-treatment, PLCβ1-immunoreactivity increased even more in neurites and continued to be present in the cells nucleus. The immunostaining pattern in cells displaying neuronal morphology did not differ between 48 h and 72 h time points (Figs. 50 E-H). However a major difference was that the vast majority of cells were NF200-positive at 72 h, but not at 48 h of AraC treatment. This is in agreement with results of Western blot analysis, showing a sharp increase in NF200-immunoreactivity in cell whole homogenates between 48 and 72 h of AraC treatment (Fig. 49B). The PLCβ1- and NF200-immunostaining patters in AraC/NT2N neurons were similar to that observed in RA/NT2N neurons (compare Figs. 46I-J and 50I-J). Thus, AraC/NT2N showed intense nuclear PLCβ1-immunoreactivity (Figs. 50I-J), whereas a weak signal was observed in projections. Again, in agreement with Western blot results, AraC/NT2N neurons displayed dense NF200 immunoreactivity in both soma and neurites (Fig. 50J).

Overall, the results shown in this chapter show that PLCβ1 expression and subcellular localization is highly regulated during the time-course of RA- and AraC-induced differentiation suggesting a possible role of PLCβ1 in neuronal differentiation.

5. ROLE OF PHOSPHOLIPASE C β1 IN NEURONAL DIFFERENTIATION

5.1. Role of PLCβ1 in AraC-induced differentiation of neuronal differentiation of NT2 progenitors

To analyze whether PLCβ1 is necessary for differentiation of NT2 cells we assayed two different strategies for siRNA knockdown of PLCB1 gene in NT2 cells. First, we tested the efficiency of four shRNA constructions cloned into pSuperior.gfp/neo vector and compared it with that obtained using ON-TARGET plus SMART pool siRNAs (see Methods), which consist of four siRNAs to the same target gene mixed together.

5.1.1. Silencing efficiency of PLCβ1 shRNAs

Four different shRNAs cloned into the pSuperior.gfp/neo vector were tested for transfection and silencing efficiency. Because this vector contains a GFP reporter gene, transfection could be directly observed by fluorescence microscopy. As negative controls, the commercial plasmid pSuperior.gfp/neo containing no insert and a non-targeting scramble shRNA were used. As shown in figure 51, only a proportion of NT2 cells expressed GFP 48 h after transfections. Fluorescence intensity varied throughout the cell population. In any case, all plasmids, except 97 shRNA, yielded similar levels of transfection that was below 50% of the total population. The transfection efficiency was even lower for the 97 shRNA construct, which in addition appeared to compromise cell viability.

Western blot analysis of PLCβ1-immunoreactivity in NT2 cell homogenates, 48 after transfection with different shRNAs, showed that all targeting shRNAs (87, 89, 97 and 99) caused a decrease of PLCβ1-expression in about 50%, suggesting that PLCβ1 was efficiently knocked down. However, no statistically significant differences were achieved with the sample used (n=2). In any case, because transfection efficiency was not complete, we decided to use commercially available siRNA pools (see Methods). Because shRNA in the pSuperior.gfp/neo vector is under the control of an inducible H1 promoter containing the tetracycline operator 2 (TetO2), these constructions are ideal for inducible knockdown of the desired gene by tetracycline treatment. Currently, we have designed a strategy to obtain a NT2 cell line for conditional knockdown of PLCβ1 using shRNAs cloned in pSuperior.gfp/neo.

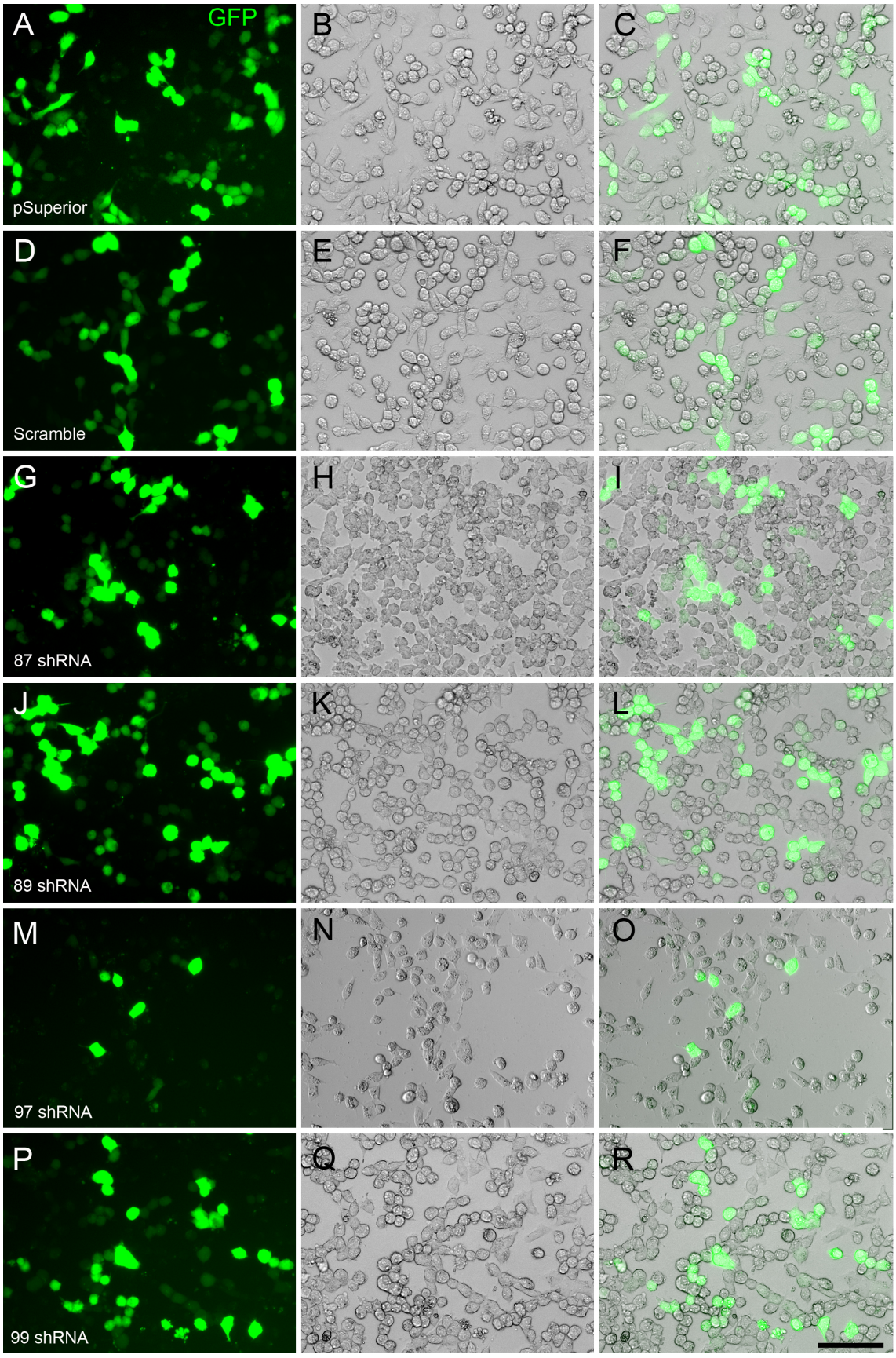

Figure 51. Evaluation of shRNA-transfection efficiency using fluorescence microscopy to visualize reporter protein GFP. NT2 cells were transfected with pSuperior.gfp/neo plasmid either with no shRNA encoding sequence (A-C) or containing non-targeting scramble RNA (D-F) or shRNAs (87, 89, 97 and 99 shRNA) targeting human PLCB1 gene (G-R). Phase contrast and GFP expression were assessed under a fluorescent microscope. Scale bar = 100 µm.

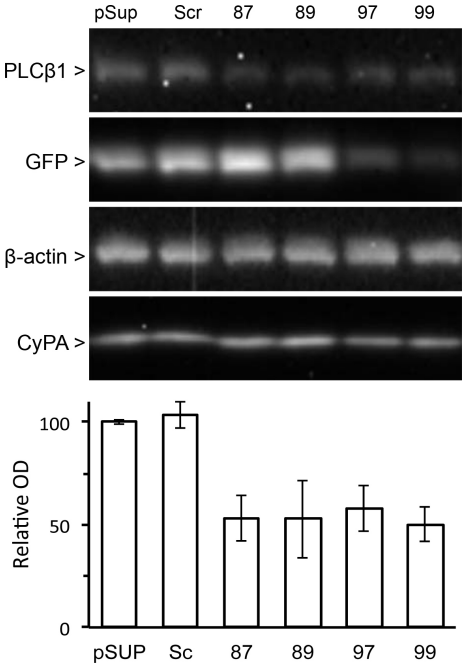

Figure 52. Western blot and semiquantitative densitometric analysis of immunoreactivity for PLCβ1, GFP, β-actin and cyclophyllin (CyPA). Immunoblots were performed in whole homogenates of NT2 progenitors cells 48 h post transfection with pSuperior.gfp/neo plasmid either with no shRNA encoding sequence (pSup) or containing non-targeting scramble RNA (Scr) or shRNAs (87, 89, 97 and 99 shRNA) targeting human PLCB1 gene. Equal amounts of total protein (30 μg) were loaded on the same gel. The y-axis of the graph shows mean percent optical density normalized to the value obtained in NT2 transfected with pSuperior.gfp/neo plasmid. All data are mean ± SEM (n=2).

5.1.2. Silencing efficiency of PLCβ1 siRNA pools

In view of the not fully satisfactory results obtained with shRNA, we used commercially available species-specific siRNAs pools (see Materials), which consist of four siRNAs to the same target gene mixed together.

First, we tested the silencing efficiency of siRNAs as well as their ability to produce a sustained knock of PLCβ1. For this purpose, NT2 cells were transfected with the siRNA pool targeting human PLCB1 gene. Transfection with a non-target pool was used as a negative control. Transfected cells were allowed to grow for 12, 24, 48, 72 or 96 h and then harvested and homogenized for SDS-PAGE and immunoblot.

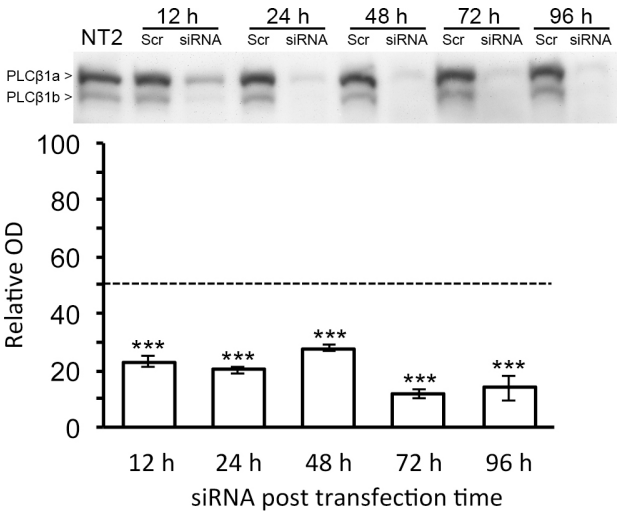

Figure 53. PLCβ1-immunoreactivity in whole homogenates form control NT2 cells or cells transfected with either non-targeting scramble siRNA (Scr) or siRNA targeting human PLCB1 gene (siRNA). Cells were harvested at post-transfection times of 12, 24, 48, 72 and 96h. 30 μg total protein was loaded in each lane and resolved in parallel. Values at each time point represent the mean percentage of optical density (OD) normalized to the corresponding value obtained in NT2 cells transfected with scramble siRNA. Repeated measures one-way ANOVA followed by Tukey's post-hoc test (***$p < 0.001$). Data are mean ± SEM (n=4).

As illustrated in Figure 53, siRNA led to a drastic decrease of PLCβ1-immunoreactivity (~80%) as soon as 12 h after transfection. Moreover, PLCβ1-knockdown was sustained up to 96 h after transfection. Next, we evaluated the specificity of targeting by analyzing the expression of PLCβ4 and β-actin on siRNA-transfected NT2 cells. As it can be appreciated in figure 54, neither PLCβ4 nor β-actin expression were affected by the siRNA pool targeting human PLCB1 transcript.

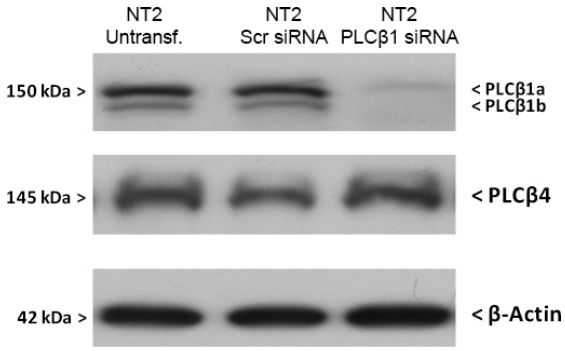

Figure 54. PLCβ1-, PLCβ4- and β-actin-immunoreactivity in whole homogenates of NT2 progenitors cells 48 h after transfection with either scramble siRNA or PLCβ1 siRNA. Equal amounts of total protein (30 μg) were loaded on the same gel. The experiment was repeated 3 times with same results.

5.1.3. Effects of PLCβ1 silencing in AraC-induced differentiation

To test whether PLCβ1 silencing affects AraC-induced differentiation, NT2 cells were transfected either with non-targeting or PLCB1 gene targeting siRNA and treated with AraC for 72 h, a time point at which neuron-specific markers are already expressed. As shown in figure 55, PLCβ1 siRNA prevented acquisition of the typical neuronal polarity induced by treatment with AraC, whereas scramble siRNA did not. Moreover, cells transfected with PLCβ1 siRNA continued to proliferate, preventing cell growth arrest induced by AraC.

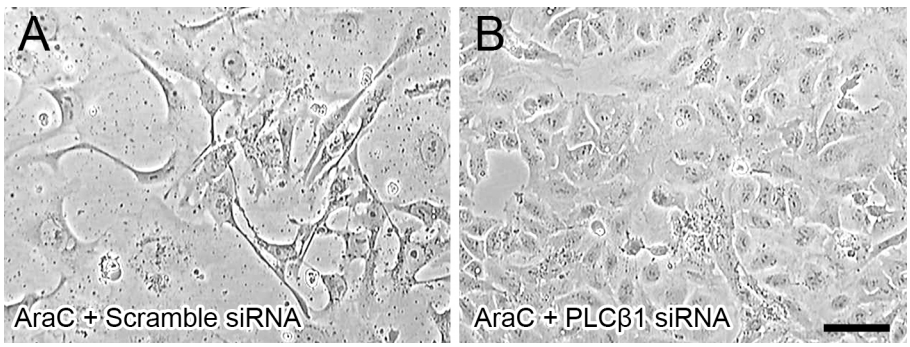

Figure 55. Phase-contrast micrographs of NT2 cells fixed 96 h after transfection with either scramble siRNA or PLCβ1 siRNA and treated with AraC for 72 h. Scale bar = 50 μm.

Western blot analysis allowed us to analyze the impact of PLCβ1 silencing in NF200 and β-III-tubulin expression after treatment with AraC for 72 h. As expected,

scramble siRNA did not prevent upregulation of PLCβ1 expression after 72 h of AraC treatment, whereas targeting siRNA caused a drastic decrease of PLCβ1 expression (Figs. 56A-B), which was clearly below basal levels (Fig. 56 B, dashed line). In NT2 cells transfected with scramble siRNA, the expression of the neuron-specific makers NF200 and β-III-tubulin increased with respect to untransfected NT2 cells as previously observed (see Section 1, Fig. 32A, H-I), whereas it was prevented by PLCβ1 siRNA (Fig. 56).

These results, demonstrate that PLCβ1 is necessary for AraC-induced neuronal differentiation of NT2 cells.

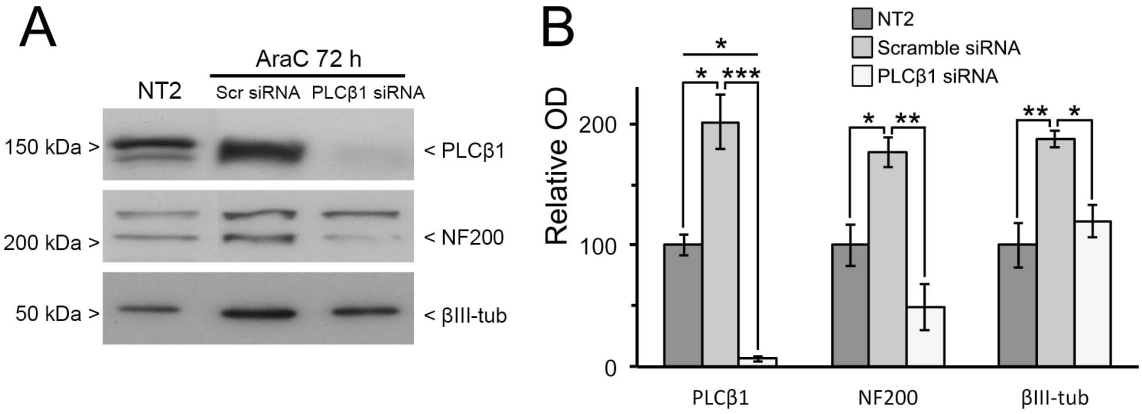

Figure 56. A. Western blot analysis of PLCβ1, NF200 and βIII-tubulin expression in NT2 cells and cells transfected either with scramble siRNA or PLCβ1 siRNA and treated with AraC for 72 h. **B.** Densitometric analysis of of PLCβ1-, NF200 and βIII-tubulin-immunoreactivity. In the three conditions mentioned in A. Equal amounts of total protein (30 μg) were loaded on the same gel and run in parallel. The y-axis of the graph shows mean of optical density normalized to the value obtained NT2 cells. One-way followed by post hoc Tukey's test (*$p < 0.05$; **$p < 0.01$; *** $p < 0.001$). Data are mean ± SEM (n=4).

5.2. Effect of PLCβ1 overexpression on NT2 progenitor cells

Results of siRNA knockdown shown that PLCβ1 is necessary for AraC-induced neuronal differentiation of NT2 progenitors prompted us to assess whether PLCβ1 overexpression is sufficient to induce neuronal differentiation of NT2 cells in the absence of any added differentiating agent. To this end, we generated PLCβ1 constructs either untagged or HA-tagged. Thus, cDNAs encoding PLCβ1a, PLCβ1b, HA- PLCβ1a and HA-PLCβ1b were cloned in pCDNA3.0 vector (see Methods).

5.2.1. Validation of constructs

First, we determined by Western blot whether these constructs encoded the expected proteins 24 h after transfection of NT2 progenitors (Fig. 57)

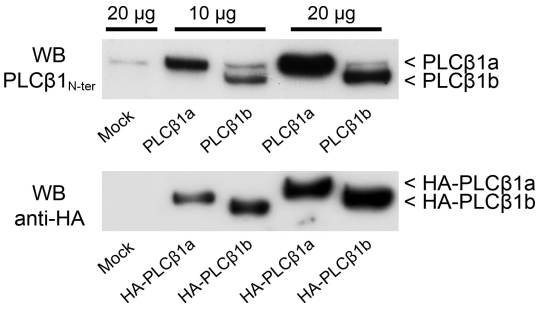

Figure 57. Western blot analysis of PLCβ1a and PLCβ1b (upper blot) and HA-PLCβ1a and HA-PLCβ1b (lower blot) overexpression 24 h after transfection. Immunoblots were performed in whole homogenates of NT2 progenitor transfected with empty plasmid alone (mock) or pCDNA-containing the sequences encoding untagged or HA-tagged splice variants PLCβ1a and PLCβ1b. Note that PLCβ1a expression is not affected by transfection with either the mock (upper blot, lane 1) of the pCDNA-PLCβ1b plasmid (upper blot, lanes 3 and 5). In conditions used for immunoblot, immunoreactivity for endogenous PLCβ1b was below the detection threshold in mock-transfected (upper blot, lane 1) as well as in PLCβ1a-transfected samples (upper blot, lanes 2 and 4).

As shown in figure 57 (upper blot), overexpression of native PLCβ1a and PLCβ1b led to the appearance of strong immunoreactive bands at the expected positions, as evidenced by Western blot analysis using the monoclonal antibody PLCβ1$_{N\text{-}ter}$ (which recognizes both splice variants). Also, transfection with pCDNA-PLCβ1a and pCDNA-PLCβ1b did not affect inmmunoreactivity of endogenous PLCβ1b and PLCβ1a, respectively (Fig. 57, upper blot). Immunoblots of homogenates from NT2 cells overexpressing either HA-PLCβ1a and PLCβ1b using a monoclonal anti-HA antibody yielded single strong immunoreactive bands at the expected positions (Fig. 57, lower blot).

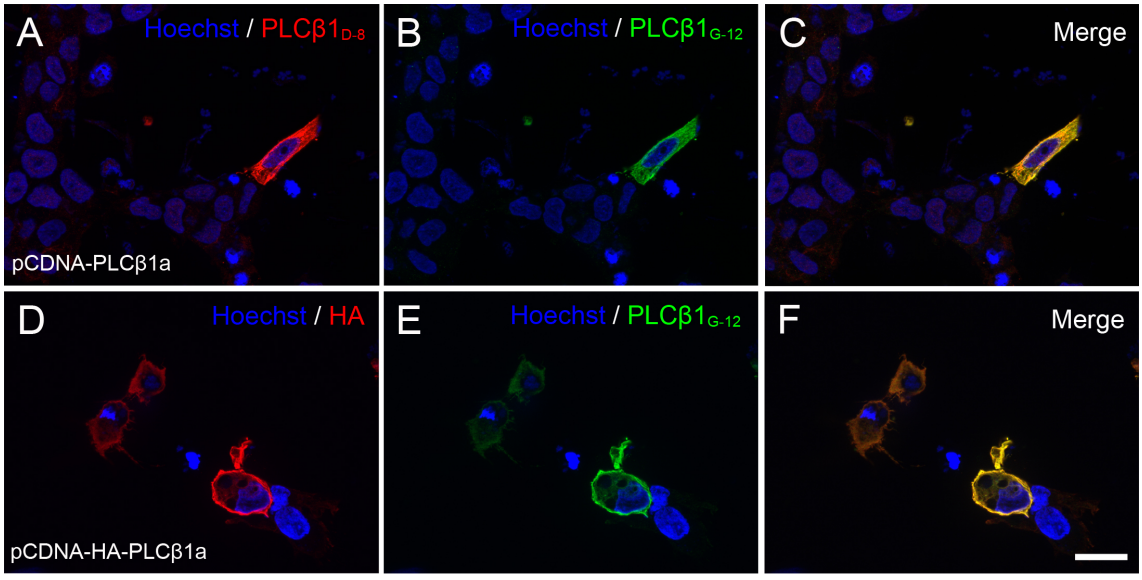

Figure 58. NT2 progenitors cells transfected with pcDNA-PLCβ1a (A) or HA-pcDNA-PLCβ1a (B), fixed 24 h after transfection and processed for double-immunofluorescence against PLCβ1$_{D\text{-}8}$ or HA (red) and PLCβ1$_{G\text{-}12}$ (green) combined with Hoechst's chromatin staining (blue). Exposure was adjusted such that endogenous PLCβ1-signal could not be visualized. Micrographs are maximum intensity projections of four consecutive optical sections separated by 0.24 µm, obtained using the structured illumination module (ApoTome). Scale bar = 20 µm.

Next we examined overexpression of the different constructs in fixed NT2 cells 24 h after transfections. For this purpose, different anti-PLCβ1 antibodies were used for by immunofluorescence and high-resolution microscopy analysis. Double-immunofluorescence analysis of PLCβ1a-transfected cells was performed by combining the mouse monoclonal PLCβ1$_{D-8}$ antibody (which recognized both splice variants) and the goat polyclonal PLCβ1$_{G-12}$, raised against the splice variant-specific tail of PLCβ1a.

As shown in figures 58A-C, under short exposure to avoid visualization of endogenous signal, strong signals were obtained with both PLCβ1$_{D-8}$ and PLCβ1$_{G-12}$ antibodies in NT2 cells transfected with the pCDNA-PLCβ1a vector. The high colocalization observed using antibodies raised in different species and directed against distant regions of PLCβ1a amino acid sequence, demonstrate the integrity of recombinant PLCβ1a protein. Similarly, high colocalization was observed by combining the mouse monoclonal PLCβ1$_{D-8}$ antibody and the rabbit polyclonal anti-HA antibody in NT2 cells transfected with the pCDNA-HA-PLCβ1a vector. (Figs. 58D-F).

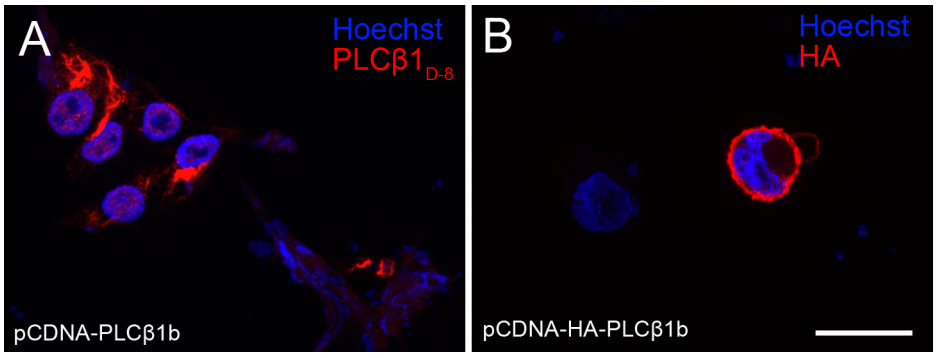

Figure 59. NT2 progenitors cells transfected with pcDNA-PLCβ1b (**A**) or HA-pcDNA-PLCβ1b (**B**), fixed 24 h after transfection and processed for immunofluorescence using the mouse monoclonal PLCβ1$_{D-8}$ or rabbit polyclonal anti-HA antibodies (red) combined with Hoechst's chromatin staining (blue). Micrographs are maximum intensity projections of four consecutive optical sections separated by 0.24 µm, obtained using the structured illumination module (ApoTome). Scale bar = 20 µm.

Because there are not available antibodies against the PLCβ1b splice variant, immunostaining in cells transfected with the pcDNA-PLCβ1b vector was performed using the monoclonal PLCβ1$_{D-8}$, whereas the rabbit polyclonal anti-HA antibody was used for assays in cells transfected with the pcDNA-HA-PLCβ1b vector. As illustrated in figures 59A and B, under short exposure, strong signal was observed in putatively PLCβ1b- and HA-PLCβ1b-transfected NT2 cells. Although immunofluorescence analysis was not fully conclusive to demonstrate overexpression of recombinant PLCβ1b, combination of immunofluorescence and Western blot results allow us to

conclude that PLCβ1b was actually overexpressed in NT2 cells transfected with the pCDNA-PLCβ1b vector.

5.2.2. Effects of PLCβ1a and PLCβ1b overexpression in cell morphology and expression of neuron-specific markers in NT2 cells

Once validated, constructs coding for the native amino acid sequences of human PLCβ1a and PLCβ1b were used to analyze the effects of their overexpression in NT2 cell morphology. 96 h after transfection with PLCβ1a, PLCβ1b or both (Figs. 60B-D), cell growth was arrested and cells acquired the typical neuronal morphology, whereas the empty vector had no effect (Fig. 60A). PLCβ1a or PLCβ1b (Figs. 60B-C) alone appeared to be more potent in promoting cell growth arrest and morphological differentiation than in combination (Fig. 60D), as suggested by the presence of a higher amount of polygonal morphologies.

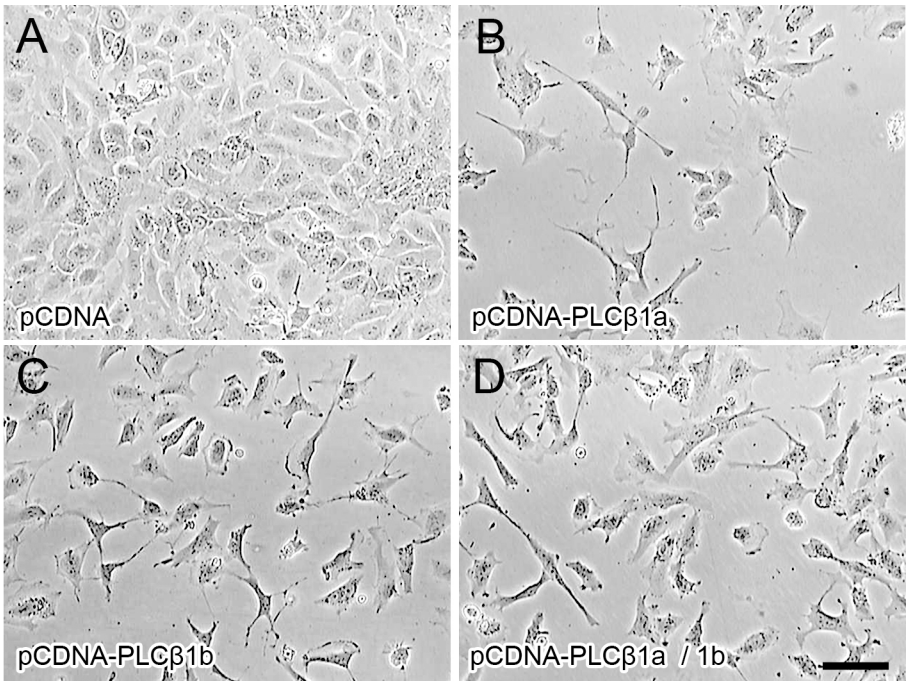

Figure 60. Phase-contrast micrographs of NT2 cells fixed 96 h after transfection with pcDNA, pcDNA-PLCβ1a, pcDNA-PLCβ1b or co-transfection of pcDNA-PLCβ1a and pcDNA-PLCβ1b plasmids. Arrowheads indicate cells displaying neurite-like processes. Scale bar = 50 μm.

To assess whether PLCβ1a or PLCβ1b overexpression promotes upregulation of neuron-specific markers, NT2 cells transfected with PLCβ1a, PLCβ1b or both were homogenized after 96 h and analyzed by Western blot. As illustrated in figure 61, PLCβ1a or PLCβ1b alone caused a ~3- and 2-fold increase in NF200 and βIII-tubulin expression, respectively, whereas co-transfection resulted in a ~2-fold increase in

NF200 expression and a moderate and statistically non-significant increase of βIII-tubulin expression. This is in agreement with the apparent higher capacity of PLCβ1a or PLCβ1b alone to induce morphological differentiation (Fig. 60). It must be noted that transfection with the mock vector also caused a moderate increase in NF200- and βIII-tubulin-immunoreactivities (Fig. 61A), probably masking to some extent the effect of PLCβ1 constructs, as OD values were normalized with respect to homogenates of mock-transfected cells.

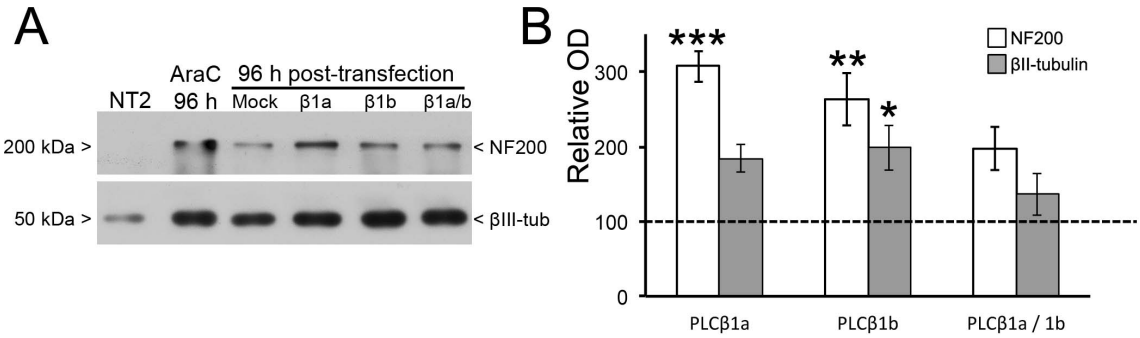

Figure 61. Immunoblots (**A**) and semiquantitative densitometric analysis (**B**) of NF200 and βIII-tubulin. Immunoblots were performed in whole homogenates of NT2 progenitor cells, NT2 cells treated with AraC for 96 h and NT2 cells transfected with an empty pcDNA, pcDNA-PLCβ1a, pcDNA-PLCβ1b or a combination of pcDNA-PLCβ1a and pcDNA-PLCβ1b. Equal amounts of total protein (5 μg) were loaded on the same. The y-axis of the graph shows mean percentage of optical density normalized to the value obtained in NT2 cells transfected with the empty (mock) plasmid. One-way followed by post hoc Tukey's test (*$p < 0.05$; **$p < 0.01$; ***$p < 0.001$). Data are mean ± SEM (n=4).

To further demonstrate the capacity of PLCβ1a and PLCβ1b to promote neuronal differentiation, we carried out double PLCβ1-NF200 immunofluorescence assays in NT2 cells 96 h after being transfected with pcDNA-PLCβ1a and pcDNA-PLCβ1b plasmids, using the pcDNA empty vector as negative control. As it can be observed in figure 62, NF200 immunoreactivity increased considerably in cells transfected with pcDNA-PLCβ1a and pcDNA-PLCβ1b as compared with neighbouring untransfected cells (Figs. 62D-I) and mock-transfected NT2 cells (Figs. 62A-C). Moreover, these changes in NF200 expression levels were correlated with changes in cell morphology, such that the appearance of cells was similar to that observed after AraC-induced differentiation (Compare Figs. 62D-I with Figs. 50E-H). Of note neither PLCβ1a nor PLCβ1b overexpression was accompanied by a marked increase in immunoreactivity within the nucleus, suggesting that nuclear translocation of PLCβ1 is saturable. Changes in expression of βIII-tubulin followed the same pattern as described for NF200 (data not shown).

Finally, assays with HA-tagged constructions confirmed the results obtained by

overexpression of native PLCβ1a and PLCβ1b. Thus, as shown in figure 63, overexpression of either HA-PLCβ1a (Figs. 63A-C) or HA-PLCβ1b (Fig. 63D) led to acquisition of neuronal polarity of transfected cells but not of neighboring untransfected cells.

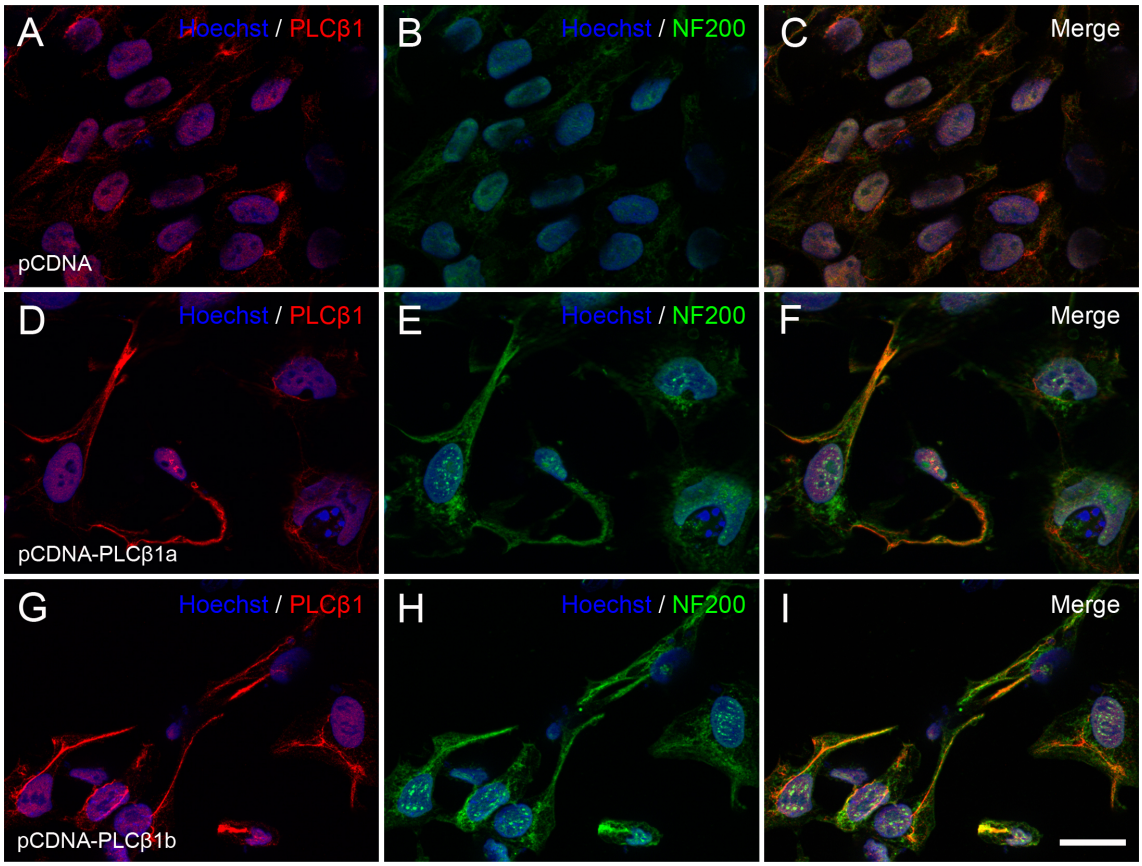

Figure 62. NT2 progenitor cells transfected with empty pCDNA (**A-C**), pcDNA-PLCβ1a (**D-F**) or pcDNA-PLCβ1b (**G-I**) fixed 96 h after transfection and processed for double immunofluorescence against PLCβ1 D-8 (red, A, D, G) and NF200 (green B, E, H), combined with Hoechst's chromatin staining (blue). Micrographs are maximum intensity projections of four consecutive optical sections separated by 0.24 µm, obtained using the structured illumination module (ApoTome). Scale bar = 25 µm.

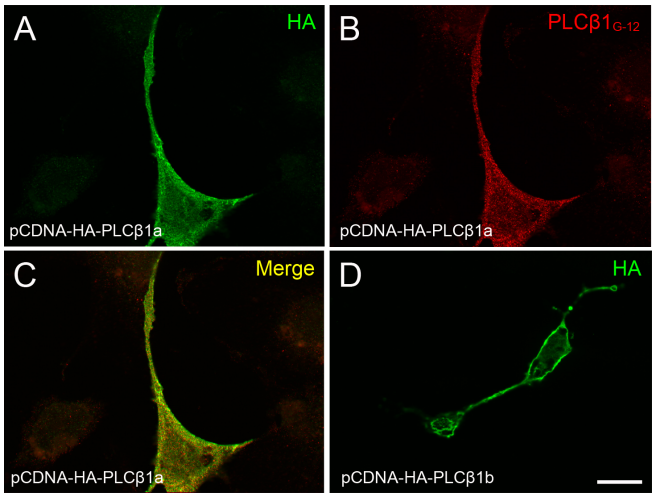

Figure 63. A-C. NT2 cells overexpressing HA-PLCβ1a, fixed 96 h after transfection and processed for double immunofluorescence to HA (green) and PLCβ1 (red). **D.** NT2 cells overexpressing HA-PLCβ1b, fixed 96 h after transfection and processed for immunofluorescence to HA (green. Micrographs are maximum intensity projections of four consecutive optical sections separated by 0.24 µm, obtained using the structured illumination module (ApoTome). Scale bar = 20 µm.

Taken together, these results show that PLCβ1 is necessary and sufficient for neuronal differentiation of NT2 cells.

5.3. Effect of PLCβ1 silencing in PC12 cell differentiation

To confirm and extend results obtained in NT2 cells we tested whether PLCβ1 silencing impairs NGF-induced differentiation of PC12 cells. First, we analyzed expression of PLCβ1 by Western blot, showing that both undifferentiated and NGF-differentiated PC12 cells express this enzyme, with no differences in OD of immunoreactive bands (Fig. 64).

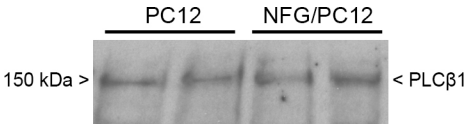

Figure 64. Western blot analysis of in whole homogenates of undifferentiated and differentitated PC12 cells (treated for 96 h with NGF 50 ng/mL). 20 μg protein/lane were loaded.

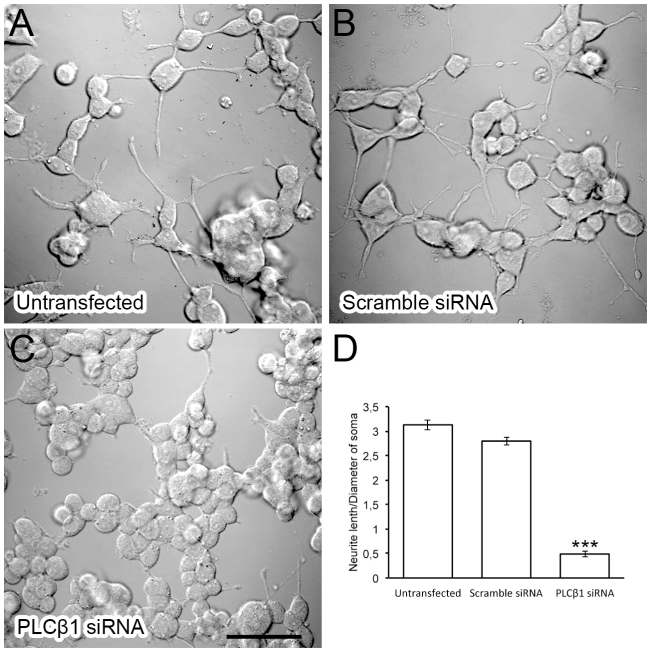

Figure 65. A-C. Phase contrast micrographs showing the morphology of PC12 cells, non-transfected (A) and transfected with scramble siRNA (B) or PLCβ1 siRNA (C) 24 h and after treating them for 96 h with NGF (50 ng/mL). Scale bar = 50 μm. **(B)** Comparison of the ratio of neurite length to cell body diameter in each condition. One-way ANOVA followed by post hoc Tukey's test (***p < 0.001). Data are mean ± SEM (n=100).

Quantitative analysis of the ratio between neurite length and diameter of cell body demonstrated that PLCβ1 knockdown using ON-TARGET plus SMART pool siRNAs (see Methods) completely abrogated NGF-induced neurite outgrowth and neuronal differentitation, whereas non-targeting scramble siRNAs did not (Fig. 65).

These results show that PLCβ1 silencing abrogates neuronal differentiation of two phenotypically distant cell lines and suggest that PLCβ1-mediated signaling participates in a universal mechanism for generic neuronal differentiation.

6. ROLE OF THE PHOSPHOLIPASE C β1-BINDING PARTNER TRANSLIN-ASSOCIATED FACTOR X IN NEURONAL DIFFERENTIATION

Recently, Scarlta and colleagues have identified the protein translin-associated factor X (TRAX) as a new binding partner of PLCβ1 (Aisiku et al., 2010), and showed that activated Gαq competes with TRAX for binding to PLCβ1, revealing a scenario in which PLCβ1, TRAX and Gαq levels, together with activity of Gq-coupled membrane receptors, would condition the location of PLCβ1 and TRAX and the possibility of these partners to interact. Interestingly, results of these studies showed that PLCβ1-TRAX association plays a key role in regulating the activity of the RISC silencing machinery, such that PLCβ1 binding to TRAX negatively regulates maturation of siRNAs targeting specific genes (Philip et al., 2012).

Based on these evidences, the expression of Gαq/11 and TRAX was analyzed during the time-course of AraC-induced neuronal differentiation.

6.1. Expression of PLCβ1-interacting proteins Gαq/11 and TRAX during AraC-induced differentiation of NT2 progenitors

In agreement with findings in RA/NT2N cells (Novak et al., 2000), expression of Gαq/11 was strongly upregulated during AraC induced differentiation of NT2 progenitors (Fig. 66A). Upregulation of Gαq/11 was observed as soon as 24 h after initiation of AraC treatment, reaching statistical significance at 48 h.

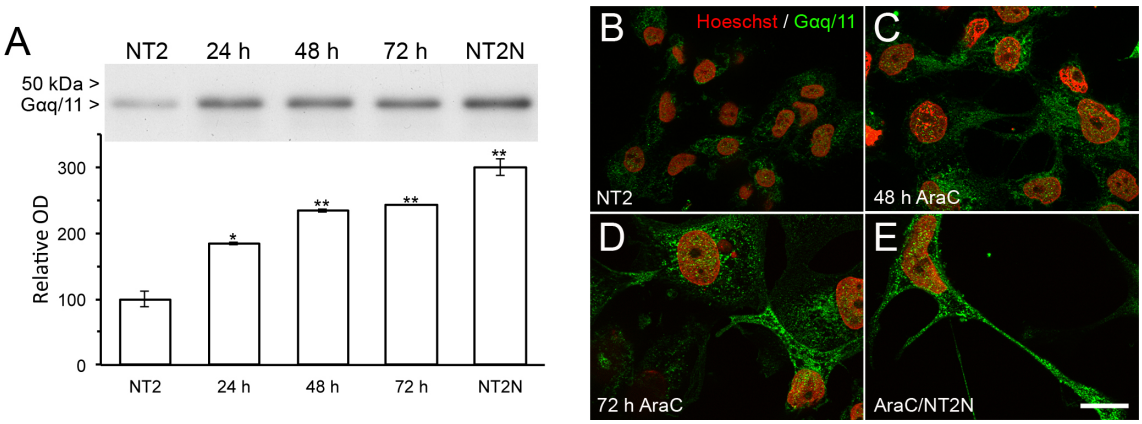

Figure 66. A. Western blot analysis of Gαq/11 expression during AraC-induced differentiation. Immunoblots were performed in whole homogenates of NT2 progenitors, AraC-treated cells (12, 24, 48 or 72 h) and AraC/NT2N cells. Equal amount of total protein for each condition (10 µg) was loaded on the same gel. The y-axis of the graph shows mean percent optical density (OD) normalized to the value obtained in NT2 progenitor cells. One-way ANOVA followed by post hoc Tukes's test (*$p < 0.05$; **$p < 0.01$). Data are mean ± SEM (n=2). **B-E.** Micrographs of NT2 cells (A), treated with AraC for 48 h (B) or 72 h (C) and differentiated AraC/NT2N neurons (D) immunolabelled for αq/11 (green) combined with Hoechst´s chromatin immunostainning (pseudocolores in red). Scale bar = 25 µm.

In line with results obtained by Western blot analysis, Gαq/11-immunofluorescence in fixed cells showed a marked increase in Gαq/11-signal after 48 h of treatment with respect to NT2 progenitors (Figs. 66B-C). Immunostaining continued to increase during differentiation (Fig. 66D), reaching a maximum at the end of treatment and being particularly intense in neurites (Figs. 66E).

Next, we analyzed TRAX expression during AraC-induced neuronal differentiation. Western blot analysis revealed that expression of TRAX remains close to basal levels during the first 48 h of treatment, and increased sharply at 72 h (Fig. 67)

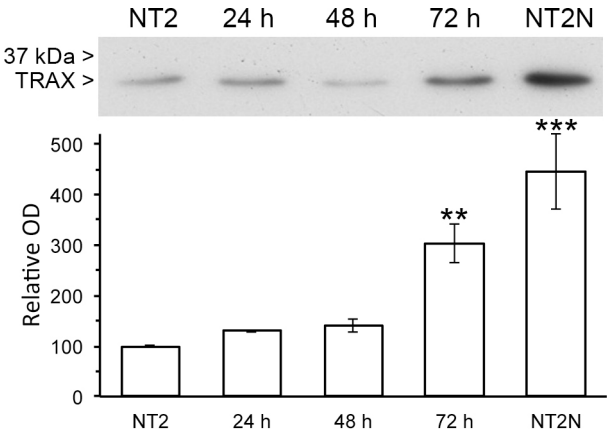

Figure 67. Semiquantitative densitometric analysis of TRAX immunoreactivity during the time course of AraC-induced neuronal differentiation of NT2 cells. Immunoblots were performed in whole homogenates of NT2 progenitor cells, NT2 cells treated with AraC 20 μM for 24, 48 or 72 h and and 6 days (NT2N). 5 μg total protein were loaded on the same gel. The y-axis of the graph shows mean optical density (OD) normalized to the value obtained in NT2 cells. One-way ANOVA followed by post hoc Tukes's test (**p < 0.01; ***p < 0.001). Data are mean ± SEM (n=5).

Comparison of the time-course of PLCβ1-, TRAX- and Gαq/11-expression during AraC-induced differentiation (Fig. 68) showed that the time-course expression of the three partners display a markedly different profiles. Thus, there is a lag time between upregulation of PLCβ1 and TRAX proteins, with an inversion of the relative expression levels at the end of differentiation caused buy a sharp downregulation of PLCβ1. At its turn, Gαq/11-expresion increases steadily until the end of differentiation, which contrast with the up-down regulation pattern of PLCβ1 and the sharp upregulation of TRAX at the end of differentiation.

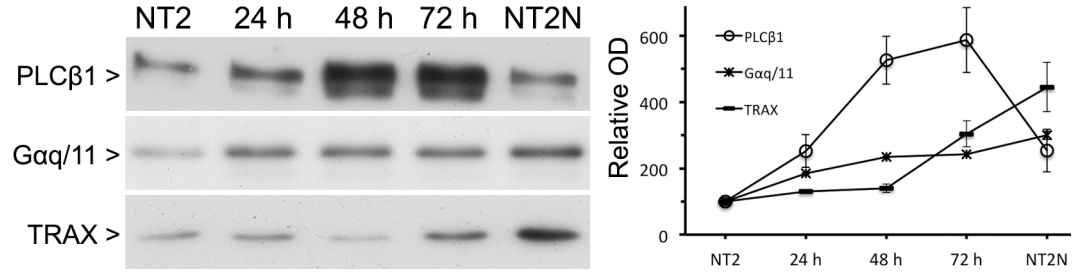

Figure 68. Immunoreactivity for PLCβ1, Gαq/11 and TRAX during the time-course of AraC-induced differentiation. Optical density values were normalized to optical density (OD) in NT2 progenitors. All data are mean ± SEM (PLCβ1, n=4; Gαq/11, n=2; TRAX, n=5).

The lag time between upregulation of PLCβ1 and TRAX prompted us to evaluate whether PLCβ1 silencing and overexpression affects TRAX upregulation, as observed for neuron-specific markers (Figs. 56, 61 and 62).

6.1.1. Effect PLCβ1 silencing on TRAX expression in AraC/NT2N neurons

As illustrated in figure 69, AraC-treatment during 72 h caused a significant increase in TRAX immunoreactivity in whole homogenates of NT2 cells transfected with non-targeting siRNA, which was reversed by siRNA targeting the human PLCB1 gene.

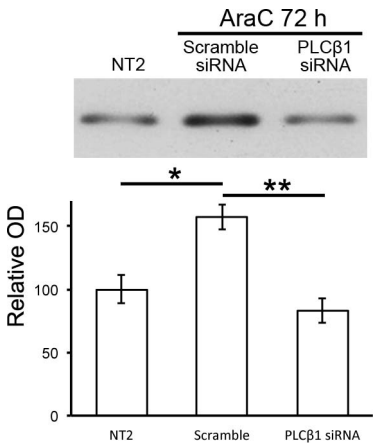

Figure 69. Semiquantitative densitometric analysis of TRAX-immunoreactivity in NT2 cells and cells transfected either with scramble siRNA or PLCβ1 siRNA and treated with AraC for 72 h. Equal amounts of total protein (5 µg) were loaded on the same gel and run in parallel. The y-axis of the graph shows mean of optical density (OD) normalized to the value obtained NT2 cells. One-way ANOVA followed by post hoc Tukey's test (*$p < 0.05$; **$p < 0.01$). Data are mean ± SEM (n=4).

6.1.2. Effect of PLCβ1 overexpression on TRAX expression in NT2 progenitors

Constructs coding for the native amino acid sequences of human PLCβ1a and PLCβ1b were used to assess whether their overexpression promotes upregulation of TRAX. To this end, NT2 cells transfected with PLCβ1a, PLCβ1b or both were homogenized after 96 h and analyzed by Western blot.

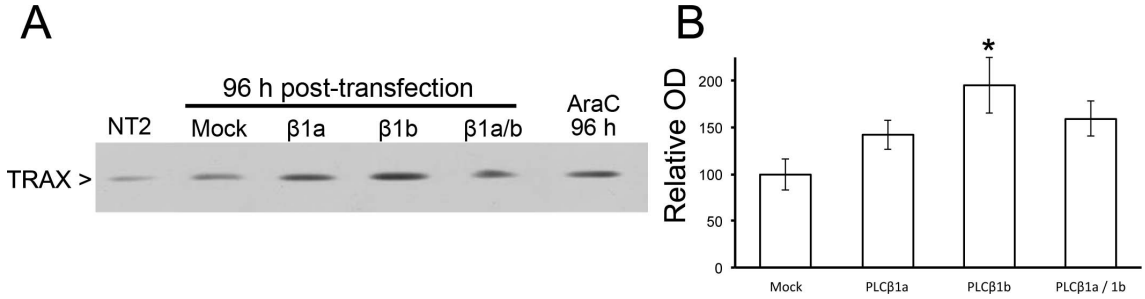

Figure 70. Semiquantitative densitometric analysis of TRAX expression. Immunoblots were performed in whole homogenates of untransfected NT2 cells, NT2 cells transfected (with pcDNA –mock-, pcDNA-PLCβ1a, pcDNA-PLCβ1b or a mix of pcDNA-PLCβ1a and pcDNA-PLCβ1b) and untransfected NT2 cells treated with AraC for 96 h. Transfected cells were lysed 96 h after transfection. 5 µg protein were loaded on the same gel. The y-axis of the graph shows mean of optical density (OD) normalized to the value obtained in mock-transfected cells. One-way ANOVA followed by post hoc Tukey's test (* $p < 0.05$). Data are mean ± SEM (n=4).

PLCβ1a or PLCβ1b alone or in combination caused an increase in TRAX expression (Figs. 70A-B), although only PLCβ1b led to a statistically significant upregulation (Fig. 70B). Because mock vector caused a moderate increase in TRAX-immunoreactivities (Fig. 70A), probably masking to some extent the effect of PLCβ1 constructs, optical density (OD) values were normalized with respect to homogenates of mock-transfected cells (Fig. 70B).

In summary these results and those obtained after PLCβ1 silencing suggest that PLCβ1 regulates TRAX expression.

6.2. Analysis of PLCβ1-TRAX interaction during AraC-induced differentiation of NT2 progenitors

6.2.1. Double PLCβ1-TRAX immunofluorescence

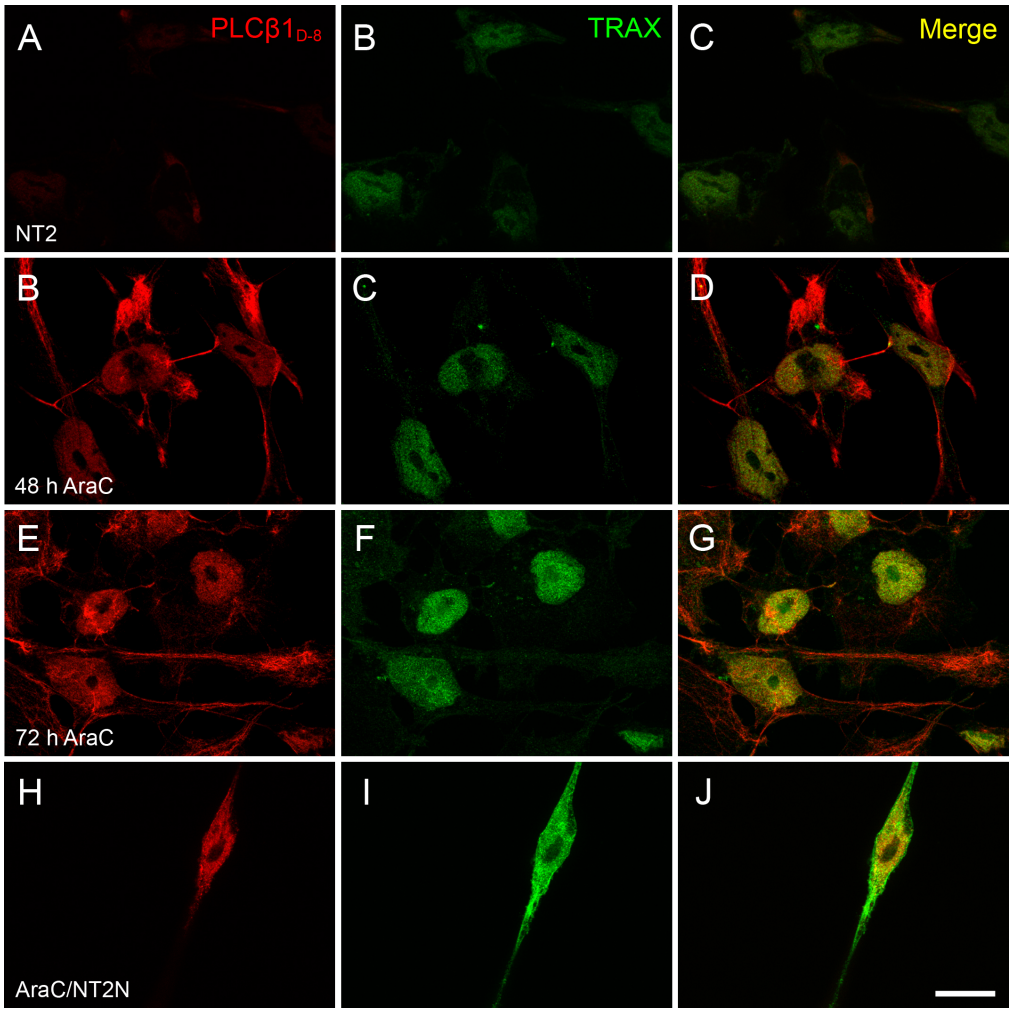

Figure 71. Double-immunofluorescence against PLCβ1$_{D-8}$ (red) and TRAX (green) in fixed NT2 progenitor cells (**A-C**), NT2 cells treated with AraC 20 μM for 48 h (**D-F**), 72 h (**G-I**) and AraC/NT2N (**J-L**). Micrographs are maximum intensity projections of four consecutive optical sections separated by 0.24 μm, obtained using the structured illumination module (ApoTome). Scale bar = 25 μm.

As a first approach to test whether PLCβ1 and TRAX interact during neuronal differentiation of NT2 cells, double immunofluorescence analysis was performed in fixed cells at different time points during AraC-induced differentiation.

As shown in figure 71, TRAX was barely detectable in NT2 progenitors (Fig. 71A-C), whereas it could be clearly observed in cell nuclei of cells treated with AraC for 48 h, where it colocalized with PLCβ1 (Fig. 71D-F). This increase was considerably in cells treated with AraC during 72 h and 6 days (NT2N cells). At the end of treatment, immunoreactivity was also observed in the cell soma and neurites (Figs. 71I-J).

The increase observed at 48 h of AraC treatment contrast with results of Western blot analysis of whole cell homogenates showing that TRAX expression is close to basal levels at this time point. This discrepancy could be due to a masking effect of nuclear upregulation caused by cytosolic and plasma membrane TRAX. Therefore, TRAX immunoreactivity was analyzed in purified subcellular fractions of NT2 cells, cells treated with AraC for 48 h and AraC/NT2N cells. As shown in figure 72, TRAX-immunoreactivity increases selectively in the nuclear fraction N as soon as 48 h after initiation of AraC treatment and even more in AraC/NT2N cells, whereas it remained unchanged in the Cyt and P2 fractions. Of note TRAX immunoreactivity was clearly detectable in Cyt and P2 fractions at the three time points analyzed. This contrasts with the absence of immunofluorescence signal in these locations, suggesting the epitope recognized by anti-TRAX antibody was masked.

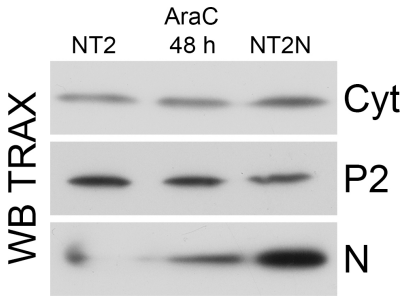

Figure 72. Western blot analysis of TRAX in Cyt, P2 and N fractions obtained from NT2 progenitor cells, NT2 cells treated for 48 h with AraC and AraC/NT2N. For each control point, equal amounts of total protein (5 μg) were loaded on the same.

6.2.2. FRET analysis of PLCβ1-TRAX interaction during AraC-induced differentiation of NT2 progenitors

To analyze whether PLCβ1-TRAX associate during AraC-induced differentiation Förster resonance energy transfer (FRET) assays were performed in NT2 cells cotransfected with TRAX-eCFP and PLCβ1-eYFP during the time-course of AraC-induced differentiation. FRET efficiency was evaluated in NT2 cells and at 3 h, 24 h, 48 h, 72 h and 96 h after initiation of AraC treatment. As seen in figure 73, FRET

efficiency increased with time following AraC treatment, reaching statistically significance as soon as 24 h after treatment. The most noticeable change was after 72-96 h of treatment; in fact, a sharp increase could be observed between 72 and 96 h of AraC treatment, although methodological shortcomings could account for this apparent drastic change. Indeed, until 72 h FRET signal was detectable in the entire cell area, whereas in cells treated with AraC during 96 h, the FRET signal was confined to a subcellular location likely corresponding to the cell nucleus, with no detectable signal in the cell body and plasma membrane, making it impossible to trace manually cell boundaries. Therefore, in cells treated with AraC for 96 h, measurement of mean FRET signal was circumscribed to the FRET-positive subcellular compartment, resulting in a overestimation of FRET efficiency at this time point. These observations are illustrated in figure 74. As it could be observed, TRAX-eCFP was distributed throughout the entire cell area in in NT2 cells (Fig. 74A), whereas PLCβ1-eYFP was mostly cytosolic (Fig. 74B), although a weak signal could be detected in the cell nucleus. FRET signal was extremely low in these cells (Fig. 74C). Consequently, no significant differences in FRET signal were observed in NT2 progenitors compared to the negative control (Fig. 73). After 72 h of treatment, no noticeable changes were observed regarding the distribution of TRAX-eCFP (Fig. 74D). In contrast, cells exhibited a strong PLCβ1-eYFP appeared associated to the plasma membrane (Fig. 74E). At this time point, FRET efficiency was significantly higher than in NT2 cells (Fig. 73). In particular, the strongest signal was observed in the plasma membrane and weaker in the cytoplasm and cell nucleus (Fig. 74F). In cells treated with AraC during 96 h, both TRAX-eCFP and PLCβ1-eYFP were localized to round structures resembling the cell nucleus (Figs. 74G-H), where strong FRET signal was detected (Fig. 74I).

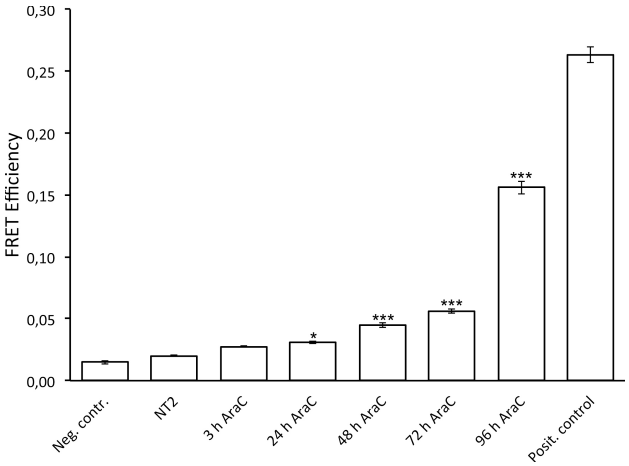

Figure 73. Quantification of FRET efficiency between TRAX-eCFP and PLCβ1-eYFP during the time-course of AraC-induced differentiation of NT2 progenitor cells. NT2 were co-transfected with TRAX-eCFP and PLCβ1-eYFP, treated with AraC and analyzed at the indicated time points. eCFP-YFP fusion protein transfected cells were used as negative and positive controls respectively. One-way ANOVA followed by post hoc Tukey's test (*p < 0.05; ***p < 0.001). Data are mean ± SEM (n=45).

By combining fluorescence images with phase-contrast images, it could be confirmed that signals corresponding to TRAX-eCFP and PLCβ1-eYFP fusion proteins as well as FRET signal was confined to the cells nucleus (Fig. 75).

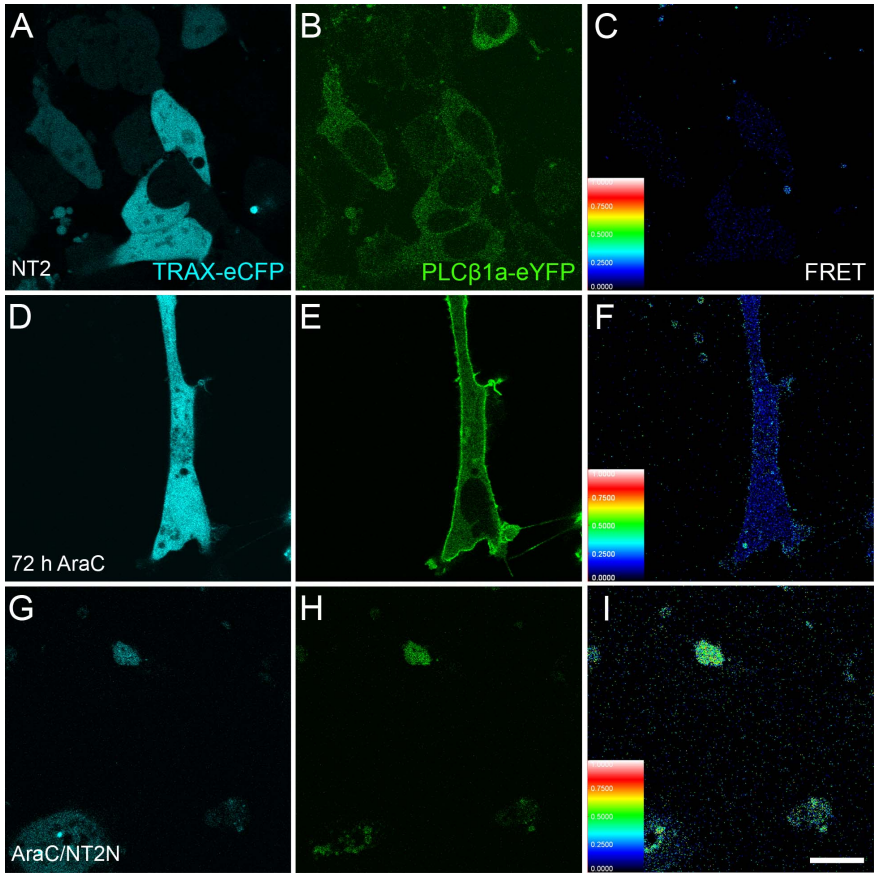

Figure 74. Immunolabeling of transfected cells with TRAX-eCFP (cyan blue) (**A**, **D**, **G**) and PLCβ1a-eYFP (green) (**B**, **E**, **H**) and FRET signals (**C**, **F**, **I**) during the AraC-induced differentiation process. Control Points: NT2 progenitor cells (**A-C**), 72 h AraC-treated NT2 cells (**D-F**) and AraC/NT2N (**G-I**). Scale bar = 25 µm.

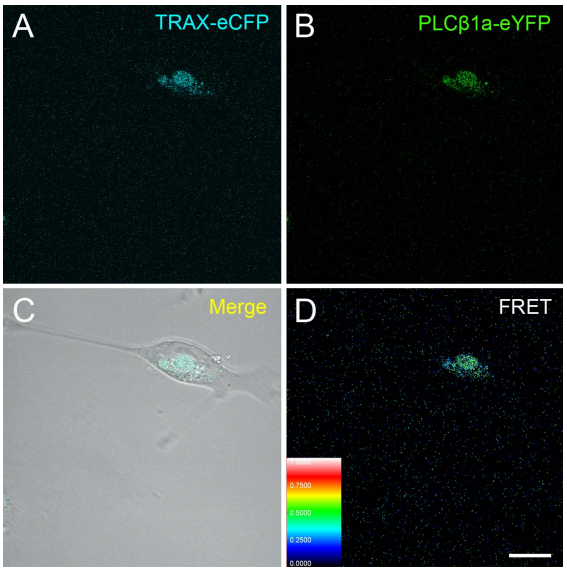

Figure 75. TRAX-eCFP (**A**), PLCβ1a-eYFP (**B**) combined with phase-contrast (**C**) and FRET signals (**D**) 96 h after the initiation of treatment with AraC. Scale bar = 20 µm.

6.3. Involvement of TRAX in neuronal differentiation of PC12 cells

On the basis of results described in this chapter, we hypothesized that, if PLCβ1-TRAX interaction was involved in neuronal differentiation, TRAX silencing (similarly to PLCβ1-silencing) would prevent differentiation of neuronal progenitors. Thus, we tested this possibility using the easily measurable model of PC12 differentiation. Given that activation of Gq-coupled membrane receptors appears to regulate PLCβ1-TRAX (Aisiku et al., 2010), the effect of Gαq/11 silencing in neuronal differentiation of PC12 cells was also analyzed. Additionally, we tested the effect of silencing of translin (the best characterized binding partner TRAX) in neuronal differentiation of PC12 cells.

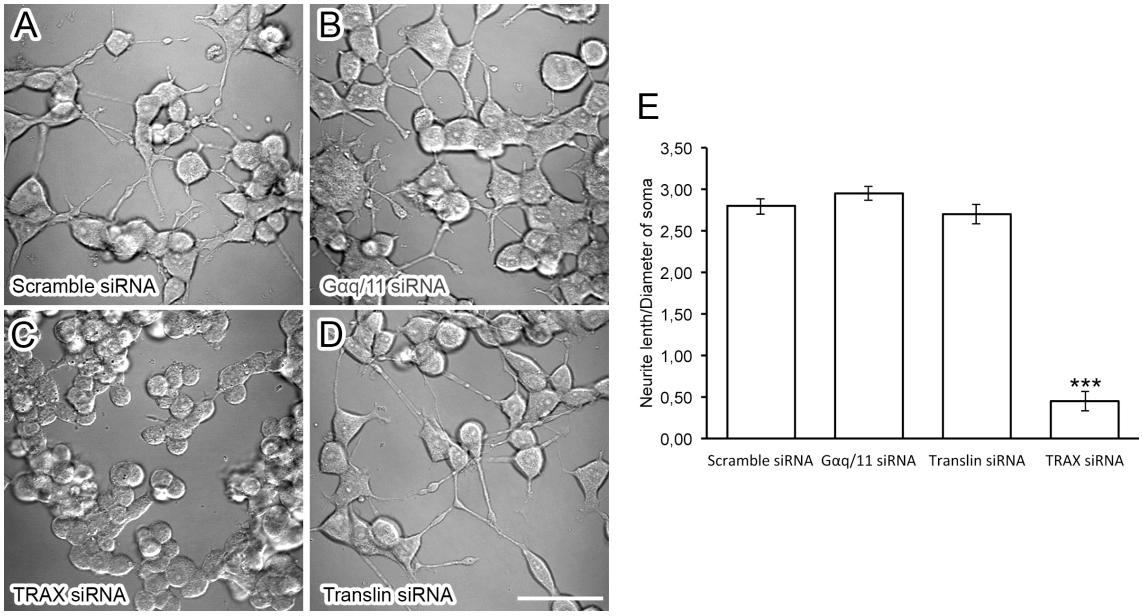

Figure 76. Phase contrast images showing the morphology of PC12 cells transfected with scramble siRNA (**A**), Gαq/11-siRNA (**B**), TRAX-siRNA (**C**), or translin-siRNA (**D**) and treated with 50 ng/mL NGF for 96 h. Scale bar = 50 μm. **(E)** Comparison of the ratio of neurite length to the cell body diameter in each condition. One-way ANOVA followed by post hoc Tukey's test (***$p < 0.001$). Data are mean ± SEM (n=100).

As shown in figure 76, silencing of TRAX, but not Gαq/11 or translin, completely abrogated NGF-induced neurite outgrowth and polarization of PC12 cells, demonstrating that, at least in PC12 cells, both PLCβ1 and TRAX are necessary for neuronal differentiation and that this requirement does not depend on Gq-signaling or integrity of the TRAX-Translin complex.

VI. DISCUSSION

1. PLCβ1a AND PLCβ1b SPLICE VARIANTS ARE EXPRESSED IN NEURONAL NUCLEI OF THE ADULT RAT CORTEX

Most of the research on signal transduction pathways based on PLCβ1 has been devoted to studying phenomena that take place at the plasma membrane. However, the work of several independent laboratories have consistently demonstrated that the phosphoinositide cycle (biosynthetic and hydrolytic machinery) is present in the cell nucleus, and may be important for various nuclear events such as mRNA export, DNA repair and gene transcription (Irvine, 2003; Martelli et al., 2005). In fact, PLCβ1 was originally identified at the nuclear level (Martelli et al., 1992; Divecha et al., 1993), and now its role in the control of cell proliferation or cell cycle progression in several cellular models is well established (Avazeri et al., 2003; Cocco et al., 2009). The evidence obtained with confocal and electron microscope analysis indicates that enzymes required for the synthesis and hydrolysis of phosphoinositides are localized at nuclear membrane and ribonucleoprotein structures of the inner nuclear matrix involved in transcript processing within the interchromatin domains (Boronenkov et al., 1998; Osborne et al., 2001; Tabellini et al., 2003; Jones and Divecha, 2004). With respect to PLCβ1, confocal and immune-electron microscopy and classic biochemical techniques provide evidence that exists in the nucleus of several cellular models. In rat liver, Swiss 3T3, MEL and PC12 cells, PLCβ1 resides in the nuclear inner matrix and lamina, and this intranuclear partitioning is further stressed in *in situ* matrix preparations which demonstrated that PLCβ1 is a structural insoluble component of the inner nuclear matrix and of the nucleolar remnant, while it is absent from the nuclear pore-lamina complex (Zini et al., 1993; Zini et al., 1994; Bertagnolo et al., 1995; Crljen et al., 2004; Fiume et al., 2009). Probably, PLCβ1 is preferentially located in subnuclear domains known as speckles, which are involved in splicing events and can be easily identified by specific markers, as the splicing factors (Bavelloni et al., 2006). Finally, it has been demonstrated that PLCβ1 and lamin B1 localize and physically interact in the nucleus of MEL cells (Fiume et al., 2009).

With these evidences in mind, we explored whether PLCβ1 is actually present in the nucleus of cells of neural origin. In our study, PLCβ1 displayed a dot-like pattern localized to chromatin-poor compartments and colocalized to a large extent with the nuclear speckle marker SC-35 (Osborne et al., 2001; Tabellini et al., 2003). In contrast, no colocalization was found with nuclear pore complex or lamin B1. Clearly, the data

reported here appear to shed new light on the presence of PLCβ1 at the neuronal nuclear compartment. As already shown in rodent and human tissues (Bahk et al., 1994; Caricasole et al., 2000; Peruzzi et al., 2002), PLCβ1 exists as two alternatively spliced variants, 138 kDa PLCβ1a (1216 aa) and 134 kDa PLCβ1b (1141 aa). These variants derived from alternative splicing at the 3' end of human PLCβ1 gene (Caricasole et al., 2000; Peruzzi et al., 2002). The PLCβ1b variant replaces the 75 C-terminal residues of PLCβ1a with 32 residues unique to PLCβ1b (Bahk et al., 1994; Caricasole et al., 2000; Peruzzi et al., 2000). The importance of the PLCβ1 C-terminal domain may rely in two aspects. First of all, C-terminal region contains determinants for Gαq and phosphatidic acid stimulation, electrostatic dependent association with membrane lipids, nuclear localization, and phosphorylation/regulation by protein kinase Cα and MAP kinase (Bahk et al., 1994; Litosch, 2000; Martelli et al., 2000; Xu et al., 2001a,b). Although, a nuclear localization motif has been mapped to a cluster of lysine residues (between 1055 and 1072) which is common to both variants (Kim et al., 1996), PLCβ1a has in its unique C-terminal a typical nuclear export signal which may result in this variant being less concentrated in the nucleus (Bahk et al., 1994). Thus, although the two splice variants of PLCβ1 have identical Gαq-interacting domains and are comparably stimulated by Gαq, have a different subcellular localization, PLCβ1a being equally distributed in the plasma membrane, in the cytoplasm and in the nucleus, and the PLCβ1b almost completely nuclear, as demonstrated by Western blot and inmunofluorescence in several cell lines (glioma C6Bu-1 and MEL cells) and in rat liver tissue (Bahk et al., 1998; Faenza et al., 2000; Crljen et al., 2004; Fiume et al., 2005). In the last 5 years, a critical role for the PLCβ1b-specific C-terminal tail in targeting this variant to the sarcolemma of cardiomyocytes has been demonstrated (Grubb et al., 2008, 2011). Our immunoblot analysis, using an antibody targeted against the common N-terminal of PLCβ1, was able to detect the presence of the two variants of PLCβ1 in different cell compartments (plasma membrane, cytosolic and nuclear fractions) Clearly, PLCβ1a was predominant over PLCβ1b in all the fractions studied, although the relative contribution of each variant to the total signal differed between subcellular compartments. Thus, PLCβ1a was more abundant than PLCβ1b in all fractions, although analysis of the PLCβ1a/ PLCβ1a ratios revealed that relative contribution of PLCβ1a was significantly higher in cytosol (Cyt) than in intact nuclei (N) and membrane fractions (P2).

The deeper understanding of the subcellular location of PLCβ1 in rat cerebral cortex presented here represents a starting point for considering additional research aimed at characterizing the distribution of its splice variants, and to shed light on the putative role of nuclear PLCβ1 pools in the regulation of cell cycle progression and differentiation in cells of neural origin. However, although there is extensive evidence highlighting the key role of nuclear PLCβ1 and its catalytic activity in cell cycle control and differentiation (see Introduction, section 1.4.1.), only indirect data exist about the role of PLCβ1 in neuronal differentiation. In this regard, it has been shown that Plcb1- and mGluR5-knockout mice (Hannan et al., 2001; Böhm et al., 2002; Spires et al., 2005) exhibit alterations in the formation of the so-called "barrels" of the somatosensory cortex, emphasizing the importance of this signal transduction for correct cortical development. Additionally, Spires et al. (2005) reported a decrease in the proportion of symmetrical synapses in the "barrel" cortex of Plcb1$^{-/-}$ mice, suggesting a transient imbalance in excitatory and inhibitory circuits (Spires et al., 2005). In line with this idea, Plcb1$^{-/-}$ mice generated by Kim et al. (1997) died suddenly at early postnatal stages and death was preceded by status epilepticus or recurrent seizures characterized by tonic-clonic or tonic extension of the whole body. Moreover, a human phenotype described by Kurian et al. (2010), which described that an homozygous deletion, involving the promoter element and exons 1, 2 and 3 of human PLCB1 gene led to tonic seizures in early infancy and, subsequently, infantile spasms and death. Interestingly, missense mutations in the SH3 domain of the human SHANK3 gene (an interaction site for PLCβ1b, see Introduction, section 1.1.4.) produces a clinical phenotype (Gauthier et al., 2010) similar to that described in Plcb1$^{-/-}$ mice (Kurian et al. (2010). These evidences in animal models and humans suggest that PLCβ1 signaling, rather than necessary for generic neuronal differentiation, is required for synaptic activity-dependent late maturation, a process in which membrane (but not nuclear) PLCβ1 would be involved. However, because all isoforms of the PLCβ family are expressed in brain cortex (Ruiz de Azúa et al., 2006), contain a nuclear localization signal (Rebecchi and Pentylana, 2000) and are expressed in neuronal nuclei (García del Caño et al., 2015), redundant PLCβs could compensate for the loss of PLCβ1 during early neuronal differentiation in brain of Plcb1$^{-/-}$ mice and patients with deletions of the PLCB1 gene promoter.

Therefore, in order to clarify whether PLCβ1 is actually required for neuronal differentiation, we used the pluripotent NTERA2/D1 (NT2) cell line, which can be

induced to differentiate *in vitro* into postmitotic NT2N neurons by retinoic acid (RA) (Andrews, 1984; Pleasure et al., 1992). Yet, the major limitations of this model are the lengthy differentiation procedure and its low efficiency, although recent studies suggest that the differentiation process can be shortened to less than one week using nucleoside analogues. Therefore, as a first step before exploring the role of PLCβ1 in neuronal differentiation of NT2 progenitors, we sought to explore whether short-term exposure of NT2 cells to the nucleoside analogue cytosine β-D-arabinofuranoside (AraC) could be a suitable method to efficiently generate mature neurons for subsequent studies.

2. NT2-DERIVED POSTMITOTIC HUMAN NEURONS CAN BE GENERATED WITH HIGH EFFICIENCY BY SHORT-TERM TREATMENT WITH THE NUCLEOSIDE ANALOGUE CYTOSINE β-D-ARABINOFURANOSIDE

NT2 derived neuronal cells *in vitro* express a plethora of neuron-specific markers at both transcript and protein levels (Pleasure et al., 1992; Cheung et al., 1999; Megiorni et al., 2005; Couillard-Despres et al., 2008; Haile et al., 2014). Our results are roughly in line with previous studies showing increased expression of NF200 (Lee and Andrews, 1986; Pleasure et al., 1992), βIII-tubulin (Megiorni et al., 2005; Couillard-Despres et al., 2008; Popovic et al., 2014) and DCX during RA-induced differentiation (Couillard-Despres et al., 2008). However, differences in culture conditions and the lack of data of the time-course expression (or election of unequal time points for analysis) make it difficult a reliable comparison between their and our results in these studies. An inherent limitation for interpretation of results arises from the heterogeneous composition of cultures during RA-induced differentiation. Indeed, the neuronal phenotype represents only a small fraction over the entire cell population before mechanical isolation of RA/NT2N cells. Of the three markers used, NF200 was clearly identified as a highly neuron-specific marker in terminal cultures, in view of the high enrichment in this protein in terminally differentiated RA/NT2N cells compared to cell samples harvested before mechanical dislodging of neuronal cells. In contrast, expression levels of βIII-tubulin and DCX were similar in samples from cultures after 28 days of treatment and in those from terminally differentiated RA/NT2N cells, indicating that these proteins were expressed in both RA/NT2N neurons and in the highly adherent non-neuronal NT2A cells. Remarkably, βIII-tubulin was already detectable in NT2 cells, reached a maximum immunoreactivity by day 7 of RA treatment, and returned to basal levels at the end of the process. This is in agreement

with a similar time-course analysis performed by Megiorni et al. (2005), even thought they used a cell aggregation method that shortens the time of the RA-induced differentiation to 3-4 weeks. Collectively, these data support and extend previous findings of the expression of neuronal markers in RA/NT2N neurons, and emphasize the caution needed in drawing conclusions about the use of βIII-tubulin for an unequivocal identification of neuronal phenotypes. In line with this conclusion, βIII-tubulin is expressed in human fetal astrocytes (Dráberová et al., 2008) as well as in undifferentiated mesenchymal stem cells (Foudah et al., 2014). Our findings show that NT2N cells derived from AraC treatment not only show neuronal morphology, but also express neuronal markers, albeit with remarkable differences in the expression profiles of βIII-tubulin and DCX during differentiation. At difference with that observed during RA-induced differentiation, in AraC-treated cultures, immunoreactivity for βIII-tubulin increased sharply at mid-treatment and reached a maximum at day 6, whereas DCX showed an up-down regulation pattern that peaked up at 48 h post-treatment. The progressive increase in expression of NeuN/Fox-3 observed during AraC-induced differentiation of NT2 progenitors, as analyzed by Western blot and immunofluorescence microscopy, further confirmed the neuronal identity of AraC/NT2N neurons. The sequential and non-matching upregulation of the early (Brown et al., 2003) and late (Mullen et al., 1992) neuronal markers DCX and NeuN/Fox-3 suggests that, beside differentiation, AraC/NT2N cells have begun a maturation process after 6 days of treatment. However, this suggestion should be considered with caution, as NeuN/Fox-3 expression has been found in non-neuronal cells, such as cultured rodent and human astrocytes and even 3T3 fibroblast cells (Darlington et al., 2008). Indeed, we also observed that part of the population of non-neuronal flat polygonal cells in our AraC-treated terminal cultures displayed weak to moderate nuclear staining for NeuN/Fox-3, leading us to consider morphological features to classify cells into non-neuronal or AraC/NT2N neuronal. Less than 10% of the cells in culture survived the uninterrupted 6-day period of AraC treatment, and only about 50% of them fulfilled the double criterion to be considered as neuronal (i.e., NeuN/Fox-3 positive nucleus and presence of neurite extensions) leading to a differentiation efficiency similar to that found after RA-differentiation. Our modified procedure, consisting of increasing cell density at mid-treatment, doubled overall cell survival and increased the percentage of neuronal cells with respect the total population

at the end of AraC treatment to 71%, respectively. Consequently, differentiation efficiency was number augmented by almost 3-fold.

The two populations identified were clearly distinguishable as demonstrated by morphometric measurements of cell nuclei and total cell area. When compared with RA/NT2N neurons, AraC/NT2N neurons displayed considerably larger nuclei and cell somata. However, due to the characteristic growth of RA/NT2N neurons in aggregates under a closed 3-D organization, measurements of nuclear and body area of these cells on images of virtual stacks could have exacerbated the differences with respect to the considerably more flattened AraC/NT2N. Indeed, the ratio of nuclear area to body area tended to get closer in both phenotypes, although it was significantly lower in AraC/NT2N neurons. An overestimation of the size of cell somata of AraC/NT2N neurons, due to limitations on accurately defining their boundaries of (see methods), could account for this difference. Morphometric analysis of neurites showed that AraC/NT2N neurons displayed a total neurite length per cell of about 180 μm^2. In a recent study, Haile et al. (2014) provided a 4.2-fold greater value for the total arborization length of RA/NT2N neurons. The much shorter time period for neurite outgrowth in our study (6 days *vs.* 5 weeks) likely accounts for this difference. Indeed, AraC/NT2N neurons were enriched in lamellar extensions and filopodia-like processes, indicative of intensive neurite outgrowth activity. In support of this idea, neurite length found here was about 20% longer than that reported by Tegenge et al. (2011) in RA-differentiated neurons using the shortened cell aggregation method described by Cheung et al. (1999). Testing longer time periods, growth factors, different matrices and/or co-culture with astrocytes will be required to determine whether AraC/NT2N neurons are able to develop longer neurite arborizations. In any case, the experimental results reported here reveal that NT2 progenitors can be committed to differentiate in a short time period and with high efficiency into cells that fulfill the generally accepted criteria for postmitotic neurons, and underline that AraC-induced differentiation of NT2 cells represents a valuable model to study molecular mechanisms underlying neuronal differentiation.

RA/NT2N neurons been shown to express a broad spectrum of neurotransmitter markers *in vitro*, including glutamatergic (Podrygajlo et al., 2009; Coyle et al., 2011), cholinergic (Guillemain et al., 2000; Saporta et al., 2000), GABAergic (Yoshioka et al., 1997; Guillemain et al., 2000; Saporta et al., 2000; Podrygajlo et al., 2009; Coyle et al., 2011), chatecolaminergic (Guillemain et al., 2000; Saporta et al., 2000) and

serotonergic (Podrygajlo et al., 2009) transcripts and/or proteins. The apparent absence of consensus on the final neurotransmitter phenotype can be attributed to differences in the neuronal differentiation protocol and culture conditions, although as discussed by Podrygajlo et al. (2009), passage number of precursors, or their genetic instability could also contribute to variability of results. Nevertheless, under the culture conditions (culture media included) described by Pleasure et al. (1992) and used here, Yoshioka et al. (1997) and Guillemain et al. (2000) reported that a considerable population of neurons possess a GABAergic phenotype, in agreement with our findings showing that RA/NT2 are mostly GABAergic. In their immunocytochemistry-based study, Guillemain et al. (2000) found that 66.5% of neurons were GABA-immunopositive, although they also reported that 51.8% and 49.5% of neurons were TH- and ChAT-immunoreactive, respectively, leading to the conclusion that many neurons were immunopositive for at least two markers. For their part, Yoshioka et al. (1997) only analyzed GAD67 transcript and protein using RT-PCR and Western blot analysis. Here, using immunofluorescence microscopy, we observed a large amount of GAD67-immunopositive and scarce VGluT1-immunopositive thin neurites, both likely corresponding to axons; hence, to the canonical distribution of these proteins. Although, due to this distribution pattern, we could not asses the proportion of neurons of each phenotype, Western blot analysis confirmed that, in our culture conditions, GABA is the major neurotransmitter in RA/NT2N cells, whereas only a weak VGluT1 signal could be observed.

Of particular interest in the present report is the finding that cells committed to differentiate by short treatment with AraC displayed a completely different neurotransmitter phenotype when compared with RA/NT2N neurons. Western blot analysis showed strong immunoreactivity for VGluT1 and ChAT in samples from terminal cultures, starting as soon as 72 h after initiation of AraC treatment. On the other hand, immunofluorescence assays evidenced that virtually all terminally differentiated neurons co-expressed both markers, suggesting that their neurotransmitter phenotype was not fully defined. Noticeably, this same phenomenon has been recently described for hippocampal embryonic neural progenitors. Thus, Bhargava et al. (2010) reported that, when cultures were obtained from brain of 18-day-old embryos, most VGluT1-positive neurons also expressed ChAT protein. On the contrary, this ability to co-express both markers of neurotransmitter phenotype was not observed in cultures from either neonatal or adult hippocampus. Results by Bhargava et al. (2010) exemplify

the importance of tissue environmental signals in specification of neurotransmitter fate. Moreover, embryonic hippocampal neurons in culture express the late neuronal marker NeuN/Fox-3 (Taguchi et al., 2014), indicating that neuronal maturation and specification of neurotransmitter phenotype are separate developmental events. As discussed by Bhargava et al. (2010), a complex combinational strategy of electrochemical coding that involves neighboring environmental signals, as well as distant afferent and retrograde signals, appear to account for specification of neurotransmitter phenotype (Johnson, 1994; Asmus et al., 2000; Landis, 2002). As a result of this developmental process neurons would loss the ability to synthesize multiple neurotransmitters. In this regard, it is likely that AraC/NT2N cells could acquire a specific neurotransmitter phenotype when engrafted in brain. In support of this, previous studies have demonstrated that RA/NT2N neurons (Saporta et al., 2000) and even NT2 progenitors (Miyazono et al., 1996) transplanted in different regions of the rodent brain are driven to differentiate in specific neurotransmitter phenotypes according to local environmental cues. Although some experimental studies using RA/NT2N grafts in animal models of stroke (Borlongan et al., 1998a,b; Saporta et al., 1999) and Huntington's disease (Hurlbert et al., 1999) have yielded promising results, others have reported either limited improvement (Bliss et al., 2006), or no effects on behavior or neurological function (Baker et al., 2000; Zhang et al., 2005; Bliss et al., 2006), which has been attributed, at least in part, to the low amount of neurons of the desired neurotransmitter phenotype, which is a key prerequisite for successful neuronal replacement. Future studies will disclose whether AraC/NT2N cells are a suitable source of glutamatergic and cholinergic neurons for replacement of cortical excitatory neurons and basal forebrain cholinergic neurons in animal models of ischemic insult and Alzheimer's disease.

More relevant to the present study, the establishment of a neuronal differentiation model for highly efficient generation of NT2-derived postmitotic human neurons offers a suitable experimental framework to approach the main aim of the present study, i.e., to analyze the possible role of PLCβ1 in neuronal differentiation.

3. PLCβ1 IS NECESSARY AND SUFFICIENT FOR NEURONAL DIFFERENTIATION OF NT2 PROGENITORS

The involvement of PLCβ1 has in cell cycle control and differentiation has been reported in various cell lines. For example, PLCβ1 activity correlates directly with

proliferation and inversely with differentiation in cultured MEL cells (Divecha et al., 1995). The endogenous activity of PLCβ1 in MEL cells decreases upon DMSO induced differentiation, which is attenuated by overexpression of PLCβ1 (Matteucci et al., 1998), which triggers cyclin D3/cdk4 activation and cell cycle progression. Interestingly, these effects are not observed by overexpression of the nuclear localization mutant PLCβ1M2b, highlighting the importance of nuclear PLCβ1-dependent signaling in cell cycle control. In contrast, rat C2C12 myoblast differentiation is characterized by an increase in PLCβ1 (Faenza et al., 2003, 2007). In these cells, overexpression of PLCβ1 results in upregulation of the member of AP-1 transcription complex c-jun, which binds to the cyclin D3 promoter and activates the cyclin D3/cdk4 pathway. Yet, at difference with that observed in MEL cells, activation of the cyclin D3/cdk4 pathway results in cell cycle arrest and differentiation, this signaling cascade being dependent on PLCβ1 catalytic activity (Ramazzotti et al., 2008).

These conflicting data reveal that results obtained in a given cell line or tissue cannot be extrapolated and, as discussed above (section 1), only indirect data exist with regard to the role of PLCβ1 in neuronal differentiation, stressing the need of easily manipulable cell culture models to clarify whether PLCβ1 is actually required for neuronal differentiation. In this study, we used human NT2 and rat adrenal pheochromocytoma PC12 cells as cell models, which have been proven to be powerful tools for investigating neuronal differentiation process. The NT2 cell line, which was derived from a human teratocarcinoma, exhibits properties that are characteristic of a committed neuronal precursor at an early stage of development. These embryonic carcinoma cells (ECCs) have long been used to study the mechanisms governing lineage commitment in the central nervous system. In particular, the effect of RA on expression of genes, enzymes and receptors has been extensively studied both in cultured and grafted NT2 cells (Damjanov and Andrews, 1983; Pleasure et al., 1992; Piontek et al., 1999; Przyborski et al., 2000). At its turn, the PC12 cell line derived from a pheochromocytoma of the rat adrenal medulla, also widely used as a model of neuronal differentiation *in vitro*, can be induced to differentiate by treatment with NGF, which causes growth arrest and morphological differentiation. Differentiated PC12 cells assume features typical of sympathetic neurons, including development electrical excitability and synthesis and storage of the catecholamines dopamine and norepinephrine (Greene and Tischler, 1976; Connolly et al., 1979; Fujita et al., 1989).

However, evidence regarding the role of PLCβ1 in neuronal differentiation of NT2 and PC12 cell lines is currently very scarce. There is only one study in which reporting that RA induced differentiation is accompanied by upregulation of PLCβ1 (Novak et al., 2000). Here we analyzed PLCβ1 expression during the time-course of RA- and AraC-induced neuronal differentiation of NT2 progenitors. Our results showed that upon exposure of NT2 cells to either RA or AraC, PLCβ1 levels drastically increase, preceding upregulation of neuron-specific markers. Of note, PLCβ1 expression remains elevated during differentiation and then fall at late stages of differentiation, when the expression of neuron-specific markers is highest. It must be also remarked, that PLCβ1 localization was mainly nuclear at the end of differentiation, as seen by immunofluorescence in fixed cells. The limitation for interpretation of results, arising form the heterogeneous composition of cultures during RA-induced differentiation (see discussion in section 2), could be circumvented by combining Western blot analysis and double immunofluorescence against PLCβ1 and the neuron-specific marker NF200. Indeed, similarly to that observed during AraC-treatment, upregulation of PLCβ1 precedes the appearance of neuron-specific markers. The strong immunofluorescence signal observed in NF200-negative non-neuronal cells (which represent the most abundant neuronal phenotype in these cultures) would explain the unchanged drastic increase in PLCβ1 levels observed by Western blot until day 28 of treatment and the marked fall in PLCβ1-immunoreactivty in neurons isolated by mechanical dislodging. Our results show that PLCβ1 expression and subcellular localization is highly regulated during the time-course of RA- and AraC-induced differentiation, suggesting a possible role of PLCβ1 in neuronal differentiation. The up-down pattern of PLCβ1 expression also suggests that temporal and spatial regulation of PLCβ1 might be relevant for proper progression of the various steps that take place during the course of neuronal differentiation steps, i.e, growth arrest, expression of neuron-specific genes and neurite extension, survival and synaptogenesis. Interestingly, such a phenomenon has been observed in the adipocyte differentiation model of 3T3-L1 fibroblasts and in C2C12 myoblasts (Faenza et al., 2007; O'Carroll et al., 2009). In these cells, PLCβ1 activity is upregulated in two phases during differentiation. The first one taking place immediately after induction of differentiation, is regulated by pERK and PKCα, and is not dependent on nuclear translocation of PLCβ1. The second one begins after 48 h, is independent of pERK and PKCα, and requires both upregulation and nuclear translocation of PLCβ1 protein.

However, despite the promising descriptive results on PLCβ1 regulation during the time-course of NT2 differentiation, assessment of whether PLCβ1 affects is involved in neuronal differentiation requires a more conclusive experimental approach. In this regard, siRNA silencing and overexpression of PLCβ1 have been proven to be potent tools for demonstrating its biological roles. These strategies require the use of appropriate cell models with short lasting differentiation periods. In this regard, neuronal differentiation of NT2 cells by short-term treatment with AraC, characterized in the present study, serves as an excellent model for our purposes. On the other hand, the use of PC12 cells is interesting to ascertain whether observations in NT2 cells are exclusive of this cell line or can be extrapolated between the phenotypically distant neuronal progenitors. Our results clearly demonstrated that siRNA silencing of human PLCB1 gene in NT2 cells impaired AraC-induced morphological differentiation. Moreover, PLCβ1 siRNAs prevented AraC-induced cell cycle arrest, and increase in expression of neuron-specific markers NF200 and βIII-tubulin. On the contrary, upon AraC treatment, NT2 cells transfected with non-targeting siRNAs stopped to grow, developed neuronal processes and expressed higher levels of NF200 and βIII-tubulin than untreated NT2. Similarly, PLCβ1 siRNAs abrogated proliferation arrest and neurite outgrowth in NGF-treated PC12 cells, clearly demonstating that PLCβ1 is a necessary mediator for AraC- and NGF-induced neuronal differentiation of NT2 and PC12 progenitors, respectively. To assess whether overexpression of PLCβ1 is sufficient to induce neuronal differentiation, NT2 progenitors were transfected with plasmid constructs coding for the native amino acid sequences of human PLCβ1a and PLCβ1b. In the absence of AraC, overexpression of both splice variants induced morphological differentiation of NT2 cells and increased levels of the neuron-specific markers NF200 and βIII-tubulin, demonstrating that PLCβ1 is not only necessary but also sufficient for neuronal differentiation of NT2 cells. Intriguingly, despite the accumulating evidence showing that the splice variant-specific carboxy-terminus of PLCβ1a and PLCβ1b posses distinct subcellular localization domains, no remarkable differences were observed between the effects elicited by overexpression of either splice variant (Grubb et al., 2008, 2011, 2012). Because these subcellular localization domains appear to govern interaction with the postsynaptic cytoskeletal scaffold (see introduction) it is likely that these domains are only relevant in mature neurons, whereas the role of PLCβ1 splice variants in early differentiation events would be redundant. In line with this idea, both variants were expressed in plasma membrane, cytosolic and nuclear

fractions of NT2 progenitors, although subtle differences in the PLCβ1a/PLCβ1b ratios were observed between fractions. However, this assumption requires experimental verification. In this regard, we have recently generated PLCβ1 constructs coding for PLCβ1 variants truncated to varying degrees in variant-specific short carboxy-terminal region, which will be used to fulfill the above mentioned purpose.

As mentioned in the introduction, molecular mechanisms responsible for the cellular responses mediated by PLCβ1 are poorly understood, and existing data are conflicting. As discussed above, PLCβ1 overexpression triggers cyclin D3/cdk4 activation in MEL and C2C12 cells, but with a completely opposite outcome. Thus, PLCβ1 expression is necessary and sufficient to promote cycle progression of MEL cells and to induce arrest in the G0/G1 phase and differentiation of C2C12 myoblasts, which only can be explained by a cross-talk between signaling pathways that control the cell cycle and those that promote cell differentiation. Future studies will be necessary to determine whether these pathways are activated by PLCβ1 in NT2 cells. Another important question that remains to be answered is whether nuclear translocation of PLCβ1 is necessary for AraC-induced differentiation of NT2 cells. Therefore, it will be necessary to test whether the nuclear localization mutant PLCβ1M2b is unable to promote neuronal differentiation of NT2 progenitors and acts in a dominant negative fashion and suppresses neuronal differentiation as it has been described for C2C12 myoblast differentiation. We are currently cloning of nuclear localization mutants of PLCβ1a and PLCβ1b, which is in an advanced stage.

4. A POSSIBLE ROLE OF TRAX-PLCβ1 INTERACTION IN NEURONAL DIFFERENTIATION

As mentioned in the introduction, TRAX (translin associated factor-X), and its binding partner protein Translin, have been implicated in a broad spectrum of biological activities, including cell growth regulation, mRNA processing and neuronal development/function (Jaendling and McFarlane, 2010), although their precise role in these processes remains to be elucidated. Recently, the interaction between PLCβ1 and TRAX has been described in cultured cells (Aisiku et al., 2010). Noticeably, it was demonstrated that Gαq competes with TRAX for PLCβ1 binding, revealing a scenario in which PLCβ1, TRAX and Gαq levels, together with activity of Gq-coupled membrane receptors, would condition the location of PLCβ1 and TRAX and the possibility of these partners to interact. A later study from the same group (Philip et al.,

2012) elegantly demonstrated that PLCβ1-TRAX association regulates the activity of the RISC silencing machinery, showing that PLCβ1 binding to TRAX negatively regulates the maturation of siRNAs targeting specific genes (Philip et al., 2012). Specifically, Philip et al. (2012) reported that overexpression of PLCβ1 reverses exogenous siRNA-mediated knockdown of LDH or GAPDH, but does not affect silencing of other genes such as cyclophilin, Hsp90 or translin. Reversal of LDH or GAPDH knockdown resulted in rescue of histone H2B levels and cell survival. These data clearly support the idea that TRAX could be a novel mediator of PLCβ1 signaling in different biological processes (Aisiku et al., 2010; Philip et al., 2012, 2103). Interestingly, endogenous miRNAs regulate gene expression during neuronal differentiation (Shi et al., 2010; Coolen et al., 2012; Palm et al., 2013; Sun et al., 2013) and that TRAX- and translin-knockout mice display a variety of neurological deficits (Chennathukuzhi et al., 2003; Stein et al., 2006; Li et al., 2008). Therefore, it is conceivable that PLCβ1-TRAX association could play a key role in neuronal differentiation by regulating endogenous miRNA activity.

Taking into consideration these evidences, we decided to characterize the expression and subcellular localization of the PLCβ1-binding partners TRAX and Gαq during neuronal differentiation of NT2 cells. Moreover, we analyzed PLCβ1-TRAX interaction in differentiating NT2 cells by Förster resonance energy transfer (FRET) and evaluated the effects of TRAX, translin and Gαq/11 silencing on differentiation of PC12 cells. The results of these assays can be summarized as follows: 1. TRAX and Gαq/11 levels are increased during AraC-induced neuronal differentiation of NT2 cells. 2. Inmunofluorescence and Western blot analysis of subcellular fractions reveal that the increase of TRAX expression during the time-course of neuronal differentiation of NT2 cells preferentially involves the cell nucleus. 3. FRET assays demonstrate that the interaction between PLCβ1 and TRAX increases during NT2 differentiation, being restricted to the nucleus at the late stages of differentiation 4. TRAX, but not tranlsin or Gαq/11 silencing, abrogates NGF-induced neuronal differentiation of PC12 cells.

Interestingly enough, the time-course of TRAX expression during AraC-induced NT2 differentiation was different from that of PLCβ1. Whereas PLCβ1 expression increased as soon as 24 h after the initiation of AraC treatment, TRAX levels began to increase significantly at 72 h, reaching a maximum at the end of the differentiation process. The difference in the time-course profile of both proteins could be explained

through a PLCβ1-mediated regulation of TRAX expression. Our results suggest that this could be the case. Indeed, silencing of PLCβ1 abrogated the increase of TRAX expression caused by AraC-treatment, whereas overexpression of PLCβ1 in absence of AraC resulted in a marked increase of TRAX levels. However, although PLCβ1 appears to regulate TRAX expression, the TRAX levels (unlike those of PLCβ1), rather than being decreased, were hugely increased at the end of differentiation. A deeper analysis of TRAX expression by Western blot analysis in subcellular fractions demonstrated that TRAX upregulation involved the cell nucleus but not the cytosol of the plasma membrane.

Although we cannot explain the mechanisms of TRAX translocation to the nucleus during neuronal differentiation, in light of our data some time-related events could be proposed. During AraC-induced differentiation, PLCβ1-immunostaining is highly increased in the cytosol until 72 h. Under these conditions, the high amount of PLCβ1 can accommodate the moderate increase of TRAX levels. It has been described that TRAX is able to compete and block Gαq binding and activation of PLCβ1 (Aisiku, 2010). During NT2 differentiation the high level of PLCβ1 can attenuate the competition between TRAX and Gαq/11. Downregulation of PLCβ1 at the end of differentiation generates a new situation in which TRAX and Gαq/11 would be competing for the interaction with a lower population of PLCβ1. Due to the higher affinity of Gαq/11 for PLCβ1 association, it is conceivable that a decrease in PLCβ1-TRAX interaction could favor the translocation of TRAX to the nucleus, as seen in other studies (Philip et al., 2012). Also, elevated and reduced levels of TRAX and PLCβ1, respectively, could be sufficient for TRAX translocation to the nucleus without the partnership of Gαq/11. Indeed, at the end of NT2 differentiation, semiquantitative Western blot analysis revealed an inversion of the relative expression levels of TRAX and PLCβ1 with respect to early stages of differentiation, and immunofluorescence assays revealed that PLCβ1-immunoreactivity was barely detectable in the cytoplasm of terminally differentiated AraC/NT2N neurons. In favor of this explanation is the fact that TRAX (but not Gαq/11) silencing did abrogate differentiation of PC12 cells. In spite of the differences between the two models, this would imply that Gαq/11 does not prevent TRAX translocation to the cell nucleus during differentitation. Further comparative studies in both cell models will be necessary to propose a solid hypothesis.

In any case, our data clearly show that TRAX is necessary for neuronal differentiation of PC12 cells and strongly suggest that is also the case for NT2 cell differentiation.

However, some questions need to be answered before establishing the biological significance of TRAX in NT2 differentiation process. TRAX was originally described as a protein forming complexes with translin (Aoki et al., 1997), and both proteins have been implicated in the control of cell cycle (Castro et al., 2000; Ishida et al., 2002), although some discrepancies have been observed depending on the cell-type used for these studies (Yang et al., 2004; Sun et al., 2006). In this regard, our results suggest that TRAX, but not translin, is necessary for NGF-induced PC12 differentiation. Whether this occurs in the same way in NT2 differentiation process remains to be answered. The time-course of translin expression, and its interaction with TRAX, during NT2 differentiation process should be performed in order to analyze whether the upregulation of nuclear TRAX is related to an increase of TRAX-translin complexes in this location. The high amount of nuclear TRAX at the end of AraC-induced NT2 differentiation suggests that this protein could be implicated in the maintenance of neuronal phenotype or in differentiated neuronal survival. Answering these key questions will be critical to define the role of TRAX in this cellular model.

Interestingly, recent studies have described some other TRAX interacting molecules, including nuclear matrix protein (CD1), an activator of DNA-dependent protein kinase (Erdemir et al., 2002) and an upstream activator of p53 (Rothbart et al., 1999). Additionally, other cytosolic proteins such as snaxip1, MEA-2, Akap9 and Sun-1 can interact with TRAX (Bray and Hecht, 2002). In this context, it will be interesting to evaluate in the future not only the role of TRAX in differentiation, maintenance of neuronal phenotype or differentiated neuronal survival, but also to analyze the signaling pathways involved in these processes.

VII. CONCLUSIONS

1. The two splice variants of phospholipase C β1, PLCβ1a and PLCβ1b, are present in membranes, cytosolic and nuclear fractions from the adult rat cerebral cortex.

1.1. Immunoblot analysis in membrane, cytosolic and nuclear fractions from the adult rat cortex showed that PLCβ1a is predominant over PLCβ1b in all fractions studied, although the relative contribution of each variant to the total signal differs between subcellular compartments.

1.2. Immunofluorescence in intact nuclei isolated from the adult rat cerebral cortex, revealed a high overlap between PLCβ1-immunostaining and the signals provided by the markers of the nuclear speckles NeuN/Fox3 and SC-35. In contrast, no co-localization of PLCβ1 with chromatin-rich domains or markers of the nuclear envelope and lamina was observed.

2. NT2 cells induced to differentiate by short-term (6 days) treatment with the nucleoside analogue cytosine β-D-arabinofuranoside (AraC) (AraC/NT2N cells) express postmitotic neuronal markers, display significant morphometric differences compared with NT2-derived non-neuronal cells and differ in neurotransmitter phenotype from NT2N neurons induced by RA (RA/NT2N cells).

2.1 Western blot and immunofluorescence analysis during the time-course of RA- and AraC-induced differentiation showed that immunoreactivity for NF200, βIII-tubulin and DCX was increased in both differentiation models.

2.2 The progressive increase in expression of NeuN/Fox-3 observed during AraC-induced differentiation of NT2 progenitors, as analysed by Western blot and immunofluorescence microscopy, confirmed the neuronal identity of AraC/NT2N neurons.

2.3 After an uninterrupted 6-day period of AraC treatment, increasing cell density at mid-treatment, about 71% of the cells in culture fulfilled the double criterion (NeuN/Fox-3 positive nucleus and neurite extensions) to be considered as neuronal, leading to a percentage of surviving terminally differentiated neurons augmented by almost 3-fold with respect to that found after RA-differentiation.

2.4 When compared with RA/NT2N neurons, AraC/NT2N neurons displayed considerably larger nuclei and cell somata, a 4.2-fold shorter total neurite length per cell and a large number of lamellar extensions and filopodia-like processes.

2.5 Cells committed to differentiate by short treatment with AraC displayed a completely different neurotransmitter phenotype when compared with RA/NT2N neurons. Using immunofluoresecence microscopy and Western blot analysis, we can conclude that, in our culture conditions, GABAergic is the major neurotransmitter phenotype in RA/NT2N cells, whereas virtually all terminally differentiated AraC/NT2N neurons co-expressed both glutamatergic and cholinergic markers.

3. Phospholipase C β1 is strongly regulated during RA- and AraC-induced differentiation of NT2 progenitors.

3.1 Combination of Western blot and double immunofluorescence showed that exposure of NT2 cells to either RA or AraC led to a drastic increase of both PLCβ1a and PLCβ1b levels that preceded upregulation of the neuron-specific markers NF200, βIII-tubulin.

3.2 Western blot and immunofluorescence assays showed that PLCβ1 expression fall at late stages of differentiation, when the expression of neuron-specific markers was highest.

3.3 At the end of differentiation, PLCβ1 localization was mainly nuclear, as seen by immunofluorescence in fixed cells.

4. Phospholipase C β1 is necessary for neuronal differentiation of NT2 and PC12 progenitors and sufficient for differentiation of NT2 progenitors.

4.1. Silencing of PLCβ1 expression impaired AraC-induced cell cycle arrest, morphological differentiation, and unpregulation of neuron-specific markers NF200 and β-III tubulin.

4.2. Silencing of PLCβ1 expression abrogated proliferation arrest and neurite outgrowth in NGF-treated PC12 cells.

4.3. Overexpression of either PLCβ1a or PLCβ1b in the absence of AraC induced morphological differentiation of NT2 cells and increased levels of the neuron-specific markers NF200 and βIII-tubulin.

5. Association of phospholipase C β1 with its binding partner translin-associated factor X (TRAX) appears to be involved in AraC-induced differentiation of NT2 cells in a translin- and Gαq/11-independent manner.

5.1. TRAX and Gαq/11 levels are increased during AraC-induced neuronal differentiation of NT2 cells.

5.2. Inmunofluorescence and Western blot analysis of subcellular fractions reveal that the increase of TRAX expression during the time-course of neuronal differentiation of NT2 cells preferentially involves the cell nucleus.

5.3. FRET assays demonstrate that the interaction between PLCβ1 and TRAX increases during NT2 differentiation, being restricted to the nucleus at the late stages of differentiation.

5.4. TRAX, but not tranlsin or Gαq/11 silencing, abrogates NGF-induced neuronal differentiation of PC12 cells.

VIII. REFERENCES

[A]

- Aisiku OR, Runnels LW, Scarlata, S (2010). Identification of a Novel Binding Partner of Phospholipase Cβ1: Translin-Associated Factor X. PLoS ONE, 5:e15001.
- Albi E, Rossi G, Maraldi NM, Viola Magno M, Cataldi S, Solimando L, Zini N (2003b). Involvement of Nuclear Phosphatidylinositol-Dependent Phospholipases C in Cell Cycle Progression During Rat Liver Regeneration. J Cell Physiol, 197:181-188.
- Andrews PW (1984). Retinoic acid induces neuronal differentiation of a cloned human embryonal carcinoma cell line in vitro. Dev Biol, 103:285-293.
- Andrews PW, Damjanov I, Simon D, Banting GS, Carlin C, Dracopoli NC, Fogh J (1984). Pluripotent embryonal carcinoma clones derived from the human teratocarcinoma cell line Tera-2. Differentiation in vivo and in vitro. Lab Invest, 50:147-162.
- Aoki K, Ishida R, Kasai M (1997). Isolation and characterization of a cDNA encoding a Translin-like protein, TRAX. FEBS Lett, 401:109-112.
- Asmus SE, Parsons S, Landis SC (2000). Developmental changes in the transmitter properties of sympathetic neurons that innervate the periosteum. J Neurosci, 20:1495-1504.
- Avazeri N, Courtot AM, Pesty A, Duquenne C, Lefevre B (2000). Cytoplasmic and nuclear phospholipase C-beta 1 relocation: role in resumption of meiosis in the mouse oocyte. Mol Biol Cell, 11:4369-4380.
- Avazeri N, Courtot AM, Pesty A, Lefevre B (2003). Meiosis resumption, calcium-sensitive period, and PLC-beta1 relocation into the nucleus in the mouse oocyte. Cell Signal, 15:1003-1010.

[B]

- Bahk YY, Lee YH, Lee TG, Seo J, Ryu SH, Suh PG (1994). Two forms of phospholipase C-β1 generated by alternative splicing. J Biol Chem, 269:8240-8245.
- Bahk YY, Song H, Baek SH, Park BY, Kim H, Ryu SH, Suh PG (1998). Localization of two forms of phosphlipase C-β1, a and b, in C6bu-1 cells. Biochim Biophys Acta, 1389:76-80.
- Baker KA, Hong M, Sadi D, Mendez I (2000). Intrastriatal and intranigral grafting of hNT neurons in the 6-OHDA rat model of Parkinson's disease. Exp Neurol, 162:350-360.

- Baker KA, Mendez I (2005). Long distance selective fiber outgrowth of transplanted hNT neurons in white matter tracts of the adult rat brain. J Comp Neurol, 486:318-330.
- Balla T (2013). Phosphoinositides: tiny lipids with giant impact on cell regulation. Physiol Rev, 93:1019-1137.
- Banerjee S, Williamson D, Habib N, Gordon M, Chataway J (2010). Human stem cell therapy in ischaemic stroke: a review. Age Ageing, 40:7-13.
- Batty IH and Nahorski SR (1992). Analysis of [3H]inositol phosphate formation and metabolism in cerebral cortical slices: evidence for a dual metabolism of 1,4-biphosphate. Biochem J, 288:807-815.
- Bavelloni A, Faenza I, Cioffi G, Piazzi M, Parisi D, Matic I, Maraldi NM, Cocco L (2006). Proteomic-based analysis of nuclear signaling: PLC beta1 affects the expression of the splicing factor SRp20 in Friend erythroleukemia cells. Proteomics, 6:5725-5734.
- Berridge MJ (1983). Rapid accumulation of inositol triphosphate reveals that agonist hydrolyse polyphosphoinositides instead of phosphatidylinositol. Biochem J, 212:849-858.
- Bertagnolo V, Marchisio M, Capitani S, Neri LM (1997). Intranuclear translocation of phospholipase C beta2 during HL-60 myeloid differentiation. Biochem Biophys Res Commun, 235:831-837.
- Bertagnolo V, Mazzoni M, Ricci D, Carini C, Neri LM, Previati M, Capitani S (1995). Identification of PI-PLC beta 1, gamma 1, and delta 1 in rat liver: subcellular distribution and relationship to inositol lipid nuclear signalling. Cell Signal, 7:669-678.
- Bertrand N, Castro DS, Guillemot F (2002). Proneural genes and the specification of neural cell fates. Nat Rev Neurosci, 3:517-530.
- Bhargava N, Das M, Edwards D, Stancescu M, Kang JF, Hickman JJ (2010). Coexpression of glutamate vesicular transporter (VGLUT1) and choline acetyltransferase (ChAT) proteins in fetal rat hippocampal neurons in culture. In Vitro Cell Dev Biol Anim, 46:685-92.
- Billi AM, Matteucci A, Faenza I, Manzoli L, Rubbini S, Gilmur RS (1997). Control of expression of PLCbeta1 by LAC repressor system: relationship between nuclear PLCbeta1 overexpression and growth factor stimulation. Biochem Biophys Res Commun, 241:122-126.
- Bliss T, Guzman R, Daadi M, Steinberg GK (2006). Cell Transplantation Therapy for Stroke. Stroke, 38:817-826.

- Böhm D, Schwegler H, Kotthaus L, Nayernia K, Rickmann M, Kfhler M, Rosenbusch J, Engel W, Flqgge G, Burfeind P (2002). Disruption of PLC-β1- mediated signal transduction in mutant mice causes age-dependent hippocampal mossy fiber sprouting and neurodegeneration. Mol Cell Neurosci, 21:584-601.
- Borlongan CV, Fournier C, Stahl CE, Yu G, Xu L, Matsukawa N, Newman M, Yasuhara T, Hara K, Hess DC, Sanberg PR (2006). Gene therapy, cell transplantation and stroke. Front Biosci, 11:1090-1101.
- Borlongan CV, Saporta S, Poulos SG, Othberg A, Sanberg PR (1998a). Viability and survival of hNT neurons determine degree of functional recovery in grafted ischemic rats. Neuroreport, 9:2837-2842.
- Borlongan CV, Tajima Y, Trojanowski JQ, Lee VM-Y, Sanberg PR (1998b). Transplantation of cryopreserved human embryonal carcinoma-derived neurons (NT2N cells) promotes functional recovery in ischemic rats. Exp Neurol, 149:310-321.
- Boronenkov IV, Loijens JC, Umeda M, Anderson RA (1998). Phosphoinositide signaling pathways in nuclei are associated with nuclear speckles containing pre-mRNA processing factors. Mol Biol Cell, 9:3547-3560.
- Bradford MM (1976). A rapid and sensitive method for the quantitation of microgram quantities of protein utilizing the principle of protein-dye binding. Anal Biochem, 72:248-254.
- Bray JD, Chennathukuzhi VM, Hecht NB (2002). Identification and characterization of cDNAs encoding four novel proteins that interact with translin associated factor-X. Genomics, 79:799-808.
- Briscoe J, Ericson J (2001). Specification of neuronal fates in the ventral neural tube. Curr Opin Neurobiol, 11:43-49
- Brown JP, Couillard-Despres S, Cooper-Kuhn CM, Winkler J, Aigner L, Kuhn HG (2003). Transient expression of doublecortin during adult neurogenesis. J Comp Neurol, 467:1-10.

[C]

- Capitani S, Cocco L, Maraldi NM, Papa S, Manzoli FA (1986). Effect of phospholipids on transcription and ribonucleoprotein processing in isolated nuclei. Adv Enzyme Regul, 25: 425-438.

- Caricasole A, Sala C, Roncarati R, Formenti E, Terstappen GC (2000). Cloning and characterization of the human phosphoinositide-specific phospholipase C-beta 1 (PLCβ1). Biochim Biophys Acta, 1517:63-72.
- Carpenter G, Ji Q (1999). Phospholipase C-γ as a signal-transducing. Exp Cell Res, 253:15-24.
- Castro A, Peter M, Magnaghi-Jaulin L, Vigneron S, Loyaux D, Lorca T, Labbé JC. (2000). Part of Xenopus translin is localized in the centrosomes during mitosis. Biochem Biophys Res Commun, 276:515-523.
- Charpentier TH, Waldo GL, Barrett MO, Huang W, Zhang Q, Harden TK, Sondek J (2014). Membrane-induced allosteric control of phospholipase C-β isozymes. J Biol Chem, 289:29545-29557.
- Chatterjee S, Pal JK (2009). Role of 5'- and 3'-untranslated regions of mRNAs in human diseases. Biol Cell, 101:251-262.
- Chennathukuzhi V, Stein JM, Abel T, Donlon S, Yang S, Miller JP, Allman DM, Simmons RA, Hecht NB (2003). Mice Deficient for Testis-Brain RNA-Binding Protein Exhibit a Coordinate Loss of TRAX, Reduced Fertility, Altered Gene Expression in the Brain, and Behavioral Changes. Mol Cell Biol, 23:6419-6434.
- Cheung WM, Fu WY, Hui WS, Ip NY (1999). Production of human CNS neurons from embryonal carcinoma cells using a cell aggregation method. Biotechniques, 26:946-948.
- Cho YS, Chennathukuzhi VM, Handel MA, Eppig J, Hecht NB (2004). The relative levels of translin-associated factor X (TRAX) and testis brain RNA-binding protein determine their nucleocytoplasmic distribution in male germ cells. J Biol Chem, 279:31514-31523.
- Chung SM, Proia AP, Klintworth GK, Watson SP, Lapetuna EG (1985). Deoxycholate induces the preferential hydrolysis poliphosphoinositides by human platelet and rat corneal phospholypase C. Biochem Biophys Res Commun, 192:411-416.
- Ciruela A, Hinchliffe KA, Divecha N, Irvine RF (2000). Nuclear targeting of the beta isoform of type II phosphatidylinositol phosphate kinase (phosphatidylinositol 5-phosphate 4-kinase) by its alpha-helix 7. Biochem J, 3:587-591.
- Claro E, Wallace MA, Lee HM, Fain JN (1989). Carbachol in the presence of guanosine 5'-O-(3-Thiotriphosphate) stimulates the breakdown of exogenous phosphatidylinositol 4,5-biphosphate, phosphatidylinositol 4-phosphate, and phosphatidylinositol by rat brain membranes. J Biol Chem, 264:18288-18295.

- Cocco L, Faenza I, Fiume R, Billi AM, Stewart Gilmour R, Manzoli FA (2006). Phosphoinositide-specific phospholipase C (PI-PLC) β1 and nuclear lipid-dependent signaling. Biochim Biophys Acta, 1761:509-521.
- Cocco L, Faenza I, Follo MY, Billi AM, Ramazzotti G, Papa V, Martelli, AM, Manzoli L (2009). Nuclear inositides: PI-PLC signaling in cell growth, differentiation and pathology. Adv Enzyme Regul, 49:2-10.
- Cocco L, Gilmour RS, Ognibene A, Letcher AJ, Manzoli FA, Irvine RF (1987). Synthesis of polyphosphoinositides in nuclei of Friend cells. Evidence for polyphosphoinositide metabolism inside the nucleus which changes with cell differentiation. Biochem J, 248:765-770.
- Cocco L, Martelli AM, Gilmour RS, Rhee SG, Manzoli FA (2001). Nuclear phospholipase C and signaling. Biochim Biophys Acta, 1530:1-14.
- Cocco L, Rubbini S, Manzoli L, Billi AM, Faenza I, Peruzzi D, Matteucci A, Artico M, Stewart Gilmour R, Goo Rhee S (1999). Inositides in the nucleus: presence and characterisation of the isozymes of phospholipase β family in NIH 3T3 cells. Biochim et Biophys Acta, 1438:295-299.
- Connolly J, Greene L, Viscarello R, Riley W (1979). Rapid, sequential changes in surface morphology of PC12 pheochromocytoma cells in response to nerve growth factor. J Cell Biol, 82:820-827.
- Couillard-Despres S, Quehl E, Altendorfer K, Karl C, Ploetz S, Bogdahn U, Winkler J, Aigner L (2008). Human in vitro reporter model of neuronal development and early differentiation processes. BMC Neurosci, 9:31.
- Coyle DE, Li J, Baccei M (2011). Regional differentiation of retinoic acid-induced human pluripotent embryonic carcinoma stem cell neurons. PLoS One, 6:e16174.
- Crljen V, Visnjic D, Banfic H (2004). Presence of different phospholipase C isoforms in the nucleus and their activation during compensatory liver growth. FEBS Lett, 571:35-42.

[D]

- D'Santos CS, Clarke JH, Divecha N (1998), Phospholipid signalling in the nucleus. Een DAG uit het leven van de inositide signalering in de nucleus. Biochim Biophys Acta, 1436:201-232.
- D'Santos C, Clarke JH, Roefs M, Halstead JR, Divecha N (2000). Nuclear inositides. Eur J of Histochem, 44:51-60.

- De Angioletti M, Lacerra G, Sabato V, Carestia C (2004). Beta+45 G --> C: a novel silent beta-thalassaemia mutation, the first in the Kozak sequence. Br J Haematol, 124:224-231.
- Damjanov I, Andrews PW (1983). Ultrastructural differentiation of a clonal human embryonal carcinoma cell line in vitro. Cancer Res, 43:2190-2198.
- Darlington PJ, Goldman JS, Cui QL, Antel JP, Kennedy TE (2008). Widespread immunoreactivity for neuronal nuclei in cultured human and rodent astrocytes. J Neurochem, 104:1201-1209.
- Dent MAR, Segura-Anaya E, Alva-Medina J, Aranda-Anzaldo A (2010). NeuN/Fox-3 is an intrinsic component of the neuronal nuclear matrix. FEBS Lett, 584:2767-2771.
- Divecha N, Banfic H, Irvine RF (1991). The polyphosphoinositide cycle exists in the nuclei of Swiss 3T3 cells under the control of a receptor (for IGF-I) in the plasma membrane, and stimulation of the cycle increases nuclear diacylglycerol and apparently induces translocation of protein kinase C to the nucleus. EMBO J, 10:3207-3214.
- Divecha N, Rhee SG, Letcher AJ, Irvine RF (1993). Phosphoinositide signaling enzymes in rat liver nuclei: phosphoinositidase C isoform β1 is specifically, but not predominantly, located in the nucleus. Biochem J, 289:617-620.
- Divecha N, Roefs M, Los A, Halstead J, Bannister A, D'Santos C (2002). Type I PIPkinases interact with and are regulated by the retinoblastoma susceptibility gene product-pRB. Curr Biol, 12:582-587.
- Divecha, N, Irvine RF (1995). Phospholipid signaling. Cell, 80:269-278.
- Downes CP, Wusterman MM (1983). Breakdown of polyphosphoinositides and not phosphatidylinositol accounts for muscarinic agonist-stimulated inositol phospholipid metabolising in rat parotid glands. Biochem J, 216:633-640.
- Dráberová E, Del Valle L, Gordon J, Marková V, Smejkalová B, Bertrand L, de Chadarévian JP, Agamanolis DP, Legido A, Khalili K, Dráber P, Katsetos CD (2008). Class III beta-tubulin is constitutively coexpressed with glial fibrillary acidic protein and nestin in midgestational human fetal astrocytes: implications for phenotypic identity. J Neuropathol Exp Neurol, 67:341-354.
- Drin G, Scarlata S (2007). Stimulation of phospholipase Cbeta by membrane interactions, interdomain movement, and G protein binding--how many ways can you activate an enzyme?. Cell Signal, 19:1383-1392.

[E]

- Eisen JA, Sweder KS, Hanawalt PC (1995). Evolution of the SNF2 family of proteins: subfamilies with distinct sequences and functions. Nucleic Acids Res, 23:2715-2723.
- Ellis MV, James SR, Perisic O, Downes CP, WilliamsRL, Katan M (1998). Catalytic domain of phosphoinositide-specific phospholipase C (PLC). Mutational analysis of residues within the active site and hydrophobic ridge of PLC-δ1. J Biol Chem, 273:11650-11659.
- Erdemir T, Bilican B, Oncel D, Goding CR, Yavuzer U (2002). DNA damage-dependent interaction of the nuclear matrix protein C1D with Translin-associated factor X (TRAX). J Cell Sci, 115: 207-216.
- Essen LO, Perisic O, Cheung R, Katan M, Williams RL (1996). Crystal structure of a mammalian phosphoinositide-specific phospholipase C-δ. Nature, 380:595-602.

[F]

- Faenza I, Bavelloni A, Fiume R, Lattanzi G,Maraldi NM, Gilmour RS, Martelli AM, Suh PG, Billi AM, Cocco L (2003). Up-regulation of nuclear phospholipase C beta 1 in myogenic differentiation. J Cell Physiol, 195:446-452.
- Faenza I, Bregoli L, Ramazzotti G, Gaboardi G, Follo MY, Mongiorgi S, Billi AM, Manzoli L, Martelli AM, Cocco L (2008). Nuclear phospholipase C beta1 and cellular differentiation. Front Biosci, 13:2452-2463.
- Faenza I, Matteucci A, Manzoli L, Billi AM, Aluigi M, Peruzzi D, Vitale M, Castorina S, Suh PG, Cocco L (2000). A role for nuclear phospholipase Cß 1 in cell cycle control. J Biol Chem, 275:30520-30524.
- Faenza I, Ramazzotti G, Bavelloni A, Fiume R, Gaboardi GC, Follo MY, Gilmour RS, Martelli AM, Ravid K, Cocco L (2007). Inositide-dependent phospholipase C signaling mimics insulin in skeletal muscle differentiation by affecting specific regions of the cyclin D3 promoter. Endocrinology, 148:1108-1117.
- Fee JA, Monsey JD, Handler RJ, Leonis MA, Mullaney SR, Hope HM, Silbert DF (1994). A Chinese hamster fibroblast mutant defective in thrombin-induced signaling has a low level of phospholipase C-beta 1. J Biol Chem, 269:21699-21708.
- Ferguson KM, Lemmon MA, Schlessinger J, Sigler PB (1995). Structure of the high affinity complex of inositol triphosphate with a phospholipase C pleckstrin homology domain. Cell, 83:1037-1046.

- Fisher SK, Haecock AM, Seguin EB, Agranoff BW (1990). Polyphosphoinositides are the major source of inositol phosphates in carbamoylcholine-stimulated SK-NSH neuroblastoma cells. Mol Pharmacol, 38:54-63.
- Fiume R, Faenza I, Matteucci A, Astolfi A, Vitalel, Martelli AM, Cocco L (2005). Nuclear Phospholipase C β1 (PLC β1) Affects CD24 Expression in Murine Erythroleukemia Cells. J Biol Chem, 280:24221-24226.
- Fiume R, Ramazzotti G, Teti G, Chiarini F, Faenza I, Mazzotti G, Billi AM, Cocco L (2009). Involvement of nuclear PLC beta1 in lamin B1 phosphorylation and G2/M cell cycle progression. FASEB J, 23:957-966.
- Foudah D, Monfrini M, Donzelli E, Niada S, Brini AT, Orciani M, Tredici G, Miloso M (2014). Expression of neural markers by undifferentiated mesenchymal-like stem cells from different sources. J Immunol Res, 2014:987678.
- Fox K, Schlaggar BL, Glazewski S, O'Leary DDM (1996). Glutamate receptor blockade at cortical synapses disrupts development of thalamocortical and columnar organization in somatosensory cortex. Proc Natl Acad Sci USA, 93:5584-5589.
- Fujita K, Lazarovici P, Guroff G (1989). Regulation of the differentiation of PC12 pheochromocytoma cells. Environ Health Perspect, 80:127-142.

[G]

- García del Caño G, Aretxabala X, González-Burguera I, Montaña M, López de Jesús M, Barrondo S, Barrio RJ, Sampedro C, Goicolea MA, Sallés J (2015). Nuclear diacylglycerol lipase-α in rat brain cortical neurons: evidence of 2-arachidonoylglycerol production in concert with phospholipase C-β activity. J Neurochem, 132:489-503.
- García del Caño G, Montaña M, Aretxabala X, González-Burguera I, López de Jesús M, Barrondo S, Sallés J (2014). Nuclear phospholipase C-β1 and diacylglycerol LIPASE-α in brain cortical neurons. Adv Biol Regul, 54:12-23.
- Garcia-Bustos JF, Marini F, Stevenson I, Frei C, Hall MN (1994). PIK1, an essential phosphatidylinositol 4-kinase associated with the yeast nucleus. EMBO J, 13:2352-2361.
- Garro MA, López de Jesus M, Ruiz de Azúa I, Callado LF, Meana JJ, Sallés J (2001) Regulation of phospholipase C beta activity by muscarinic acetylcholine and 5-HT2 receptors in crude and synaptosomal membranes from human cerebral cortex. Neuropharmacology, 40:686-695.

- Gauthier J, Champagne N, Lafrenière RG, Xiong L, Spiegelman D, Brustein E, Lapointe M, Peng H, Côté M, Noreau A, Hamdan FF, Addington AM, Rapoport JL, Delisi LE, Krebs MO, Joober R, Fathalli F, Mouaffak F, Haghighi AP, Néri C, Dubé MP, Samuels ME, Marineau C, Stone EA, Awadalla P, Barker PA, Carbonetto S, Drapeau P, Rouleau GA; S2D Team (2010). De novo mutations in the gene encoding the synaptic scaffolding protein SHANK3 in patients ascertained for schizophrenia. Proc Natl Acad Sci USA, 107:7863-7868.
- Gonzales ML, Anderson RA (2006). Nuclear phosphoinositide kinases and inositol phospholipids. J Cell Biochem, 97:252-260.
- Greene LA, Tischler AS (1976). Establishment of a noradrenergic clonal line of rat adrenal pheochromocytoma cells which respond to nerve growth factor. Proc Natl Acad Sci USA, 73:2424-2428.
- Grobler JA, Hurley JH (1998). Catalysis by phospholipase C δ1 requires that Ca2+ bind to the catalytic domain, but not the C2 domain. Biochemistry, 37:5020-5028.
- Grubb DR, Iliades P, Cooley N, Yu YL, Luo J, Filtz TM, Woodcock EA (2011) Phospholipase Cbeta1b associates with a Shank3 complex at the cardiac sarcolemma. FASEB J, 25:1040-1047.
- Grubb DR, Luo J, Yu YL, Woodcock EA (2012). Scaffolding protein Homer 1c mediates hypertrophic responses downstream of Gq in cardiomyocytes. FASEB J, 26:596-603.
- Grubb DR, Vasilevski O, Huynh H, Woodcock EA (2008). The extreme C-terminal region of phospholipase C β1 determines subcellular localization and function; the “b” splice variant mediates alpha1-adrenergic receptor responses in cardiomyocytes. FASEB J, 22:2768-2774.
- Guillemain I, Alonso G, Patey G, Privat A, Chaudieu I (2000a). Human NT2 neurons express a large variety of neurotransmission phenotypes in vitro. J Comp Neurol, 422:380-395.
- Guillemain I, Gaboyard S, Fontes G, Saunier M, Privat A, Patey G (2000b). Differential expression of Bcl-2-related proteins in differentiating NT2 cells. Neuroreport, 11:1421-1425.
- Guo Y, Golebiewska U, D'Amico S, Scarlata S (2010). The small G protein Rac1 activates phospholipase Cδ1 through phospholipase Cβ2. J Biol Chem, 285:24999-25008.

[H]

- Haile Y, Fu W, Shi B, Westaway D, Baker G, Jhamandas J, Giuliani F (2014). Characterization of the NT2-derived neuronal and astrocytic cell lines as alternative in vitro models for primary human neurons and astrocytes. J Neurosci Res, 92:1187-1198.
- Hammond SM, Caudy AA, Hannon GJ (2001). Post-transcriptional gene silencing by double-stranded RNA. Nat Rev Genet, 2:110-119.
- Hannan AJ, Blakemore C, Katsnelson A, Vitalis T, Huber KM, Bear M (2001). PLC-beta1, activated via mGluRs, mediates activity-dependent differentiation in cerebral cortex. Nat Neurosci, 4:282-288.
- Hara K, Yasuhara T, Maki M, Matsukawa N, Masuda T, Yu SJ, Ali M, Yu G, Xu L, Kim SU, Hess DC, Borlongan CV (2008). Neural progenitor NT2N cell lines from teratocarcinoma for transplantation therapy in stroke. Prog Neurobiol, 85:318-34.
- Harlan JE, Hajduk PJ, Yoon HS, Fesik SW (1994). Pleckstrin homology domains bind to phosphatidylinositol-4,5-biphosphate. Nature, 371:168-170.
- Hartley RS, Margulis M, Fishman PS, Lee VM, Tang CM (1999a). Functional synapses are formed between human NTera2 (NT2N, hNT) neurons grown on astrocytes. J Comp Neurol, 407:1-10.
- Hartley RS, Trojanowski JQ, Lee VM (1999b). Differential effects of spinal cord gray and white matter on process outgrowth from grafted human NTERA2 neurons (NT2N, hNT). J Comp Neurol, 415:404-418.
- Hecht NB (2004). Translin-associated Factor X Is Post-transcriptionally Regulated by Its Partner Protein TB-RBP, and Both Are Essential for Normal Cell Proliferation. J Biol Chem, 279:12605-12614.
- Hecht, N.B (2004). The Relative Levels of Translin-associated Factor X (TRAX) and Testis Brain RNA-binding Protein Determine Their Nucleocytoplasmic Distribution in Male Germ Cells. J Biol Chem, 279:31514-31523.
- Hicks S, Jezyk MR, Gershburg S, Seifert JP, Harden TK, Sondek J (2008). General and Versatile Autoinhibition of PLC Isozymes. Mol Cell, 31:383-394.
- Hurlbert MS, Gianani RI, Hutt C, Freed CR, Kaddis FG (1999). Neural transplantation of hNT neurons for Huntington's disease. Cell Transplant, 8:143-151.

[I]

- Igarashi H, Knott JG, Schultz RM, Williams CJ (2007). Alterations of PLCβ1 in mouse eggs change calcium oscillatory behavior following fertilization. Dev Biol, 312:321-330.
- Ignatius MJ, Chandler CR, Shooter EM (1985). Nerve growth factor-treated, neurite-bearing PC12 cells continue to synthesize DNA. J Neurosci, 5:343-351.
- Irvine RF (2003). Nuclear lipid signalling. Nat Rev Mol Cell Biol, 4:349-360.
- Ishida R, Okado H, Sato H, Shionoiri C, Aoki K, Kasai M (2002). A role for the octameric ring protein, Translin, in mitotic cell division. FEBS Lett, 525:105-110.

[J]

- Jaendling A, McFarlane RJ (2010). Biological roles of translin and translin-associated factor-X: RNA metabolism comes to the fore. Biochem J, 429:225-234
- Jessell TM (2000). Neuronal specification I the spinal cord: inductive signals and transcriptional codes. Nat Rev Genet, 1:20-29.
- Jones DR, Divecha N (2004). Linking lipids to chromatin. Curr Opin Genet Dev, 14:196-202.

[K]

- Kelley GG, Reks SE, Ondrako JM, Smrcka AV (2001). Phospholipase C-ε: a novel Ras effector. EMBO J, 20:743-754.
- Keune Wj, Bultsma Y, Sommer L, Jones D, Divecha N (2011). Phosphoinositide signalling in the nucleus. Adv Enzyme Regul, 51:91-99.
- Kim CG, Park D, Rhee SG (1996). The role of carboxyl-terminal basic amino acids in Gqα-dependent activation, particulate association, and nuclear localization of phospholipase C-β1. J Biol Chem, 271:21187-21192.
- Kim D, Jun KS, Lee SB, Kang NG, Min DS, Kim YH, Ryu SH, Suh PG, Shin HS (1997). Phospholipase C isozymes selectively couple to specific neurotransmitter receptors. Nature, 389:290-293.
- Kim MJ, Min DS, Suh PG (1998). A cytosolic, Gαq and βγ intensitive splice variant of phospholipase C-β4. J Biol Chem, 273:3618-3624.
- Kleppner SR, Robinson KA, Trojanowski JQ, Lee VM (1995). Transplanted human neurons derived from a teratocarcinoma cell line (Ntera2) mature, integrate and survive for over 1 year in the nude mouse brain. J Comp Neurol, 357:618-636.

- Koh HY, Kim D, Lee J, Lee S, Shin HS (2008). Deficits in social behavior and sensorimotor gating in mice lacking phospholipase Cbeta1. Genes Brain Behav, 7:120-128.
- Koh HY. Phospholipase C-β1 and schizophrenia-related behaviors (2013). Adv Biol Regul, 53:242-248.
- Kondziolka D, Steinberg GK, Wechsler L, Meltzer CC, Elder E, Gebel J, Decesare S, Jovin T, Zafonte R, Lebowitz J, Flickinger JC, Tong D, Marks MP, Jamieson C, Luu D, Bell-Stephens T, Teraoka J (2005). Neurotransplantation for patients with subcortical motor stroke: a phase 2 randomized trial. J Neurosurg, 103:38-45.
- Kondziolka D, Wechsler L, Goldstein S, Meltzer C, Thulborn KR, Gebel J, Jannetta P, DeCesare S, Elder EM, McGrogan M, Reitman MA, Bynum L (2000). Trasplantation of cultured human neuronal cells for patients with stroke. Neurology, 55:565-569.
- Kumar V, Jong YJI, O'Malley KL (2008). Activated nuclear metabotropic glutamate receptor mGlu5 couples to nuclear G(q/11) proteins to generate inositol 1,4,5-triphosphate-mediated nuclear Ca2+ release. J Biol Chem, 283:14072-14083.
- Kurian MA, Meyer E, Vassallo G, Morgan NV, Prakash N, Pasha S, Hai NA, Shuib S, Rahman F, Wassmer E, Cross JH, O'Callaghan FJ, Osborne JP, Scheffer IE, Gissen P, Maher ER (2010). Phospholipase C beta 1 deficiency is associated with early onset epileptic encephalopathy. Brain, 133:2964-2970.
- Kuriki H, Tamiya-Koizumi K, Asano M, Yoshida S, Kojima K, Nimura Y (1992). Existence of phosphoinositide-specific phospholipase C in rat liver nuclei and its change during liver regeneration. J Biochem, 111:283-286.
- Kuvichkin VV (2002). DNA-lipid interactions in vitro and in vivo. Bioelectrochemistry, 58:3-12.

[L]

- Lamond AI, Spector DL (2003). Nuclear speckles: a model for nuclear organelles. Nat Rev Mol Cell Biol, 4:605-612.
- Landis SC (2002). Quick-change artist: from excitatory to inhibitory synapse in minutes. Nat Neurosci, 5:503-504.
- Lee SB, Rhee SG (1996). Molecular cloning, splice variants, expression, and purification of phospholipase C-δ4. J Biol Chem, 271:25-31.

- Lee SB, Shin SH, Hepler JR, Gilman AG, Rhee SG (1993). Activation of phospholipase C-beta 2 mutants by G protein alpha q and beta gamma subunits. J Biol Chem, 268:25952-25957.
- Lee VM, Andrews PW (1986). Differentiation of NTERA-2 clonal human embryonal carcinoma cells into neurons involves the induction of all three neurofilament proteins. J Neurosci, 6:514-521.
- Lee VM, Hartley RS, Trojanowski JQ (2000). Neurobiology of human neurons (NT2N) grafted into mouse spinal cord: implications for improving therapy of spinal cord injury. Prog Brain Res, 128:299-307.
- Li W, Laishram RS, Anderson RA (2013). The novel poly(A) polymerase Star-PAP is a signal-regulated switch at the 3'-end of mRNAs. Adv Biol Regul, 53:64-76.
- Li Z, Wu Y, Baraban JM (2008). The Translin/Trax RNA binding complex: clues to function in the nervous system. Biochim Biophys Acta, 1779:479-485.
- Litosch I (2000). Regulation of phospholipase C-β1 activity by phosphatidic acid. Biochemistry, 39:7736-7743.
- Liu M, Simon MI (1996). Regulation by cAMP-dependent protein kinease of a G protein-mediated phospholipase C. Nature, 382:83-87.
- Liu Y, Ye X, Jiang F, Liang C, Chen D, Peng J, Kinch LN, Grishin N. V, Liu Q (2009). C3PO, an endoribonuclease that promotes RNAi by facilitating RISC activation. Science, 325:750-753.
- Lo Vasco VR, Cardinale G, Polonia P (2012). Deletion of PLCB1 gene in schizophrenia-affected patients. J Cell Mol Med, 16:844-851.
- Lodish H, Berk A, Zipursky SL, Matsudaira P, Baltimore D and Darnell J. 2000. Molecular Cell Biology. FreemanWH and Company. New York, USA.
- López I, Mac EC, Ding J, Hamm HE, Lomasney JW (2001). A novel bifunctional phospholipase C that is regulated by Gα12 and stimulates the Ras/Mitogen-activated protein kinase pathway. J Biol Chem, 276:2758-2765.
- Lukinovic-Skudar V, Donlagic L, Banfic H, Visnjic D (2005). Nuclear phospholipase C-beta1b activation during G2/M and late G1 phase in nocodazole-synchronized HL-60 cells. Biochim Biophys Acta, 1733:148-156.
- Lyon AM, Tesmer VM, Dhamsania VD, Thal DM, Gutierrez J, Chowdhury S, Suddala KC, Northup JK, Tesmer JJ (2011). An Autoinhibitory Helix in the C-Terminal Region of Phospholipase C-β Mediates $G\alpha_q$ Activation. Nat Struct Mol Biol, 18:999-1005.

[M]

- Maki M, Kitaura Y, Satoh H, Ohkouchi S, Shibata H (2002). Structures, functions and molecular evolution of the penta-EF-hand Ca2+-binding proteins. Biochim Biophys Acta, 1600:51-60.
- Manzoli L, Billi AM, Rubbini S, Bavelloni A, Faenza I, Gilmour RS (1997). Essential role for nuclear phospholipase C b1 in insulin-like growth factor 1-induced mitogenesis. Cancer Res, 57:2137-2139.
- Marmiroli S, Ognibeneli A, Bavelloni A, Cintill C, Cocco, Maraldi NM (1994). Interleukin lα Stimulates Nuclear Phospholipase C in Human Osteosarcoma SaOS-2 Cells. J Biol Chem, 269:13-16.
- Martelli AM, Billi AM, Manzoli L, Faenza I, Aluigi M, Falconi M, De PA, Gilmour RS, Cocco L (2000). Insulin selectively stimulates nuclear phosphoinositide-specific phospholipase C (PI-PLC) beta1 activity through a mitogen-activated protein (MAP) kinase-dependent serine phosphorylation. FEBS Lett, 486:230-236.
- Martelli AM, Cocco L, Bareggi R, Tabellini G, Rizzoli R, Ghibellini MD, Narducci P (1999). Insulin-like growth factor-I-dependent stimulation of nuclear phospholipase C beta 1 activity in Swiss 3T3 cells requires an intact cytoskeleton and is paralleled by increased phosphorylation of the phospholipase. J Cell Biochem, 72:339-348.
- Martelli AM, Fiume R, Faenza I, Tabellini G, Evangelista C, Bortul R, Follo MY, Falà F, Cocco L (2005). Nuclear phosphoinositide specific phospholipase C (PI-PLC)-beta 1: a central intermediary in nuclear lipid-dependent signal transduction. Histol Histopathol, 20:1251-1260.
- Martelli AM, Gilmour RS, Neri LM, Manzoli L, Corps AN, Cocco L (1991). Mitogen-stimulated events in nuclei of Swiss 3T3 cells. Evidence for a direct link between changes of inositol lipids, protein kinase C requirement and the onset of DNA synthesis. FEBS Lett, 283:243-246.
- Martelli MA, Stewart Gilmour R, Bertagnolo V, Neri LM, Manzoli L, Cocco L (1992). Nuclear localization and signalling activity of phosphoinositidase Cβ in Swiss 3T3 Cells. Nature, 358:242-245.
- Martínez-Morales PL, Revilla A, Ocaña I, González C, Sainz P, McGuire D, Liste I (2013). Progress in stem cell therapy for major human neurological disorders. Stem Cell Rev, 9:685-699.

- Matteucci A, Faenza I, Gilmour RS, Manzoli L, Billi AM, Peruzzi D, Bavelloni A, Rhee SG, Cocco L (1998). Nuclear but not cytoplasmic phospholipase C ß1 inhibits differentiation of erythroleukemia cells. Cancer Res, 58:5057-5060.
- McOmish CE, Burrows E, Howard M, Scarr E, Kim D, Shin HS, Dean B, van den Buuse M, Hannan AJ (2008a). Phospholipase C beta1 knockout mice exhibit endophenotypes modelling schizophrenia which are rescued by environmental enrichment and clozapine administration. Mol Psychiatry, 13:661-672.
- McOmish CE, Burrows EL, Howard M, Hannan AJ (2008b). PLC-β1 knockout mice as a model of disrupted cortical development and plasticity: behavioral endophenotypes and dysregulation of RGS4 gene expression. Hippocampus, 18:824-834.
- Megiorni F, Mora B, Indovina P, Mazzilli MC (2005). Expression of neuronal markers during NTera2/cloneD1 differentiation by cell aggregation method. Neurosci Lett 373:105-109.
- Meltzer CC, Kondziolka D, Villemagne VL, Wechsler L, Goldstein S, Thurlborn KR, Gebel J, Elder EM, DeCesare S, Jacobs S (2001). Serial [18F] fluorodeoxyglucose positron emission tomography after human neuronal implantation for stroke. Neurosurgery, 49:586-591.
- Memedula S, Belmont AS (2003). Sequential recruitment of HAT and SWI/SNF components to condensed chromatin by VP16. Curr Biol, 13:241-246.
- Mittnacht S (1998). Control of pRB phosphorylation. Curr Opin Genet Dev, 8:21-27.
- Miyara F, Pesty A, Migne C, Djediat C, Huang XB, Dumont-Hassan M, Debey P, Lefevre B (2008). Spontaneous calcium oscillations and nuclear PLC-beta1 in human GV oocytes. Mol Reprod Dev, 75:392-402.
- Miyazono M, Nowell PC, Finan JL, Lee VM, Trojanowski JQ (1996). Long-term integration and neuronal differentiation of human embryonal carcinoma cells (NTera-2) transplanted into the caudoputamen of nude mice. J Comp Neurol, 376:603-613.
- Montaña M, García del Caño G, López de Jesús M, González-Burguera I, Echeazarra L, Barrondo S, Sallés J (2012). Cellular neurochemical characterization and subcellular localization of phospholipase C β1 in rat brain. Neuroscience, 222:239-68.
- Mortillaro MJ, Blencowe BJ, Wei X, Nakayasu H, Dull L, Warren SL, Sharp PA, Berezney R (1996). A hyperphosphorylated form of the large subunit of RNA polymerase II is associated with splicing complexes and the nuclear matrix. Proc Natl Acad Sci USA, 93:8253-8257.

- Mullen RJ, Buck CR, Smith AM (1992). NeuN, a neuronal specific nuclear protein in vertebrates. Development, 116:201-211.
- Musch T, Oz Y, Lyko F, Breiling A (2010). Nucleoside drugs induce cellular differentiation by caspase-dependent degradation of stem cell factors. PLoS One, 5:e10726.

[N]

- Nagano K, Fukami K, Minagawa T, Watanabe Y, Ozaki C, Takenawa T (1999). A novel phospholipase C-δ4 (PLC-δ4) splice variant as a negative regulator of PLC. J Biol Chem, 274:2872-2879.
- Nelson PT, Kondziolka D, Wechsler L, Goldstein S, Gebel J, DeCesare S, Elder EM, Zhang PJ, Jacobs A, McGrogan M, Lee VM, Trojanowski JQ (2002). Clonal human (hNT) neuron grafts for stroke therapy: neuropathology in a patient 27 months after implantation. Am J Pathol, 160:1201-1206.
- Neri LM, Borgatti P, Capitani S, Martelli AM (1998). Nuclear diacylglycerol produced by phosphoinositide-specific phospholipase C is responsible for nuclear translocation of protein kinase C-α. J Biol Chem, 273:29738 -29744.
- Neri LM, Capitani S, Borgatti P, Martelli AM (1999). Lipid signalling and cell responses at the nuclear level. Histol Histopathol, 14:321-335.
- Nishizuka Y (1984). Turnover of inositol phospholipids and signal transduction. Science, 225:1365-1370.
- Novak JE, Agranoff BW, Fisher SK (2000). Increased expression of Gαq/11 and of phospholipase-Cβ1/4 in differentiated human NT2-N neurons: enhancement of phosphoinositide hydrolysis. J Neurochem, 74:2322-2330.

[O]

- O'Carroll SJ, Mitchell MD, Faenza I, Cocco L, Gilmour RS (2009). Nuclear PLCbeta1 is required for 3T3-L1 adipocyte differentiation and regulates expression of the cyclin D3-cdk4 complex. Cell Signal, 21:926-935.
- O'Malley KL, Jong YJ, Gonchar Y, Burkhalter A, Romano C (2003). Activation of metabotropic glutamate receptor mGlu5 on nuclear membranes mediates intranuclear Ca2+ changes in heterologous cell types and neurons. J Biol Chem, 278:28210-28219.

- O'Leary DD, Ruff NL, Dyck RH (1994). Development, critical period plasticity, and adult reorganizations of mammalian somatosensory systems. Curr Opin Neurobiol, 4:535-544.
- Osborne SL, Thomas CL, Gschmeissner S, Schiavo G (2001). Nuclear PtdIns(4,5)P2 assembles in a mitotically regulated particle involved in pre-mRNA splicing. J Cell Sci, 114:2501-2511.
- Öz S, Maercker C, Breiling A (2013). Embryonic carcinoma cells show specific dielectric resistance profiles during induced differentiation. PLoS One, 8:e59895.

[P]

- Payrastre B, Nievers M, Boonstra J, Breton M, Verkleij AJ, Van Bergen en Henegouwen P.M.P (1992). A Differential Location of Phosphoinositide Kinases, Diacylglycerol Kinase, and PhospholipaseC in the Nuclear Matrix. J Biol Chem, 267:5078-5084.
- Peruzzi D, Aluigi M, Manzoli L, Billi AM, Di Giorgio FP, Morleo M, Martelli AM, Cocco L (2002). Molecular characterization of the human PLC β1 gene. Biochim Biophys Acta, 1584:46- 54.
- Peruzzi D, Calabrese G, Faenza I, Manzoli L, Matteucci A, Gianfrancesco F, Billi AM, Stuppia L, Palka G, Cocco L (2000). Identification and chromosomal localization by fluorescence in situ hybridisation of human gene of phosphoinositide specific phospholipase C β1. Biochim Biophys Acta, 1484:175-182.
- Philip F, Guo Y, Aisiku O, Scarlata S (2012). Phospholipase Cβ1 is linked to RNA interference of specific genes through translin-associated factor X. FASEB J, 26:4903-4913.
- Philip F, Sahu S, Caso G, Scarlata S (2013). Role of Phospholipase C-β in RNA interference. Adv Biol Regul, 53:319-330.
- Piontek J, Chen CC, Kempf M, Brandt R (1999). Neurotrophins differentially regulate the survival and morphological complexity of human CNS model neurons. J Neurochem, 73(1):139-146.
- Plantavid M, Rosignol L, Chap H, Douste-Blazy L (1986). Studies of endogenous polyphosphoinositide hydrolysis in human platelet membranes. Evidence that polyphosphoinositides remain inaccessible to phosphochesterase in the native membrane. Biochim Biophys Acta, 875:147-156.

- Pleasure SJ, Page C, Lee VM (1992). Pure, postmitotic, polarized human neurons derived from NTera 2 cells provide a system for expressing exogenous proteins in terminally differentiated neurons. J Neurosci, 12:1802-1815.
- Podrygajlo G, Song Y, Schlesinger F, Krampfl K, Bicker G (2010). Synaptic currents and transmitter responses in human NT2 neurons differentiated in aggregate culture. Neurosci Lett, 468:207-210.
- Podrygajlo G, Tegenge MA, Gierse A, Paquet-Durand F, Tan S, Bicker G, Stern M (2009). Cellular phenotypes of human model neurons (NT2) after differentiation in aggregate culture. Cell Tissue Res, 336:439-452.
- Popovic J, Stanisavljevic D, Schwirtlich M, Klajn A, Marjanovic J, Stevanovic M (2014). Expression analysis of SOX14 during retinoic acid induced neural differentiation of embryonal carcinoma cells and assessment of the effect of its ectopic expression on SOXB members in HeLa cells. PLoS One, 9:e91852.
- Przyborski SA, Morton IE, Wood A, Andrews PW (2000). Developmental regulation of neurogenesis in the pluripotent human embryonal carcinoma cell line NTERA-2. Eur J Neurosci, 12:3521-3528.

[R]

- Ramazzotti G, Faenza I, Gaboardi GC, Piazzi M, Bavelloni A, Fiume R, Manzoli L, Martelli AM, Cocco L (2008). Catalytic activity of nuclear PLC-PLCβ_1 is required for its signalling function during C2C12 differentiation. Cell Signal, 20:2013-2021.
- Rameh LE y Cantley LC (1999). The role of phosphoinositide 3-kinase lipid products in cell function. J Biol Chem, 274:8347-8350.
- Rando OJ, Zhao K, Janmey P, Crabtree GR (2002). Phosphatidylinositol-dependent actin filament binding by the SWI/SNF-like BAF chromatin remodeling complex. Proc Natl Acad Sci USA, 99: 2824-2829.
- Razzini G, Brancaccio A, Lemmon MA, Guarnieri S, Falasca M (2000). The role of the pleckstrin homology domain in membrane targeting and activation of phospholipase C-β1. J Biol Chem, 275:14873-14881.
- Rebecchi MJ, Pentyala SN (2000). Structure, function, and control of phosphoinositide-specific phosphoplipase C. Physiol Rev, 80:1291-1335.
- Rhee SG (2001).Regulation of phosphoinositide-specific phospholipase C. Annu Rev Biochem, 70:281-312.

- Rhee SG, Bae YS (1997). Regulation of phosphoinositide-Specific phospholipase C isoenzymes. J Biol Chem, 272:15045-15048.
- Rhee SG, Suh PG, Ryu SH, Lee SY (1989). Studies of inositol phospholipid-specific phospholipase C. Science, 244:546-550.
- Robbins J, Dilworth SM, Laskey RA, Dingwall C (1991). Two interdependent basic domains in nucleoplasmin nuclear targeting sequence: identification of a class of bipartite nuclear targeting sequence. Cell, 64:615-623.
- Ruiz de Azúa I, del Olmo E, Pazos A, Sallés J (2006). Transmembrane signaling through phospholipase C-beta in the developing human prefrontal cortex. J Neurosci Res, 84:13-26.

[S]

- Sallés J, López de Jesus M, Goñi O, Fernandez-Teruel A, Driscoll P, Tobena A, Escorihuela RM (2001). Transmembrane signaling through phospholipase C in cortical and hippocampal membranes of psychogenetically selected rat lines. Psychopharmacology, 154:115-125.
- Saporta S, Borlongan CV, Sanberg PR (1999). Neural transplantation of human neuroteratocarcinoma (hNT) neurons into ischemic rats. A quantitative dose-response analysis of cell survival and behavioral recovery. Neuroscience, 91:519-525.
- Saporta S, Willing AE, Colina LO, Zigova T, Milliken M, Daadi MM, Sanberg PR (2000). In vitro and in vivo characterization of hNT neuron neurotransmitter phenotypes. Brain Res Bull, 53:263-238.
- Saunders CM, Larman MG, Parrington J, Cox LJ, Royse J, Blayney LM, Swann K, Lai FA (2002). PLC zeta: a sperm-specific trigger of Ca2+ oscillations in eggs and embryo development. Development, 129:3533-3544.
- Schramp M, Hedman A, Li W, Tan X, Anderson R (2012). PIP kinases from the cell membrane to the nucleus. Subcell Biochem, 58:25-59.
- Shen X, Ranallo R, Choi E, Wu C (2003). Involvement of actin-related proteins in ATP-dependent chromatin remodeling. Mol Cell, 12:147-155.
- Shuman, S. (1991). Recombination Mediated by Vaccinia Virus DNA Topoisomerase I in *Escherichia coli* is Sequence Specific. Proc Natl Acad Sci USA, 88:10104-10108.
- Shuman, S. (1994). Novel Approach to Molecular Cloning and Polynucleotide Synthesis Using Vaccinia DNA Topoisomerase. J Biol Chem, 269:32678-32684.

- Smith CD, Wells WW (1983). Phosphorylation of rat liver nuclear envelopes II. Characterization of in vitro lipid phosphorylation. J Biol Chem, 258:9368-9373.
- Song C, Hu CD, Masago M, Kariya KI, Yamawaki-Kataoka Y, Shibatohge M, Wu D, Satoh T, Kataoka T (2001). Regulation of a novel human phospholipase C, PLC-ε, through membrane targeting by Ras. J Biol Chem, 276:2752-2757.
- Spector DL (1993). Macromolecular domains within the cell nucleus. Annu Rev Cell Biol, 9:265-315.
- Spector DL, Fu XD, Maniatas T (1991). Associations between distinct premRNA splicing components and the cell nucleus. EMBO J, 10:3467-3481.
- Spires TL, Molnár Z, Kind PC, Cordery PM, Upton AL, Blakemore, Hannan AJ (2005). Activity-dependent Regulation of Synapse and Dendritic Spine Morphology in Developing Barrel Cortex Requires Phospholipase C-β1 Signalling. Cereb Cortex, 15:385-393.
- Stein JM, Bergman W, Fang Y, Davison L, Brensinger C, Robinson MB, Hecht NB, Abel T (2006). Behavioral and neurochemical alterations in mice lacking the RNA-binding protein translin. J Neurosci, 26:2184-2196.
- Suh PG, Park JI, Manzoli L, Cocco L, Peak JC, Katan M, Fukami K, Kataoka T, Yun S, Ryu SH (2008). Multiple roles of phosphoinositide-specific phospholipase C Isozymes. BMB Rep, 41:415-434.
- Sun CN, Cheng HC, Chou JL, Lee SY, Lin YW, Lai HL, Chen HM, Chern Y (2006). Rescue of p53 blockage by the A(2A) adenosine receptor via a novel interacting protein, translin-associated protein X. Mol Pharmacol, 70:454-466.
- Sun F, Guo W, Du J, Ni Z, Sun Q, Yao Y (2013). Widespread, abundant, and diverse TE-associated siRNAs in developing wheat grain. Gene, 522:1-7.

[T]

- Tabellini G, Bortul R, Santi S, Riccio M, Baldini G, Cappellini A, Billi AM, Berezney R, Ruggeri A, Cocco L, Martelli AM (2003). Diacylglycerol kinase-theta is localized in the speckle domains of the nucleus. Exp Cell Res, 287:143-154.
- Taguchi K, Watanabe Y, Tsujimura A, Tatebe H, Miyata S, Tokuda T, Mizuno T, Tanaka M (2014). Differential expression of alpha-synuclein in hippocampal neurons. PLoS One, 9:e89327.
- Takeuchi H, Oike M, Paterson HF, Allen V, Kanematsu T, Ito Y, Erneux C, Katan M, Hirata M (2000). Inhibition of Ca(2+) signalling by p130, a phospholipase-C-related

catalytically inactive protein: critical role of the p130 pleckstrin homology domain. Biochem J, 349:357-368.

- Tegenge MA, Roloff F, Bicker G (2011). Rapid differentiation of human embryonal carcinoma stem cells (NT2) into neurons for neurite outgrowth analysis. Cell Mol Neurobiol, 31:635-643.
- Thompson RJ (1973). Studies on RNA synthesis in two populations of nuclei from the mammalian cerebral cortex. J Neurochem, 21:19-40.
- Topham MK, Bunting M, Zimmerman GA, McIntyre TM, Blackshear PJ, Prescott SM (1998). Protein kinase C regulates the nuclear localization of diacylglycerol kinase-zeta. Nature, 394:697-700.
- Trojanowski JQ, Kleppner SR, Hartley RS, Miyazono M, Fraser NW, Kesari S, Lee VMY (1997). Transfectable and transplantable post-mitotic human neurons: a potential "platform" for gene therapy of nervous system diseases. Exp Neurol, 144:92-97.
- Trojanowski JQ, Mantione JR, Lee JH, Seid DP, You T, Inge LJ, Lee VM (1993). Neurons derived from a human teratocarcinoma cell line establish molecular and structural polarity following transplantation into the rodent brain. Exp Neurol, 122:283-294.

[U]

- Udawela M, Scarr E, Hannan AJ, Thomas EA, Dean B (2011). Phospholipase C beta 1 expression in the dorsolateral prefrontal cortex from patients with schizophrenia at different stages of illness. Aust N Z J Psychiatry, 45:140-147.

[V]

- Vann LR, Wooding FB, Irvine RF, Divecha N (1997). Metabolism and possible compartmentalization of inositol lipids in isolated rat-liver nuclei. Biochem J, 327:569-576.

[W]

- Waldo GL, Ricks TK, Hicks SN, Cheever ML, Kawano T, Tsuboi K, Wang X, Montell C, Kozasa T, Sondek J, Harden TK (2010). Kinetic scaffolding mediated by a phospholipase C-beta and Gq signaling complex. Science, 330:974-980.

- Wang J, Boja ES, Oubrahim H, Chock PB (2004). Testis Brain Ribonucleic Acid-Binding Protein/Translin Possesses Both Single-Stranded and Double-Stranded Ribonuclease Activities. Biochemistry, 43:13424-13431.
- Wang T, Pentyala S, Elliot JT, Dowal L, Gupta E, Rebecchi MJ, Scarlata S (1999). Selective interaction of the C2 domains of phospholipase C-beta1 and -beta2 with activated Galphaq subunits: an alternative function for C2-signaling modules. Proc Natl Acad Sci USA, 96:7843-7846.
- Wen W, Yan J, Zhang M (2006). Structural characterization of the split pleckstrin homology domain in phospholipase C-gamma1 and its interaction with TRPC3. J Biol Chem, 281:12060-12068.
- Wu D, Jiang H, Katz A, Simon MI (1993). Identification of critical regions on phospholipase C-beta 1 required for activation by G-proteins. J Biol Chem, 268:3704-3709.

[X]

- Xu A, Suh PG, Marmy-Conus N, Pearson RB, Seok OY, Cocco L, Gilmour RS (2001a). Phosphorylation of nuclear phospholipase C β1 by extracellular signalregulated kinase mediates the mitogenic action of insulin-like growth factor I. Mol Cell Biol, 21:2981-2990.
- Xu A, Wang Y, Xu LY, Gilmour RS (2001b). Protein kinase C a-mediated negative feedback regulation is responsible for the termination of insulin-like growth factor I induced activation of nuclear phospholipase C β1 in Swiss 3T3 cells. J Biol Chem, 276:14980-14986.
- Xu SL, Choi RC, Zhu KY, Leung KW, Guo AJ, Bi D, Xu H, Lau DT, Dong TT, Tsim KW (2012). Isorhamnetin, A Flavonol Aglycone from Ginkgo biloba L, Induces Neuronal Differentiation of Cultured PC12 Cells: Potentiating the Effect of Nerve Growth Factor. Evid Based Complement Alternat Med, 2012:278273.

[Y]

- Yamamoto T, Takeuchi H, Kanematsu T, Allen V, Yagisawa H, Kikkawa U, Watanabe Y, Nakasima A, Katan M, Hirata M (1999). Involvement of EF hand motifs in the Ca2+-dependent binding of the pleckstrin homology domain to phosphoinositides. Eur J Biochem, 265:481-490.

- Yang S, Cho YS, Chennathukuzhi VM, Underkoffler LA, Loomes K, Hecht NB (2004). Translin-associated factor X is post-transcriptionally regulated by its partner protein TB-RBP, and both are essential for normal cell proliferation. J Biol Chem, 279:12605-12614.
- Ye X, Huang N, Liu Y, Paroo Z, Huerta C, Li P, Chen S, Liu Q, Zhang H (2011). Structure of C3PO and Mechanism of Human RISC Activation. Nat Struct Mol Biol, 18:650-657.
- Yin HL, Janmey PA (2003). Phosphoinositide regulation of the actin cytoskeleton. Annu Rev Physiol, 65:761-789.
- York JD, Majerus PW (1994). Nuclear phosphatidylinositols decrease during S phase of the cell cycle in HeLa cells. J Biol Chem, 269:7847-7850.
- Yoshioka A, Yudkoff M, Pleasure D (1997). Expression of glutamic acid decarboxylase during human neuronal differentiation: studies using the NTera-2 culture system. Brain Res, 767:333-339.
- Yu H, Fukami K, Watanabe Y, Ozaki C, Takenawa T (1998). Phosphatidylinositol 4,5-bisphosphate reverses the inhibition of RNA transcription caused by histone H1. Eur J Biochem, 251:281-287.

[Z]

- Zhang C, Saatman KE, Royo NC, Soltesz KM, Millard M, Schouten JW, Motta M, Hoover RC, McMillan A, Watson DJ, Lee VM, Trojanowski JQ, McIntosh TK (2005). Delayed transplantation of human neurons following brain injury in rats: a long-term graft survival and behavior study. J Neurotrauma, 22:1456-1474.
- Zhao K, Wang W, Rando OJ, Xue Y, Swiderek K, Kuo A, Crabtree GR (1998). Rapid and phosphoinositol-dependent binding of the SWI/SNF-like BAF complex to chromatin after T lymphocyte receptor signaling. Cell, 95:625-636.
- Zini N, Martelli AM, Cocco L, Manzoli FA, Maraldi NM (1993). Phosphoinositidase C isoforms are specifically localized in the nuclear matrix and cytoskeleton of Swiss 3T3 cells. Exp Cell Res, 208:257-269.
- Zini N, Mazzoni M, Neri LM, Bavelloni A, Marmiroli S, Capitani S, Maraldi NM (1994). Immunocytochemical detection of the specific association of different PIC isoforms with cytoskeletal and nuclear matrix compartments in PC12 cells. Eur J Cell Biol, 65:206-213.